

Revista **ALCONPAT**

Latin American Journal of Quality Control, Pathology and Construction Recovery

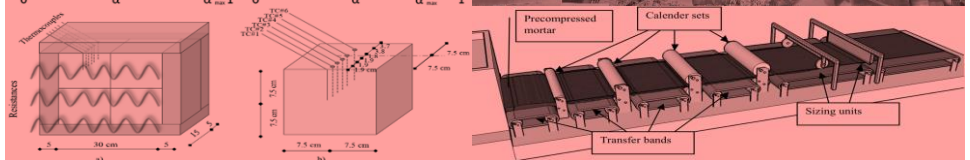
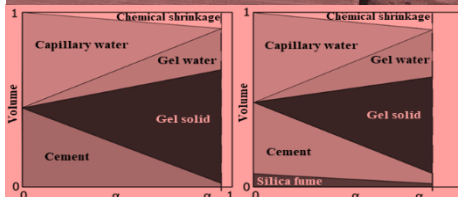
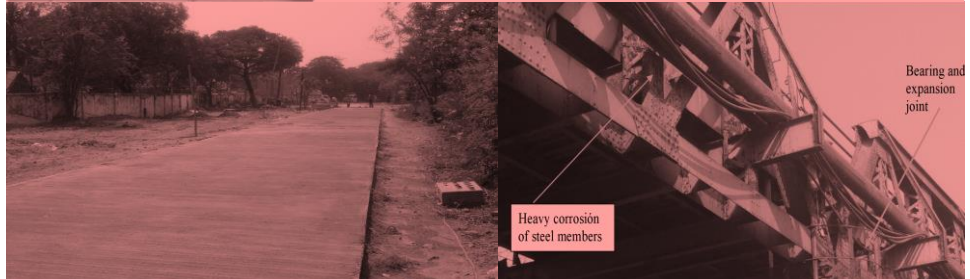
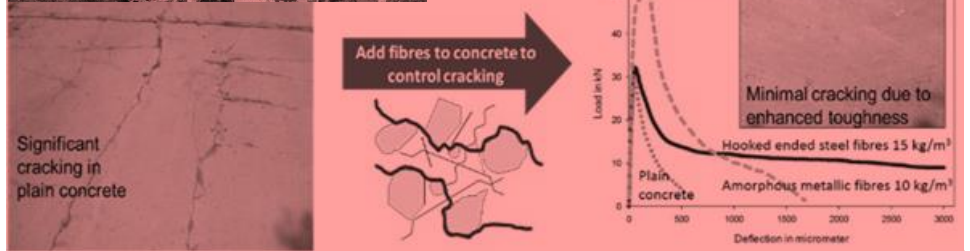
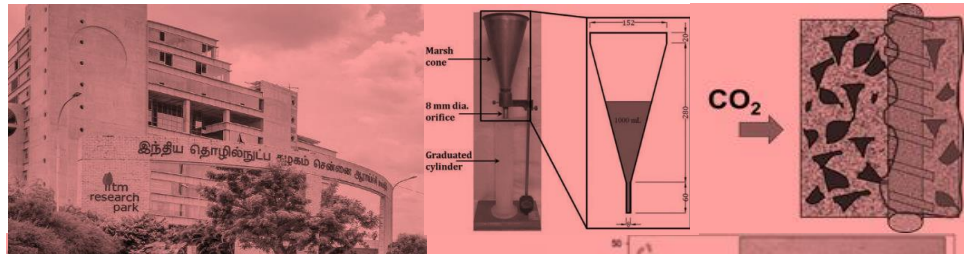
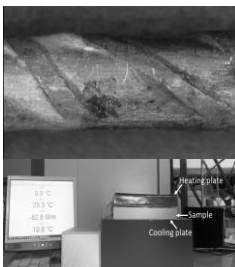
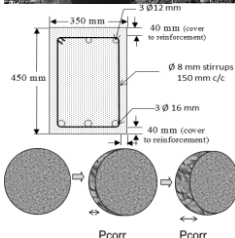
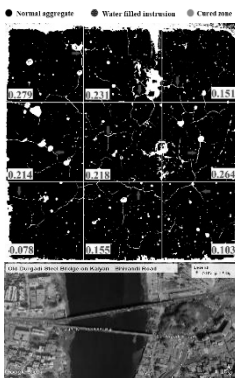
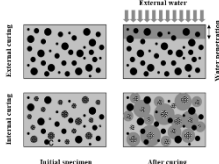
DOI: <http://dx.doi.org/10.21041/ra.v10i2>
editorial.revista.alconpat@gmail.com

eISSN: 2007-6835

Volume 10

May – August 2020

Issue 2



Latin American Journal of Quality Control, Pathology and Construction Recovery

<http://www.revistaalconpat.org>



ALCONPAT International

Founders members:

Liana Arrieta de Bustillos – **Venezuela**
Antonio Carmona Filho - **Brazil**
Dante Domene – **Argentina**
Manuel Fernández Cánovas – **Spain**
José Calavera Ruiz – **Spain**
Paulo Helene, **Brazil**

Board of Directors International:

President of Honor

Angélica Ayala Piola, **Paraguay**

President

Carmen Andrade Perdriz, **Spain**

Managing Director

Pedro Castro Borges, **Mexico**

Executive Secretary

José Iván Escalante García, **Mexico**

Technical Vice President

Enio Pazini Figueiredo, **Brazil**

Administrative Vice President

Luis Álvarez Valencia, **Guatemala**

Manager

Paulo Helene, **Brazil**

Revista ALCONPAT

Editor in Chief:

Dr. Pedro Castro Borges
Centro de Investigación y de Estudios Avanzados del
Instituto Politécnico Nacional, Unidad Mérida
(CINVESTAV IPN – Mérida)
Merida, Yucatan, **Mexico**

Co-Editor in Chief:

Dr. Francisco Alberto Alonso Farrera
Universidad Autónoma de Chiapas
Tuxtla Gutiérrez, Chiapas, México

Executive Editor:

Dr. José Manuel Mendoza Rangel
Universidad Autónoma de Nuevo León,
Facultad de Ingeniería Civil
Monterrey, Nuevo Leon, **Mexico**

Associate Editors:

Dr. Manuel Fernandez Canovas
Universidad Politécnica de Madrid.
Madrid, **Spain**

Ing. Raúl Husni

Facultad de Ingeniería Universidad de Buenos Aires.
Buenos Aires, **Argentina**

Dr. Paulo Roberto do Lago Helene
Universidade de São Paulo.
São Paulo, **Brazil**

Dr. José Iván Escalante García
Centro de Investigación y de Estudios Avanzados del
Instituto Politécnico Nacional (Unidad Saltillo)
Saltillo, Coahuila, **Mexico**.

Dr. Mauricio López.
Departamento de Ingeniería y Gestión de la Construcción,
Escuela de Ingeniería, Pontificia Universidad Católica de
Chile
Santiago de Chile, **Chile**

Dra. Oladis Troconis de Rincón
Centro de Estudios de Corrosión
Universidad de Zulia
Maracaibo, **Venezuela**

Dr. Fernando Branco Universidad
Técnica de Lisboa
Lisboa, **Portugal**

Dr. Pedro Garcés Terradillos
Universidad de Alicante
San Vicente, **Spain**

Dr. Andrés Antonio Torres Acosta
Instituto Tecnológico y de Estudios Superiores de
Monterrey, Querétaro
Querétaro, **Mexico**

Dr. Luiz Fernández Luco
Universidad de Buenos Aires –
Facultad de Ingeniería – INTECIN
Buenos Aires, **Argentina**

RAV10N2, May – August 2020

Message from the Editor in Chief

**JOURNAL OF THE LATIN-AMERICAN
ASSOCIATION OF QUALITY CONTROL,
PATHOLOGY AND RECOVERY OF
CONSTRUCTION**

<http://www.revistaalconpat.org>

With great satisfaction, we present the second issue of the tenth year of the ALCONPAT Journal.

The aim of the journal is to publish case studies within the scope of the Association, namely quality control, pathology and recovery of constructions, including basic and applied research, reviews and documentary research.

This edition presents our eighth Special Issue, this time dedicated to advances in science and technology of concrete for celebrating the extensive academic trajectories of Dr. Ravindra Gettu and Dr. Venkatesh Kodur, who were honored during the 3rd R N Raikar Memorial International Conference, held in Mumbai, India in December 2018.

This V10N2 issue begins with a work from **India**, where Ravindra Gettu and colleagues present a review about a decade of research carried out at IIT Madras on cementitious systems. It has shown that the partial replacement of portland cement with supplementary cementitious materials (SCMs) has significant benefits, as well as limitations. The SCMs do not adversely affect the long-term compressive strength and drying shrinkage of concretes, though there may be some compromise in workability and the resistance against plastic shrinkage cracking. Through the assessment of the chloride ingress rate in concrete and chloride threshold of steel, it is evident that the use of SCMs could significantly enhance the service life under chloride attack, though there is a reduction of the carbonation resistance. More importantly, SCMs can lead to significant reduction of the carbon footprint of concrete, and hence, are essential to achieve sustainability.

In the second work, from **Spain**, Carmen Andrade presents a review about the limitations of the models of corrosion initiation with indications to overcome them. Performance-based design of durability is at present a trend considered in fib Model Code (MC2010). However, we are still far from accurately predicting the performance of a structure in a specific environment, in spite of which performance-based requirements are introduced in the concrete specifications of large infrastructures demanding 100 years or more of service life. The depassivation step and the propagation period with considerations on their probabilistic treatment are also commented. It is proposed to consider corrosion onset as a “deterioration or initiation Limit State” (DLS or ILS). An example of calculation the time to cover-cracking induced corrosion is included.

The third work of this issue is from **Turkey**, where B. Y. Pekmezci and E. Y. Tuncel present an experimental study that was planned and executed for the application of Phase Change Materials (PCM) containing fiber-reinforced cementitious panels on buildings. The objective of their research was to enhance the thermal performance of the panels. PCM containing composites showed higher latent heat capacity and lower thermal conductivity.

Reinforcement with chopped fibers compensated the strength loss due to PCM in cementitious panels. Specific fracture energy of the panels increased with increase of PCM ratio. PCM containing fiber reinforced cementitious panels showed great potential for energy efficient buildings with enhanced thermal and mechanical properties.

In the fourth article, from **Canada**, M. Aqel and D. K. Panesar decouple the physical and chemical effects of limestone filler (LF), when used as a cement replacement. The effects were decoupled using LF and a chemically inert material (brucite $Mg(OH)_2$). Paste, and mortar specimens were steam cured for 16 hours at 55°C. The heat of hydration, thermal analysis, x-ray diffraction, and compressive strength, were evaluated at 16 hours and at 28 days. LF can adversely affect the properties through dilution effect. However, heterogeneous nucleation compensates for the dilution effect at 16 hours while the production of mono-carboaluminate compensates for the dilution effect at 16 hours and 28 days. The study could be broadened by considering a wider temperature range. The originality lies in the method of decoupling the physical and chemical effects. Measurable effects of the physical and chemical contribution of LF are evident on the mechanical and transport material properties.

The fifth work, by Alejandro Durán-Herrera and colleagues, from **Mexico** discuss the synergetic effect of a super-absorbent polymer in combination with a calcium nitrite corrosion inhibitor that were evaluated as a combined technology to improve concrete durability in High Performance Concrete. The effect of these technologies was evaluated by measuring the following parameters: autogenous and drying shrinkage, surface electrical resistivity and the non-steady-state chloride migration coefficient. The results indicated that the synergistic effect of SAP + CNI improves autogenous shrinkage and surface electrical resistivity.

The sixth work in this issue is written by A. H. Akca and N. Özyurt from **Turkey**. The relation between crack growth and reduction in the compressive strength after high temperature exposure and after air re-curing was investigated in this study. Concrete specimens were heated to 1000°C and they were subjected to air re-curing for 28 days. During re-curing period, their heated surfaces were monitored by using a digital single-lens reflex camera and the images were analyzed by using image analysis software. After cooling, the maximum reduction in the compressive strength of concrete was 49.5% and that of air re-cured concrete was 66.8%. Image analyses showed high correlations between crack growth and reduction in the compressive strength. This non-destructive method has the potential to represent the extent of damage in concrete after high temperature exposure.

In the seventh work, from **USA**, V. K. R. Kodur and A. Agrawal present an approach to evaluate residual capacity of fire-damaged concrete structures. The advanced analysis approach involves capturing response in three stages; namely, structural response at ambient conditions (prior to fire exposure), thermo-mechanical response during fire exposure, and post-fire residual response after cooling down of the structural member. The proposed approach is implemented in a comprehensive numerical model developed in the finite element computer program ABAQUS for specifically evaluating residual capacity of an RC beam after exposure to different fire scenarios. Predictions from

the numerical model are utilized to highlight importance of each stage of analysis in evaluating realistic residual capacity of fire damaged concrete members.

In the eighth work, from **Mexico**, Pedro Castro and colleagues discuss the passivation process quality considering polarization periodicity, passivation consolidation parameters, and data treatment. Passivation process quality in steel reinforcement affects a structure's planned future service life. Some research has addressed this phenomenon, but its study is complicated by the limits of analogue-era data, dispersion in corrosion rate data, and their interpretation. Two series of small reinforced concrete beams were built using two water/cement ratio and two curing/storage combinations and exposed to marine environment. Polarization periodicity had no effect on passivation/depasivation during passivation but on the data treatment. The curing and storage process influenced the tendency towards depasivation. Post-curing storage type affected cumulative corrosion rate from 1 to 5 $\mu\text{A}\cdot\text{day}/\text{cm}^2$; this is equivalent to the margin of uncertainty in interpretation.

The article that closes this edition is written by S. S. Bhonge and colleagues from **India** who describe the need for a rehabilitation methodology for the evaluation of distress and a proposal of likely remedial measures for a 100 year old Steel Bridge on the Ulhas River at km 1/ 800 on Bhiwandi road, Kalyan, near Mumbai. The bridge was constructed in 1914 during the British era, making it a heritage bridge, by British engineers with a unique structural arrangement of jack arch decking and warren truss girder with verticals. A structural audit in 2000 revealed the deterioration of steel parts and concrete initiated long ago because of the humid environment in the area. Durgadee Bridge showed various signs of distress like major cracks in masonry abutments, heavy corrosion of the mild steel structural members, non-functioning of expansion joints and bearings, failure and deterioration of jack arch roof plates, de-bonding of concrete and exposed reinforcement etc. The paper describes the draft policy/ proposed stages of rehabilitation and repair, proposed methodology and procedure for corrosion protection.

We are confident that the articles in this issue will constitute an important reference for those readers involved with questions related with science and technology of concrete. We thank the authors for participating in this issue, and for their willingness and effort to present high quality articles and meet the established timelines.

On behalf of the Editorial Board

Pedro Castro Borges
Editor in Chief

Surendra Manjrekar
Guest Editor

Commentary on the special issue

by
Ravindra Gettu
and
Venkatesh Kodur

In 2018, we were honored together at a Symposium on Advances in Science & Technology of Concrete, organized by the India Chapter of the American Concrete Institute, Mumbai, 2018, as part of the 3rd R N Raikar Memorial International Conference. It was humbling for us to be the company of the previous honorees, Profs. Suru Shah, Nemy Banthia and P.A.M Basheer, as well as to receive the warmth and hospitality of the conference organizers, especially Surendra Manjrekar, and the many friends, well-wishers and researchers, who participated in this event. It is of great pleasure that we are recognized again together in this special issue of the Revista ALCONPAT, and are grateful to the Association, and Pedro Castro Borges, in particular, for the generous gesture.

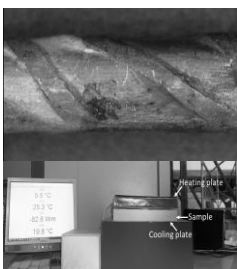
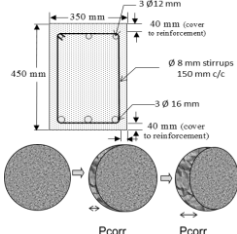
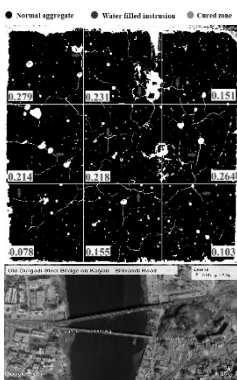
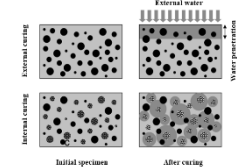
We fondly recall our visit to Tuxtla, Gutiérrez, Chiapas, México, for CONPAT 2019, and the opportunity to meet many ALCONPAT members, and have fruitful discussions with Latin American researchers and students.

The scientific community working in the science and technology of concrete has always been characterized by camaraderie and friendly discussions. The problems are often the same in many parts of the world, and there is always a lot to learn from the experiences of others. The exchange of ideas also prevents the same mistakes from being repeated. New techniques and technologies developed in some regions can be implemented better in other regions as we become wiser to overcome the limitations and constraints. Standards and codes formulated painstakingly in certain places can be used and improved upon in other countries. Our field of structural concrete does not evolve so rapidly, which has positives and negatives, and consequently information reaches all corners of the world fast enough for implementation.

Journals such as Revista ALCONPAT has the ability to focus on scientific questions that are relevant to practice and the effort taken to bring together high-quality papers in each issue is certainly commendable. We thank all the authors and the editors who have made this issue, one which is very special to us, possible.

Professor Venkatesh K. R. Kodur, Michigan State University, East Lansing, USA

Professor Ravindra Gettu, Indian Institute of Technology Madras, Chennai, India



CONTENT

REVIEW

- | | Page |
|--|-----------|
| R. G. Pillai, R. Gettu, M. Santhanam: Use of supplementary cementitious materials (SCMs) in reinforced concrete systems – Benefits and limitations. | 147 - 164 |
| C. Andrade: Rebar corrosion modelling and deterioration limit state. | 165 – 179 |

BASIC RESEARCH

- | | |
|--|-----------|
| E. Y. Tuncel, B. Y. Pekmezci: Sustainable fiber reinforced cementitious panels containing PCM: Mechanical and thermal performance. | 180 – 190 |
| M. Aqel, D. Panesar: Physical and chemical effects of limestone filler on the hydration of steam cured cement paste and mortar. | 191 - 205 |
| A. Durán-Herrera, J. A. Canul-Polanco, R. Dávila-Pompermayer, L. G. López-Yépez, P. Valdez-Tamez: Synergetic effect of a super-absorbent polymer and a calcium nitrite corrosion inhibitor in high performance concrete durability. | 206 - 218 |
| A. H. Akca, N. Özyurt: Image analysis on disintegrated concrete at the post-heating stage. | 219 - 229 |
| V. K. R. Kodur, A. Agrawal: A numerical approach for evaluating residual capacity of fire damaged concrete members. | 230 - 242 |
| J. A. Briceño-Mena, M. G. Balancán Zapata, P. Castro-Borges: Passivation process quality in reinforced concrete: effects of polarization periodicity and passivation consolidation parameters on data treatment. | 243 - 258 |

DOCUMENTAL RESEARCH

- | | |
|---|-----------|
| S. S. Bhonge, P. Dalwi, J. K. Kulkarni, S. K. Manjrekar: Recommendations for rehabilitation & corrosion protection of 100-year-old steel bridge (Durgadee) across heavily polluted river near Mumbai, India. | 259 - 273 |
|---|-----------|

Use of supplementary cementitious materials (SCMs) in reinforced concrete systems – Benefits and limitations

R. G. Pillai¹ , R. Gettu^{1*} , M. Santhanam¹

*Contact author: gettu@iitm.ac.in

DOI: <https://doi.org/10.21041/ra.v10i2.477>

Reception: 07/01/2020 | Acceptance: 08/04/2020 | Publication: 30/04/2020

ABSTRACT

About a decade of research carried out at IIT Madras on cementitious systems has shown that the partial replacement of portland cement with supplementary cementitious materials (SCMs) has benefits as well as limitations. The SCMs do not adversely affect the long-term compressive strength and drying shrinkage of concretes, though there may be some compromise in workability and the resistance against plastic shrinkage cracking. Through the assessment of the chloride ingress rate in concrete and chloride threshold of steel, it is evident that the use of SCMs could significantly enhance the service life under chloride attack, though there is a reduction of the carbonation resistance. More importantly, SCMs can lead to significant reduction of the carbon footprint of concrete, and hence, are essential to achieve sustainability.

Keywords: supplementary cementitious materials, limestone calcined clay, mechanical properties, microstructure, durability.

Cite as: Pillai, R. G., Gettu, R., Santhanam, M. (2020), “Use of supplementary cementitious materials (SCMs) in reinforced concrete systems – Benefits and limitations”, Revista ALCONPAT, 10 (2), pp. 147 – 164, DOI: <https://doi.org/10.21041/ra.v10i2.477>.

¹ Department of Civil Engineering, Indian Institute of Technology Madras, Chennai, India.

Legal Information

Revista ALCONPAT is a quarterly publication by the Asociación Latinoamericana de Control de Calidad, Patología y Recuperación de la Construcción, Internacional, A.C., Km. 6 antigua carretera a Progreso, Mérida, Yucatán, 97310, Tel.5219997385893, alconpat.int@gmail.com, Website: www.alconpat.org

Responsible editor: Pedro Castro Borges, Ph.D. Reservation of rights for exclusive use No.04-2013-011717330300-203, and ISSN 2007-6835, both granted by the Instituto Nacional de Derecho de Autor. Responsible for the last update of this issue, Informatics Unit ALCONPAT, Elizabeth Sabido Maldonado, Km. 6, antigua carretera a Progreso, Mérida, Yucatán, C.P. 97310.

The views of the authors do not necessarily reflect the position of the editor.

The total or partial reproduction of the contents and images of the publication is strictly prohibited without the previous authorization of ALCONPAT Internacional A.C.

Any dispute, including the replies of the authors, will be published in the first issue of 2021 provided that the information is received before the closing of the third issue of 2020.

Uso de materiales cementicios suplementarios (SCM) en sistemas de concreto armado - Beneficios y limitaciones

RESUMEN

Alrededor de una década de investigación realizada en IIT Madras sobre sistemas cementosos ha demostrado que el reemplazo parcial de cemento portland con materiales cementosos suplementarios (SCM) tiene beneficios y limitaciones. Los SCM no afectan negativamente la resistencia a la compresión a largo plazo y la contracción por secado de los hormigones, aunque puede haber algún compromiso en la trabajabilidad y la resistencia contra el agrietamiento por contracción plástica. A través de la evaluación de la tasa de ingreso de cloruro en el hormigón y el umbral de cloruro de acero, es evidente que el uso de SCM podría mejorar significativamente la vida útil bajo ataque de cloruro, aunque hay una reducción de la resistencia a la carbonatación. Más importante aún, los SCM pueden conducir a una reducción significativa de la huella de carbono del hormigón y, por lo tanto, son esenciales para lograr la sostenibilidad.

Palabras clave: materiales cementicios suplementarios, arcilla calcinada, caliza, propiedades mecánicas, microestructura, durabilidad.

Uso de materiais cimentícios suplementares (SCMs) em sistemas de concreto armado - Benefícios e limitações

RESUMO

Cerca de uma década de pesquisa realizada no IIT Madras em sistemas cimentícios mostrou que a substituição parcial do cimento Portland por materiais cimentícios suplementares (SCMs) traz benefícios e limitações. Os SCMs não afetam adversamente a resistência à compressão a longo prazo e o encolhimento por secagem dos concretos, embora possa haver algum comprometimento na trabalhabilidade e na resistência contra trincas por encolhimento do plástico. Através da avaliação da taxa de entrada de cloreto no concreto e no limiar de aço do cloreto, é evidente que o uso de SCMs poderia melhorar significativamente a vida útil sob ataque de cloreto, embora haja uma redução da resistência à carbonatação. Mais importante, os SCMs podem levar a uma redução significativa da pegada de carbono do concreto e, portanto, são essenciais para alcançar a sustentabilidade.

Palavras-chave: materiais cimentícios suplementares, argila calcificada calcária, propriedades mecánicas, microestrutura, durabilidade.

1. INTRODUCTION

Since the 1990s, many leading researchers started advocating the use of supplementary cementitious materials (SCMs), such as fly ash (PFA) and ground granulated blast-furnace slag (GGBS) due to their ability to partially substitute cement and even make it a more effective binder in concrete (Dhir and Jones, 1994; Malhotra and Ramezaniyanpour, 1994; Mehta, 1994, 2001). The benefits that were initially demonstrated in reinforced concrete structures included the (i) reduction of the carbon footprint by using the SCMs that are waste products, (ii) enhancement of the strength of the aggregate-paste interfaces and concrete; (iii) decrease in the permeability; (iv) increase in electrical resistivity; (v) lowering of the risk of alkali-silica reaction; (vi) reduction of the heat evolution during hydration; (vii) enhancement of the resistance to chlorides and sulphates; and (viii) reduction in the cost of concrete. Many research findings over the past couple of decades have also shown that the incorporation of SCMs, with a concurrent decrease in the ordinary

portland clinker content in concrete, is perhaps the most viable way towards sustainability, especially when a long corrosion-free service life is expected. This is mainly brought about by the enhanced durability, reduced carbon footprint and lower raw material demand – all without sacrificing strength (Chatterjee, 2018; Scrivener et al., 2018). Also, the use of SCMs can increase the ratio between the tensile or flexural strength and the compressive strength of concrete. Regarding corrosion resistance, the use of SCMs can tremendously increase the resistance to the ingress of chlorides and the enhancement of the electrical resistance of concrete can reduce the rate of corrosion of the embedded steel. Nevertheless, simple substitution, by weight, of cement with a SCM without any appropriate modification of the mix-design, and/or the processes of making and placing the concrete may lead to some limitations. These include (i) the higher potential for plastic shrinkage cracking (due to higher paste content, less bleeding and lower early strength gain), (ii) slower evolution of strength (due to slower hydration), (iii) leaching of heavy metals, (iv) undesired thixotropy, (v) lower surface hardness, (vi) lower chloride threshold, and (vii) faster carbonation (due to lower carbonatable material content). These issues have raised concerns about the problems that could occur if the material and structural designs are not done adequately. At present, more than 75% of cement available in India is made by blending ground clinker or intergrinding the ordinary portland clinker with PFA, GGBS, limestone, calcined clay or other SCMs. Moreover, the clinker content is expected to decrease further in the years to come – mainly due to the advantages associated with the long list of engineering properties, and those associated with the economics and climate change. Therefore, it is important that the benefits of using the SCMs are emphasized appropriately, along with the limitations and measures for their mitigation.

Researchers at IIT Madras have worked on several projects related to the behaviour and properties of cementitious systems with SCMs and have studied their workability, mechanical properties, dimensional stability, durability and corrosion resistance, among other aspects. These studies have enhanced the knowledge about the short- and long-term performance of concretes with blended binders, as well as the confidence to guide their applications in the Indian and other contexts. Major real-scale applications of SCMs that have stemmed from this experience include the construction, over the past 15 years or so, of various reinforced concrete buildings, on the IIT Madras campus, with a cumulative built-up area of about 126,000 m² with concrete containing fly ash, and fibre-reinforced concrete road stretches of more than 1 km length with high volumes of fly ash (see Figure 1a). Also, the recently completed complex of four 10-storey commercial buildings (in the IIT Madras Research Park Phase II) with about 80,000 m² of built-up area used GGBS in the normal and self-compacting fair-faced concrete façades (see Figure 1b). The remaining sections of this paper provide previews of findings from the relevant research projects conducted by the authors and their research group on various SCMs, such as fly ash, slag and limestone calcined clay.



(a)



(b)

Figure 1. FRC pavement on IIT Madras campus, and (b) the SCC building in the IIT Madras Research.

2. FRESH CONCRETE PROPERTIES

The presence of SCMs could increase the superplasticizer demand to achieve the required flow or workability. They could also affect the evolution of the various rheological characteristics as a function of time. Consequently, the flow responses of the blended binder system would differ significantly from that of an ordinary portland cement (OPC) system with the same water-binder ratio (w/b), depending mainly on the particle size distribution and particle shape of SCMs. A simple method such as Marsh Cone test has been used extensively to assess the variations in the behaviour of cement pastes with various superplasticizers and SCMs (Jayasree and Gettu, 2008, 2012; Jayasree et al., 2011; John and Gettu, 2014). Figure 2 shows the flow time (in log scale) versus the superplasticizer/binder dosage for pastes with (i) OPC, (ii) OPC with 30% replacement with fly ash (i.e., FA30), and (iii) limestone calcined clay cement (LC3) pastes; all with w/b = 0.40 and a PCE based superplasticizer (Nair, 2018). The flow times corresponding to the saturation dosage of superplasticizers (indicated by vertical lines in Figure 2b) for the pastes with FA30 and LC3 pastes are higher than that for OPC paste. These results show that the mortars and concretes made with fly ash and limestone calcined clay systems would exhibit differences in flow response and workability (Jayasree and Gettu, 2010; Nair 2018). However, such challenges can be mitigated with the appropriate corrections in the mixture proportioning – i.e., by adjusting the paste, superplasticizer, and water content.

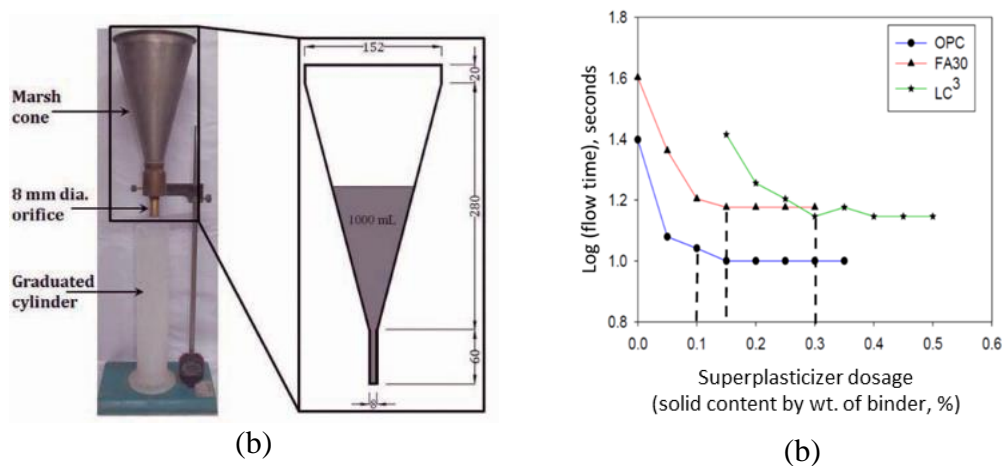


Figure 2. Marsh cone test setup and flow time curve (Nair, 2018; Mohan, 2019)

The increase in cohesiveness of the paste due to the higher fineness of the SCMs reduces the rise of bleed water. This is generally beneficial because bleeding produces defects within the concrete, typically at the interfaces between the coarse aggregates or steel reinforcing bars and the paste. However, the absence of bleed water leads to the evaporation of water from the concrete surface when it is subjected to drying, resulting in plastic shrinkage. Preventing plastic shrinkage cracking is a major challenge in many construction sites – although covering/curing of concrete is generally practiced. Sirajuddin and Gettu (2018) studied the susceptibility to cracking during the first few hours after placing the concrete using the restrained plastic shrinkage test (ASTM C1579, 2013) and found that the partial replacement of OPC with SCMs can increase the tendency for plastic shrinkage cracking in concrete, especially when replacement levels are high. This is attributed to the significant less replenishment of moisture at the surface subjected to drying leading to higher capillary stresses. If the gain in strength is slow during the early hours, the tensile stresses induced due to moisture loss could be higher than the tensile strength of the concrete – leading to cracking of concrete during the early hours. It was seen that 15% replacement with fly ash and slag increased the crack area by about 20 and 100%, respectively. At 30% replacement with fly ash and slag, the

crack area increased by about 40 percent and four-fold, respectively. Other results can be seen in Table 1, where OPC is the control concrete; FA15 and FA30 are concretes with 15 and 30% replacement with fly ash, respectively; and SG15 and SG30 are concretes with 15 and 30% replacements with slag (Sirajuddin and Gettu, 2018). This study strongly suggests that curing should be initiated earlier in mortars and concretes with SCMs and/or appropriate mitigation measures must be adopted, such as the incorporation of about 1 kg/m³ of short polypropylene fibres or shrinkage reducing admixtures in concrete.

Table 1. Data from tests for plastic shrinkage cracking potential

Mix ID	Crack initiation time (min)	Crack parameters				% increase in crack area	% increase in mean crack width
		Crack area (mm ²)	Crack length (mm)	Maximum crack width (mm)	Mean crack width (mm)		
OPC	207	97	263	0.68	0.37	-	-
FA15	180	121	303	0.93	0.40	24	7
FA30	167	138	333	1.03	0.42	42	12
SG15	197	225	427	1.25	0.53	132	42
SG30	183	402	444	1.73	0.91	313	144

3. COMPRESSIVE STRENGTH AND ELASTIC MODULUS

Compressive strength is probably the most important parameter influencing the structural performance of concrete systems. Hence, many researchers have investigated the effect of SCMs on the compressive strength of concrete. However, there are still negative perceptions and restrictions on the use of SCMs for major infrastructure projects, mainly because of the lack of awareness on the advantages of such materials and the possible variations in the quality and type of SCMs available from various sources. To address such issues, experimental data has been obtained for concretes that are typically used in the Indian construction sector to quantify the evolution of their strengths (Dhandapani et al., 2018; Sakthivel, 2019; Sakthivel et al., 2019). Though the early-age compressive strength of blended binder concretes could be lower than that of OPC concrete, Figure 3 shows that the eventual values can be much higher, especially for replacement levels of 15% of fly ash and slag (see Figure 3a & Figure 3b). Figure 3c shows that ternary blends with 60% OPC, 20% slag and 20% fly ash can exhibit higher compressive strengths at later ages than concretes without SCMs. This indicates a need for appropriately planning the schedule for curing and formwork removal while using concretes with SCMs. Figure 4 shows that the concretes with various SCMs exhibit adequate elastic modulus, as predicted by various standards and codes. Altogether, it can be concluded that the performance of SCM based concretes is good in terms of the mechanical properties.

4. EVOLUTION OF SHRINKAGE

Ongoing tests at IIT Madras on the shrinkage of concretes with blended binders indicate that the incorporation of SCMs does not alter the drying shrinkage strain evolution significantly (see 4-year

data in Figure 5). It can be concluded that replacement of OPC by $\leq 30\%$ of slag and fly ash, at the same w/b, will not change the ultimate strains due to drying shrinkage. This is of considerable relevance to design practices because most shrinkage models do not directly give provisions for the estimating shrinkage in concretes with SCMs. The findings also indicate that the shrinkage models calibrated for OPC concretes (i.e., without SCMs) can be used for concretes with SCMs, with some recalibration, if needed.

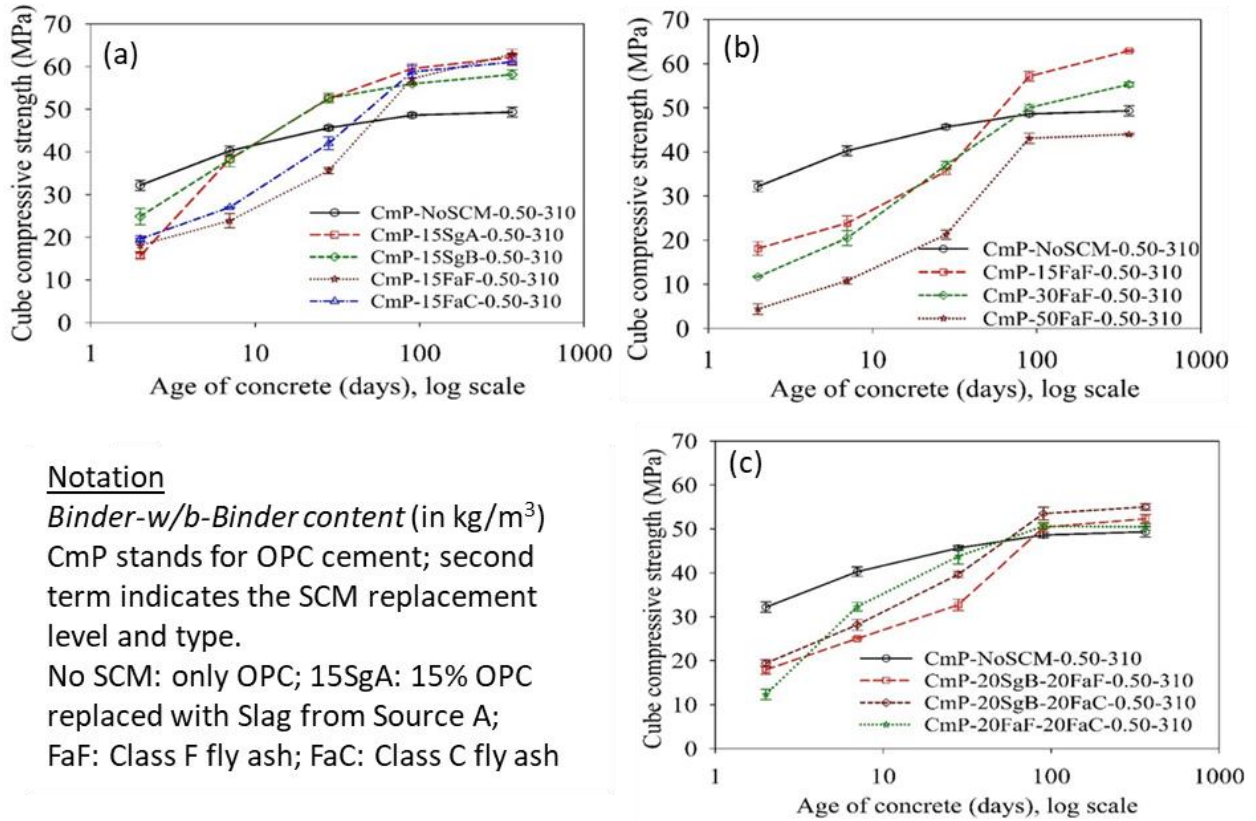


Figure 3. Compressive strength evolution in concretes with blended binders (Sakthivel et al., 2019)

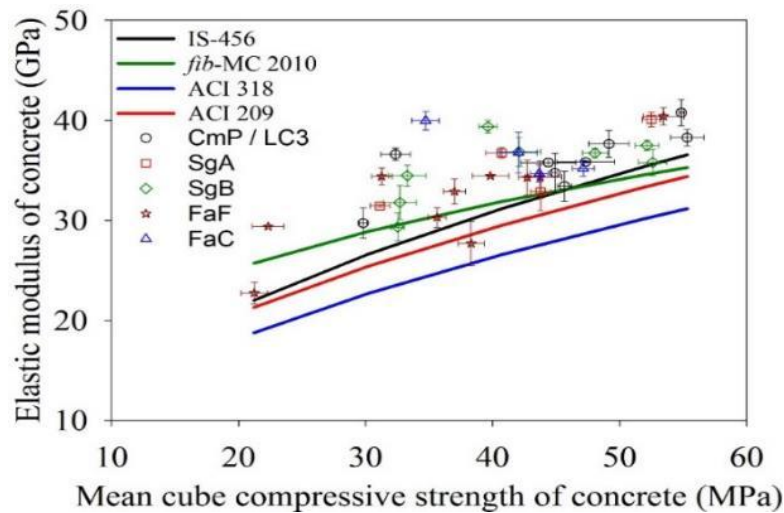


Figure 4. Elastic modulus of various concretes with SCMs

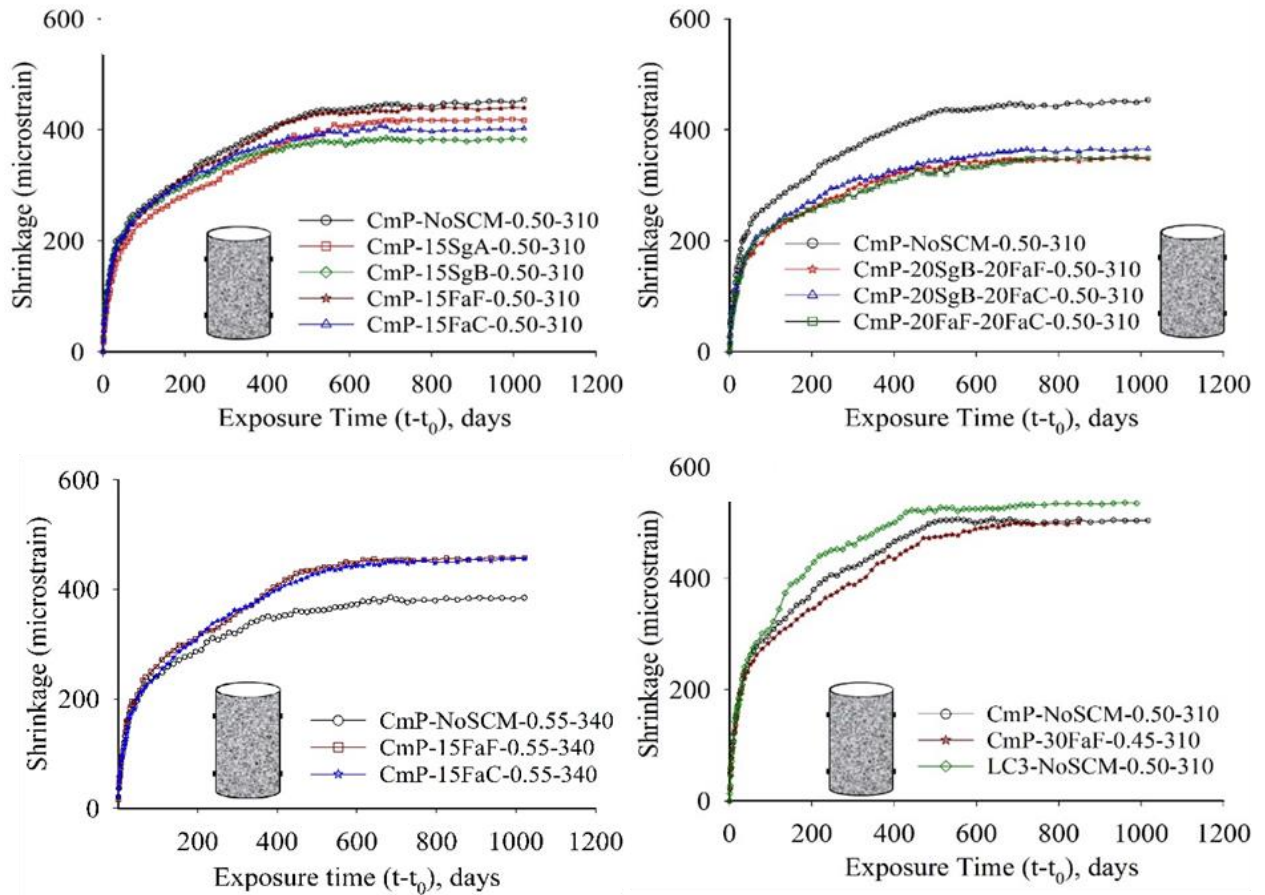


Figure 5. Drying shrinkage in concrete specimens with SCMs [Nomenclature: Cement Type - SCM replacement level and type - w/b - total binder content] (Sakthivel, 2019)

5. TOUGHNESS AND CRACK RESISTANCE

Concrete pavements are being used more extensively in many parts of the world, and this type of application is promising for the use of high volumes of fly ash in concrete. However, there could be problems (see Figure 6) of significant cracking due to the shrinkage and fatigue loading. Such problems cannot be resolved by just increasing the compressive strength of concrete and require targeted enhancement of the toughness, which is the key influencing parameter in providing adequate crack resistance. The incorporation of (steel, polymer, amorphous metal and glass) fibres for improving the toughness has been studied extensively at IIT Madras (see the image on the right in Figure 6), leading to guidelines for testing and design (Nayar and Gettu, 2015, 2016, 2020). Further work has also shown that steel fibres can dramatically prevent crack propagation in cracked concrete under a range of loading conditions (Jose et al., 2018; Stephen and Gettu, 2019a, 2019b).

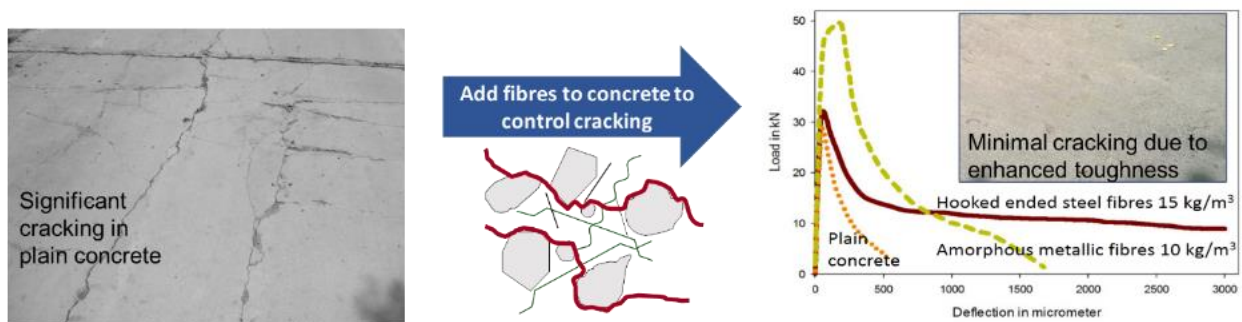
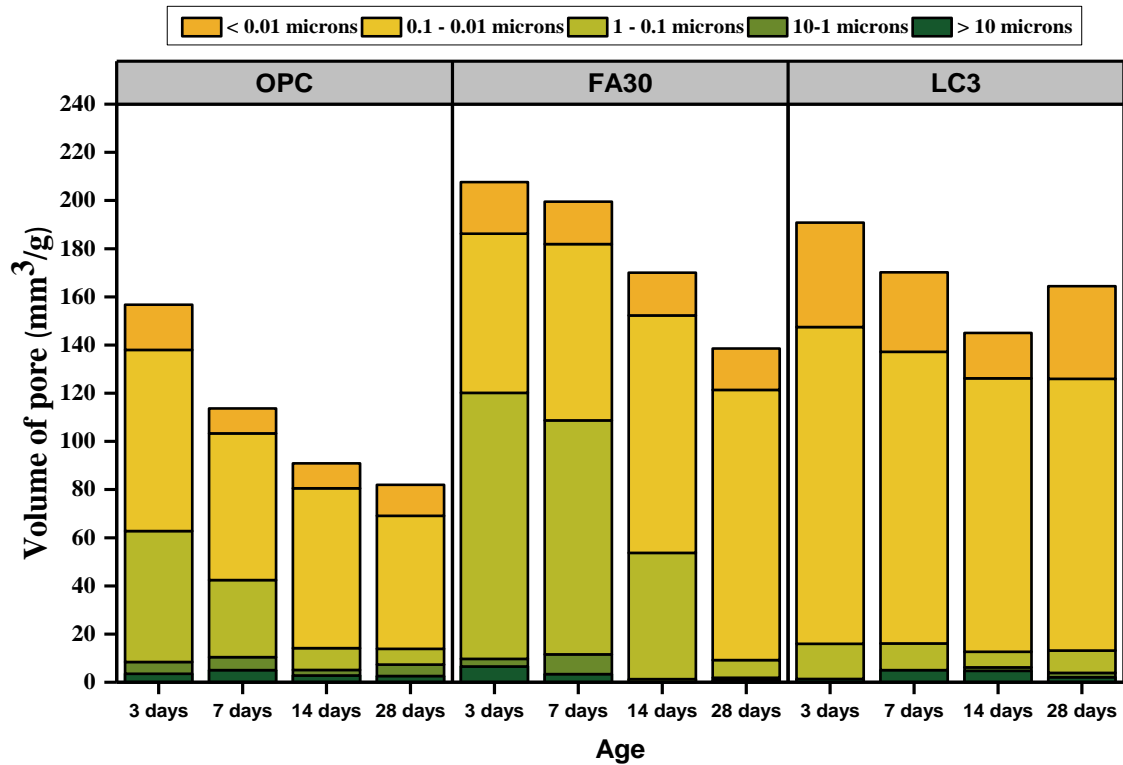


Figure 6. Role of hooked-end steel and amorphous metallic fibres in concrete with high volume fly ash to enhance toughness and reducing cracking.

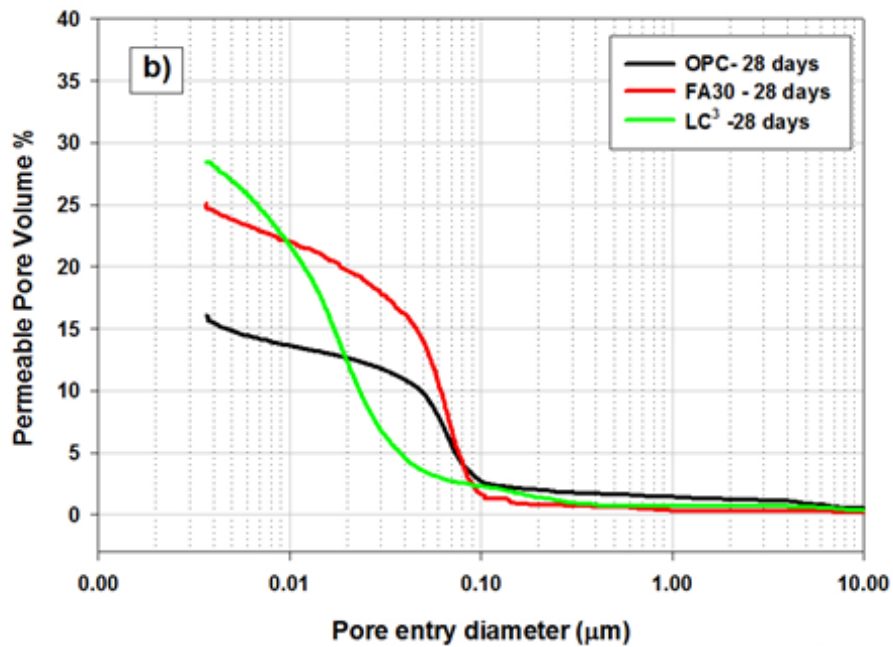
6. EVOLUTION OF MICROSTRUCTURE AND PERMEABILITY

Concretes with blended binder systems exhibit a more refined pore structure than OPC systems because of the additional/prolonged hydraulic and pozzolanic reactions. Dhandapani and Santhanam (2020) performed extensive studies on the evolution of microstructure in binders with various SCMs, especially LC3 systems. Figure 7(a) shows the evolution of pore sizes in hardened cement pastes with a w/b ratio of 0.35 and prepared with (i) OPC, (ii) OPC with fly ash (at 30% replacement dosage), and (iii) LC3. The results clearly indicate that slower reacting SCMs, like fly ash, result in a retardation of about 14 days to exhibit significant refinement of pores, whereas the faster reacting SCMs, like limestone-calcined clay, exhibit much finer pores even as early as 3 days. Figure 7(b) shows the pore size distributions in OPC, FA30 and LC3 systems at 28 days of curing. One important lesson is that the concretes with fly ash will require prolonged curing to exploit the full potential. More refinement of pores will improve the resistivity of the system, as seen in Figure 8 for concretes with SCMs, in particular LC3 systems. Consequently, the resistivity higher will lead to better chloride resistance and lower corrosion rates.

Due to the refined pore structure, concretes with SCMs also exhibit lower permeability (Dhanya and Santhanam, 2017). The charge passed in the rapid chloride penetration test is a good indicator of the permeability of concrete; Figure 9 indicates the significant resistance to charge transfer, especially when the replacement levels of slag and Class F fly ash are more than 30%. On the other hand, the performance of calcareous (Class C) fly ash is rated less than that of Class F fly ash and slag. Note that at 15% replacement level, both slag and Class C fly ash exhibit similar performance. Figure 10 shows data from water sorptivity tests, indicating that SCM based concretes show only marginally lower sorptivity than OPC concretes. The literature does not also provide any consensus on the water sorptivity and chloride penetration of concretes with SCMs. The authors believe that with appropriate mix-design, placement and curing practices, the positive aspects of SCMs can be exploited to enhance the durability of reinforced concrete systems.



(a) Pore volume distribution at different ages



(b) Pore size distribution at 28 days

Figure 7. Pore size distribution of different binder systems (Dhandapani and Santhanam, 2017)

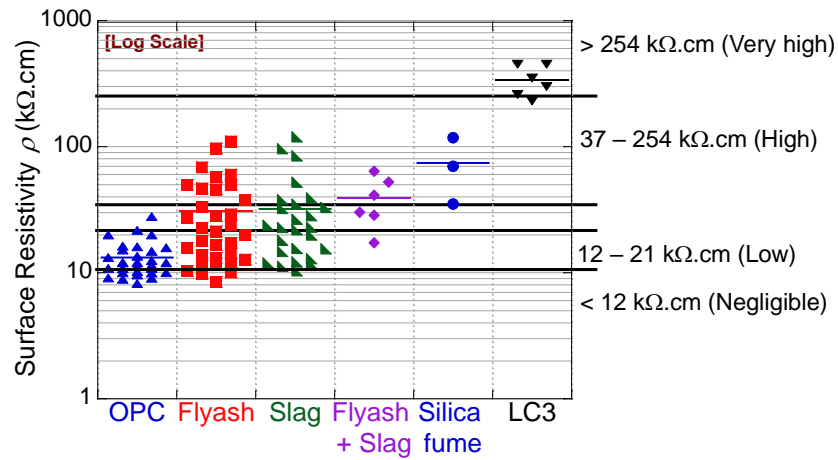


Figure 8. Wenner 4-probe surface resistivity of concretes with various SCMs

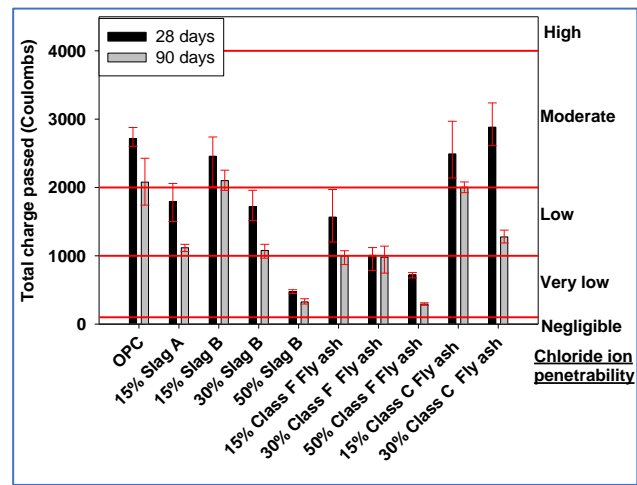


Figure 9. Results of rapid chloride penetration tests on concrete with different SCMs (binder content of 310 kg/m³, w/b of 0.5) (Dhanya, 2015)

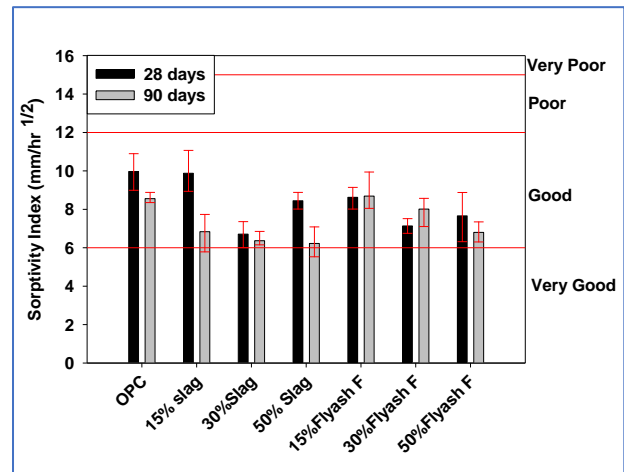
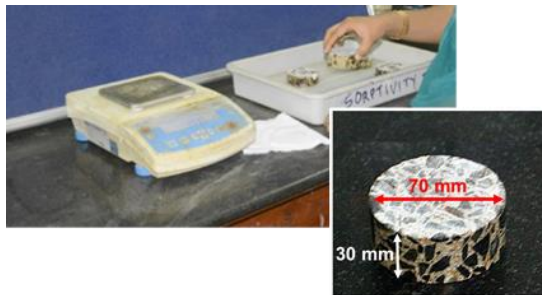


Figure 10. Results of water sorptivity tests on concretes with different SCMs (binder content of 380 kg/m³ and w/b of 0.4) (Dhanya, 2015)

7. CHLORIDE RESISTANCE, CHLORIDE THRESHOLD AND SERVICE LIFE

Many reports suggest that the resistance of concretes against chloride ingress can be greatly enhanced by using SCMs. The refined pore structure and enhanced chloride binding capacity are the major reasons for this. Figure 11a shows chloride profiles (ASTM C1556 tests) of concretes moist cured for 1 year; the curves for FA30 and LC3 systems exhibit steeper slopes than that for the OPC system – indicating lower chloride diffusion coefficients and better chloride binding capacity, which can be attributed to higher concentration of reactive alumina in the SCMs. Also, fly ash and LC3 systems exhibit about 75% in the chloride diffusion coefficients (see Figure 11b), with the LC3 systems possessing better chloride binding capability than those with fly ash. Pillai et al. (2018), and Dhandapani and Santhanam (2020) showed that the SCM type greatly influences the ageing factor or decay constant for the chloride diffusion coefficient. The appropriate choice of ageing factor is important to obtain more realistic service life estimates. See Table 2 for the recommended ranges of ageing factors for various binder systems; to be conservative, one may choose a lower value in the range given. For example, for systems with OPC, Class F fly ash, Class C fly ash, slag and LC3, it is recommended to use ageing factors of 0.1, 0.6, 0.4, 0.4 and 0.4, respectively, for the initial estimation of service life. The service life estimates can be refined by collecting field samples to obtain chloride profiles, and then determining the chloride diffusion coefficients and ageing factors at later ages.

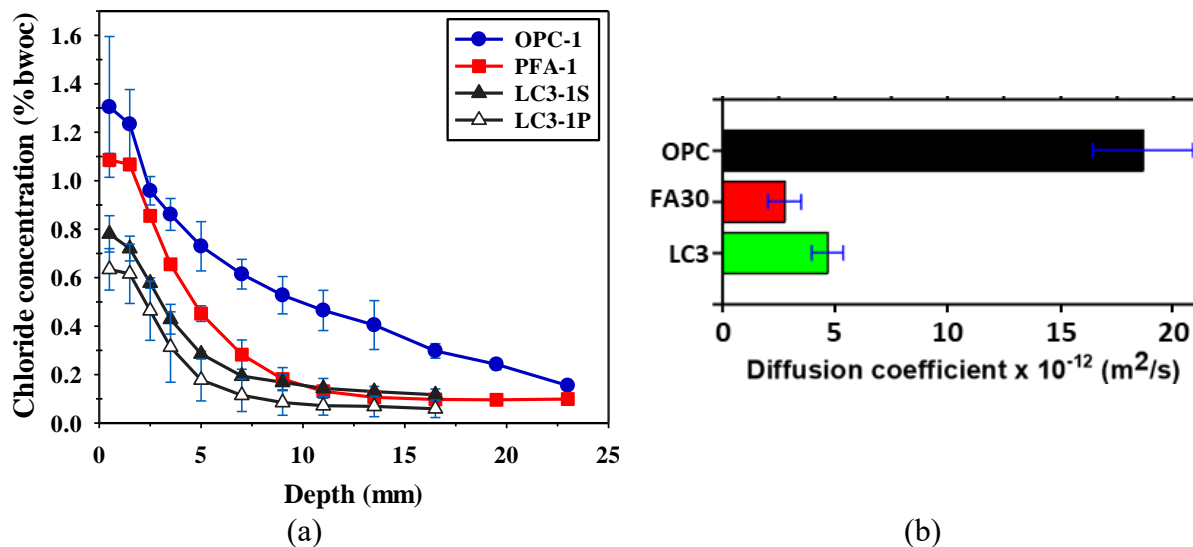


Figure 11. Chloride profiles and chloride diffusion coefficients of concretes with OPC, fly ash and LC3 (Dhandapani et al., 2018)

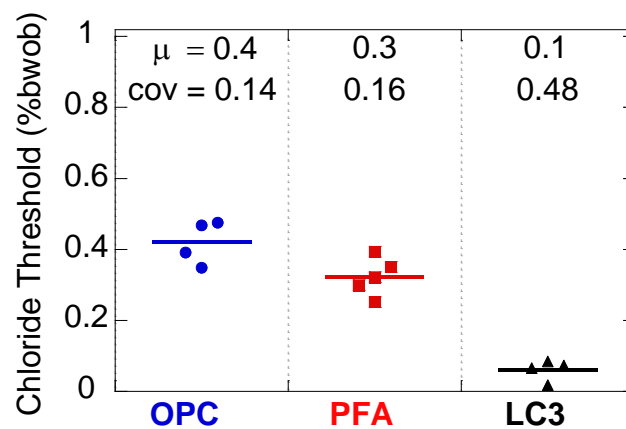
Table 2. Recommended ranges of ageing factors for different binders

Binder type	Recommended range of ageing factor
OPC	0.1-0.3
Class F fly ash	0.6-0.8
Class C fly ash	0.4-0.6
Slag	0.4-0.6
Calcined clay	0.4-0.5

Service life can be defined primarily as the time taken to initiate corrosion (say, the corrosion free service life) for assessing the influence of SCMs, though it has been shown that fly ash can be beneficial in the propagation phase even in cracked concretes (Sangoju et al., 2011, 2015). For obtaining such service life estimates, in addition to the chloride diffusion coefficient and its decay constant, quantitative estimates of chloride threshold are essential. The test procedures adopting macrocell corrosion measurements do not adequately detect the corrosion initiation in highly resistive concrete systems (such as those with LC3 and with SCMs and low w/b ratios). In such systems, corrosion initiates with macrocells or microcells forming on the same steel rebar, which is not detected in typical macrocell test methods like ASTM G109 (Rengaraju et al., 2018). Also, linear polarization resistance techniques have limitations in detecting corrosion in highly resistive concrete systems (Rengaraju et al., 2019). Hence, an accelerated chloride threshold test method (hr-ACT test method) was developed to accommodate chloride threshold tests in highly resistive (hr) concrete systems (Pillai et al. 2018, Rengaraju, 2019). This test uses a lollipop-type steel-mortar specimen, the linear polarization resistance and/or the electrochemical impedance spectroscopy technique, and a statistical procedure to detect corrosion initiation. Consequently, probabilistic estimates of chloride threshold of various steel-cementitious systems could be developed (see Table 3). As seen in Table 3 and in Figure 12, there is a noticeable reduction in the chloride threshold from OPC to fly ash (i.e., PFA) to LC3 systems (from about 0.4 to 0.1 % by weight of binder), which can be attributed to the lower pH in the PFA and LC3 systems.

Table 3. Chloride thresholds of various steel-cementitious systems (determined using hr-ACT test)

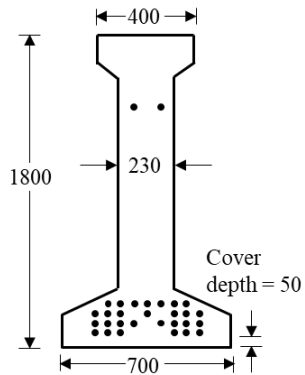
Water-binder ratio	Type of binder	Type of steel	Chloride threshold (%bwob)	
			Mean	Coefficient of variation
0.4	OPC	Uncoated TMT/QST steel	0.47	0.10
	OPC + fly ash		0.30	0.10
0.5	OPC	Uncoated TMT/QST steel	0.40	0.14
	OPC + fly ash		0.31	0.16
	OPC	Prestressing steel – Unstressed	0.40	0.17
	OPC + fly ash		0.23	0.15



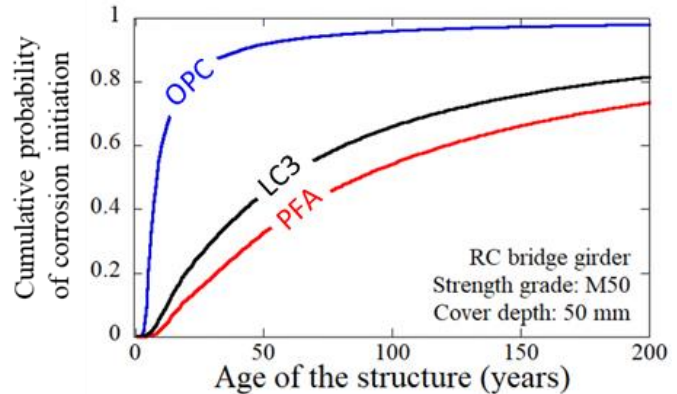
%bwob - percent by weight of binder

Figure 12. Chloride threshold of systems without and with SCMs (μ: mean, cov: coefficient of variation)

Nevertheless, one should note that achieving long service life is a consequence of the synergistic effect of many parameters (primarily the chloride diffusion coefficient, ageing factor and chloride threshold). In order to demonstrate the potential to enhance the service life of reinforcement concrete structures under chloride exposure through the incorporation of blended binders, a bridge girder (see Figure 13(a)) having a cover depth (d) of 50 mm, and exposed to a surface chloride concentration of 0.8% by weight of binder, is considered. The cumulative probabilities of corrosion initiation were obtained using the solution of Fick's 2nd Law of Diffusion, in a MATLAB® programme SL-Chlor, considering d , D_{cl} and Cl_{th} as random variables (Pillai et al. 2018; Rengaraju, 2019). Figure 13(b) shows that SCM based systems can generally yield much longer service lives than the OPC systems.



(a) Cross-section of the girder used
(All dimensions are in mm)



(b) Probabilistic estimate of corrosion-free service life

Figure 13. Case study demonstrating the synergistic effect of chloride diffusion coefficient, ageing coefficient and chloride threshold for various binder systems (Pillai et al. 2018)

8. CARBONATION RESISTANCE

The resistance to the penetration of CO_2 is generally good in OPC systems because of the high calcium hydroxide buffer. However, due to prolonged pozzolanic reactions, SCM-based concretes exhibit lower calcium hydroxide buffers and consequently, lower resistance to carbonation. Due to less availability of $Ca(OH)_2$ in SCM based systems, the CO_2 is able to carbonate the CSH at an earlier time – leading to rapid progression of the carbonation front. Dhanya (2015) showed, from accelerated carbonation studies under 1% CO_2 , that carbonation depths in concretes having more than 15% of the OPC replaced with Class F fly ash could be much higher than with only OPC as the binder (see Figure 14). On the other hand, the increase in carbonation for slag-substituted mixes was not significant. Natural carbonation results from recent studies have also shown greater penetration depths for SCM blended concretes. Therefore, corrosion initiation due to carbonation can be expected to occur earlier in concretes with SCMs, if exposed without any coating. However, the propagation of corrosion would still depend on the availability of moisture and oxygen, as well as on the conductivity (or conversely, resistivity) of the medium – these factors are expected to compensate and yield a situation favourable to the SCMs. Considering all these aspects it is possible to effectively design an SCM based concrete for situations where carbonation could govern the durability. Hence, it is cautioned not to refrain from using concretes with SCMs - rather engineers could adopt mitigation measures, such as anti-carbonation coatings, to compensate for the adverse effects due to potentially faster carbonation.



Fracture surface across specimens of 100 × 100 × 500 mm

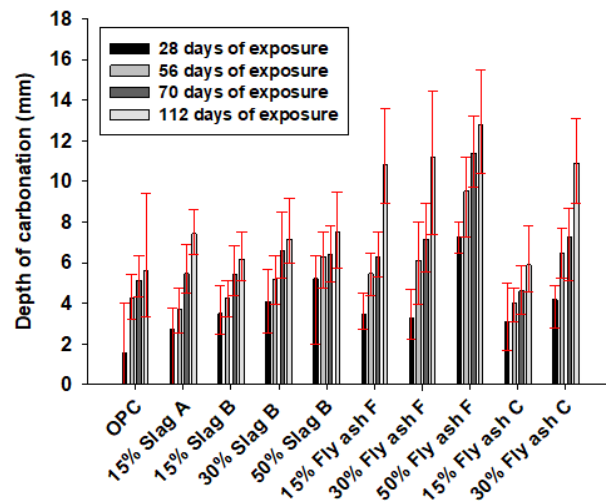


Figure 14. Accelerated carbonation depths in concretes with different SCMs (binder content of 310 kg/m³; w/b of 0.5)

9. CARBON FOOTPRINT

Partial substitution of OPC with SCMs can lead to significant reduction in the CO₂ emissions associated with the production of cement; and hence, the production of concrete. In order to quantify the positive aspects related to the carbon footprint and environmental impact of concretes with blended binders, extensive investigations have been undertaken at IIT Madras using life cycle assessment (LCA) performed with data from various cement plants in India (Gettu et al., 2016, 2018, 2019). Figure 15 shows the CO₂ emissions obtained for one of the case studies considering M50 concretes. These values are in the ranges reported in the literature; e.g., Flower and Sanjayan (2007) gave values of about 0.13 kg/kg for OPC concrete, and the embodied carbon values given by Hammond and Jones (2008) yield CO₂ emissions of 0.13-0.16 kg/kg. More importantly, the plots indicate that in concretes with only OPC, more than 75% of the CO₂ emissions are associated with the cement, while the majority of the remaining 25% of the CO₂ emissions is associated with the transportation and electricity. This is also in agreement with the observations of Flower and Sanjayan (2007) and Marceau et al. (2007). Upon replacement of OPC with SCMs or blended binders, significant reduction in emissions is observed. It is seen that the use of fly ash and GGBS decreases the CO₂ emissions by about 26% and 21% - similar to ranges reported by Flower and Sanjayan (2007). The LC3 concretes are very promising in terms of CO₂ emissions, with a 30-35% reduction compared to OPC concretes with similar compressive strengths. In general, the use of locally available SCMs at higher dosages leads to significant reduction in the carbon footprint of concrete industry.

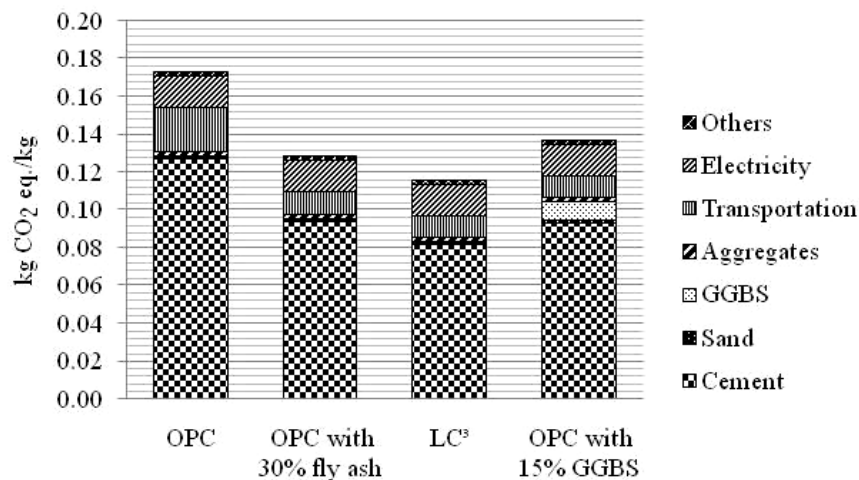


Figure 15. Carbon dioxide emissions for M50 concretes with different binders (Gettu et al., 2016)

10. CONCLUSIONS

For more than a decade, researchers at IIT Madras have been working on several aspects of SCMs and their performance in reinforced concrete systems. Various aspects related to fresh properties, hardened properties and durability (corrosion and transport) properties have been studied. Based on such studies with relevance to the Indian context, the following conclusions can be drawn:

- Workability of concretes can be influenced by the incorporation of SCMs and can be adjusted with the use of superplasticizers.
- There is a higher potential for plastic shrinkage cracking due to the use of SCMs, which can be mitigated by the addition of polypropylene fibres or prolonged moist curing. However, drying shrinkage of concretes with blended binders did not practically differ from that of OPC concrete.
- Concretes with SCMs were able to meet the compressive strength, elastic modulus, and shrinkage requirements as typically required for OPC concretes.
- Significant pore refinement occurs in concretes with SCMs, which in turn enhances its electrical resistivity and resistance to chlorides and reduces corrosion rates
- Curing is essential to exploit the full potential of concretes with SCMs in terms of both strength and durability
- Chloride threshold depends not only on the steel type but also on the cementitious binder used. It is seen that the use of SCMs can reduce the chloride threshold. However, the significant enhancement against the chloride ingress rate compensates for such reduction in chloride threshold and the synergistic effect results in longer service lives of fly ash, slag, and LC3 systems than OPC systems.
- Some of the SCMs have less resistance against carbonation, which can be addressed by adequate mixture proportioning, and mitigation measures such as anti-carbonation coatings.
- Considering the possibility of significant reduction in carbon footprint, it is evident that the use of SCMs is essential towards enhancing the durability and sustainability of concrete structures.

11. ACKNOWLEDGEMENTS

Many researchers have been cautioning against unrestricted use of SCMs in concrete construction and drawing attention to possible negative repercussions of using them. On the other hand, it is evident that the SCMs provide, debatably, the most viable option for sustainable concrete technology. This work is an acknowledgement of the arguments given by these researchers over the years, and an attempt to provide a balanced view, based on extensive experimental studies carried out over more than a decade.

The authors express deep gratitude to their research scholars, students and project staff for their dedication and hard work that has led to the many interesting and important results obtained, such as those summarised in this paper. They have made possible the many projects, which have been taken to successful completion. These works have been carried out mainly in the Construction Materials Research Laboratories of the Department of Civil Engineering, including the IIT Madras-Lafarge Laboratory for Durability and Long-term Performance of Concrete; the help of the staff of these facilities is gratefully acknowledged. Thanks are also due to the sponsors and funding agencies for their generous support in the various phases of our research work over the years.

This paper is a revised version of that corresponding to a keynote lecture at the 3rd RN Raikar Memorial International Conference on Advances in Science & Technology of Concrete, Mumbai, 2018, and appearing in its proceedings. The previous version was also adapted and translated to Spanish for the Revista Hormigón, (ISSN-0325-8947) in 2019.

12. REFERENCES

- Chatterjee, A. K. (2018). *Cement production technology: Principles and practice*. CRC Press, Boca Raton, USA, 419 p.
- Dhandapani, Y., Santhanam, M. (2017). *Assessment of pore structure evolution in the limestone calcined clay cementitious system and its implications for performance*. Cement and Concrete Composites, 84:36-47. <https://doi.org/10.1016/j.cemconcomp.2017.08.012>
- Dhandapani, Y., Sakthivel, T., Santhanam, M., Gettu, R., Pillai, R. G. (2018). *Mechanical properties and durability performance of concretes with limestone calcined clay cement (LC3)*. Cement and Concrete Research, 107:136-151. <https://doi.org/10.1016/j.cemconres.2018.02.005>
- Dhandapani, Y., Santhanam, M. (2020), *Investigation on the microstructure-related characteristics to elucidate performance of composite cement with limestone-calcined clay combination*, Cement and Concrete Research, 129, 22 p. <https://doi.org/10.1016/j.cemconres.2019.105959>
- Dhanya, B. S. (2015). *Study of the influence of supplementary cementitious materials on selected durability parameters of concrete*, Doctoral Thesis, IIT Madras, Chennai, India, 361 p.
- Dhanya, B. S., Santhanam, M. (2017). *Performance evaluation of rapid chloride permeability test in concretes with supplementary cementitious materials*, Materials and Structures, 50:67, 9 p. <https://doi.org/10.1617/s11527-016-0940-3>
- Dhir, R. K., Jones, M. R., Eds. (1994). *Euro-cements: Impact of ENV 197 on concrete construction*, Proc. National Seminar (Dundee, UK). E&FN Spon, London, 240 p.
- Flower, D. J. M., Sanjayan, J. G. (2007). *Green house gas emissions due to concrete manufacture*. The International Journal of Life Cycle Assessment, 12:282. <https://doi.org/10.1065/lca2007.05.327>
- Gettu, R., Patel, A., Rathi, V., Prakasan, S., Basavaraj, A. S., Maity, S. (2016). *Sustainability assessment of cements and concretes in the Indian context: Influence of supplementary cementitious materials*, Proc. Fourth Intl. Conf. on Sustainable Construction Materials and Technologies (Las Vegas, USA), Eds. N. Ghafoori, P. Claisse, E. Ganjian and T.R. Naik, paper

S299, 142-1150.

- Gettu, R., Pillai, R. G., Santhanam, M., Basavaraj, A. S., Rathnarajan, S., Dhanya, B. S. (2018). *Sustainability-based decision support framework for choosing concrete mixture proportions*. Materials and Structures, 52 (122), 17 p. <https://doi.org/10.1617/s11527-019-1425-y>
- Gettu, R., Patel, A., Rathi, V., Prakasan, S., Basavaraj, A. S., Palaniappan, S., Maity, S. (2019). *Influence of supplementary cementitious materials on the sustainability parameters of cements and concretes in the Indian context*, Materials and Structures, 52:10, 11 p. <https://doi.org/10.1617/s11527-019-1321-5>.
- Hammond, G. P., Jones, C. I. (2008). *Embodied energy and carbon in construction materials*. Proceedings of the Institution of Civil Engineers, Energy 161(2): 87-98. <https://doi.org/10.1680/ener.2008.161.2.87>
- Jayasree, C., Gettu, R. (2008). *Experimental study of the flow behaviour of superplasticized cement paste*. Materials and Structures, 41:1581-1593. <https://doi.org/10.1617/s11527-008-9350-5>
- Jayasree, C., Gettu, R., (2010). *Correlating properties of superplasticized paste, mortar and concrete*. Indian Concrete Journal, 84(7):7-18.
- Jayasree, C., Gettu, R. (2012). "Choice of compatible cement-superplasticizer combinations", ICI J. (Indian Concrete Institute), 12(4): 14-31.
- Jayasree, C., Murali Krishnan, J., Gettu, R. (2011). *Influence of superplasticizer on the non-newtonian characteristics of cement paste*, Materials and Structures, 44(5): 929-943. <https://doi.org/10.1617/s11527-010-9677-6>
- John, E., Gettu, R. (2014). *Effect of temperature on flow properties of superplasticized cement paste*, ACI Materials Journal, 111(1): 67-76.
- Jose, S., Gettu, R., Indhuja, S. (2018). *Flexural toughness characterization of steel, polymer and glass fibre reinforced concrete based on the notched beam test*, The Indian Concr. J., 92(2): 35-50.
- Malhotra, V. M., Ramezani pour, A. A., (1994). *Fly ash in concrete*, 2nd ed., Canada Centre for Mineral and Energy Technology, Ottawa, 307 p.
- Marceau, M., Nisbet, M. A., Van Geem, M. G. (2007). *Life cycle inventory of portland cement concrete*, Portland Cement Association, Skokie, Illinois, USA, 121 p.
- Mehta, P. K., Ed., (1999). *Concrete technology for sustainable development in the twenty-first century*, Proc. Intl. Symp. (Hyderabad). Cement Manufacturers' Association, New Delhi, 538 p.
- Mehta, P. K. (2001). *Reducing the environmental impact of concrete*, Concrete International., 23(10):61-66.
- Mohan, M. K. (2019). *Flowable, bleed resistant cementitious grouts and performance specifications for applications in post-tensioned concrete systems*, MS Thesis, Department of Civil Engineering, IIT Madras, Chennai, 149 p.
- Nair, V. G. N. (2018). *Experimental study of the flow behaviour of superplasticized pastes and concretes with limestone calcined clay cement (LC3)*. MS Thesis, Department of Civil Engineering, IIT Madras, Chennai, 119 p.
- Nayar, S. K., Gettu, R. (2015). *Synergy in Toughness by Incorporating Amorphous Metal and Steel Fibers*, ACI Mater. J., 112(6): 821-827. <https://doi.org/10.14359/51687857>
- Nayar, S. K., Gettu, R. (2016). *Benefits of using amorphous metallic fibres in concrete slabs-on-grade*, RILEM Technical Letters, 122-128. <https://doi.org/10.21809/rilemtechlett.2016.20>
- Nayar, S. K., Gettu, R. (2020). *Mechanistic–empirical design of fibre reinforced concrete (FRC) pavements using inelastic analysis*, Sādhanā, 45:19, 7 p. <https://doi.org/10.1007/s12046-019-1255-1>
- Pillai, R. G., Gettu, R., Santhanam, M., Rengaraju, S., Dhandapani, Y., Rathnarajan, S., Basavaraj, A. S. (2018). *Service life and life cycle assessment of reinforced concrete systems with limestone calcined clay cement (LC3)*. Cement and Concrete Research, 118: 111-119. <https://doi.org/10.1016/j.cemconres.2018.11.019>

- Rengaraju, S., Godara, A., Alapati, P., Pillai, R. G. (2018), *Macrocell corrosion mechanisms of prestressing strands in various concretes*, Mag. Concr. Res. (ICE, UK), 72(4): 194-206. <https://doi.org/10.1680/jmacr.18.00284>
- Rengaraju, S. (2019), *Electrochemical response and chloride threshold of steel in highly resistive concrete systems*, Ph.D. Thesis, Department of Civil Engineering, IIT Madras, Chennai, 252 p.
- Rengaraju, S., Neelakantan, L., Pillai, R. G. (2019), *Investigation on the polarization resistance of steel embedded in highly resistive cementitious systems—An attempt and challenges*, Electrochimica Acta, 308: 131-141. <https://doi.org/10.1016/j.electacta.2019.03.200>
- Sakthivel, T. (2019). *Effect of the incorporation of slag, fly ash, and limestone calcined clay on the compressive strength, elastic modulus and shrinkage of concrete*, Ph.D. Thesis, Department of Civil Engineering, IIT Madras, Chennai, 194 p.
- Sakthivel, T., Gettu, R., Pillai, R. G. (2019). *Compressive strength and elastic modulus of concretes with fly ash and slag*. J. Institution of Engineers (India): Series A, 10 p. <https://doi.org/10.1007/s40030-019-00376-w>
- Sangoju, B., Gettu, R., Bharatkumar, B. H., Neelamegam, M. (2011). *Chloride-induced corrosion of steel in cracked OPC and PPC concretes: Experimental study*, Journal of Materials in Civil Engineering, 23(7): 1057-66. [https://doi.org/10.1061/\(ASCE\)MT.1943-5533.0000260](https://doi.org/10.1061/(ASCE)MT.1943-5533.0000260)
- Sangoju, B., Pillai, R. G., Gettu, R., Bharatkumar, B. H., Iyer, N. R. (2015). *Use of portland pozzolana cement to enhance the service life of reinforced concrete exposed to chloride attack*, Journal of Materials in Civil Engineering, 27(11): 04015031, 8 p. [https://doi.org/10.1061/\(ASCE\)MT.1943-5533.0001293](https://doi.org/10.1061/(ASCE)MT.1943-5533.0001293)
- Scrivener, K., John, V. M., Gartner, E. M. (2017). *Eco-efficient cements: Potential economically viable solutions for a low-CO₂ cement-based materials industry*. United Nations Environment Programme, Paris, 50 p.
- Sirajuddin, M., Gettu, R. (2018). *Plastic shrinkage cracking of concrete incorporating mineral admixtures and its mitigation*. Materials and Structures, 51(48), 10 p. <https://doi.org/10.1617/s11527-018-1173-4>
- Stephen, S. J., Gettu, R. (2019a). *Rate-dependence of the tensile behaviour of fibre reinforced concrete in the quasi-static regime*, Materials and Structures, 52:107, 9 p., with Supplementary Material published online, 6 p. <https://doi.org/10.1617/s11527-019-1405-2>
- Stephen, S. J., Gettu, R. (2019b). *Fatigue response of cracked fibre reinforced concrete*, Proc. Intl. Conf. on Innovative Materials for Sustainable Civil Engineering, RILEM Week (Nanjing, China), p. 6.

Rebar corrosion modelling and deterioration limit state

C. Andrade^{1*} 

*Contact author: candrade@cimne.upc.edu

DOI: <https://doi.org/10.21041/ra.v10i2.478>

Reception: 08/12/2019 | Acceptance: 09/04/2020 | Publication: 30/04/2020

ABSTRACT

In present work the limitations of the models of corrosion initiation with indications to overcome them, are presented. Performance based design of durability is at present a trend considered in fib Model Code (MC2010). However, we are still far from accurately predicting the performance of a structure in a specific environment, in spite of which performance-based requirements are introduced in the concrete specifications of large infrastructures demanding 100 years or more of service life. Also are commented the depassivation step and the propagation period with considerations on their probabilistic treatment. It is proposed to consider corrosion onset as a “deterioration or initiation Limit State” (DLS or ILS). An example of calculation the time to cover-cracking induced corrosion is included.

Keywords: concrete; chlorides; carbonation; corrosion; reliability.

Cite as: Andrade, C. (2020), “*Rebar corrosion modelling and deterioration limit state*”, Revista ALCONPAT, 10(2), pp. 165 – 179, DOI: <https://doi.org/10.21041/ra.v10i2.478>.

¹ International Centre for Numerical Methods in Engineering (CIMNE), Spain.

Legal Information

Revista ALCONPAT is a quarterly publication by the Asociación Latinoamericana de Control de Calidad, Patología y Recuperación de la Construcción, Internacional, A.C., Km. 6 antigua carretera a Progreso, Mérida, Yucatán, 97310, Tel.5219997385893, alconpat.int@gmail.com, Website: www.alconpat.org

Responsible editor: Pedro Castro Borges, Ph.D. Reservation of rights for exclusive use No.04-2013-011717330300-203, and ISSN 2007-6835, both granted by the Instituto Nacional de Derecho de Autor. Responsible for the last update of this issue, Informatics Unit ALCONPAT, Elizabeth Sabido Maldonado, Km. 6, antigua carretera a Progreso, Mérida, Yucatán, C.P. 97310.

The views of the authors do not necessarily reflect the position of the editor.

The total or partial reproduction of the contents and images of the publication is strictly prohibited without the previous authorization of ALCONPAT Internacional A.C.

Any dispute, including the replies of the authors, will be published in the first issue of 2021 provided that the information is received before the closing of the third issue of 2020.

Modelado de la corrosión de la armadura y estado límite de deterioro

RESUMEN

En el presente trabajo se analizan las limitaciones de los modelos de iniciación de la corrosión con indicaciones prácticas para superarlas. Es una tendencia mundial el desarrollo de normativa basada en prestaciones como se plasmó en el Código Modelo MC2010 del FIB. Sin embargo, los modelos de predicción todavía adolecen de mucha incertidumbre cuando se aplican a una estructura específica, a pesar de lo cual es creciente el número de especificaciones en grandes infraestructuras que exigen 100 años o más de vida útil. También se comentan la etapa de despasivación y el período de propagación con consideraciones sobre su tratamiento probabilístico. Se propone considerar el inicio de la corrosión como un "estado límite de deterioro o iniciación" (DLS o ILS) con un ejemplo de cálculo.

Palabras clave: hormigón; cloruros; carbonatación; corrosión; fiabilidad.

Modelagem da corrosão da armadura e estado limite de deterioração

RESUMO

O presente trabalho analisa as limitações dos modelos de iniciação à corrosão com indicações práticas para superá-los. É uma tendência global desenvolver regulamentos baseados em desempenho, conforme incorporados no Código do modelo FIB MC2010. No entanto, os modelos de previsão ainda sofrem grande incerteza quando aplicados a uma estrutura específica, apesar do aumento do número de especificações em grandes infraestruturas que requerem 100 anos ou mais de vida útil. O estágio de despassivação e o período de propagação também são discutidos com considerações sobre seu tratamento probabilístico. Propõe-se considerar o início da corrosão como um "estado limite de deterioração ou iniciação" (DLS ou ILS) com um exemplo de cálculo.

Palavras-chave: concreto; cloretos; carbonatação; corrosão; confiabilidade.

1. INTRODUCTION

Prediction of service life related to reinforcement corrosion is at present a developing matter because mathematical models have been published (Tuutti, 1982; Bakker, 1994; CONTECVET Manual, 2001; DURACRETE, 1998; MC 2010, 2012) and it is increasing the demand of predefined service life beyond 100 years in the critical infrastructures. The models are usually based in assuming that the carbonation front or the chloride threshold penetrates by diffusion therefore, Fick's second law in non-steady-state conditions, is applied. However, it has to be emphasized that there is not a model that could have been applied to concrete structures older than 30 years and that the cements and the concretes fabricated around one century ago, are different than present ones. This lack of long term verification is important to be remembered by the designers and prescriptors, because frequently it is found in the international contracts requests of 120 or 150 years of service life, which have to be considered more as a guess than a fact. There is not a manner, at present, to distinguish by testing a concrete lasting 100 years without corrosion of another having 120 years of service life. In spite of this limitation it is certainly important to study further the tests and the models related to durability in order, precisely, of improving present understanding and fill the gaps in knowledge.

The uncertainty in the prediction has led to the application of risk analysis and probabilistic concepts and thus, in Model Code 2010 (MC 2010, 2012) it is defined the several limit state functions (LSF) related to carbonation, chloride ingress, frost attack, and leaching. The consideration of the uncertainties aims into the need to identify which kind of limit state should be

applied to processes related to concrete durability and which probability of corrosion or deterioration would be adequate.

In present work some of the aspects related to the limitations of the rebar corrosion models and its probabilistic aspects will be commented attending to the typical sequence of: initiation period, depassivation limit and corrosion propagation, to end with some considerations on the limit state associated to corrosion.

1.1 Initiation period

Carbonation and chloride ingress are identified as the two main causes of rebar corrosion (Bazant, 1979; Tuutti, 1982; CONTECVET Manual, 2001; DURACRETE, 1998; MC 2010, 2012). Carbonation is a process in which its rate is almost constant along the life, and then the typical square root law can be applied (see equation [1]) where V_{CO_2} is the rate of carbonation under reference conditions and x_c is the carbonation depth.

$$x_c(t) = k_{CO_2} \cdot \sqrt{t} \quad [1]$$

This V_{CO_2} depends on the chosen concrete mix (w/c-ratio, cement type and mineral additions) and on the influence of the execution or of the environmental conditions (mean relative humidity and CO₂-concentration). In general, the carbonation progresses faster when the RH of the exterior of concrete is between 45 and 65%. The carbonation depth decreases with higher RH (Bakker, 1994) (figure 1). The introduction of this effect into equation [1] is made by the available models in several manners. They are:

- By using a root different (for instance cubic root) than the square. The result is in general an attenuation of the carbonation depth

$$x_c(t) = k_{CO_2} \cdot \sqrt[3]{t} \quad [1']$$

- By multiplying by a « climatic factor » (W_{Rain}) (Bakker, 1994; Galan et al. 2010) usually smaller than the unity, for instance by taking into account « the wetness period » per year (days of rain per year with respect to 365).

$$x_c(t) = k_{CO_2} \cdot W_{Rain} \cdot \sqrt{t} \quad [1'']$$

In figure 1 it is given results of the comparison of rates of carbonation (Galan et al. 2010) of tests of specimens in Madrid's climate during 4 years of two kind of concretes (with w/c ratios of 0.45 and 0.6 and in accordance, 400 and 300 Kg of cement by m³ of concrete) exposed outdoor sheltered and exposed to rain. The resulting equation in these tests is given next. This relation may be different in other climates.

$$V_{CO_2}(sheltered) = 1.4 V_{CO_2}(non\ sheltered) + 1.6 \quad [1a]$$

Comparison of exposure classes and concretes

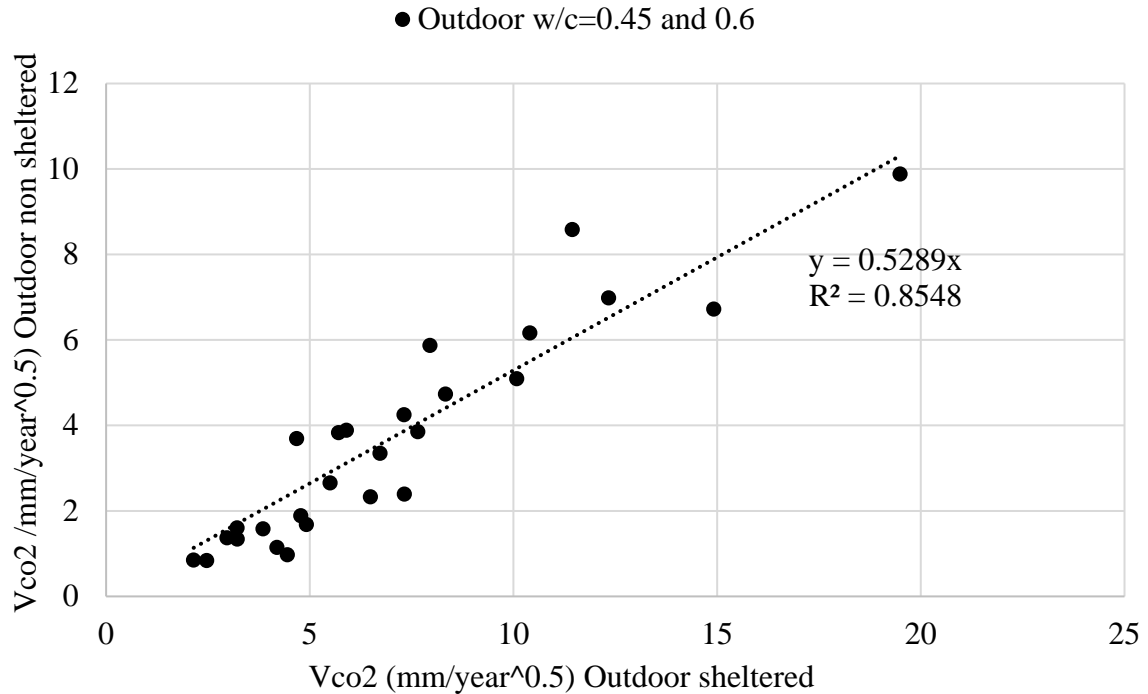


Figure 1. Relation between the velocity of carbonation in non-sheltered from rain and protected from rain conditions in the climate of Madrid.

This equation leads to apply an exponent of 0.31 instead of 0.5 in [1'] and as indicated in the figure 1, means that the rate of carbonation exposed to rain is approximately the half of that when the same concrete is sheltered from rain (Madrid climate).

In the case of *chloride penetration*, the calculation is made through the expression named “equation of the error function” (equation [2]) where $C(x, t)$ is the critical chloride concentration leading to depassivation inside the concrete at a distance x for a time t , C_s is the surface or external chloride concentration, and D_{ap} is the Apparent Diffusion Coefficient:

$$C(x, t) = C_s \left(1 - \operatorname{erf} \frac{x}{2\sqrt{D_{ap}t}}\right) \quad [2]$$

With respect to the chloride ingress three main limitations have been identified in the application of equation [2] (Andrade, 2014):

1. The decrease of the Apparent Diffusion coefficient with time (Mangat and Molloy, 1994),
2. The variation of the surface concentration with time due the variability of external climate and the carbonation (Andrade, 1997),
3. The development of a maximum in the chloride profile instead of having that maximum in the concrete surface (Andrade et al, 2015).

The decrease with time of the chloride diffusion coefficient is empirically addressed (Mangat and Molloy, 1994) by considering that D_{ap} decreases with time (figure 2) following equation [3] where n = “aging factor”, D_0 = the diffusion coefficient at the initial testing time t_0 (usually 28 days) and t_i is the period until when the coefficient is assumed to decrease:

$$D_{ap}(t) = D_0 \cdot \left(\frac{t_i}{t_0}\right)^{-n} \quad [3]$$

This equation indicates that the initial value of the D_{ap} is changed for a smaller one for the calculations in equation [2]. Although generally accepted, it is not indicated how or when to test the decrease and the period of time of its application. In consequence, if the period of application is long time, it leads into a too low diffusion coefficient as shown in figure 2, where it can be deduced that depending on the aging factor (n) considered, the decrease may be of one or two orders of magnitude. Then, due to the uncertainties on the extrapolation from a short term test to long term, the decrease has to be limited. One possible “good practice” is to limit, depending on the type of cement, the decrease to 1 year (Portland cement), 5 years (cement with mineral addition other than slags or limestone) or 10 years (cements with slag as mineral addition) or to a decrease of to limit to a maximum of one order of magnitude. Finally, a modification to this equation has been proposed by Gulikers (Tang and Gulikers, 2007) (see equation [4])

$$D_{ap} = \frac{D_0}{1-n} \cdot \left(\frac{t_0}{t_1}\right)^n \quad [4]$$

By calculating D_{ap} through this expression, the same result is obtained by means of finite elements methods or by the analytical direct calculation of equation [2].

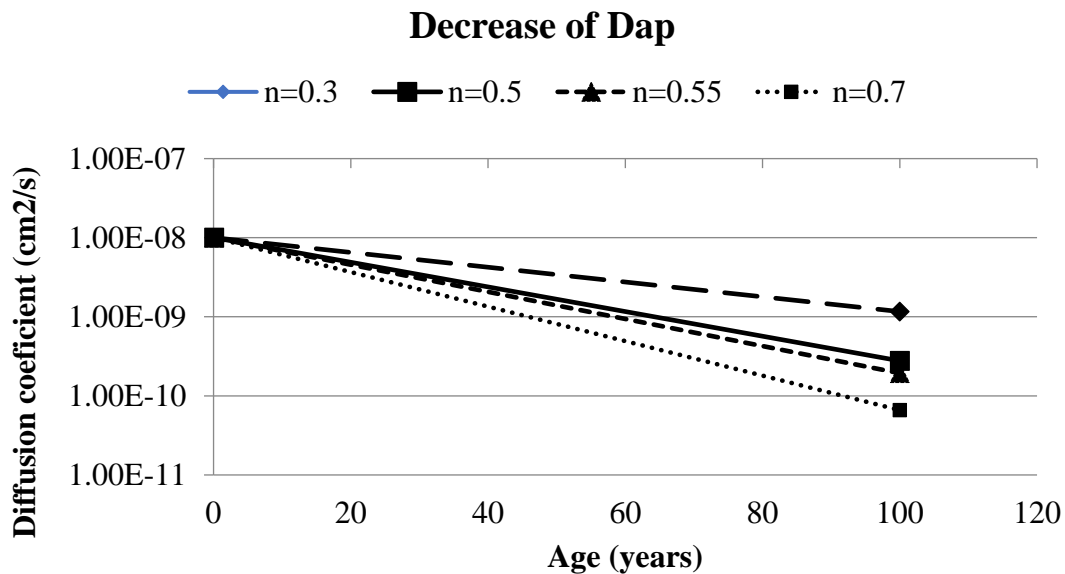


Figure 2. Decrease of Apparent Diffusion coefficient with time in function of aging factors ranging from 0.3 to 0.7.

To overcome the problem of a variable surface concentration it is viable to use the surface concentration obtained in a natural diffusion test lasting 90 days. This time is long enough to allow bidding to reach equilibrium with the external chloride concentration.

The other main limitation is related to the building up of a “pic” or maximum in the chloride concentration of a profile (figure 3-left) (Andrade, 2015). This maximum has been attributed to “convection” by capillary absorption, although it seems more likely that it is due to the carbonation of the surface, but these reasons are not sufficient to explain how it is possible that the surface concentration could be lower than the external one, because the chloride concentration is almost nil at the concrete surface in figure 3. It has to be also remarked, that, in order to calculate the

Apparent diffusion coefficient, D_{ap} , equation [2] can be fitted into this profile shape with the maximum, providing the “zero” depth (figure 3-right) is considered that of the maximum position (Andrade, 2015) because the profile from the maximum evolves following Fick’s law. That is, the fitting of equation [2] should not be made by extrapolating the maximum back to the surface, because the surface concentration would be much higher than the real one. The value of x_0 in the figure (distance from surface to the maximum position) should be added to the result of calculation of the depth of the chloride threshold (Andrade, 2015) from equation [2]. What is unknown is how the chlorides deplete at the surface and how the maximum moves inwards, that is, the law of its evolution with time to long term.

$$\text{Chloride threshold depth} = x_0 + x(\text{calculated from } x_0) \quad [5]$$

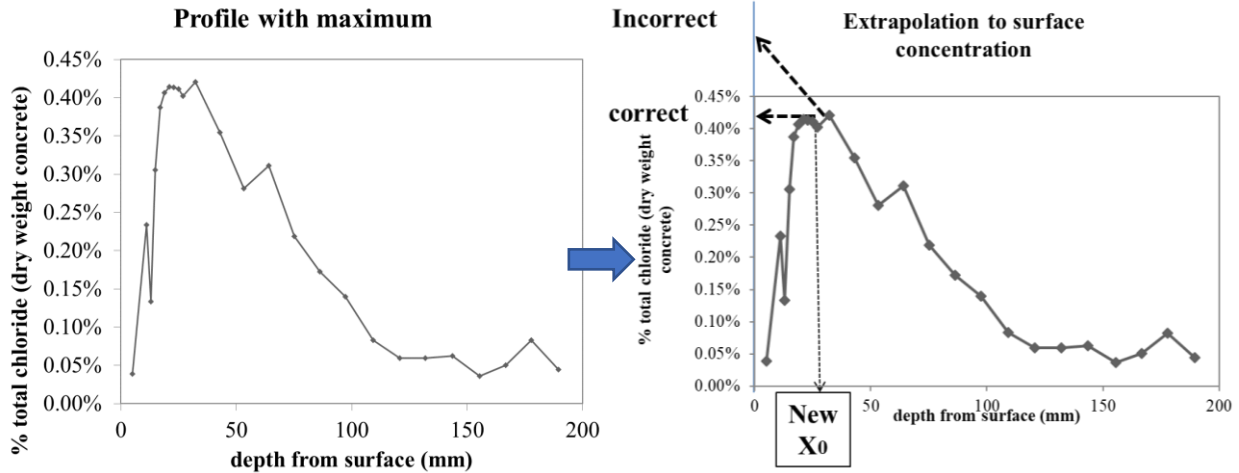


Figure 3. Left: Typical maximum in chloride concentration in the interior of the concrete and not at its surface. Right: extrapolation to obtain the chloride surface concentration to be used in the calculations

1.2 Depassivation step

It is assumed that depassivation means starting of corrosion, but it is not easy to identify the onset of corrosion in the real structures because the initial depassivated zone can be so small (figure 4) that it is not noticed. No external sign can be detected until concrete cover cracks or corrosion spots appear on the surface. No changes in the serviceability of the concrete are detected at depassivation onset. Then, unless electrochemical monitoring of the corrosion parameters is made, there is not the possibility to detect corrosion initiation. Even performing an electrochemical monitoring, the identification of depassivation in real conditions is not an easy task due to the changes in temperature and moisture. This difficulty of how to detect and measure the depassivation onset will not be addressed in present work; however some considerations on the consequences of this fact will be mentioned next.



Figure 4. Small spots of corrosion due to chloride attack

Two main aspects will be analysed on the depassivation process: its duration and the variability of the chloride threshold. The duration because depassivation is not an instantaneous process, but it lasts a period of time due to the intrinsic heterogeneity of the concrete which make the threshold front to be irregular.

For *carbonation* the corrosion threshold is reached when the pH value drops below 8-9, which precisely coincide with the phenolphthalein colour-change from purple to colourless. Due to the presence of aggregates this carbonation front is not fully steep (Thiery, 2007) but additionally is irregular and then the surface of the bar will be depassivated irregularly (figure 5), what is maintained until the front advances deeper. The variability of the front can be characterized by an averaged value and a standard deviation (for instance resulting in between the 15% and the 25% of the coefficient of variation).

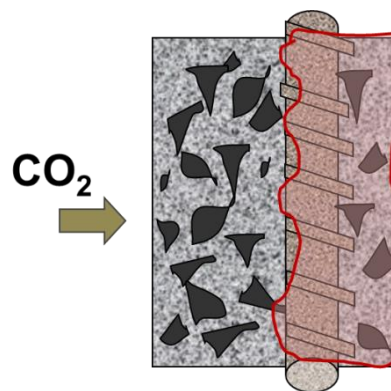


Figure 5. Irregularities that may appear in the carbonation front which lead into a localized depassivated rebar surface.

With respect to the *chloride process*, the corrosion starts when certain critical chloride concentration enters in contact to the steel surface. The normal value considered in numerous standards is of 0.4% by weight of cement, although values as higher as 2-3% may not developed corrosion in some circumstances. Then, the threshold is not a fixed quantity, but is a range of values (Izquierdo et al. 2004; Markeset, 2009) that can be treated statistically. The distribution from Izquierdo et al. (Izquierdo et al. 2004) is given in figure 6. It has an averaged value of $C_x = 0.70\%$

(by concrete mass) with a standard deviation of $\pm 0.20\%$. The statistical distribution of Marqueset (Marqueset, 2009) found in real structures is almost similar (bridges in Norway where cores were drilled until the bar and observation of incipient corrosion was identified as the chloride threshold).

D. Izquierdo 2004 G. Marqueset 2009

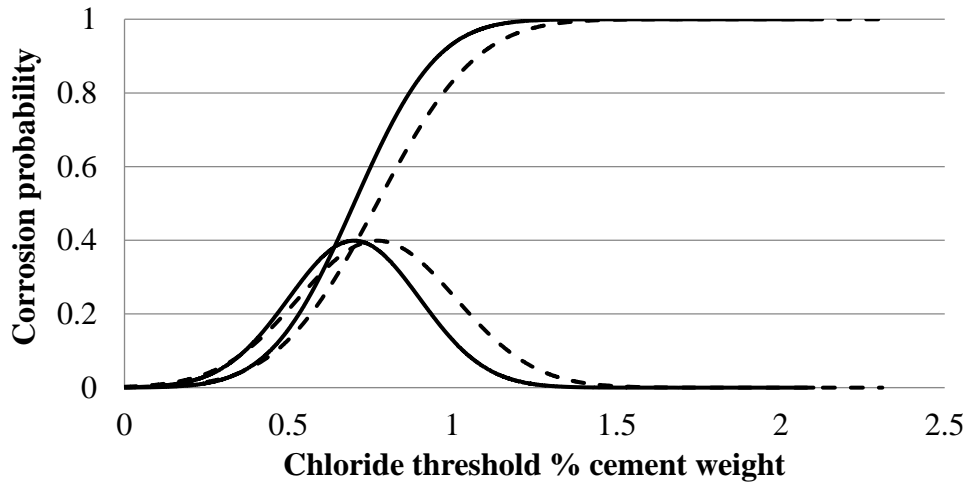


Figure 6. Statistical distributions of the chloride threshold by Izquierdo et al (plain line) (Izquierdo et al. 2004) made in laboratory conditions and by Marqueset (discontinuous line) (Marqueset, 2009) measured in real structures.

1.3 Propagation of corrosion

The progressive corrosion advance and loss in cross diameter of the bar and the oxides formed will induce several structural consequences which were described in CONTECVET Manual (2001) (figure 7):

- (a) Decrease in cross section and bar ductility.
- (b) Cover cracking
- (c) Steel/concrete bond deterioration and
- (d) Load-bearing capacity loss in regarding ULS.

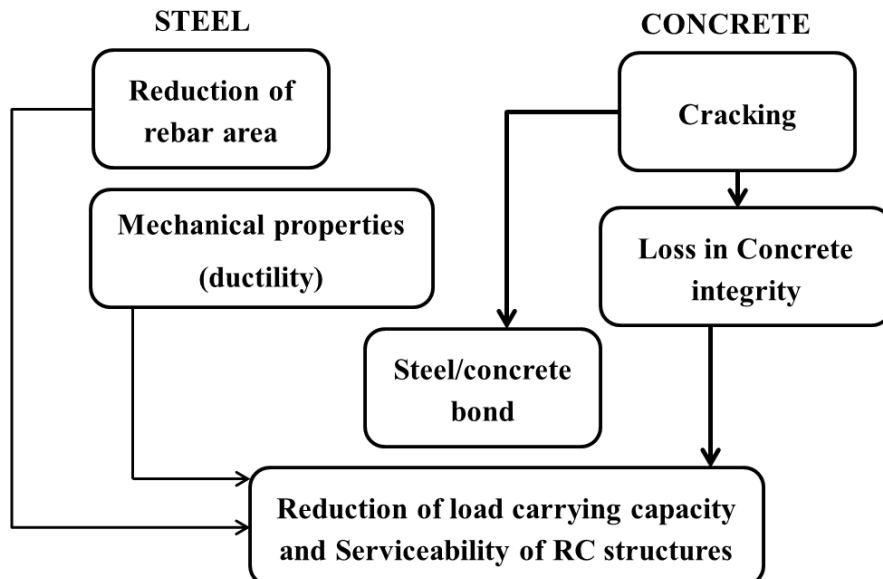


Figure 7 Consequences of rebar corrosion (CONTECVET Manual, 2001).

In order to calculate the time to reach one of these “failure” conditions it is necessary to have a model for the evolution of the bar diameter loss. A model was proposed years ago by Andrade et al (Andrade, 1989; Andrade, 2004) based in that of Tuutti (Tuutti, 1982). The preliminary model has been updated more recently (Andrade, 2017) which is shown in figure 8 as a bilinear propagation model expressed by the equation [5]:

$$t_p = t_{p1} + t_{p2} = \frac{P_{corr1}}{V_{corr1}} + \frac{P_{corr2}}{V_{corr2}} \quad [5]$$

Where t_p is the propagation period, P_{corr} is the loss in bar diameter or “accumulated corrosion”, V_{corr} is the corrosion rate, ϕ_0 is the initial diameter, ϕ_t is the final one after t years of corrosion. The conversion factor between V_{corr} and I_{corr} is: V_{corr} (mm/year) = 0.0116 · I_{corr} ($\mu A/cm^2$). Figure 8 presents the complete service life model (Tuutti, 1982; Andrade, 2017) having in mind the possibility that the corrosion rate is not only constant (line A in figure 8) but that it might be also presenting a two-step behaviour: line B would be the case when the corrosion decreases with time and line C that when it increases with time (for example when the cover cracks due to the corrosion in very wet environment). It also shows a “failure condition” of cracking (limit state of cover cracking parallel to the bars) depending on the degree of corrosion (Andrade, 2017).

The corrosion rate depends on the concrete porosity, the degree of water saturation and the temperature of each local environment. Taking the exposure classes defined in the European standard EN 206, in Table 1 are given values of the V_{corr} (considering linear its progress) and time of wetness (W_t) with the expected standard deviations (CONTECVET Manual, 2001; DURACRETE, 1998). It is also given the pitting factor, α .

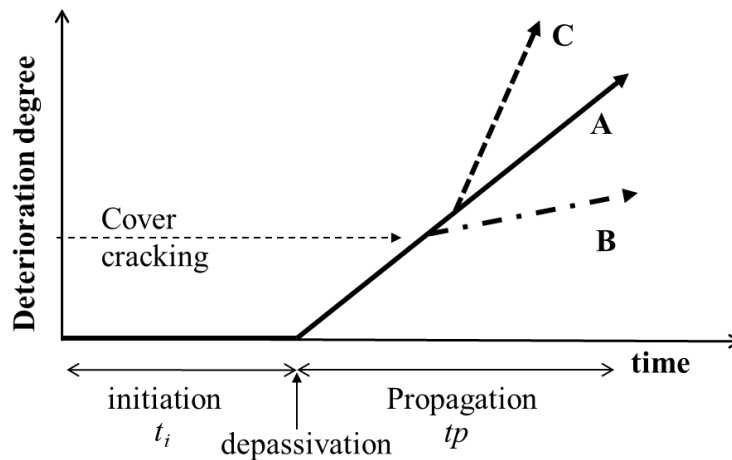


Figure 8. Service life model with the trends of the propagation period

Table 1. Values of V_{corr} , W_v and the pitting factor α from (2.3)

EXPOSURE CLASSES	$V_{corr, a}$ [mm/year]			W_t [-]			α pitting factor		
	Mean	St. Dev.	Distr.	Mean	St. Dev.	Distr.	Mean	St. Dev.	Distr.
No risk of corrosion	0	-	D	0	-	D	-	-	-
CARBONATION (Totally carbonated)									
Sheltered	0.002	0.003	W	0.5	0.12	N	2	0	D
Unsheltered	0.005	0.007	W	0.75	0.20	N	2	0	D

CHLORIDE INITIATED CORROSION									
Wet	0.004	0.006	W	1	0.25	N	9.28	4.04	N
Cyclic wet-dry	0.030	0.040	W	0.75	0.20	N	9.28	4.04	N
Airborne sea water	0.030	0.040	W	0.5	0.12	N	9.28	4.04	N
Submerged	Not expected or 0.010								
Tidal zone	0.070	0.100	W	1	0.25	N	9.28	4.0 4	N

As the climate may be constant or repeated every year, the accumulated corrosion or corrosion depth, P_{corr} , (see figure 9), which is the loss in diameter $P_{corr} = \Delta\phi = \phi_0 - \phi_i$, can be, as previously commented, linear with respect to the time (line A in figure 8) or can be considered a two-linear trend where the corrosion decreases with time ($V_{corr1} > V_{corr2}$ - line B) or increases ($V_{corr1} < V_{corr2}$ - line C).

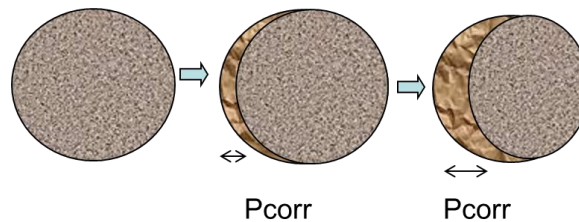


Figure 9. Evolution of the loss in diameter P_{corr} with the advance of the aggressive front.

If the corrosion is localized, there is a dependence of the maximum pit depth from the homogeneous corrosion by which it is possible to establish that (Gonzalez et al, 1995, CONTECVET Manual, 2001):

$$I_{pit} = I_{corr} \cdot \alpha \quad [6] \quad \text{or} \quad P_{pit} = P_{corr} \cdot \alpha \quad [6']$$

Where α is the “pitting factor” (see table 1) which accounts for the maximum pit depth. That is, the maximum pit depth is α times deeper than if the corrosion would have been homogeneous. The average value is $\alpha = 10$, although it may range in the case of chloride attack from 3 to 15 times.

2. CORROSION LIMIT STATES

The evolution towards a performance based durability design has added the probabilistic treatment to the calculation of the concrete durability, as developed in Duracrete project (DURACRETE, 1998) and incorporated into the fib Model Code 2010 (MC 2010, 2012) to the above conventional treatment. For the probabilistic treatment, a Limit State Function is defined whose general formulation is next given as equation [7]. A probability of failure is associated to the depassivation step. Thus:

$$P\{\} = P_{dep} = P\{t_{SL} - t_{ini}\} < P_0 \quad [7]$$

where:

- $P\{\}$ is the probability that depassivation occurs,
- t_{SL} is the design service life [years],

- t_{ini} is the initiation period [years],
- P_0 is the target failure probability

This general expression is particularized for each deterioration process. In the case of reinforcement corrosion, the traditional limit state considered is the time to steel depassivation. However, as mentioned this limit state does not fulfil the classical definition of SLS of the standards ISO 16204 (ISO, 2012) and ISO 2394 (ISO, 2015) for the SLS: *a state which corresponds to conditions beyond which specified serviceability requirements for a structure or its components are no longer satisfied*, because when corrosion just starts, any detrimental effect is produced at the structural level and any sign of damage or any effect is detected. All serviceability requirements continue being fulfilled during the first stages of the corrosion process. It seems much more appropriate the definition of an “Initiation” or “Deterioration Limit State” ILS or DLS, given in ISO standard 13283 (ISO, 2008) as: *a state which corresponds to the initiation of significant deterioration of a component of the structure*.

A consequence of this proposal is that the reliability associated to the depassivation may not be that of a typical SLS (probabilities of around 10%), but should be one considering the consequences of the corrosion initiation only, which are negligible in general. These consequences were mentioned before (figure 7) and having taken a corrosion propagation model and suggested values of V_{corr} , it is possible to analyze the effect of the deterioration level in the consequences of corrosion and select the most adequate reliability level. Further, the designer should as well, verify the standard SLS or the ULS. The procedure for the design (full probabilistic) briefly would include:

- The identification of the possible corrosion rate in the particular exposure class (see table 1).
- The calculation of the reduced area of the bars, the reduced concrete properties and concrete/bar bond at different times and plotting of a diagram as that of figure 8.
- Taken the selected V_{corr} and its standard deviation, calculate the probability to reach a $P_{corr} = 50 \mu\text{m}$ (associated to induce an incipient crack around the bars, that is, the DLS). This probability of failure has not to composery be the 10% as suggested in (MC 2010, 2012).
- The time of propagation so calculated will be the extra time added to the initiation period as service life time.

2.1 Example: Verification of cover cracking induced corrosion

For the sake of describing an example, cover cracking induced corrosion (parallel to the bars and not transversal to them due to the flexural loads) is proposed to be considered as a SLS, because when the cover in parallel to the bars a “*condition state beyond that of the design*” is reached in the same manner than when the cracks are transversal to the bars. The limit state of cracking induced corrosion can be calculated as suggested in MC2010 (MC 2010, 2012) through the equation [8]:

$$P\{\} = P_{crack} = P\{t_{SL} - t_{ini} - t_{prop} > 0\} < P_0 \quad [8]$$

where: $P\{\}$ is probability that parallel cracks are produced, t_{SL} is the design service life [years], t_{ini} is initiation period [years], t_{prop} is propagation period [years], P_0 is target failure probability. Figure 10 shows for the sake of illustration of the example, the probability of cover cracking (for bar diameter loss of $P_{corr} = 100 \mu\text{m}$ (Andrade et al. 2017) associated to the cover cracking) for several chloride diffusion coefficients (and corrosion rates associated to the concrete quality) in a hypothetical element of 5 cm in cover and a service life of 100 years.

The most important deductions from these figures are that the cover cracking probability is not unique, but varies with the rate of chloride ingress and of the corrosion rate. Other input parameters, as the aging factor or the coefficient of variation also influence the probability of reaching $P_{corr} =$

100 μm of diameter loss within the life time period. It is worth to notice that, logically, the probability of cover cracking when reaching 100 μm of diameter loss is smaller as the concrete is of higher quality, because the depassivation will be produced later. Reversely, lower quality concretes show that a higher probability is found at the end of the target service life. Then, it cannot be established a single value as a unique failure probability, but would depend on the concrete quality. The fact that the reliability is structure-dependent is general and that is why the semi-probabilistic format with general “safety factors” is the normal method in the existing Codes. In order to take a particular safety factor numerous cases and their economic consequences have to be analyzed, in order to select the optimum giving the highest safety at the minimum cost.

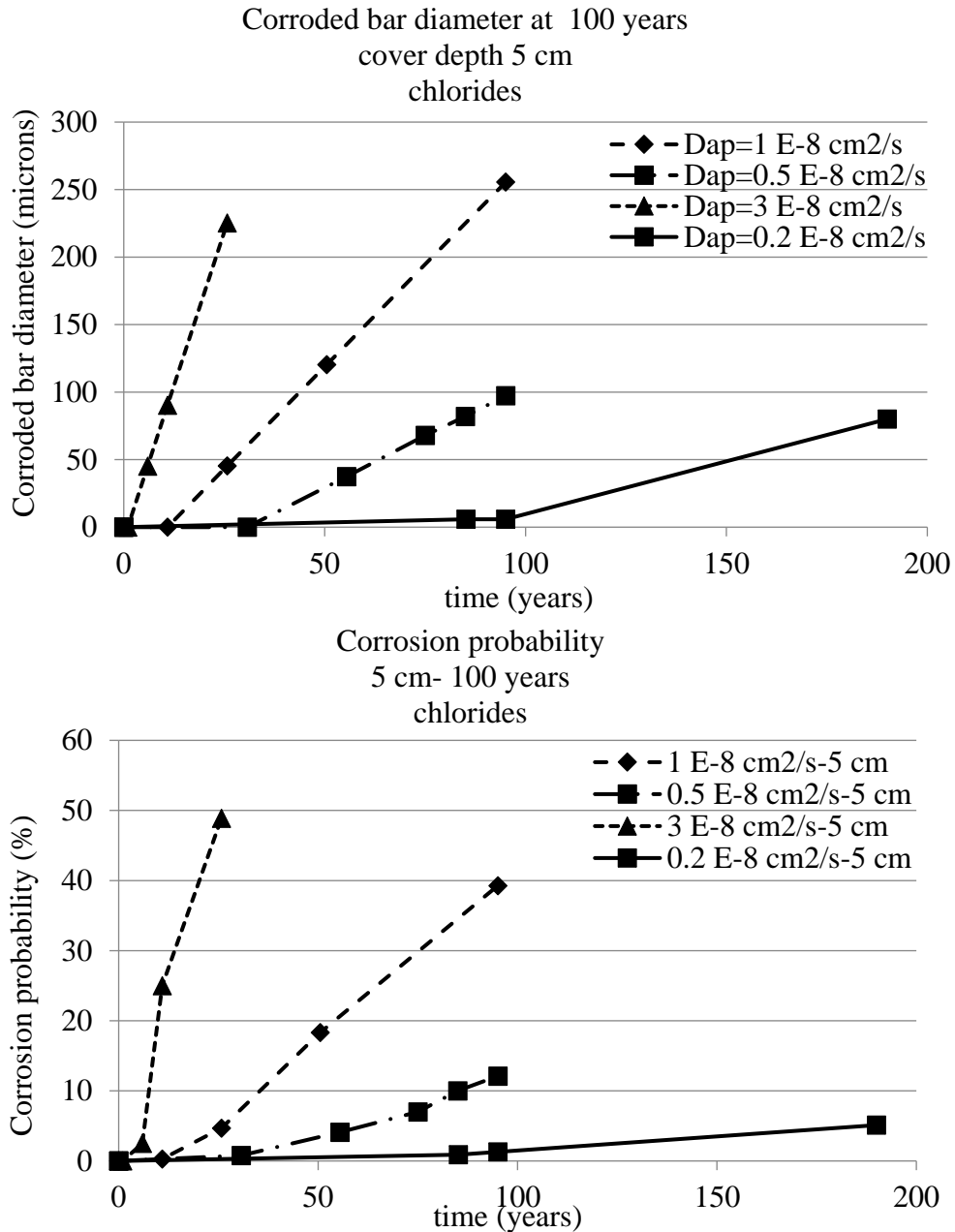


Figure 10. In the upper part is given the time to reach $P_{corr} = 100 \mu\text{m}$ of diameter loss for several $D_{ap,Cl}$. In the bottom part is given the probability of failure which is different depending on the value of $D_{ap,Cl}$ and associated corrosion rate.

2.2 Verification of ULS

The methodology of calculation of the ULS is similar to the one of calculation for the DLS or SLS through the determination of the accumulated corrosion, P_{corr} , from the exterior part of the reinforcement (figure 9) and the consideration of the corresponding general or localized loss of section. Then, from the reduced section of the bar, concrete and from the decreased steel/concrete bond, the loss in load bearing capacity of the concrete section can be recalculated. It is out of present work a detailed explanation. This detailed explanation can be found in Contecvet Manual (CONTECVET Manual, 2001) and the published Reports from Duracrete project (DURACRETE, 1998).

3. CONCLUSIONS

In spite of the progresses made in the calculation of service life in the last 20 years and the publication of models in the MC2010 (MC 2010, 2012), still numerous uncertainties remain and predictions at 100 years are not accurate enough. In present work, it has been tried to propose some advances with respect to present knowledge. These are:

- Carbonation model: the need to take into account an environmental factor, for example when the structure is outdoors exposed to rain. This factor should be determined with its standard deviation.
- Chloride model: the variations of the surface concentration and of the diffusion coefficient should be taken into account in the model based in Fick's law, as well as the possibility that the maximum in concentration is produced in the interior of the concrete and not in its surface. The concentration of the maximum is the "driven force" (the equivalent to the surface concentration) for the advance of the chloride profile.
- Corrosion propagation: the model is based in the Accumulated corrosion (P_{corr}) and the corrosion rate (V_{corr}). This last depends on the degree of concrete water saturation (time of wetness) and on the temperature.
- A new Deterioration Limit state (DLS) as defined by ISO 13283 is proposed for the sake of the calculations. Its reliability would depend on the importance of the structure and the consequences of the corrosion. This probability of failure may not be the 10% associated until present to depassivation (MC 2010, 2012). General safety factors should be deduced and help to define the most adequate probability in combination to the economical optimization.
- The Limit States (SLS and ULS) should be the same than for a non-deteriorated structure but considering the reduction of the bar section, the cover cracking and the loss in bond as developed in Contecvet Manual.

4. ACKNOWLEDGEMENTS

The author is grateful to the funds provided by the Ministry of Economy, Industry and Competitiveness of Spain. Also is grateful to the fruitful discussions in the committee TG 8.3 of Commission 8: Durability of fib, and with the members of the JCSS dealing with "Environmental loads chapter" of the Probabilistic Model Code.

5. REFERENCES

- Andrade, C. (2014). *2013 W.R. Whitney Award Lecture: Probabilistic Treatment of the Reinforcement Corrosion*. Corrosion, vol. 70, No. 6. pp. 643-651, <https://doi.org/10.5006/1049>
- Andrade, C. (2017), *Reliability analysis of corrosion onset: initiation limit state*, Journal of Structural Integrity and Maintenance, Pages 200-208, <https://doi.org/10.1080/24705314.2017.1388693>
- Andrade, C., Alonso, C., Gulikers, J., Polder, R., Cigna, R., Vennesland, Ø., Salta, M., Raharinaivo, A., Elsener, B. (2004). "RILEM TC 154-EMC: Electrochemical Techniques for Measuring Metallic Corrosion. Recommendations Test methods for on-site corrosion rate measurement of steel reinforcement in concrete by means of the polarization resistance method." Materials and Structures, 37(273): 623-643.
- Andrade, C., Alonso, C., Rodríguez, J. (1989), "Remaining service life of corroding structures", Proceedings IABSE Symposium on Durability, Lisbonne, pp. 359-363
- Andrade, C., Climent, M. A., de Vera, G. (2015), *Procedure for calculating the chloride diffusion coefficient and surface concentration from a profile having a maximum beyond the concrete Surface*, Materials and Structures 48:863–869, <https://doi.org/10.1617/s11527-015-0543-4>
- Andrade, C., Díez, J. M., Cruz Alonso, A. (1997) "Mathematical modelling of a concrete surface "skin effect" on Diffusion in chloride contaminated media". Advances Cement Based Materials, vol.6 (2), 39-44. [https://doi.org/10.1016/S1065-7355\(97\)00002-3](https://doi.org/10.1016/S1065-7355(97)00002-3)
- Bakker, R. (1994), "Prediction of service life reinforcement in concrete under different climatic conditions at given cover", Corrosion and Protection of Steel in Concrete International Conference, Sheffield (U.K.), R.N. Swamy Ed.
- Bazant, Z. P. (1979), *Physical Model for steel corrosion in concrete sea structures. Theory and application*. ASCE Journal of structural Division, June- ST6-p. 14551 (1138-1153)
- CONTECVET Manual (2001), *A validated user's manual for assessing the residual life of concrete structures*, DG Enterprise, CEC. (The manual can be downloaded from the web site of www.ietcc.csic.es)
- DURACRETE (1998), *Probabilistic Performance based durability design of concrete structures*, Brite EuRam Project 95 – 1347.
- Galan I., Andrade C., Mora P., Sanjuan M. A. (2010), *Sequestration of CO2 by Concrete Carbonation*, Environ. Sci. Technol. 44, 3181–3186.
- Gonzalez J.A., Andrade C, Alonso C, Feliu S. (1995), *Comparison of rates of general corrosion and maximum pitting penetration on concrete embedded steel reinforcement*. Cement and Concrete Research; 25(2): 257-264.
- International Organization for Standardization (ISO) (2012), *ISO 16204-Durability — Service life design of concrete structures*.
- International Organization for Standardization (ISO) (2015), *ISO 2394- General principles of reliability for structures*.
- International Organization for Standardization (ISO) (2008), *ISO 13283- General principles on the design of structures for durability*.
- Izquierdo, D., Alonso, C., Andrade, C., Castellote, M. (2004). *Potentiostatic determination of chloride threshold values for rebar depassivation Experimental and statistical study*, Electrochimica Acta, 49(17-18): 2731-2739, <https://doi.org/10.1016/j.electacta.2004.01.034>
- Mangat, P. S., Molloy, B. T. (1994), *Predicting of long term chloride concentration in concrete*. Materials and Structures, 27, 338-346. <https://doi.org/10.1007/BF02473426>
- Markeset, G. (2009), *Critical chloride content and its influence on service life predictions Critical chloride content and its influence on service life predictions*, Materials and Corrosion, 60, No. 8593-596, <https://doi.org/10.1002/maco.200905288>

- MC 2010 (2012), *The fib Model Code for Concrete Structures 2010*. fib <http://www.fib-international.org/fib-model-code-2010> .
- Tang, L., Gulikers, J. (2007), *On the Mathematics of Time-dependent Apparent Chloride Diffusion Coefficient in Concrete*. Cement and Concrete Research, Volume 37, Issue 4, Pages 589-595, <https://doi.org/10.1016/j.cemconres.2007.01.006>
- Thiery, M., Villain, G., Dangla, P., Platret, G. (2007), *Investigation of the carbonation front shape on cementitious materials: Effects of the chemical kinetics*, Cement and Concrete Research, 37(7), 1047–1058, <https://doi.org/10.1016/j.cemconres.2007.04.002>
- Tuutti, K. (1982), “*Corrosion of steel in concrete*”, Swedish Cement and Concrete Institute (CBI) n° 4-82. Stockholm.

Sustainable fiber reinforced cementitious panels containing PCM: Mechanical and thermal performance

B. Y. Pekmezci^{1*} , E. Y. Tuncel² 

*Contact author: pekmezci1@itu.edu.tr

DOI: <http://dx.doi.org/10.21041/ra.v10i2.479>

Reception: 26/11/2019 | Acceptance: 11/02/2020 | Publication: 30/04/2020

ABSTRACT

An experimental study was planned and executed for the application of Phase Change Materials (PCM) containing fiber-reinforced cementitious panels on buildings. The objective of the research was to enhance the thermal performance of the panels. Panels with the dimensions of 60x120x2.5 cm were produced and experimental investigations about the thermal and the mechanical performance of the composites were carried out. PCM containing composites showed higher latent heat capacity and lower thermal conductivity. Reinforcement with chopped fibers compensated the strength loss due to PCM in cementitious panels. Specific fracture energy of the panels increased with increase of PCM ratio. PCM containing fiber reinforced cementitious panels showed great potential for energy efficient buildings with enhanced thermal and mechanical properties.

Keywords: energy efficiency, phase change materials, fiber reinforced cementitious composites.

Cite as: Pekmezci, B. Y., Tuncel, E. Y. (2020), “Sustainable fiber reinforced cementitious panels containing PCM: Mechanical and thermal performance”, Revista ALCONPAT, 10 (2), pp. 180 – 190, DOI: <http://dx.doi.org/10.21041/ra.v10i2.479>.

¹ Department of Civil Engineering, Faculty of Civil Engineering, Istanbul Technical University, Istanbul, Turkey.

² Department of Architecture, Faculty of Architecture, Istanbul Technical University, Istanbul, Turkey.

Legal Information

Revista ALCONPAT is a quarterly publication by the Asociación Latinoamericana de Control de Calidad, Patología y Recuperación de la Construcción, Internacional, A.C., Km. 6 antigua carretera a Progreso, Mérida, Yucatán, 97310, Tel.5219997385893, alconpat.int@gmail.com, Website: www.alconpat.org

Responsible editor: Pedro Castro Borges, Ph.D. Reservation of rights for exclusive use No.04-2013-011717330300-203, and ISSN 2007-6835, both granted by the Instituto Nacional de Derecho de Autor. Responsible for the last update of this issue, Informatics Unit ALCONPAT, Elizabeth Sabido Maldonado, Km. 6, antigua carretera a Progreso, Mérida, Yucatán, C.P. 97310.

The views of the authors do not necessarily reflect the position of the editor.

The total or partial reproduction of the contents and images of the publication is strictly prohibited without the previous authorization of ALCONPAT Internacional A.C.

Any dispute, including the replies of the authors, will be published in the first issue of 2021 provided that the information is received before the closing of the third issue of 2020.

Paneles cementosos sostenibles reforzados con fibra que contienen PCM: Rendimiento mecánico y térmico

RESUMEN

Se planificó y ejecutó un estudio experimental para la aplicación de materiales de cambio de fase (PCM) que contienen paneles cementosos reforzados con fibra en edificios. El objetivo de la investigación fue mejorar el rendimiento térmico de los paneles. Se produjeron paneles con unas dimensiones de 60x120x2,5 cm y se llevaron a cabo investigaciones experimentales sobre el rendimiento térmico y mecánico de los compuestos. Los compuestos que contienen PCM mostraron mayor capacidad de calor latente y menor conductividad térmica. El refuerzo con fibras cortadas compensó la pérdida de resistencia debido a PCM en paneles cementosos. La energía de fractura específica de los paneles aumentó con el aumento de la relación PCM. Los paneles cementosos reforzados con fibra que contenían PCM mostraron un gran potencial para edificios energéticamente eficientes con propiedades térmicas y mecánicas mejoradas.

Palabras clave: eficiencia energética, materiales de cambio de fase, compuestos cementosos reforzados con fibra.

Painéis cimentícios reforçados com fibra sustentável contendo PCM: Desempenho mecânico e térmico

RESUMO

Um estudo experimental foi planejado e executado para a aplicação de materiais de mudança de fase (PCM) contendo painéis cimentícios reforçados com fibra em edifícios. O objetivo da pesquisa foi melhorar o desempenho térmico dos painéis. Painéis com dimensões de 60x120x2,5 cm foram produzidos e investigações experimentais sobre o desempenho térmico e mecânico dos compósitos foram realizadas. Os compósitos contendo PCM apresentaram maior capacidade de calor latente e menor condutividade térmica. O reforço com fibras cortadas compensou a perda de força devido ao PCM em painéis de cimento. A energia de fratura específica dos painéis aumentou com o aumento da razão PCM. Os painéis cimentícios reforçados com fibra de PCM mostraram grande potencial para edifícios com eficiência energética, com propriedades térmicas e mecânicas aprimoradas.

Palavras-chave: eficiência energética, materiais de mudança de fase, compósitos cimentícios reforçados com fibra.

1. INTRODUCTION

The use of solar energy has become a promising method to reach energy efficient solutions throughout the last century. Improving the thermal properties of building members will contribute to the efficient use of energy by preventing heat gain/loss through the building envelope. More over thermal comfort became important with development of panel and thin building envelope systems due to their low thermal mass. Phase change materials (PCM) are favorable materials for thermal applications because of their large contribution to the thermal mass of a building and thus providing “inertia” against temperature fluctuations.

Sustainability has become a goal for global development and for the effective use of reliable, sustainable and modern energy. This goal has been revealed among the objectives of United Nations (UN) 2030 (United Nations, 2015; Esseghir and Khouni, 2014).

On the other hand, energy consumption in the world is increasing significantly. This rise in consumption is also causing environmental problems. In the last two decades this increase has reached 30% (Sharifi et al., 2017; Chen et al., 2017; Chwieduk et al., 2003; Papadopoulos et al., 2002; IEA, 2016).

Considering that 60% of energy consumption is consumed by buildings due to heating and cooling operations, it should be considered that reducing this consumption will make a significant contribution to global energy consumption. Passive air conditioning methods can be applied to reduce energy consumption in buildings. Passive air conditioning technologies can be used in conjunction with traditional methods to create hybrid systems (Geetha and Velraj, 2012; Akeiber et al., 2012).

PCMs are materials with high latent heat capacity. With PCMs, it is possible to store high amount of energy in order to control the heat fluctuations in the indoor environment and to increase comfort (Mehling and Cabeza, 2008; Souayfane et al., 2016). When the ambient temperature rises above the melting temperature of the PCMs, the PCM performs a phase conversion from solid to liquid. During this conversion heat accumulates at high temperatures. It also solidifies when the temperature falls below the melting temperature of the ambient temperature and releases the stored heat. This process prevents high fluctuations in ambient temperature. PCMs stay at a nearly constant temperature during phase changes to prevent over-heating and cooling of the environment (Sharifi et al., 2017; Raoux and Wuttig, 2009).

With utilization of PCM in building materials, cooling and heating loads of the buildings can be reduced. Due to the high latent heat storage capacity of PCMs, which means a greater heat storage per unit volume than other building materials (Sharma et al., 2009), thermal inertia of the building that uses PCM integrated building materials will be greater (Singh Rathore et al., 2020). Microencapsulation, which is the process of enclosing the micron size particles of solid, liquid and gasses in an inert shell, is one of the methods that can be used to integrate PCM into other materials. Microencapsulated PCMs have been used in many researches to enhance the thermal performance of building materials (Barreneche et al., 2013; Arce et al., 2012; Thiele et al., 2015, Su et al., 2012; Borreguero et al. 2014; Li et al., 2019; Tuncel and Pekmezci, 2018). Although there is a common conclusion on the success of the PCMs on thermal performance enhancement, their effects on the mechanical properties of the building materials which they are integrated in, still need further examination for reliable applications.

2. EXPERIMENTAL STUDY

In this study, experiments were carried out to determine the mechanical and thermal properties of cement composite panels containing PCM. Calender extrusion which is a sustainable production method has been used in the production of panels. Panels with PCM content of 2.5% and 5%, and panels which are not containing PCM (0%), were produced in the production using the calender extrusion system. The schematic representation of calender extrusion fiber reinforced cementitious panel production system is given in Figure 1.

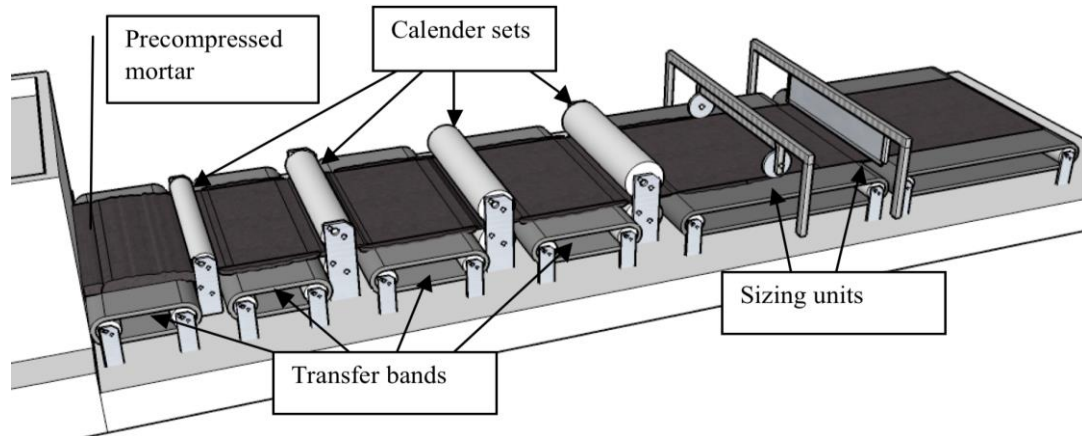


Figure 1. Calender extrusion line perspective (Pekmezci, 2015).

The dimensions of the produced samples were 60x120x2.5 cm. The ambient environmental conditions were 18°C temperature and 65% relative humidity. The produced panel specimens were brought to the dimensions necessary for the experimental study, and experiments were carried out. Discrete glass fibers were used in the production of composites. Tests were carried out at 18°C ambient temperature.

Cement was White Cement obtained from Cimsa Cement Factory Turkey. A polycarboxylate based superplasticizer, which was obtained from SIKA Turkey, was used for production of specimens. The properties of Cimsa White Cement are given in Table 1. CEM-FIL Anti-Crak HP 74/12 chopped glass strands were used as the reinforcement. The manufacturer-supplied properties of the fibers are presented in Table 2. The properties of PCM (provided by the manufacturer) are presented in Table 3.

Table 1. Properties of cement

Property	Value
Setting time, initial (minute)	115
Le chatelier opening (mm)	1.0
Compressive strength, 2 days, MPa	37.0
Compressive strength, 28 days, MPa	60.0
SO ₃ (%)	3.45
Unsoluble residue (%)	0.16
Ignition loss (%)	3.10
Cl ⁻ (%)	0.011

Table 2. Properties of glass fiber.

Fiber Length	12 mm
Aspect ratio (length / diameter)	74
Filament Diameter	14 - 19 μm
Loss on Ignition (%) (ISO 1887: 1995)	0.80 - 2.00
Moisture (%) (ISO 3344: 1997)	0.50 max
Specific Gravity	2.68 g/cm ³
Material	Alkali Resistant Glass
Chemical Resistance	very high
Modulus of elasticity	72 GPa
Tensile Strength	1700 MPa

Table 3. Properties of PCM

Product type	Powder
Melting point (approx. in °C)	23
Overall storage capacity (approx. in kJ/kg)	135
Latent heat capacity (approx. in kJ/kg)	100

In design of the composite panels, two different PCM amount were used (2.5% and 5.0% of total mass). A plain mixture that did not include PCM was also produced for comparison. In all mixtures, the fiber ratio was used as 2% of total volume. Water / cement ratio is kept as 0.40. The workability of the mixtures, which is suitable for calender extrusion, is provided by superplasticizer and viscosity modifier. The mix proportions of the mixtures used in the study are given in Table 4.

Table 4. Mixture proportions.

Mixture #	Cement kg/m ³	Sand kg/m ³	Water/cement ratio	PCM (% total w.)	Glass fiber (% total vol.)	WR admixture (% cement w.)
I	666	1332	0.4	-	2	2
II	617	1234	0.4	2,5	2	2
III	577	1154	0.5	5	2	2

3. RESULTS AND DISCUSSION

3.1 Thermal conductivity and mechanical properties

The thermal conductivity tests were conducted according to ISO 8301:1991 using a heat flow meter apparatus (Ahlborn) on plain and PCM composites. Figure 2 shows thermal conductivity test setup. Specimens with dimensions of 350 x 350 x 25 mm were used for the thermal conductivity measurements and were kept in saturated lime water at 21±1°C temperature for 28 days. Specimens were dried at 60°C until they achieved constant weight to avoid any moisture-based test error. Testing began when the specimen came to room temperature. Determination of the thermal conductivity was performed at a steady state condition with a mean temperature of +10°C at the center of the cross-section of sample.



Figure 2. Thermal conductivity test setup.

The thermal conductivity of the panels were 0.33 W/mK, 0.31 W/mK and 0.29 W/mK for panels including 0%, 2.5% and 5% PCM by total mass respectively. Although the ratio of PCM, leads to

a change in the thermal conductivity values, this change is not significant when evaluated from the viewpoint of heat insulation.

The mechanical properties of the composites were based on the 28-day uniaxial compressive strength test and the simple beam four-point bending test. Compressive strength tests were conducted on 40 mm cube specimens. For flexural tests, beam specimens of 45 mm width and 25 mm height were used. The length of the beam was 350 mm while the span length was 300 mm. A closed-loop testing machine (MTS Criterion 5500) was used in both tests and load-deflection curves were generated in the flexural tests. The specific fracture energy values (W_f) of the specimens were also determined in accordance with the recommendation of the RILEM 50-FMC Technical Committee (RILEM TCS, 1985). Tests were conducted at 18°C. Five individual specimens were tested for each group.

Figure 3 shows the results of the compressive strength test. It is clear from the figure that as the PCM ratio increases, the compressive strength of the matrix decreases. When the variation of the compressive strength values with the PCM ratios of matrix is examined, the compressive strength of the matrix is decreased by 7.5% and 10% when the PCM is used by 2.5% and 5%, respectively.

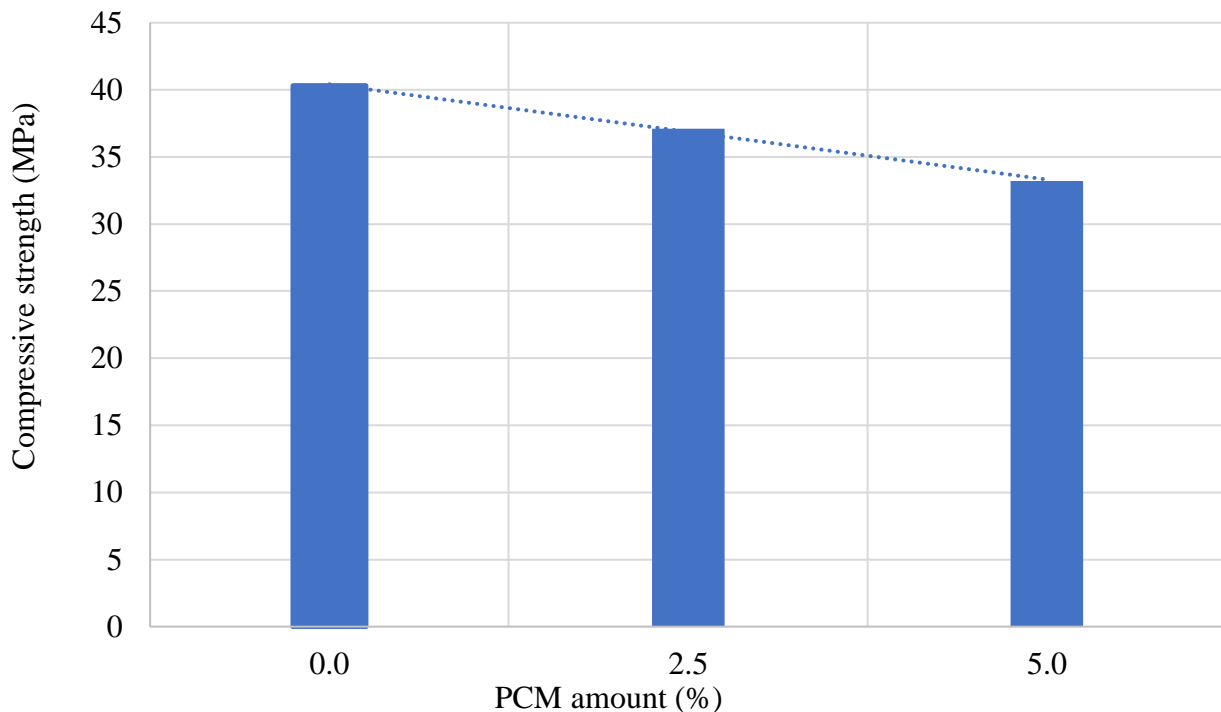


Figure 3. Relation of compressive strength with the PCM ratio of the panels.

Figure 4 shows the variation of flexural strength values with PCM amount. It is clear that flexural strengths decrease as the amount of PCM in the mixture increases. When the PCM content is 2.5% and 5%, the flexural strengths decrease by 7% and 13%, respectively.

Figure 5 shows the variation of specific fracture energy values with PCM amount. The specific fracture energy values increase as the PCM amount of the mixture increases in contrast to the strength values. The specific fracture energy increase was 31% and 40% for PCM ratios of 2.5 and 5%, respectively. This increase in specific fracture energy values can be attributed to an increase in deformation capacity. As the amount of PCM in the mixture increases, the ductility of the composites also increases due to the specific fracture energy value.

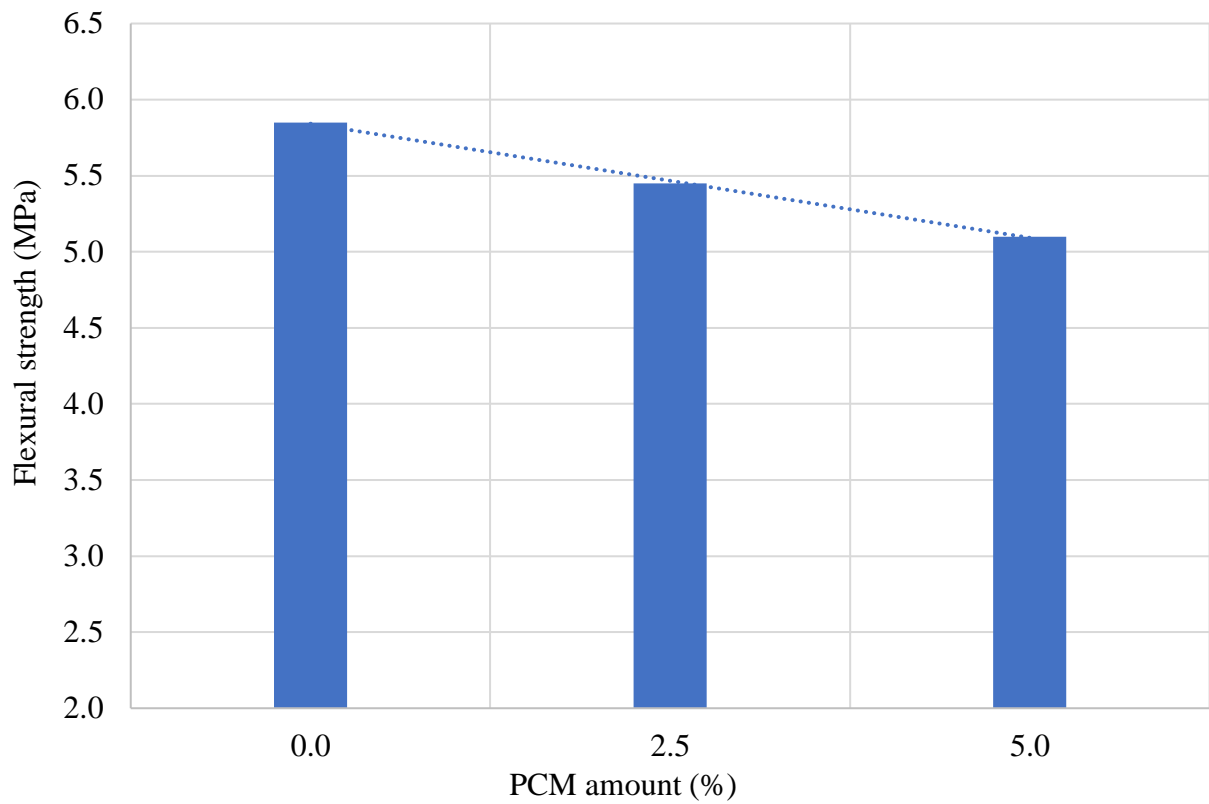


Figure 4. Relation of flexural strength with the PCM ratio of the panels.

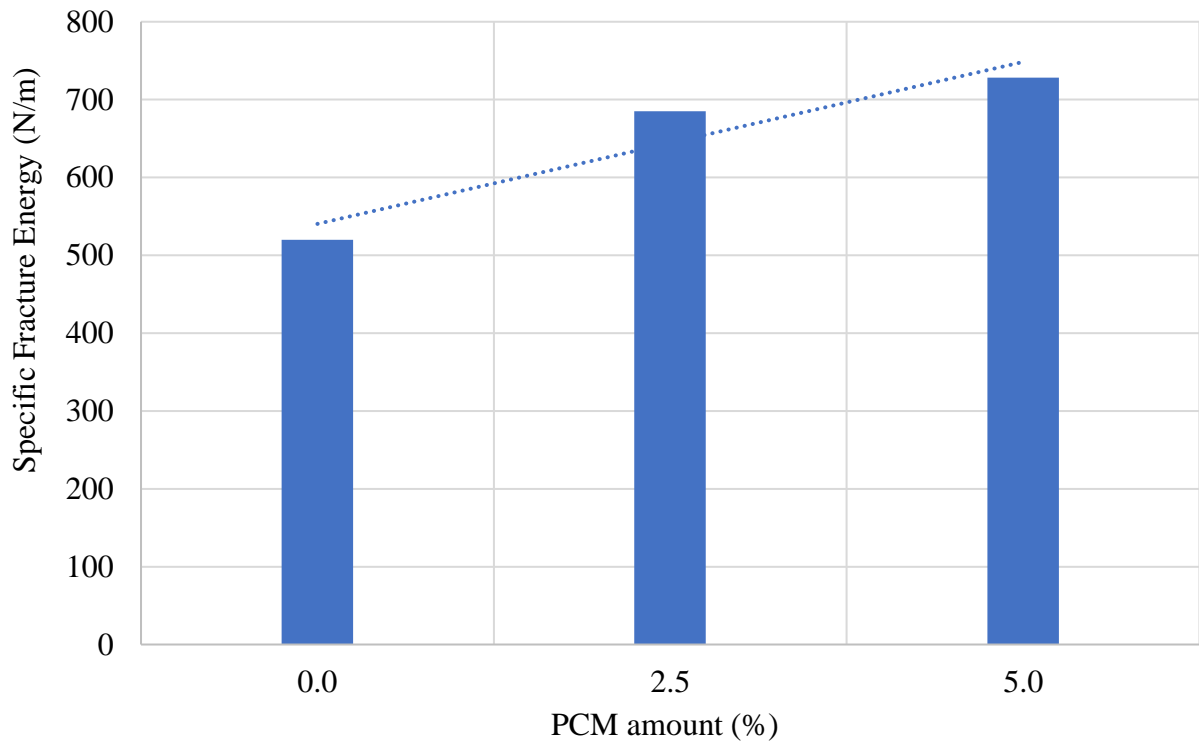


Figure 5. Relation of specific fracture energy with the PCM ratio of the panels.

3.2 Microstructure

The micrograph of the microencapsulated PCM in the cement matrix is shown in Figure 6. When we look at the Figure 6, it can be said that the microencapsulated PCM provides good bonding with the cement matrix and there are no cracks at the interface. However, it is observed that the PCM retains its spherical shape. This shows that microencapsulated PCMs during mixing, processing and curing can be used without deterioration.

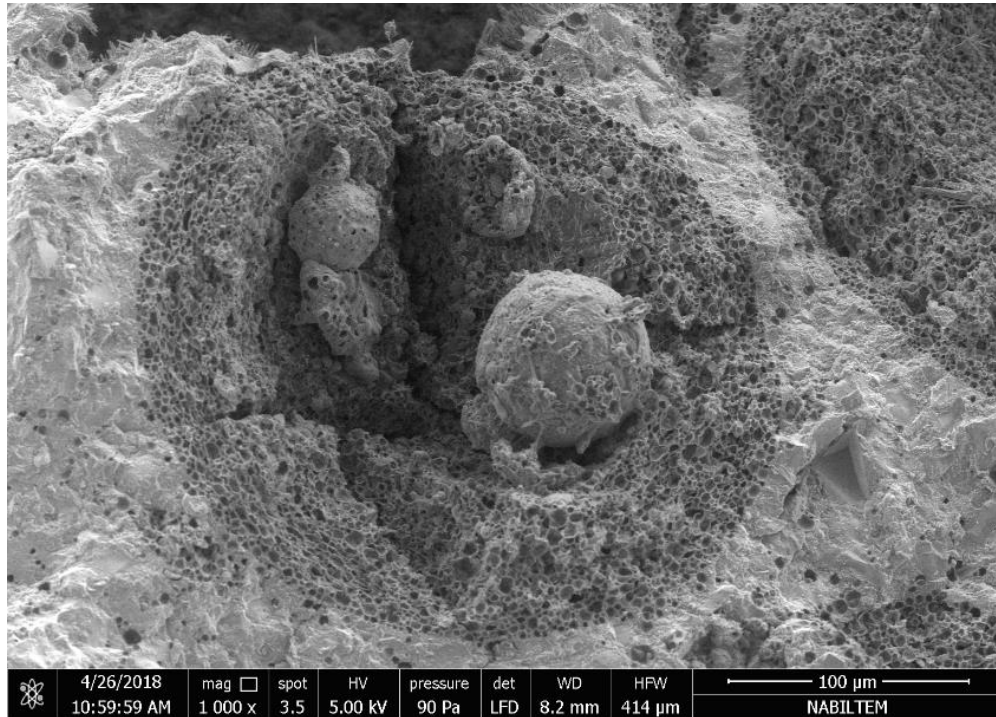
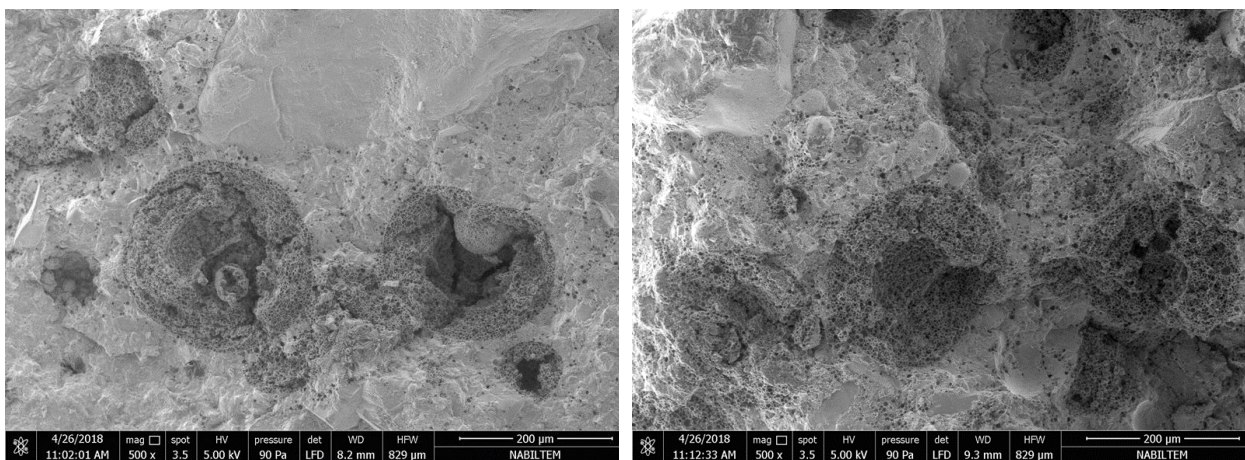


Figure 6. Microencapsulated PCM in cement matrix.

In the Figure 7, the distribution of microencapsulated PCMs in the cement based matrix is shown in the case of using PCM at different ratios.

Figures 7a and 7b show SEM images of mixtures containing 2.5% and 5% PCM, respectively. It is clear that the microencapsulated PCMs are placed closer to each other at 5% use, but the PCM capsules do not contact each other while preserving the integrity of the mortar phase there between.



(a) 2.5% PCM

(b) 5.0% PCM

Figure 7. Microencapsulated PCM distribution in cement matrix.

3.3 Thermal heat storage performance

The inner walls of two rooms of equivalent size were covered with the produced panel samples and the temperature changes in the rooms were monitored. Panels without PCM were applied to one of the rooms while panel samples containing PCM containing 5% were applied to the other room. In order to obtain the best performance from the PCM, measurements were made in the equivalent rooms having 50 m³ volume built in the main laboratory building. The main laboratory's air conditioning was shut down for four days during a vacation and the temperature in the main laboratory was allowed to fluctuate depending on natural conditions. In this process, the maximum temperature in the laboratory reached 28°C during the daytime hours and the minimum temperature remained at 15°C during the night hours. The maximum fluctuation in the room was measured as 3°C in the room where PCM-free panels were used, while 1°C was used for the room where PCM including panels were used.

4. CONCLUSIONS

Within the scope of this experimental study, the following conclusions can be drawn;

- The cementitious composite panels including PCM's are promising in terms of mechanical properties. Although PCM usage causes decrease on strength values, this decrease is not dramatic to prevent the use of the composite panels in situ. Moreover, PCM usage helps to increase the specific fracture energy values.
- Although the ratio of PCM used leads to a change in the thermal conductivity values, this change is not significant when evaluated from the viewpoint of heat insulation.
- The maximum fluctuation in the room was measured as 3°C in the room where PCM-free panels were used, while 1°C was used for the room where PCM including panels were used.

5. REFERENCES

- Akeiber, H., Nejat, P., Majid, M.Z.A, Wahid, M.A., Jomehzadeh, F., Famileh, I.Z., Calautit, J.K., Hughes, B.R., Zaki, S.A. (2016). *A review on phase change material (PCM) for sustainable passive cooling in building envelopes*. *Renewable and Sustainable Energy Reviews*. 60:1470–1497. <https://doi.org/10.1016/j.rser.2016.03.036>.
- Arce, P., Castellón, C., Castell, A., Cabeza, L. F. (2012). *Use of microencapsulated PCM in buildings and the effect of adding awnings*. *Energy and Buildings*. 44: 88–93. <https://doi.org/10.1016/j.enbuild.2011.10.028>.
- Barreneche, C., Navarro, M. E., Fernández, A. I., Cabeza, L. F. (2013). *Improvement of the thermal inertia of building materials incorporating PCM. Evaluation in the macroscale*. *Applied Energy*. 109: 428–432. <https://doi.org/10.1016/j.apenergy.2012.12.055>.
- Borreguero, A. M., Serrano, A., Garrido, I., Rodríguez, J. F., Carmona, M. (2014). *Polymeric-SiO₂-PCMs for improving the thermal properties of gypsum applied in energy efficient buildings*. *Energy Conversion and Management*. 87: 138–144. <https://doi.org/10.1016/j.enconman.2014.07.027>.
- Chen, B., Yang, Q., Li, J. S., Chen, G. Q. (2017). *Decoupling analysis on energy consumption, embodied GHG emissions and economic growth — The case study of Macao*. *Renewable and Sustainable Energy Reviews*. 67: 662–672. <https://doi.org/10.1016/j.rser.2016.09.027>.
- Chwieduk, D. (2003). *Towards sustainable-energy buildings*. *Applied Energy* 76 (1–3): 211–217. [https://doi.org/10.1016/S0306-2619\(03\)00059-X](https://doi.org/10.1016/S0306-2619(03)00059-X).
- Esseghir, A.; Khouni, L.H. (2014). *Economic growth, energy consumption and sustainable development: The case of the Union for the Mediterranean countries*. *Energy*. 71: 218-225. <https://doi.org/10.1016/j.energy.2014.04.050>.

- Geetha, N. B.; Velraj, R. (2012). *Passive cooling methods for energy efficient buildings with and without thermal energy storage – A review*. Energy Education Science and Technology Part A: Energy Science and Research. 29(2): 913-946.
- International Energy Agency, IEA, (2016). *IEA Headline Energy Data*, <https://www.iea.org>, last accessed: 12.02.2017.
- Li, C., Yu, H., Song, Y., Liu, Z. (2019). *Novel hybrid microencapsulated phase change materials incorporated wallboard for year-long year energy storage in buildings*. Energy Conversion and Management. 183: 791–802. <https://doi.org/10.1016/j.enconman.2019.01.036>.
- Mehling, H.; Cabeza, L.F. (2008), *Heat and Cold Storage with PCM: An up to Date Introduction in to Basics and Applications*, Springer, Berlin, Heidelberg. 308 pp. ISBN: 978-3-540-68556-2, e-ISBN: 978-3-540-68557-9. <https://doi.org/10.1007/978-3-540-68557-9>.
- Papadopoulos, A. M.; Theodosiou, T. G.; Karatzas, K.D. (2002). *Feasibility of energy savingrenovation measures in urban buildings: the impact of energy prices and theacceptable pay back time criterion*. Energy and Buildings 34(5):455–466. [https://doi.org/10.1016/S0378-7788\(01\)00129-3](https://doi.org/10.1016/S0378-7788(01)00129-3).
- Pekmezci, B.Y., *Utility of Colloidal Nano-silica in Processing of Fiber Reinforced Cementitious Composites*. Sobolev, K. and Shah S. P. Editors. Nanotechnology in Construction Proceedings of NICOM5, Springer. pp. 501-506. ISBN: 978-3-319-17087-9 eISBN: 978-3-319-17088-6. <https://doi.org/10.1007/978-3-319-17088-6>
- Raoux, S., Wuttig, M. (Eds.) (2009). *Phase Change Materials: Science and Applications*, Springer, 446 pp. ISBN: 978-0-387-84873-0, e-ISBN: 978-0-387-84874-7. <https://doi.org/10.1007/978-0-387-84874-7>.
- RILEM TCS, (1985). *Determination of the fracture energy of mortar and concrete by means of three-point bend tests on notched beams*. Materials and Structures, 18(106): 285-290. <https://doi.org/10.1007/BF02472918>.
- Sharifi, N. P., Shaikh, A. A. N., Sakulich, A. R. (2017), *Application of phase change materials in gypsum boards to meet building energy conservation goals*. Energy and Buildings. 138:455–467. <https://doi.org/10.1016/j.enbuild.2016.12.046>.
- Sharma, A., Tyagi, V. V., Chen, C. R., Buddhi, D. (2009). *Review on thermal energy storage with phase change materials and applications*. Renewable and Sustainable Energy Reviews, 13(2): 318–345. <https://doi.org/10.1016/j.rser.2007.10.005>.
- Singh Rathore, P.K., Shukla, S.K., Gupta, N.K. (2020). *Potential of microencapsulated PCM for energy savings in buildings: A critical review*. Sustainable Cities and Society. 53. <https://doi.org/10.1016/j.scs.2019.101884>.
- Souayfane, F., Fardoun, F., Biwale, P.H. (2016). *Phase change materials (PCM) for cooling applications in buildings: A review*. Energy and Buildings. 129:396–431. <https://doi.org/10.1016/j.enbuild.2016.04.006>.
- Su, J. F., Wang, X. Y., Wang, S. B., Zhao, Y. H., Huang, Z. (2012). *Fabrication and properties of microencapsulated-paraffin/gypsum-matrix building materials for thermal energy storage*. Energy Conversion and Management. 55: 101–107. <https://doi.org/10.1016/j.enconman.2011.10.015>.
- Thiele, A. M., Jamet, A., Sant, G., Pilon, L. (2015). *Annual energy analysis of concrete containing phase change materials for building envelopes*. Energy Conversion and Management. 103: 374–386. <https://doi.org/10.1016/j.enconman.2015.06.068>.
- Tuncel, E. Y., Pekmezci, B. Y. (2018). *A sustainable cold bonded lightweight PCM aggregate production: Its effects on concrete properties*. Construction and Building Materials. 181: 199-216. <https://doi.org/10.1016/j.conbuildmat.2018.05.269>.

United Nations, (2015), *Resolution adopted by the General Assembly on 25 September 2015*, General Assembly A/Res/70/1, Transforming our world: the 2030 Agenda for Sustainable Development. Seventieth session, 21 October 2015, pp. 35.
https://www.un.org/ga/search/view_doc.asp?symbol=A/RES/70/1&Lang=E
https://www.un.org/en/development/desa/population/migration/generalassembly/docs/globalcompact/A_RES_70_1_E.pdf

Physical and chemical effects of limestone filler on the hydration of steam cured cement paste and mortar

M. Aqel¹. D. K. Panesar^{2*} 

*Contact author: d.panesar@utoronto.ca

DOI: <http://dx.doi.org/10.21041/ra.v10i2.481>

Reception: 26/10/2019 | Acceptance: 12/02/2020 | Publication: 30/04/2020

ABSTRACT

The aim of the paper is to decouple the physical and chemical effects of limestone filler (LF), when used as a cement replacement. The effects were decoupled using LF and a chemically inert material (brucite $Mg(OH)_2$). Paste, and mortar specimens were steam cured for 16 hours at 55°C. The heat of hydration, thermal analysis, x-ray diffraction, and compressive strength, were evaluated at 16 hours and at 28 days. LF can adversely affect the properties through dilution effect. However, heterogeneous nucleation compensates for the dilution effect at 16 hours while the production of mono-carboaluminate compensates for the dilution effect at 16 hours and 28 days. The study could be broadened by considering a wider temperature range. The originality lies in the method of decoupling the physical and chemical effects. Measurable effects of the physical and chemical contribution of LF are evident on the mechanical and transport material properties.

Keywords: limestone filler; compressive strength; heterogeneous nucleation; dilution.

Cite as: Aqel, M., Panesar, D. K. (2020), “*Physical and chemical effects of limestone filler on the hydration of steam cured cement paste and mortar*”, Revista ALCONPAT, 10 (2), pp. 191 – 205, DOI: <http://dx.doi.org/10.21041/ra.v10i2.481>

¹ Concrete Engineer, Materials Engineering and Research Office, Ministry of Transportation Ontario, Canada.

² Professor, Department of Civil and Mineral Engineering, University of Toronto, Canada.

Legal Information

Revista ALCONPAT is a quarterly publication by the Asociación Latinoamericana de Control de Calidad, Patología y Recuperación de la Construcción, Internacional, A.C., Km. 6 antigua carretera a Progreso, Mérida, Yucatán, 97310, Tel.5219997385893, alconpat.int@gmail.com, Website: www.alconpat.org

Responsible editor: Pedro Castro Borges, Ph.D. Reservation of rights for exclusive use No.04-2013-011717330300-203, and ISSN 2007-6835, both granted by the Instituto Nacional de Derecho de Autor. Responsible for the last update of this issue, Informatics Unit ALCONPAT, Elizabeth Sabido Maldonado, Km. 6, antigua carretera a Progreso, Mérida, Yucatán, C.P. 97310.

The views of the authors do not necessarily reflect the position of the editor.

The total or partial reproduction of the contents and images of the publication is strictly prohibited without the previous authorization of ALCONPAT Internacional A.C.

Any dispute, including the replies of the authors, will be published in the first issue of 2021 provided that the information is received before the closing of the third issue of 2020.

Efectos físicos y químicos del relleno de piedra caliza sobre la hidratación de la pasta y el mortero de cemento curados al vapor

RESUMEN

El objetivo del artículo es disociar los efectos físicos y químicos del material filler calcáreo (FC), cuando es usado como sustitución del cemento. Los efectos fueron de disociados usando FC químicamente inerte (brucita $Mg(OH)_2$). Las muestras de pasta y mortero fueron curadas a vapor por 16 h a $55^\circ C$. El calor de hidratación, el análisis térmico, la difracción de rayos-x y la resistencia a la compresión fueron evaluados a las 16 h y a los 28 días. El FC puede afectar adversamente las propiedades a través del efecto de dilución. No obstante, la nucleación heterogénea compensa el efecto de dilución en 16 h, mientras la producción de mono-carboaluminato compensa el efecto de dilución a las 16 h y 28 días. El estudio puede ser ampliado considerando un rango de temperatura más amplio. La originalidad reside en el método de disociar los efectos físicos y químicos. Efectos mensurables de la contribución física y química de la FC son evidentes en las propiedades mecánicas y de transporte de material.

Palabras llave: relleno de piedra caliza; fuerza compresiva; nucleación heterogénea; dilución.

Efeitos físicos e químicos do filler calcário na hidratação de pasta de cimento e argamassa curadas à vapor

RESUMO

O objetivo do artigo é dissociar os efeitos físicos e químicos do material filler calcário (FC), quando usado como substituição do cimento. Os efeitos foram dissociados usando FC quimicamente inerte (brucita $Mg(OH)_2$). As amostras de pasta e argamassa foram curadas a vapor por 16 h a $55^\circ C$. O calor de hidratação, a análise térmica, a difração de raios-x e a resistência à compressão foram avaliados às 16 h e aos 28 dias. O FC pode afetar adversamente as propriedades através do efeito de diluição. No entanto, a nucleação heterogênea compensa o efeito de diluição em 16 h, enquanto a produção de mono-carboaluminato compensa o efeito de diluição em 16 h e 28 dias. O estudo pode ser ampliado considerando uma faixa de temperatura mais ampla. A originalidade reside no método de dissociar os efeitos físicos e químicos. Efeitos mensuráveis da contribuição física e química da FC são evidentes nas propriedades mecânicas e de transporte de material.

Palavras-chave: filler calcário; resistência a compressão; nucleação heterogênea; diluição.

1. INTRODUCTION

Global cement production was estimated to be 4.0 billion tonnes in 2013 owing to the fact that concrete is the second most consumed material on earth after water (U.S. Geological Survey 2014, European Federation for Precast Concrete 2014). Cement production has a significant environmental impact as it is responsible for 7% of worldwide manmade CO_2 emission (Benhelal et al. 2013). This is due to the fact that one tonne of cement produces approximately 900 kg of CO_2 of which 450 kg is produced from the decomposition of raw materials and 360 kg from burning fuel (Benhelal et al. 2013). Replacing cement with supplementary cementing materials or fillers such as limestone filler (LF) has been one approach to reduce the negative environmental impact of concrete (Mohammadi and South 2016) In addition, LF can reduce the cost of cement production. This is mainly due to the relatively lower cost and hardness of LF compared to cement clinker (Celik et al. 2015).

LF has been accepted as a cement replacement in many standards around the world. For example, the use of interground limestone as a cement replacement has been accepted in many standards in Europe since 1960, Canadian Standard Association (CSA) in 1983, and ASTM C150 in 2004. However, all of these standards have set a maximum interground limestone content which ranges from 5% to 15% (Tennis et al. 2011, Hooton et al. 2007).

When replacing cement, LF influences the behavior of cement through physical and chemical effects. The physical effect is caused by (i) modification of particle size distribution, (ii) dilution and (iii) heterogeneous nucleation. Modification of particle size distribution and heterogeneous nucleation can improve the properties of concrete whereas dilution has adverse effect. The chemical effect of LF is caused by the chemical reaction between LF with monosulfate and calcium aluminate hydrate in the hydrated cement system.

1.1 Physical effect of LF

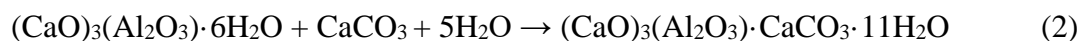
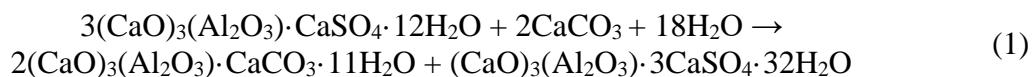
(i) Modification of the particle size distribution due to the presence of LF is primarily attributed to its relatively lower hardness compared to cement, and so when ground it yields a wider particle size distribution (Gao 2012, Sellevold et al. 1982). This allows LF to improve the particle size distribution when added to the cement (Sellevold et al. 1982). Furthermore, LF can decrease the water demand by replacing some of the water in the voids. This water provides additional reduction in the friction between solid particles and thus improves the workability (Hawkins et al. 2003). However, this effect could be masked by the higher water adsorption when LF fineness increases (Schmidt 1992). When LF particles are finer than cement, LF can reduce the bleeding of concrete through water adsorption at replacement levels greater than 5%. At a replacement level less than 5%, the bleeding is only influenced by the surface area of the cement (Moir and Kelham 1993).

(ii) Dilution effect occurs when the cement content is reduced due to cement replacement by LF (Irassar 2009). The reduction in the cement content decreases the hydration products and thus adversely affects the compressive strength at early and later ages, porosity and permeability of concrete. The effect of dilution masks any other LF effects at replacement level higher than 5%. Below 5%, the dilution effect is minimized (Tsvivilis et al. 2003). Although dilution influences the properties of the cement system at all ages it is mainly observed after 3 days (Kenai et al. 2004). Before 3 days, a portion of the dilution effect is compensated for by the heterogeneous nucleation effect of LF.

(iii) Portion of the hydration products precipitates on the surface of LF particles (Irassar 2009). This effect depends mainly on the fineness of LF. The increase in LF fineness increases the nucleation sites for the precipitation of the hydration products (Ezziane et al. 2010). This accelerates the cement hydration process and results in faster early age strength gain (Irassar 2009). In addition, the surface area of LF will accommodate some of the hydration products, which reduces the thickness of the hydration products coating unhydrated cement particles (Lin and Meyer 2009). This allows the inner part of unhydrated cement particles to hydrate sooner and thus accelerate the hydration process.

1.2 Chemical effect of LF

The chemical interaction between LF and other hydration products was debated. However, research work in the past 20 years proved that LF is not a chemically inert material but rather a partially reactive material (Hooton et al. 2007, Hawkins et al. 2003). LF reacts with monosulfate $((\text{CaO})_3(\text{Al}_2\text{O}_3)\cdot\text{CaSO}_4\cdot 12\text{H}_2\text{O})$ and calcium aluminate hydrate $((\text{CaO})_3(\text{Al}_2\text{O}_3)\cdot 6\text{H}_2\text{O})$ to form calcium mono-carboaluminate $(3\text{CaO}\cdot\text{Al}_2\text{O}_3\cdot\text{CaCO}_3\cdot 11\text{H}_2\text{O})$ as presented in Equations 1 and 2 (Kakali et al. 2000, Bentz 2006, Kuzel et al. 1996). The reactions between LF and monosulfate and calcium aluminate hydrate take place after the exhaustion of sulfate ions in the system (Wang 2010). In addition, the fineness of LF influences these reactions; the higher the fineness of LF the more LF is consumed in these reactions (Hooton et al 2007).



The influence of LF on the concrete properties cured at ambient temperature (i.e., 23°C) have been fairly reported in the literature (Hooton et al. 2007, Hawkins et al. 2003, Irassar 2009). However, the results in the literature often vary and in many cases contradict. This contradiction is evident in the workability, mechanical properties and durability performance results (Tennis et al. 2011, Ramezani-pour and Hooton 2013, Sirisawat et al. 2014). Furthermore, information on the influence of LF when the concrete is steam cured is limited. While the influence of LF is caused by a combination of physical and chemical effects no elaboration on the influence of each effect has been reported. Therefore, it is essential to identify the influence of each effect to understand how LF interacts in the cement system and to optimize the use of LF for the precast/prestressed applications.

The aim of this paper is to decouple the physical and chemical effects of LF on paste and mortar systems. This was achieved by using LF and an inert filler (brucite, $\text{Mg}(\text{OH})_2$ which will be referred to as Mg) with similar particle size distribution and fineness. The concept of using inert material to evaluate the effect of a reactive material is not new. However, no research work has been done to utilize this concept to decouple the physical and chemical effects of LF and quantify the contribution of each effect separately.

Mg is an inert material by nature but could chemically react with the amorphous silica in fly ash under sulphate rich environment (Zhang et al. 2014, Moore et al. 2009). However, this condition at which Mg can chemically react does not apply in this study and therefore, Mg was considered an inert material. Mg was used to evaluate and measure the combined physical effects of LF while LF was used to measure the combined physical and chemical effects. The difference in performance between LF and Mg mixtures is attributed to the chemical reaction of LF.

The physical and chemical effects of LF on the heat of hydration, chemical composition, and cube compressive strength, were evaluated. The heat of hydration of cement pastes was measured at 23°C and 55°C for a duration of 72 hours using Isothermal Calorimetry. The chemical composition of cement pastes was measured at 16 hours (following steam curing) and at 28 days using thermal analysis. The cube compressive strength of mortars were evaluated at 16 hours and 28 days.

2. EXPERIMENTAL PROGRAM

2.1. Materials

CSA type HE cement with no interground limestone was used. The cement was supplied by Lafarge Canada Inc. The physical and chemical properties of cement are presented in Table 1. LF and Mg were supplied by Omya Canada Inc. and Aldon Corporation, respectively. The selection of Mg was based on the chemical reactivity and hardness. Mg is an inert material and has similar Mohs Hardness (i.e., 3) compared to LF (Moore et al. 2009, Santhanam 2013). The hardness of Mg and LF should be similar to avoid introducing a new variable in the compressive strength results (Zhang et al. 2011). LF had a Blaine fineness of 1125 m^2/kg , median particle size of 3 μm and specific gravity of 2.7. The supplied Mg had a Blaine fineness of 1450 m^2/kg , median particle size of 4 μm and specific gravity of 2.4. Since the particle size distribution and the Blaine fineness of the supplied LF and Mg were different, both materials required modification in particle size distribution to achieve similar particle size distribution and Blaine fineness. This modification consisted of sieving LF and Mg using 10 μm , 7 μm , 5 μm and 2 μm sieves and using equal proportion retained on each sieve. The sieving was conducted to ensure similar particle size distribution of LF and Mg. In addition, the portion of LF passing 2 μm sieve was ground so that the final LF product

has similar Blaine fineness compared to Mg namely, $1450 \pm 30 \text{ m}^2/\text{kg}$. The particle size distribution of cement, LF and Mg is presented in Figure 1. The fine aggregate (natural sand) and coarse aggregate (crushed limestone) were supplied by Dufferin Aggregates. The specific gravity of the sand was 2.72 and the fineness modulus was 2.84. Plastol 6400, a high-range water reducer (HRWR), supplied by Euclid Chemical was used.

Table 1. Chemical and physical properties of cement

Chemical and Physical Properties	HE Cement
SiO ₂ (%)	19.7
Al ₂ O ₃ (%)	5.0
Fe ₂ O ₃ (%)	3.3
CaO (%)	61.8
MgO (%)	2.5
SO ₃ (%)	4.1
Na ₂ O _{eq} (%)	0.7
C ₃ S (%)	54.0
C ₃ A (%)	8.0
C ₄ AF (%)	10.0
C ₂ S (%)	14.0
LOI at 1150 °C (%)	0.9
Blaine (m ² /kg)	505

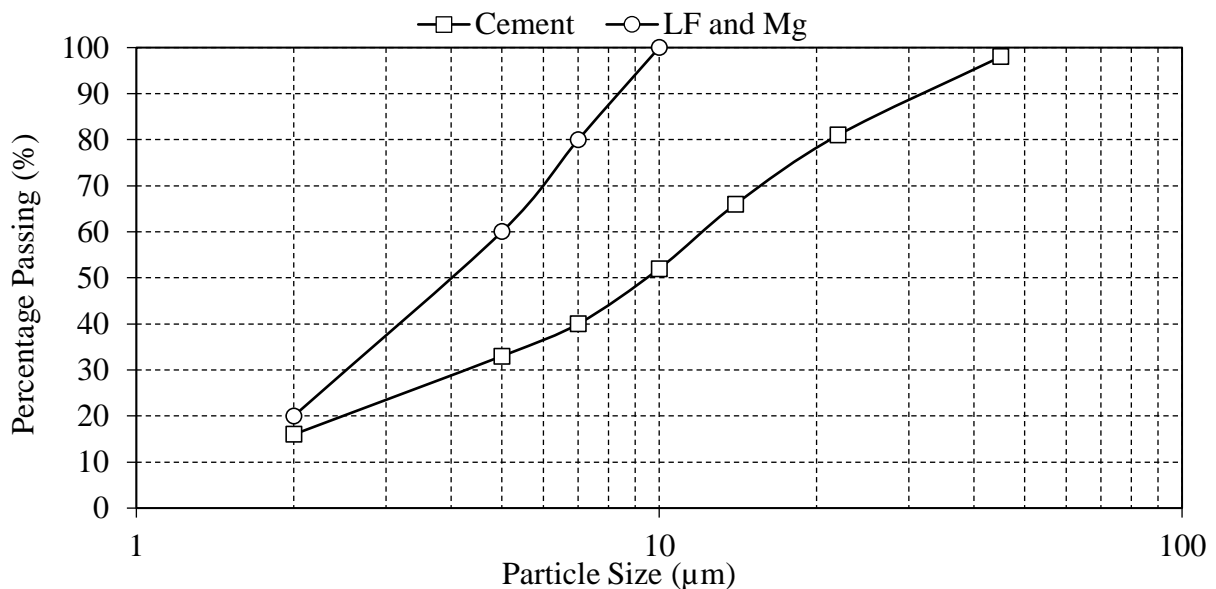


Figure 1. Particle size distribution of cement, LF and Mg

2.2. Mix design

Three mix designs were evaluated. For each mix design, cement paste, and mortar were prepared. The details of the mixtures are presented in Table 2 for cement paste and mortar mixes. LF and Mg were used to replace 15% by weight of the cement. The water-to-cement ratio (w/c) was kept constant in the paste, mortar and concrete at 0.34. LF and Mg were not considered as cementing materials in the w/c ratio calculation. This was done in accordance with the Canadian Standards Association CSA A23.1-14. The use of 0.34 w/c ratio was to represent a typically used w/c in self-consolidating concrete (Esmailkhanian et al. 2014, Celik et al. 2015). No HRWR was used in

cement pastes to prevent any variation in the heat of hydration or thermal analysis results. The sand-to-cement ratio in the mortar mixtures was 2.

Table 2. Cement paste and mortar mixture details

Mix ID	Cement (% by weight)	Cement replacement (% by weight)		Sand/Cement ratio for mortar	w/c Ratio
		LF	Mg		
C	100	0	0	2	0.34
LF	85	15	0	2	
Mg	85	0	15	2	

2.3. Curing regime

Paste, and mortar specimens were steam cured at 55°C and 95% relative humidity (RH) for 16 hours as presented in Figure 2. A 0.45 m³ Cincinnati Sub-Zero environmental chamber was used. A maximum curing temperature of 55°C was used in order to prevent any formation of delayed ettringite (Brunetaud et al. 2006). Following steam curing, the specimens were placed in limewater at 23°C until tested.

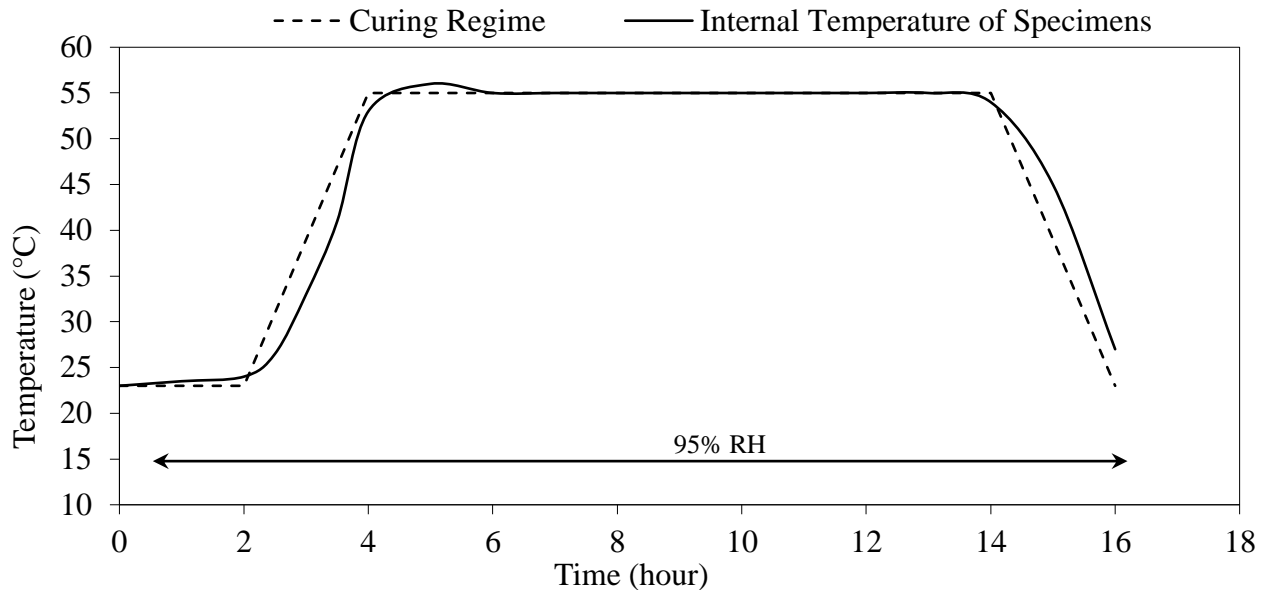


Figure 2. Steam curing regime

2.4. Test methods

Cement paste specimens were used for the heat of hydration, and thermal analysis. Mortar specimens were used for cube compressive strength.

2.4.1 Heat of hydration

For each paste mixture, the heat of hydration was measured at 23°C and 55°C over a period of 72 hours in accordance with ASTM C1702-09 Method B. Three samples were tested for each paste mixture. Pastes cured at 23°C were tested using an isothermal calorimeter (TAM Air) manufactured by Thermometric. At 55°C, I-Cal 8000 isothermal calorimeter manufactured by Calmetrix was used. Before mixing the cement pastes, all materials were preconditioned to a temperature within $\pm 2^\circ\text{C}$ of the isothermal calorimeter testing temperature. This was done by placing the materials in the environmental chamber set at $\pm 2^\circ\text{C}$ of the isothermal calorimeter testing temperature for 2 hours.

2.4.2 Thermal analysis

Calcium hydroxide ($\text{Ca}(\text{OH})_2$), calcium carbonate (CaCO_3) and magnesium hydroxide ($\text{Mg}(\text{OH})_2$) contents were measured at 16 hours and 28 days using Thermal Gravimetric /Differential Thermal Analysis (TG/DTA). For each mix design, two TG/DTA tests were conducted. The tests were conducted using Netzsch SA Simultaneous Thermal Analyzer with a maximum temperature of 1100°C and $10^\circ\text{C}/\text{min}$ heating rate. $\text{Ca}(\text{OH})_2$ content was used to evaluate the hydration products for each mixture. The paste samples were freeze-dried until a constant mass was achieved. In freeze-drying process, the paste samples were frozen in liquid nitrogen to stop the hydration reactions. Thereafter, the paste samples were placed under vacuum at -10°C . Under these conditions, the free water in the cement paste samples is transformed from a solid state to gas state without going through the liquid state. The use of freeze-drying instead of heat drying was to prevent the loss of any chemically bonded water.

CaCO_3 content was used to calculate the amount of LF that was consumed in the chemical reaction. The initial CaCO_3 content (prior to mixing), expressed in percentage by weight (wt%), was calculated according to Equation 3. The final CaCO_3 content was calculated using TG/DTA mass loss at approximately 680 to 800°C as presented in Equation 4 (Maria 2011). The amount of reacted LF was calculated using Equation 5.

$$\text{Initial CaCO}_3 \text{ Content (wt\%)} = \frac{\text{Mass of LF}}{\text{Total Mass (cement+LF+water)}} \times 100 \quad (3)$$

$$\text{Final CaCO}_3 \text{ Content (wt\%)} = \text{Mass loss (680 – 800}^\circ\text{C)} \times \frac{\text{Molar Mass of CaCO}_3}{\text{Molar Mass of CO}_2} \quad (4)$$

$$\text{Reacted LF (wt)} = \text{Initial CaCO}_3 \text{ content} - \text{Final CaCO}_3 \text{ content} \quad (5)$$

Similarly, the initial content of Mg was calculated using Equations 6. Mass loss corresponding to the decomposition of Mg between 350 and 400°C was used to calculate the final Mg content as presented in Equation 7. $\text{Ca}(\text{OH})_2$ content was measured using TG/DTA mass loss between 450 to 500°C as presented in Equation 8 (Maria 2011).

$$\text{Initial Mg Content (wt\%)} = \frac{\text{Mass of Mg}}{\text{Total Mass (cement+Mg+water)}} \times 100 \quad (6)$$

$$\text{Final Mg Content (wt\%)} = \text{Mass loss (350 – 400}^\circ\text{C)} \times \frac{\text{Molar Mass of Mg(OH)}_2}{\text{Molar Mass of H}_2\text{O}} \quad (7)$$

$$\text{Measured Ca(OH)}_2 \text{ Content (wt\%)} = \text{Mass loss (450 – 500}^\circ\text{C)} \times \frac{\text{Molar Mass of Ca(OH)}_2}{\text{Molar Mass of H}_2\text{O}} \quad (8)$$

2.4.3 Mortar compressive strength

For each mortar mixture, three cubes were tested at 16 hours and 28 days for compressive strength in accordance to ASTM C109-12.

2.4.4 X-Ray diffraction

The x-ray diffraction was used to identify the calcium monocarboaluminate phase. At 28 days, paste samples were dried in a vacuum oven at 38°C for 24 hours. Prior to x-ray testing, the samples were crushed and sieved to obtain a powder with particle size of less than $45\mu\text{m}$.

3. RESULTS AND DISCUSSION

3.1. Heat of hydration

The total heat released during the first 40 hours of hydration from each paste cured at 23°C and 55°C is presented in Figure 3. At curing temperature of 23°C, during the first 12 hours of hydration, mixes made with LF and Mg showed higher total heat released compared to control mixture made of 100% cement. At approximately 14 hours, the total heat released from all mixes were similar. After 14 hours, control mixture made of 100% cement showed higher total heat released compared to mixes made with LF and Mg. At curing temperature of 55°C, mix LF showed higher total heat released compared to mix Mg and control mixture made of 100% cement. Mix Mg showed higher total heat released in the first 18 hours of hydration compared to control mixture made of 100% cement. After 18 hours, mixes made with Mg and 100% cement had similar total heat released. The increase in the total heat released of HE cement paste with the addition of fine particles (i.e., LF and Mg) was due to the acceleration in hydration reaction which is in alignment with the literature (Kumar et al. 2013, Ye et al. 2007, Pera et al. 1999). The precipitation of the hydration products from the pore solution is assumed to be similar on the surface of LF and Mg particles since both materials have similar physical characteristics.

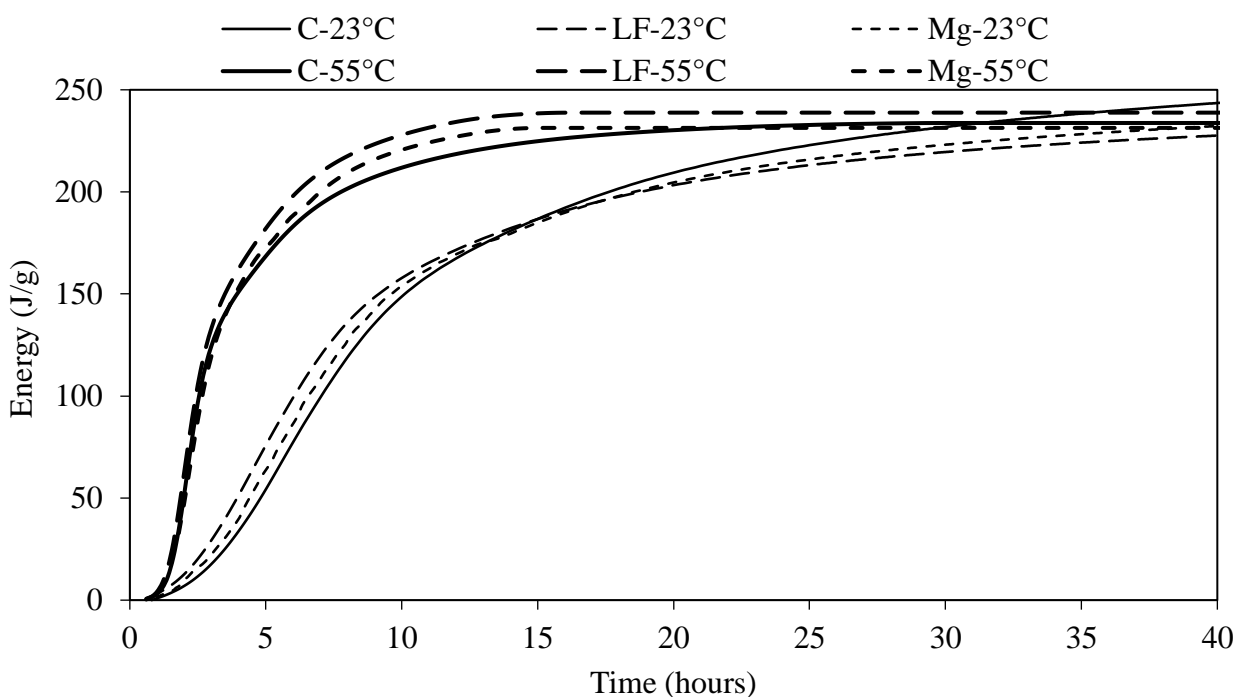


Figure 3. Effect of curing temperature (23°C and 55°C) on the total heat released of cement pastes

The physical effect of LF (the difference in the results between control mixture made of 100% cement and mix Mg) increased the heat of hydration compared to control mixture made of 100% cement. This increase is caused by the heterogeneous nucleation which causes acceleration in the hydration rate. The chemical effect of LF (the difference in the results between mix LF and mix Mg) showed an additional increase in the heat of hydration. This increase in heat of hydration was caused by the chemical reaction of LF and calcium aluminate which is an exothermic chemical reaction (Chowaniec 2012). The combined effect (physical and chemical) of LF was influenced by curing temperature. This was evident in total heat released after 40 hours where LF reduced the total heat released when cured at 23°C and increased the total heat released at 55°C compared to control mix made of 100% cement.

3.2. Thermal analysis

The thermal analysis was used to measure the amount of reacted LF and to confirm that Mg is chemically inert material. In addition, a relative evaluation of hydration products was conducted using $\text{Ca}(\text{OH})_2$ content. The mass loss from TG analysis and the DTA results are presented in Figures 4 and 5, respectively. Figure 4 presents the mass loss with temperature. Figure 5(a) presents DTA results for control mixture made with 100% cement while Figures 5(b) and (c) present DTA results for mixes made with LF and Mg, respectively. Based on the measured data, $\text{Ca}(\text{OH})_2$, CaCO_3 , and Mg contents were calculated using Equations 3 through 8. The results in Figures 4 and 5(b) showed that the addition of LF increased $\text{Ca}(\text{OH})_2$ content at 16 hours compared to control mixture made with 100% cement. The content of $\text{Ca}(\text{OH})_2$ increased from 7.4 wt% in control mixture made of 100% cement to 8.6 wt% in mix LF. This is expected as the additional surface area provided by LF acts as nucleation sites for the precipitation of the hydration products. This accelerates the hydration process resulting in a higher $\text{Ca}(\text{OH})_2$ content in mix LF compared to control mixture made of 100% cement. At 28 days, the $\text{Ca}(\text{OH})_2$ content in mix LF and control mixture made of 100% cement were approximately similar (11.9 wt% in control mixture made of 100% cement and 12.2 wt% in mix LF).

The amount of reacted LF in mix LF was 1.4 wt% at 16 hours and 2.5 wt% at 28 days. Dividing the amount of reacted LF by the initial CaCO_3 content yields the percentage of reacted LF to the total available LF in the system (11.8% at 16 hours and 21.6% at 28 days). The amount of the reacted LF at 16 hours was approximately 55% of the amount of reacted LF at 28 days. This indicates that the reaction of LF took place early during the hydration process and explains the higher heat of hydration in mix LF compared to mix Mg and control mixture made of 100% cement.

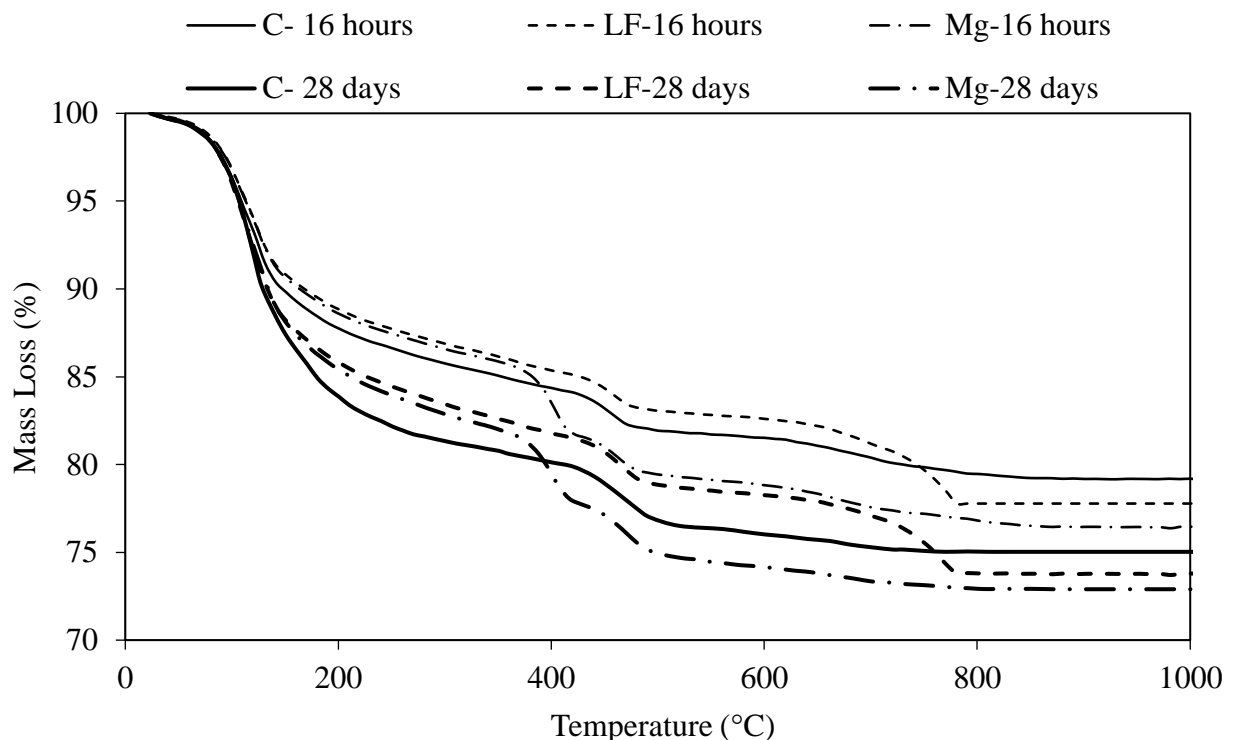


Figure 4. Effect of mixture design on the TG mass loss of cement pastes at 16 hours and 28 days.

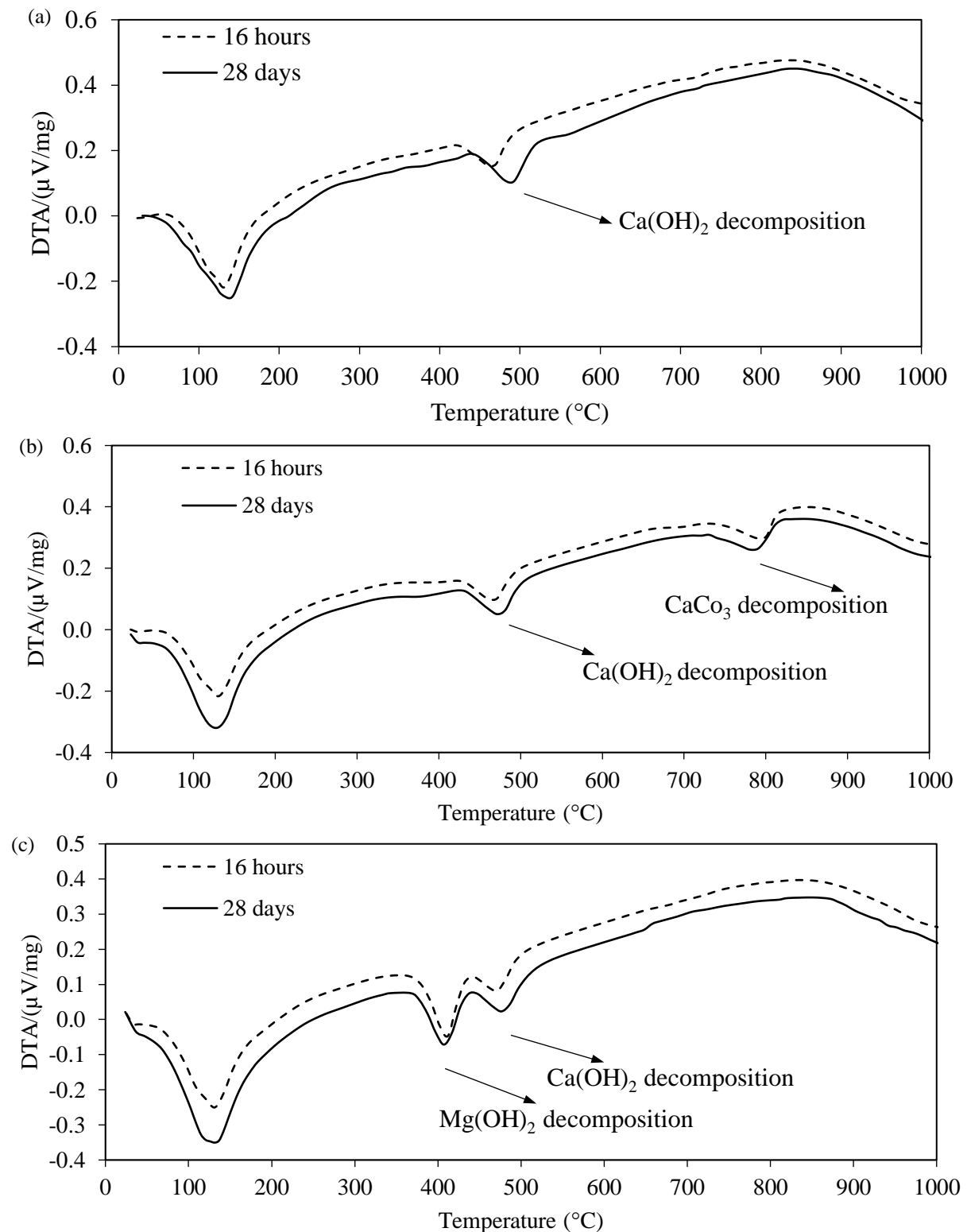


Figure 5. Effect of mixture design on DTA results of cement pastes at 16 hours and 28 days (a) 100% cement, (b) LF and (c) Mg

The addition of Mg also increased $\text{Ca}(\text{OH})_2$ content at 16 hours compared to control mixture made of 100% cement as presented in Figures 4 and 5(c). The content of $\text{Ca}(\text{OH})_2$ increased from 7.4 wt% in control mixture made of 100% cement to 8.2 wt% in mix Mg. This is due to the additional surface area provided by Mg that acts as nucleation sites. At 28 days, mix Mg and control mixture

made of 100% cement showed similar $\text{Ca}(\text{OH})_2$ content (11.9 wt%). The initial and final contents of Mg were similar (11.6 wt%) regardless of testing age (i.e., 16 hours or 28 days). This confirms the chemically inert behaviour of Mg.

3.3 X-Ray diffraction

The x-ray diffraction was used to confirm the presence of calcium monocarboaluminate in the hydrated cement paste in mix LF. Figure 6 presents the x-ray diffraction results for the control mix (Figure 6.a) and LF mix (Figure 6.b). The results showed that a peak at approximately $12^\circ 2\theta$ representing calcium mono-carboaluminate was observed in mix LF while monosulfate peak was observed in the x-ray diffraction results of the control mix.

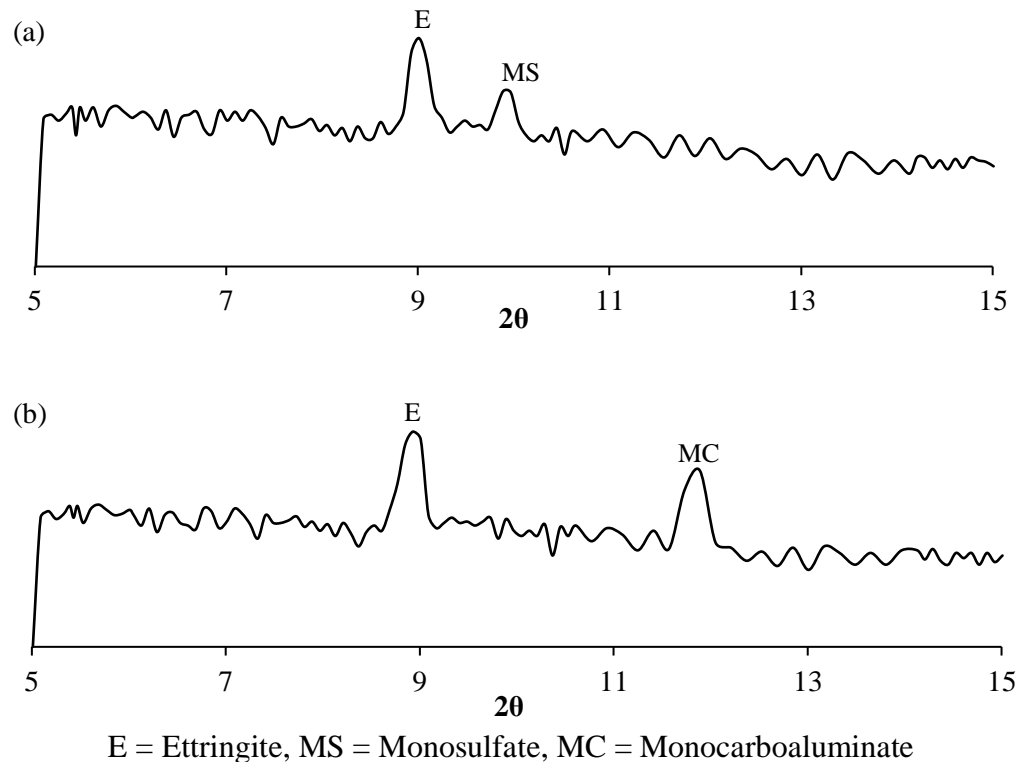


Figure 6: X-Ray diffraction analysis of cement pastes at 28 days (a) 100% cement and (b) LF

3.4. Compressive strength of mortar

The results of the cube compressive strength of mortars at 16 hours and 28 days are presented in Figure 7. Each column in the figure represents the average of three tests. The coefficients of variation were below 5%. At 16 hours, the addition of LF and Mg increased the cube compressive strength by 7% and 3%, respectively. At 28 days, the strength of all mixes was approximately similar (90 to 94 MPa).

The increase in the 16-hour compressive strength with the addition of Mg (physical effect of LF) was caused by two factors. Firstly, the fine particles of Mg fill the voids between the larger particles which reduces the porosity and increase the strength. Secondly, the increase in hydration rate with the addition of Mg increases the hydration products and thus reduces the porosity and increase the strength. This agrees with the results obtained from the heat of hydration, and thermal analysis. The chemical effect of LF (the difference between mix LF and mix Mg) showed that the production of calcium mono-carboaluminate increases the strength at 16 hours. Although a distinct effect of LF and Mg was observed in heat of hydration, thermal analysis, and compressive strength results at 16 hours, no effect was observed at 28 days. This is due to dilution effect which is in alignment with the literature (Irassar 2009, Tsvivilis et al. 2003, Kenai et al. 2004).

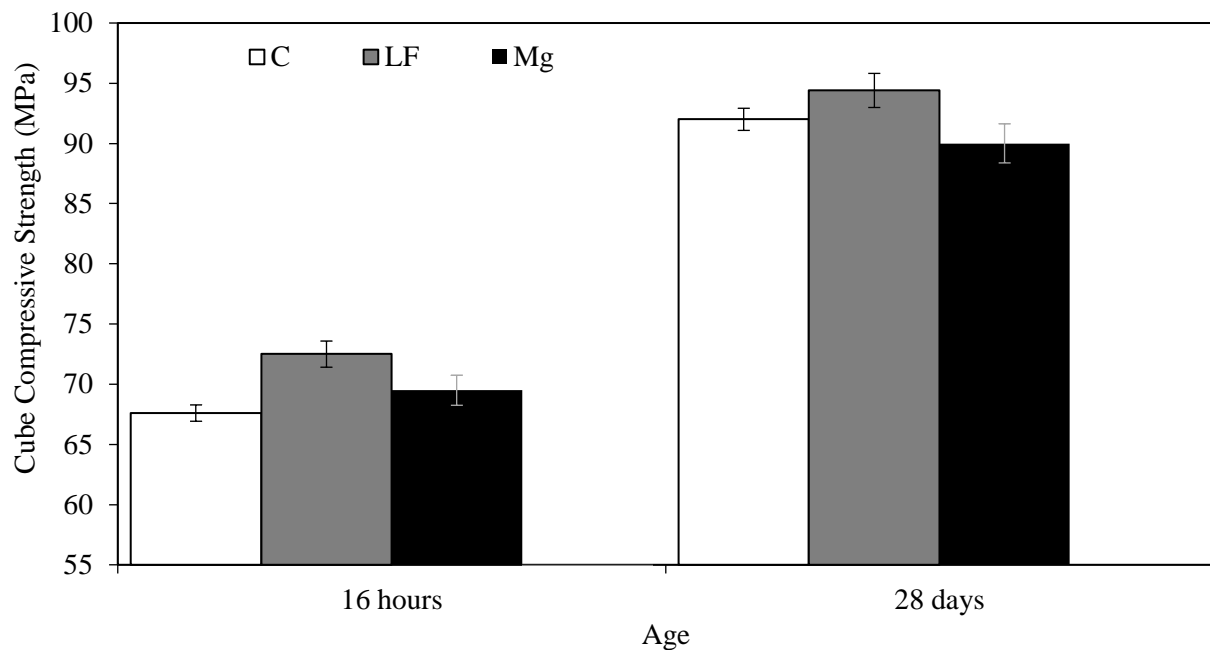


Figure 7. Effect of effect of LF and Mg filler on the cube compressive strength of mortars at 16 hours and 28 days compared to control mix

3.5. Physical and chemical effects of LF

LF has physical and chemical effects that influence the properties of concrete. These effects occur simultaneously and is difficult to evaluate the contribution of each effect individually. However, by using an inert material such as Mg with similar physical properties to LF, the physical and chemical effects of LF could be decoupled. The thermal analysis confirmed the chemically inert behavior of Mg. The difference in performance between mix LF (physical and chemical effects) and mix Mg (physical effect) defines the influence of the chemical effect of LF (i.e., calcium mono-carboaluminate). In the following discussion, the combined effect of modification of particle size distribution, dilution and heterogeneous nucleation is referred to as the physical effect of LF whereas the chemical reaction of LF is referred to as the chemical effect of LF.

At 16 hours, the physical and chemical effects of LF increased the compressive strength of mortar. At 28 days, the physical effect of LF had a negative impact on the compressive strength of mortar. To the contrary, the chemical effect of LF increased the compressive strength of mortar. Further study is required to examine the interplay between the permeability, sorptivity, and pore distribution.

4. CONCLUSION

The following conclusions are drawn from the results of this study:

- The physical effect of LF increases the compressive strength of mortar at 16 hours. This increase is due to the acceleration in the hydration rate and reduction in the porosity. However, the increase in the compressive strength of mortar was diminished at 28 days due to the dilution effect.
- The reactivity of LF and the production of calcium mono-carboaluminate had an important role in enhancing the compressive strength and microstructure of mortar specimens at 16 hours and at 28 days.

5. ACKNOWLEDGMENTS

This research was supported by the Ministry of Transportation of Ontario Highway Infrastructure Innovations Funding Programme. Opinions expressed in this report are those of the authors and may not necessarily reflect the views and policies of the Ministry of Transportation of Ontario. The authors would like to acknowledge NSERC Research Tools and Instruments Research Grant for the environmental chamber. The authors would like to acknowledge Holcim Canada for providing the cement and Omya Canada for providing the limestone, Euclid Admixture Canada Inc. for providing the chemical admixtures and Dufferin Aggregates for providing the sand and coarse aggregate.

6. REFERENCES

- ASTM International (2010). “*ASTM C1202: Standard test method for electrical indication of concrete's ability to resist chloride ion penetration.*”, West Conshohocken, PA, USA.
- ASTM International (2012). “*ASTM C109: Standard test method for compressive strength of hydraulic cement mortars (Using 2-in. or [50-mm] Cube Specimens).*”, West Conshohocken, PA, USA.
- ASTM International (2013). “*ASTM C1585: Standard test method for measurement of rate of absorption of water by hydraulic-cement concretes.*”, West Conshohocken, PA, USA.
- ASTM International (2009). “*ASTM C1702: Standard test method for measurement of heat of hydration of hydraulic cementitious materials using isothermal conduction calorimetry.*”, West Conshohocken, PA, USA.
- Benhelal, E., Zahedi, G., Shamsaei, E., Bahadori A., (2013). “*Global strategies and potentials to curb CO₂ emissions in cement industry.*” *Journal of Cleaner Production*, 51, 142–161. <https://doi.org/10.1016/j.jclepro.2012.10.049>
- Bentz, D. (2006), “*Modeling the influence of limestone filler on cement hydration using CEMHYD3D.*” *Cement and Concrete Composites*, 28 (2), 124–129. <https://doi.org/10.1016/j.cemconcomp.2005.10.006>
- Bentz, D., Irassar, E., Bucher, B., Weiss, W., (2009). “*Limestone fillers conserve cement: part 1: an analysis based on power's model.*” *Concrete International*, 31 (11), 41–46.
- Brunetaud, X., Linder, R., Divet, L., Duragrin, D., Damidot, D. (2006). “*Effect of curing conditions and concrete mix design on the expansion generated by delayed ettringite formation.*” *Materials and Structures*, 40 (6), 567–578. <https://doi.org/10.1617/s11527-006-9163-3>
- BIBM (2014), *European Precast Concrete Factbook*, 1–12. URL: <https://bibm.eu/wp-content/uploads/2019/07/BIBM-Factbook-2014.pdf>
- Celik, K., Meral, C., Petek Gursel, A., Mehta, P. K., Horvath, A., Monteiro, P. J. M. (2015). “*Mechanical properties, durability, and life-cycle assessment of self-consolidating concrete mixtures made with blended Portland cements containing fly ash and limestone powder.*” *Cement and Concrete Composites*, 56, 59–72. <https://doi.org/10.1016/j.cemconcomp.2014.11.003>
- Chowaniec, O., (2012). “*Limestone addition in cement.*” Doctoral Thesis, École Polytechnique Fédérale de Lausanne, Lausanne, Switzerland.
- Canadian Standards Association (CSA) (2009). “*A23.1/A23.2: Concrete materials and methods of concrete construction/test methods and standard practices for concrete.*”, Ottawa, Canada.
- Canadian Standards Association (CSA) (2014). “*A23.1/A23.2: Concrete materials and methods of concrete construction/test methods and standard practices for concrete.*”, Ottawa, Canada.
- Esmailkhanian, B., Khayat, K. H., Yahia, A., Feys, D. (2014). “*Effects of mix design parameters and rheological properties on dynamic stability of self-consolidating concrete.*” *Cement and Concrete Composites*, 54, 21-28, <https://doi.org/10.1016/j.cemconcomp.2014.03.001>

- Ezziane, K., Kadri, E., Hallal, A., Duval, R. (2010). “*Effect of mineral additives on the setting of blended cement by the maturity method.*” *Materials and Structures*, 43(3), 393–401. <https://doi.org/10.1617/s11527-009-9498-7>
- Gao, F. (2012). “*Advances in polymer nanocomposites, types and applications*”. 1st ed. Woodhead Publishing, England.
- Hawkins, P., Tennis, P., Detwiler, R., (2003). “*The use of limestone in Portland cement: a state-of-the-art review.*” EB227, The Portland Cement Association (PCA), 5–36. ISBN: 0-89312-229-7.
- Hooton, D., Nokken, M., Thomas, M., (2007). “*Portland-limestone cement: state-of-the-art report and gap analysis for CSA A 3000.*” SN3053, Cement Association of Canada, 1–59.
- Irassar, E. (2009). “*Sulfate attack on cementitious materials containing limestone filler - a review.*” *Cement and Concrete Research*, 39 (3), 241–254. <https://doi.org/10.1016/j.cemconres.2008.11.007>
- Kakali, G., Tsvivilis, S., Aggeli, E., and Bati, M., (2000). “*Hydration products of C₃A, C₃S and Portland cement in the presence of CaCO₃.*” *Cement and Concrete Research*, 30 (7), 2–6. [https://doi.org/10.1016/S0008-8846\(00\)00292-1](https://doi.org/10.1016/S0008-8846(00)00292-1)
- Kenai, S., Soboyejo, W., Soboyejo, A. (2004). “*Some engineering properties of limestone concrete.*” *Materials and Manufacturing Processes*, 19 (5), 949–961. <https://doi.org/10.1081/AMP-200030668>
- Kumar, A., Oey, T., Falla, G. P., Henkensiefken, R., Neithalath, N., Sant, G. (2013). “*A comparison of intergrinding and blending limestone on reaction and strength evolution in cementitious materials.*” *Construction and Building Materials*, 43, 428–435. <https://doi.org/10.1016/j.conbuildmat.2013.02.032>
- Kuzel, H., Baier, H. (1996). “*Hydration of calcium aluminate cements in the presence of calcium carbonate.*” *European Journal of Mineralogy*, 8(1), 129–141. <https://doi.org/10.1127/ejm/8/1/0129>
- Lin, F., Meyer, C. (2009). “*Hydration kinetics modeling of Portland cement considering the effects of curing temperature and applied pressure.*” *Cement and Concrete Research*, 39 (4), 255–265. <https://doi.org/10.1016/j.cemconres.2009.01.014>
- Maria, F. (2011). “*Handbook of thermogravimetric system of minerals and its use in geological practice.*” Geological Institute of Hungary, Budapest, 13–55. ISBN 978-963-671-288-4.
- Mohammadi, J., South, W. (2016). “*Effects of intergrinding 12% limestone with cement on properties of cement and mortar.*” *Journal of Advanced Concrete Technology*, 14 (5), 215–228. <https://doi.org/10.3151/jact.14.215>
- Moir, G., Kelham, S. (1993). “*Performance of limestone-filled cements.*” Building Research Establishment report. Her Maj.'s Stat. Off. London, Watford, 245, ISBN: 0851255671
- Moore, J., Stanitski, C., Jurs, P. (2009). “*Principles of chemistry: the molecular science.*” 1st ed., Brooks Cole, USA, 143–148. ISBN0495390798.
- Péra, J., Husson, S., Guilhot, B. (1999). “*Influence of finely ground limestone on cement hydration.*” *Cement and Concrete Composites*, 21 (2), 99–105. [https://doi.org/10.1016/S0958-9465\(98\)00020-1](https://doi.org/10.1016/S0958-9465(98)00020-1)
- Ramezaniapour, A. M., Hooton, R. D. (2013). “*Sulfate resistance of Portland-limestone cements in combination with supplementary cementitious materials.*” *Materials and Structures*, 46 (7), 1061–1073. <https://doi.org/10.1617/s11527-012-9953-8>
- Santhanam, M. (2013). “*Performance of cement-based materials in aggressive aqueous environments.*” RILEM State-of-the-Art Reports, 10, 75–90.
- Schmidt, M. (1992). “*Cement with interground additives– capabilities and environmental relief, part I.*” *Zement- Kalk-Gips*, 45 (2), 64–69.
- Sellevoid, E., Bager, D., Klitgaard-Jensen, E., Knudsen, T. (1982). “*Silica fume-cement pastes: hydration and pore structure.*” *Condensed Silica Fume in Concrete*, Institutt for Bygningsmateriallære, Norges Tekniske Høgskole, Norway, BML 82.610, 19–50.

- Sirisawat, I., Baingam, L., Saengsoy, W., Krammart, P., and Tangtermsirikul, S. (2014). “*Sodium and magnesium sulfate resistance of mortars with interground limestone and limestone powder replacing cements*”. *Journal of Advanced Concrete Technology*, 12 (10), 403-412. <https://doi.org/10.3151/jact.12.403>
- Tennis, P. D., Thomas, M. D. A., Weiss, W. J. (2011), *State-of-the-Art Report on Use of Limestone in Cements at Levels of up to 15%*, SN3148, Portland Cement Association, Skokie, Illinois, USA, 78 pages.
- Tikkanen, J., Cwirzen, A., and Penttala, V. (2011). “*Mineral powder concrete – effects of powder content on concrete properties.*” *Magazine of Concrete Research*, 63 (12), 893–903. <https://doi.org/10.1680/mac.10.00048>
- Tsivilis, S., Tsantilas, J., Kakali, G., Chaniotakis, E., and Sakellariou, A. (2003). “*The permeability of Portland limestone cement concrete.*” *Cement and Concrete Research*, 33 (9), 1465–1471. [https://doi.org/10.1016/S0008-8846\(03\)00092-9](https://doi.org/10.1016/S0008-8846(03)00092-9)
- Geological Survey, U. S. (2014). *Mineral commodity summaries*; February. <https://doi.org/10.3133/70100414>
- Wang, J. (2010). “*Hydration mechanism of cements based on low-CO₂ clinkers containing belite, ye’elimite and calcium alumino-ferrite.*” PhD Thesis, University of Lille, France.
- Yang, C. C., Chiang, C. T. (2005). “*On the relationship between pore structure and charge passed from RCPT in mineral-free cement-based materials.*” *Materials Chemistry and Physics*, 93 (1), 202–207. <https://doi.org/10.1016/j.matchemphys.2005.03.044>
- Ye, G., Liu, X., De Schutter, G., Poppe, M., Taerwe, L. (2007). “*Influence of limestone powder used as filler in SCC on hydration and microstructure of cement pastes.*” *Cement and Concrete Composites*, 29 (2), 94–102. <https://doi.org/10.1016/j.cemconcomp.2006.09.003>
- Zhang, T., Vandeperre, L. J., Cheeseman, C. R (2014). “*Formation of magnesium silicate hydrate (M-S-H) cement pastes using sodium hexametaphosphate.*” *Cement and Concrete Research*, 65, 8–14. <https://doi.org/10.1016/j.cemconres.2014.07.001>
- Zhange, P., Li, S. X., and Zhange, Z. F. (2011). “*General relationship between strength and hardness.*” *Materials Science and Engineering: A*, 529, 62–73. <https://doi.org/10.1016/j.msea.2011.08.061>

Synergetic effect of a super-absorbent polymer and a calcium nitrite corrosion inhibitor in high performance concrete durability

A. Durán-Herrera*^{id}, J. A. Canul-Polanco^{id}, R. Dávila-Pompermayer^{id},
L. G. López-Yépez^{id}, P. Valdez-Tamez^{id}

*Contact author: alejandro.duranhr@gmail.com

DOI: <https://doi.org/10.21041/ra.v10i2.450>

Reception: 22/11/2019 | Acceptance: 05/03/2020 | Publication: 30/04/2020

ABSTRACT

In this research, the synergetic effect of a super-absorbent polymer in combination with a calcium nitrite corrosion inhibitor were evaluated as a combined technology to improve concrete durability in High Performance Concrete. For this purpose, Portland cement mortars with a water/cement ratio of 0.4 and a substitution of 9.5% of cement by silica fume were produced. The effect of this technologies was evaluated by measuring the following parameters: autogenous and drying shrinkage, surface electrical resistivity and the non-steady-state chloride migration coefficient. The results indicate that the synergistic effect of SAP + CNI improves autogenous shrinkage and surface electrical resistivity.

Keywords: high performance concrete; super-absorbent polymer; calcium nitrite corrosion inhibitor; silica fume; durability.

Cite as: Durán-Herrera, A., Canul-Polanco, J. A., Dávila-Pompermayer, R., López-Yépez, L. G., Valdez-Tamez, P. (2020), "Synergetic effect of a superabsorbent polymer and a calcium nitrite corrosion inhibitor in high performance concrete durability", Revista ALCONPAT, 10 (2), pp. 206 – 218, DOI: <https://doi.org/10.21041/ra.v10i2.450>.

¹ Universidad Autónoma de Nuevo León, Facultad de Ingeniería Civil, Nuevo León, México.

Legal Information

Revista ALCONPAT is a quarterly publication by the Asociación Latinoamericana de Control de Calidad, Patología y Recuperación de la Construcción, Internacional, A.C., Km. 6 antigua carretera a Progreso, Mérida, Yucatán, 97310, Tel.5219997385893, alconpat.int@gmail.com, Website: www.alconpat.org

Responsible editor: Pedro Castro Borges, Ph.D. Reservation of rights for exclusive use No.04-2013-011717330300-203, and ISSN 2007-6835, both granted by the Instituto Nacional de Derecho de Autor. Responsible for the last update of this issue, Informatics Unit ALCONPAT, Elizabeth Sabido Maldonado, Km. 6, antigua carretera a Progreso, Mérida, Yucatán, C.P. 97310.

The views of the authors do not necessarily reflect the position of the editor.

The total or partial reproduction of the contents and images of the publication is strictly prohibited without the previous authorization of ALCONPAT Internacional A.C.

Any dispute, including the replies of the authors, will be published in the first issue of 2021 provided that the information is received before the closing of the third issue of 2020.

Efecto sinérgico de un polímero súper-absorbente y un aditivo inhibidor de la corrosión base nitrito de calcio en la durabilidad del concreto de alto desempeño

RESUMEN

En esta investigación, se evaluó el efecto sinérgico de un polímero súper-absorbente en conjunto con un inhibidor de corrosión de nitrito de calcio, como una tecnología combinada para mejorar la durabilidad de un Concreto de Alto Desempeño. Para este propósito, se produjeron morteros de cemento Portland con una proporción de agua/cemento de 0.4 y una sustitución de 9.5% de cemento por microsilíce. El efecto de estas tecnologías fue evaluado midiendo los siguientes parámetros: las retracciones autógena y por secado, la resistividad eléctrica superficial y el coeficiente de migración de cloruros en estado no estacionario. Los resultados indican que el efecto sinérgico del SAP + CNI mejora la retracción autógena y la resistividad eléctrica superficial.

Palabras clave: concreto de alto desempeño; polimeropolímero súper-absorbente; anhibidorinhibidor de la corrosión base nitrito de calcio; microsilíce; durabilidad.

Efeito sinérgico de um polímero super absorvente e um aditivo inibidor de corrosão à base de nitrito de cálcio na durabilidade do concreto de alto desempenho

RESUMO

Nesta pesquisa, o efeito sinérgico de um polímero super absorvente (SAP) e um inibidor de corrosão do nitrito de cálcio (CNI) foi avaliado como uma tecnologia combinada para melhorar a durabilidade do Concreto de Alto Desempenho. Para isso, foram produzidas argamassas de cimento Portland com uma relação água/cimento de 0,4 e uma adição de 9,5% de sílica ativa. O efeito dessas tecnologias foi avaliado medindo-se os seguintes parâmetros: retração autógena e por secagem, resistividade elétrica da superfície e coeficiente de migração de cloretos em estado não estacionário. Os resultados indicam que o efeito sinérgico do SAP + CNI melhora a retração autógena e a resistividade elétrica superficial.

Palavras-chave: concreto de alto desempenho; polímero super absorvente; inibidor de corrosão baseado em nitrito de cálcio; microsilíce; durabilidade.

1. INTRODUCTION

It is well known that high performance concrete (HPC) has better mechanical and durability properties than conventional concrete (Zhutovsky S. et. al., 2012). In HPC, supplementary cementitious materials (SCM), such as silica fume (SF) are commonly used to achieve a superior performance in terms of mechanical and durability performance (Lothenbach B. et. al., 2011). However, despite these benefits, the presence of silica fume in HPC could adversely originate early age cracking attributed to the hydration process (Pendergrass B. et. Al., 2014).

Calcium nitrite admixtures (CNI) are used as corrosion inhibitors since the 1980's to extend the service life of reinforced concrete, and are commonly used in HPC for marine constructions (Gaidis J.M., 2004). In the presence of CNI, concrete setting times could be delayed (M.A. Quraishi, et. al., 2016; Hansson C.M. et al., 1998), but in this work we are expecting that the presence of SF could counteract this delay.

Because the fineness of SF, it is well knowknown that in the presence of this SCM, concrete shrinkage will be increased, mainly at early ages. With the inclusion of CNI we are expecting that

shrinkage could be further augmented and consequently the a reduction of the potential durability. Therefore, a proposed solution to this issue could be the implementation of internal curing trough a superabsorbent polymer (SAP).

For the positive results it has shown to mitigate early age shrinkage (Snoeck D. et al., 2015), internal curing is known as a feasible technology to diminish the early age cracking of HPC (Craeye B. et al., 2011; Cusson D. et al., 2010). TheseThis technology consists in the introduction of a porous material within the fresh concrete, a highly porous material that could absorb a significant amount of water that will be released within the porous network of concrete as the relative humidity and internal pore pressure decreases. For this purpose, superabsorbent polymers and lightweight aggregates are the most common agents used to implement internal curing (Jensen O. et. Al al., 2001). However, the use of SAP has proved a better performance in terms of water absorption capacity (Mechtcherine V. et. Al al., 2012).

To implement this technology in HPC, the dosage of superabsorbent polymer that should be used could be determined through the modified Powers hydration model (T.C. Powers, et. Al al., 1948; Jensen O. et al., 2000; Jensen O. et al., 2002), a model that is explained by two different hydration systems, an open water-entrained system and a closed system isolated from an external source of water. Figure 1 illustrates the importance of internal curing in HPC, because in this concretes, the higher densification level of the cementitious matrix will prevent external curing to be effective (water penetration) through all the depth of concrete, a condition that could be solved through the implementation of internal curing.

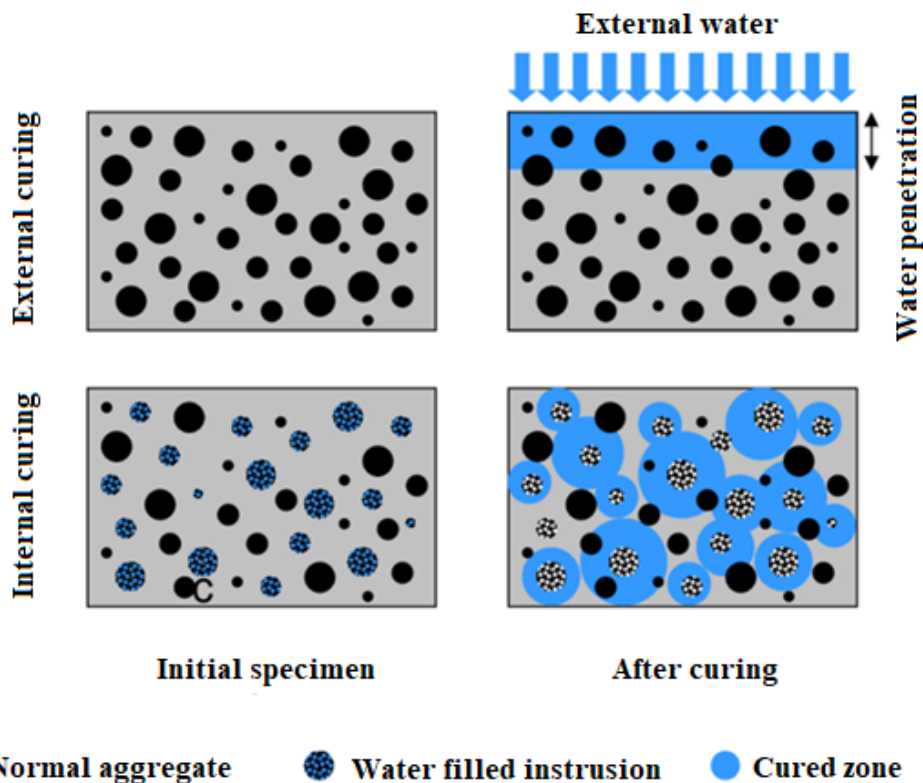


Figure 1. Internal water curing vs external water curing in HPC (I. De la Varga et al., 2012)

Hence, returning to the concern of the use of CNI and SF in concrete. Because CNI could modify the setting time and hydration rate of a cementitious matrix (M.A. Quraishi, et al., 2016; Hansson C.M. et al., 1998), it is expected that the internal curing method with SAP could decrease these mentioned effects.

Most of the published research work about the effect of CNI in portland cement based concrete, evaluate the effect of this admixture through corrosion electrochemical tests, but leave aside the

evaluation of the effect of this admixture regarding setting times and hydration rate (Hansson C.M. et al., 1998). In this project, is expected that the internal curing method with SAP will influence the hydration of the cementitious system and counteract the setting times delay associated to the presence of CNI, therefor it was mainly focused in the evaluation of the synergetic effect of CNI and SAP in fresh and hardened stage properties of an HPC with SF, such as: autogenous shrinkage, drying shrinkage, surface electrical resistivity and the non-steady chloride migration coefficient.

2. PROCEDURE

Materials used for the production of the mortars:

- An ASTM C 150 Type V Ordinary Portland cement (OPC), with a Blaine fineness of 363 m²/kg, a specific gravity of 3.1 and a loss on ignition (LOI) of 3.37 %.
- An ASTM C 1240 dry condensed silica fume (SF) with a BET specific surface area of 21.63 m²/g, a specific gravity of 2.2, a LOI of 2.63 % and a SiO₂ content of 95 %.
- An ASTM C 33 crushed limestone aggregate (FA) from Monterrey, Mexico, with a maximum nominal size of 5 mm, a dry specific gravity of 2.61 and a water absorption of 2.2%.
- A polyacrylamide-potassium polyacrylate super absorbent polymer (SAP) with an absorption of 25 g/g, a specific gravity of 1.004 and a desorption of 90% in pore solutions extracted from a set of ten cementitious pastes (Type V OPC + SF) with a water-to-binder ratio (w/b) of 0.4 and a silica fume dosage of 9.5 % in substitution of the mass of Portland cement.
- A poly-carboxylate based superplasticizer (SP) with a solids content of 51.8%, a specific gravity of 1.1.
- A calcium nitrite corrosion inhibitor admixture (CNI) with a solids content of 51.6% and a specific gravity of 1.3.

Mortars were prepared with a w/c of 0.40 and a silica fume addition of 9.5% by mass. The paste proportions were established according to the modified hydration Powers model for Portland Cement-Silica Fume (PC-SF) cementitious systems (T.C. Powers, et. Al., 1948; Jensen O. et al., 2000; Jensen O. et al., 2002), that analytically evaluate the hydration degree (α) for the same cementitious matrix exposed to an external open curing system or to an internal closed system isolated from the external curing water. For this project, the system was closed isolated with and without internal curing (see figure 2). The diagram in figure 2 present the volumetric phase distribution in a cementitious paste: capillary water, gel water (p_w) gel solid (b_w), and chemical shrinkage (CS). The CS and b_w were calculated by the Test ASTM C 1608 and thermogravimetric analysis (TGA) correspondingly. The gel water amount was considered 0.19 g/g for cement and 0.5 g/g for silica fume (Sellevold E. J. et al., 1998).

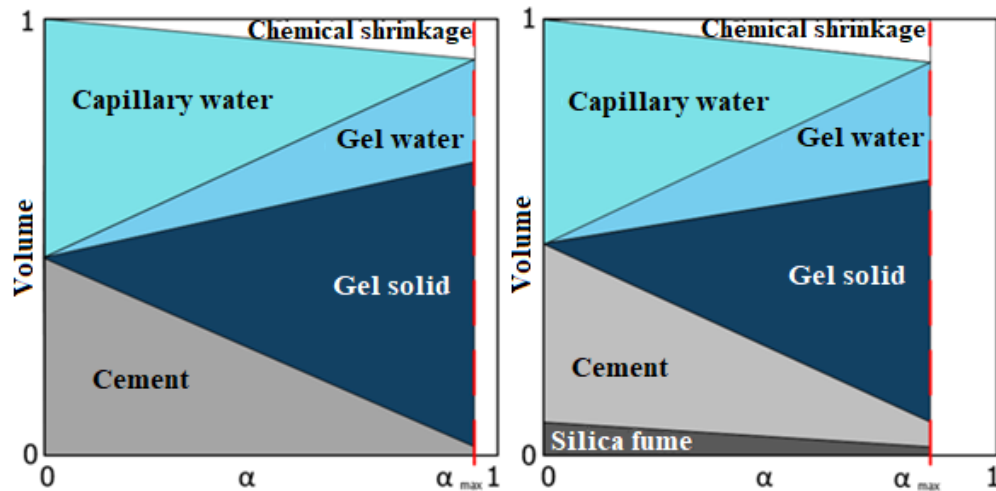


Figure 2. Volumetric phase distribution and hydration level in a cementitious paste with w/c of 0.4, without SF (left) and with SF (right), illustrated according to the Powers' model. In the figure it is observed how the volumetric phase distribution change with the hydration degree (α), in the presence of a SCM.

Equation 1 was used to calculate b_w :

$$b_w = (M_{1000\text{ }^\circ\text{C}} - M_{105\text{ }^\circ\text{C}} - M_{\text{CO}_2}) / (M_{1000\text{ }^\circ\text{C}} / \{1 - \text{LOI}_{\text{cem}}\}) \quad (1)$$

Where:

- $M_{1000\text{ }^\circ\text{C}}$ is the mass of the sample at 1000 °C in grams
- $M_{105\text{ }^\circ\text{C}}$ is the mass of the sample at 105 °C in grams
- M_{CO_2} is the mass loss due to decarbonation of the CaCO_3 , usually between 650-800 °C.
- LOI_{cem} is the loss of ignition of the cement

The required amount of internal curing water (IC_w) to mitigate autogenous shrinkage in a Portland cement-silica fume cementitious paste with a w/c ratio of 0.40 was calculated according to equations 2 and 3:

$$\text{IC}_w = (\text{Cem}) * (0.42 + 0.5 (s/c)) - (w/c) \quad (2)$$

$$\text{IC}_s = (\text{IC}_w / \text{abs}) / \text{des} \quad (3)$$

Where:

- Cem is the amount of cement in kg/m^3
- w/c is the water/cement ratio of the paste
- s/c the microsilica /cement ratio
- IC_w is the amount of internal curing water in kg/m^3
- IC_s is the amount of SAP in kg/m^3
- abs is the absorption of SAP in grams
- des is the desorption of SAP in grams

The dosage of CNI was 2% respect to the mass of the cementitious materials. A target consistency (spread) of 24 ± 1 cm was established for the whole set of mortar mixtures, and it was measured in the ASTM C 230 flow table, according to the procedure described in ASTM C 1437, but without the drops specified in the standard procedure. To maintain constant the water-to-cement ratio, the amount of water in the admixtures was considered as part of the reaction water. Mixtures were prepared in an epicyclical type mixer that meets the requirements of ASTM C 305, through the

following mixing procedure:

1. Materials were added to the mixer in the following order: fine aggregates, cement, silica fume, SAP and water. The mixing procedure begins 30 seconds after. For mixtures without SAP, mixing started immediately after the addition of water.
2. Then, materials were mixed at low speed for 4 minutes.
3. In this step, for mixture CNI, this admixture was dosed three minutes after mixing started (*without turning off the mixer*) and mixing continued for one additional minute at low speed.
4. After SP was dosed, mixing continued for one additional minute at low speed.
5. After an accumulated mixing time of 5 minutes, the mixer was turned off for 30 seconds to scrap the sides and bottom of the bowl with a trowel.
6. Then, the mixing process continued for three minutes at high speed.
7. *For mixture SAP + CNI, CNI was dosed at the beginning of this step (5.5 minutes after mixing started).*

For the whole set of mortars, the fresh stage properties characterization consisted on the determination of the consistency (spread) according to ASTM C 1437, but without any drop of the flow table; the air content and unit weight were determined according to ASTM C 85. Autogenous shrinkage was evaluated according to ASTM C 1698, after the final setting time of the concrete but in the mortar fraction of the material determined according ASTM C 403, and up to an age of 28 days. Measurements of the lineal autogenous strain was made by triplicate trough a flexible corrugated mold and a dilatometer.

The four mixtures evaluated in this work are identified according to the nomenclature that appears in table 1, and the proportions for all these mixtures, with the aggregated in dry condition are reported in table 2.

Table 1. Mixture identifications (ID)

ID	Materials
REF	PC + SF
SAP	PC + SF + SAP
CNI	PC + SF + CNI
SAP+CNI	PC + SF + SAP + CNI

Table 2. Mixture proportions in kg/m³, FA in dry condition

Mixture	OPC	SF	Water	IC _w	SP	FA	SAP	CNI
REF	485.1	46.1	225.7	----	3.2	1513.8	----	----
SAP	481.7	45.8	224.1	32.5	3.2	1414.3	1.4	----
CNI	485.8	46.1	220.9	----	3.2	1506.7	----	10.7
SAP+CNI	481.3	45.7	217.0	32.5	3.2	1404.3	1.4	10.6

At the end of the mixing process, prismatic specimens with dimensions of 50 x 50 x 250 mm, were casted for the determination of the drying shrinkage, according to ASTM C 596 (four samples were casted for each mixture); cylindrical specimens with dimensions of 10 cm in diameter by 20 cm in height, were casted to perform the surface electrical resistivity tests (SER) according to AASHTO TP 95, with a device that operates according to the Four-Point Wenner Array Probe Test (AASHTO TP 95, 2011), as well as the non-steady chloride migration coefficient according to NT Build 492). The results of these two methods present good correlations and are commonly reported as durability indexes of concrete and as an indicator of the cement paste quality (T.C. Powers, et. Al., 1948). Specimens were demolded at 24 hours and placed in a curing room that meets the required controlled conditions established by ASTM C 31 (23°C ± 2°C and RH ≥ 95%).

3. RESULTS AND DISCUSSION

3.1 Hydration parameters

For OPC and SF, the hydration parameters were obtained from the Powers Model (T.C. Powers, et al., 1948; Jensen O. et al., 2000; Jensen O. et al., 2002) through TGA (including the determination of the amount of calcium hydroxide, CH) and CS measurements, and were calculated according to equation 1-3. The results were used to calculate the internal curing water and the amount of SAP to be dosed and are summarized in in Table 3.

Table 3. Hydration parameters of the cementitious materials from TGA and CS measurements

Cementitious	b_w (g/g)	p_w (g/g)	CS (ml/100g)	CH g/g	(α)
OPC	0.23	0.19	6.03	0.16	1
SF	0	0.5	19.66	1.7	-----

Through equations 1-3 and the values reported for the hydration parameters in Table 3, theoretically indicate that in a closed system the cementitious paste (OPC and SF) will reach a α of 1 if the final w/c ratio is 0.47. In our experimental work, the cementitious paste was set to have a w/c ratio of 0.40 and an s/c of 0.095, therefore in order to reach a w/c of 0.47; the amount of internal curing water to add in terms of w/c ratio should be 0.07. The required mass of water for internal curing (ICw), and the required dosage of SAP to implement internal curing within the mortar, are reported in table 4.

Table 4. Parameters to calculate the amounts of ICw and SAP to implement internal curing in a closed water system.

w/c _{closed}	w/c	X	s/c	ICw (kg/m ³)	SAP (kg/m ³)
0.47	0.40	0.07	0.095	33.8	1.5

$$X = w/c_{\text{closed}} - w/c$$

3.2 Fresh stage properties

The fresh stage properties are presented in table 5. All the mixtures achieved the target spread of 24 ± 1 cm. The results of air content and unit weight exhibit that the substitution of sand by SAP increased the air content and subsequently decreased the unit weight. For mixtures CNI and CNI+SAP, the fresh stage properties were similar to the reference mixture.

Table 5. Fresh stage properties of mortars

Mixture	Spread (cm)	Air content (%)	Unit weight (kg/m ³)
REF	24	1.4	2359
SAP	24	2.1	2283
CNI	24	1.3	2358
CNI+SAP	23	2.4	2295

Table 6. Setting times

Mixture	Initial (min)	Final (min)
REF	220	285
SAP	297	383
CNI	195	245
SAP+CNI	248	307

Because it is known that CNI could have an influence on the setting times (Hansson C.M. et al., 1998) and that SAP could also decrease setting times, the determination of this property was included in the experimental program of this work. The results of setting times reported in Table 6 indicate that alone, the dosages of CNI accelerate the initial and final setting times by 25 and 40 minutes, and that SAP delay these setting times by 1h:17m and 1h:38m respectively. In mixture SAP+CNI, the combined effect leads to a negligible delay in the initial and final setting times, of 28 and 22 minutes respectively. The acceleration or delay in setting times originated by CNI, SAP and SAP+CNI are negligible and do not represent any problem for practical applications.

3.3 Autogenous and drying shrinkage.

The results of autogenous shrinkage (AS) presented in Figure 3 at ages of 64 hours and 28 days exhibit the great benefit of SAP to counteract AS by 97% and 89% respectively. The presence of CNI significantly increases AS by 89% and 78% respectively, but in combination with SAP this undesired performance was opposite counteracting the volumetric instability and leading to AS reductions of 79% and 69% respectively.

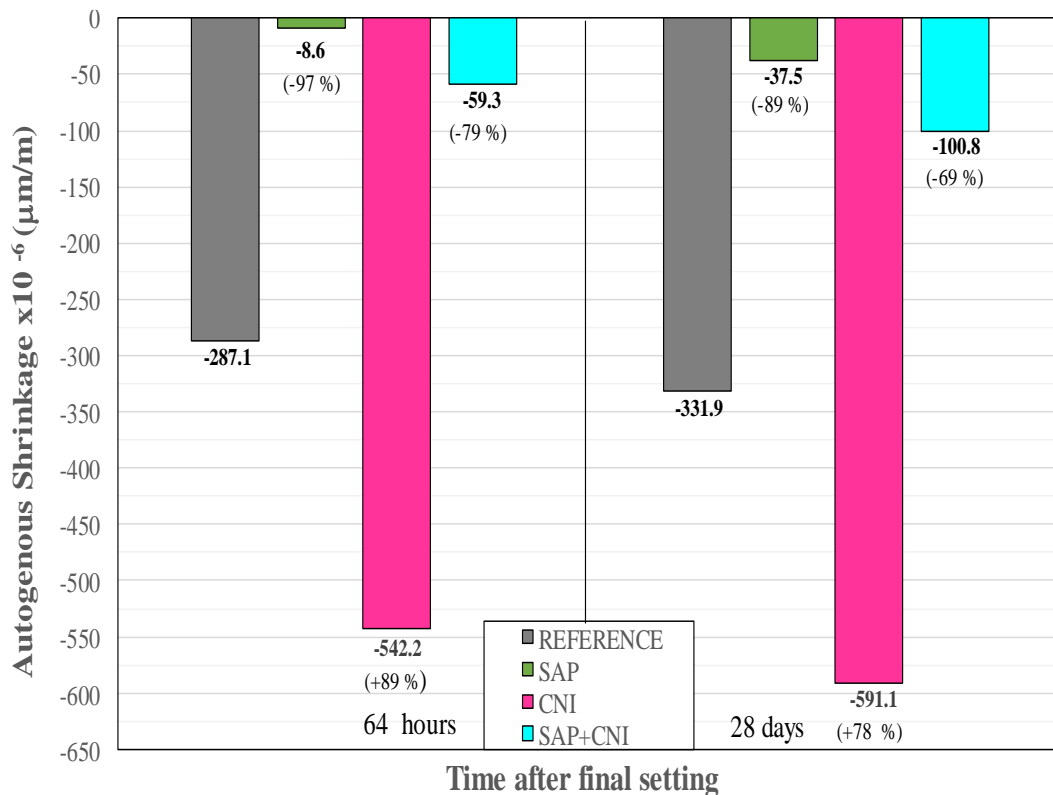


Figure 3. Autogenous shrinkage at 64 hours and 28 days

For Reference, SAP and CNI mixtures, the results of drying shrinkage (DS) reported in Figure 4, at an age of 70 days (595, 620 and 645 μm respectively), clearly illustrate that SAP and CNI do not have a mayor effect in this property, however, by combining the two admixtures, DS increases to 765 μm , representing a minor increase of 145 μm in comparison to the average DS of the other three mixtures (620 μm).

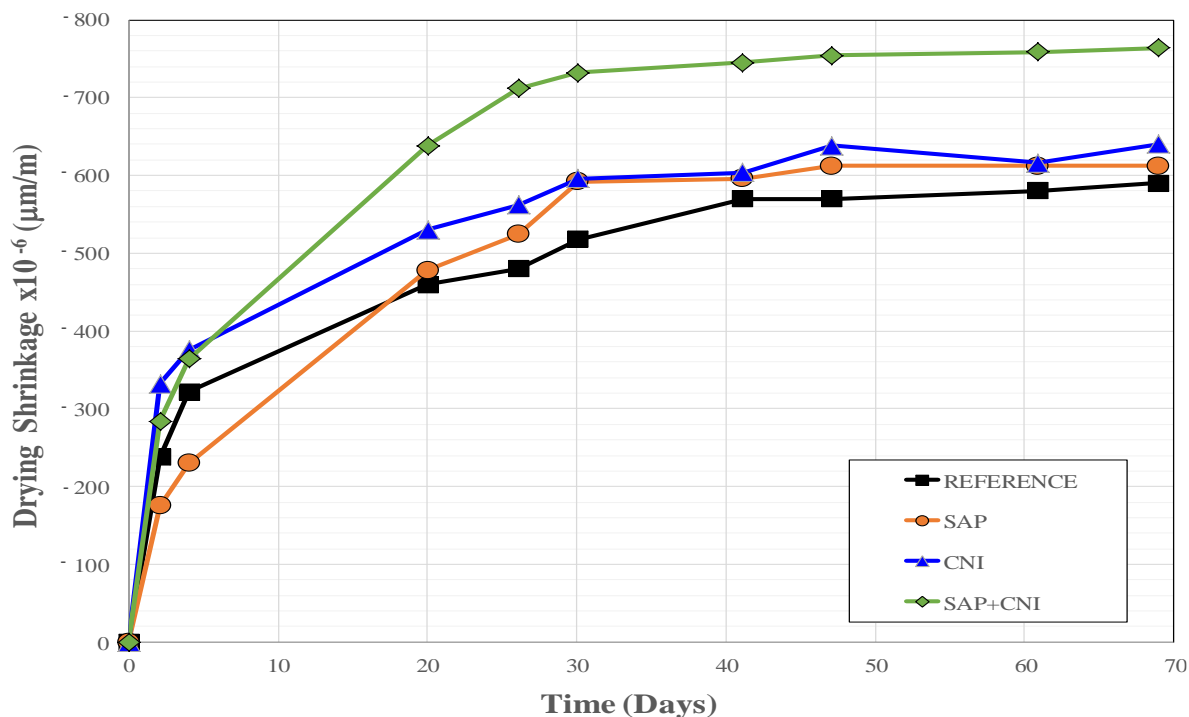


Figure 4. Drying shrinkage at the age 70 days

3.4 Surface electrical resistivity (SER) and chloride migration coefficient (D_{nssm})

The results reported in Figure 5, indicate that for all the ages reported in this figure, CNI slightly improved SER within a range of 10% to 13%. According to the qualitative classification reported in the standard test method for this tests AASHTO TP 95, the results for reference and CNI mixtures present a very low chloride Ion Permeability Potential. At 28 days, the presence of SAP originates a reduction of 36%, suggesting that the chloride ion permeability potential was affected and passes from very low to low, however at 70 and 114 days the reductions remains almost the same (38% and 32%), also that at this two ages the concrete recovers the very low chloride ion permeability potential. Mixture SAP + CNI presented a similar trend with reductions of 31%, 32% and 37% at the ages of 28, 70 and 114 days respectively.

Surface electrical resistivity is an indirect measure of both porosity and diffusivity. The electrical current flowing through the hydrated paste is due to an electrolytic process mainly resulting from the flow of ions present in the pore solution (K. O. Ampadu, et al., 1999) on the other hand, when the concentration of ionic species such as sodium and potassium decreases, this will lead to a decrease in ionic conductivity and therefore to an increase of the electrical resistivity (C. Shi, 2004). It seems that the increase of SER, originated by the presence of CNI, is the result of the decrease in the flow of electric current because of the probable decrease in ionic conductivity in the pore solution.

Among others, factors that affect SER results are porosity, water content, the presence of supplementary cementitious materials and the w/c ratio. For mixtures with CNI it is also important to highlight that this technique could provide slightly underestimated results (AASHTO TP 95, 2011).

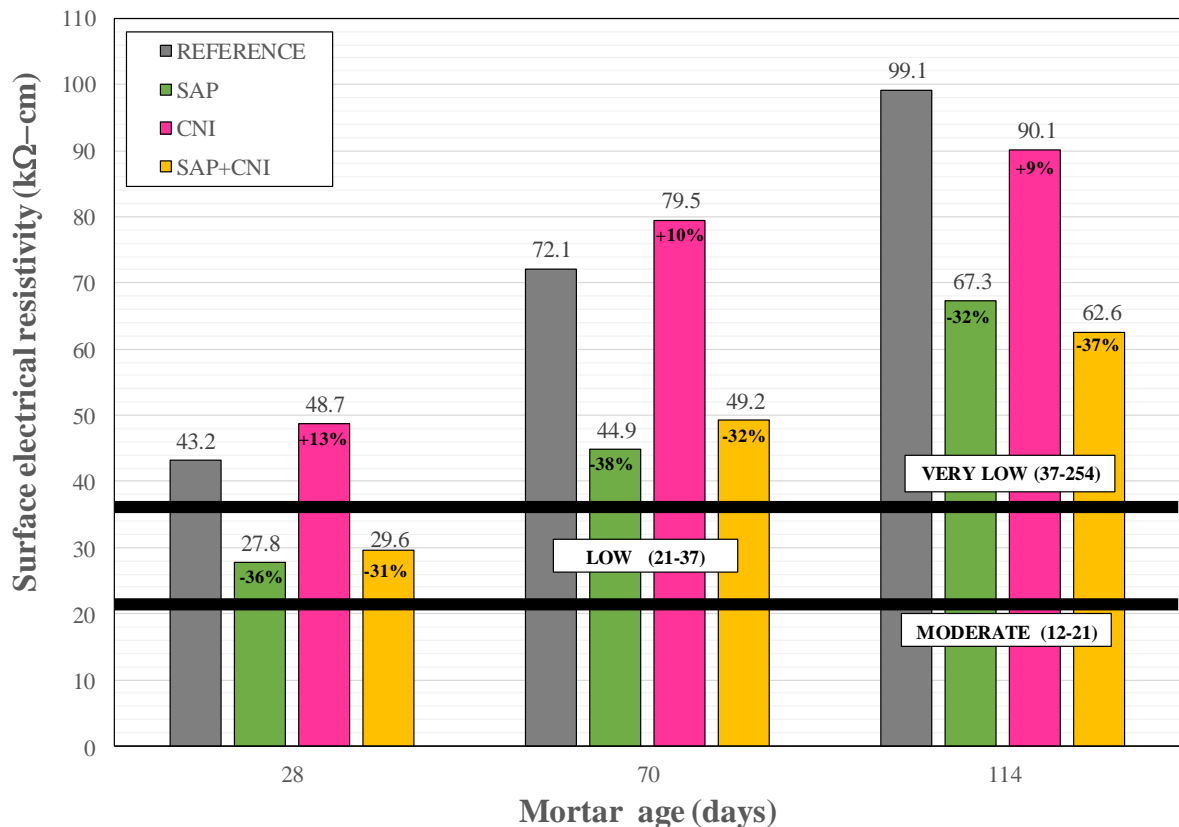


Figure 5. Development of surface electrical resistivity up to an age of 114 days, indication the three levels for the potential permeability of chloride ions according to AASHTO TP 95

Results in Table 7 indicate that the three technologies (SAP, CNI and SAP+CNI) increased D_{nssm} by 38, 30 and 122%. Even though, these increments could be perceived as very high, the qualitative classification established for this test method (Nilsson L., et al., 1998) indicate that for HPC with these technologies, the potential resistance to the ingress of chlorides is extremely high ($D_{nssm} < 2.5 \times 10^{-12} \text{ m}^2/\text{s}$) for mixtures SAP and CNI, and very high ($D_{nssm} = 2.2 - 5.0 \times 10^{-12} \text{ m}^2/\text{s}$) for mixture SAP+CNI. The coefficients of variation reported in table 7 are included as a reference of the uncertainty that could be expected for measurements made by triplicate.

Analysing the absolute differences for setting times, SER and D_{nssm} , we can observe that mixtures with SAP presented the higher values. This behaviour is attributed mainly to the increase in the water/cementitious ratio that could result during the very early ages, because it is considered that SAP does not effectively retain all calculated internal curing water, liberating part of it in a period comprised between the time when the specimens were casted and the time when the concrete reach its final setting time. Even though this slight adverse effect of SAP results, SER and D_{nssm} indicates that in terms of durability (qualitative) the effect is negligible.

Table 7. Chloride Migration Coefficient (D_{nssm}) at 114 days

Mixture	D_{nssm} ($\times 10^{-12} \text{ m}^2/\text{s}$)	Coefficient of variation (%)
REF	1.46	4.44
SAP	2.01	7.04
CNI	1.90	5.03
SAP+CNI	3.25	9.14

If the SAP voids are empty, ions have to travel a slightly longer route to pass the void, but if SAP voids are full with liquid, they may provide an expressway without obstacles for ion transport. However, the liquid in the void may be wholly or partly held within a swelled SAP particle and the transport properties in a swelled SAP particle are not known (Marianne T. H. et al., 2015). This statement could be the reason of the higher coefficients (D_{nssm}) obtained for the mixtures with SAP.

4. SUMMARY AND CONCLUSIONS

Based in the analysis of the results obtained for the mortars evaluated in this work, the following conclusions can be drawn:

- Results of surface electrical resistivity indicate that SAP has the most detrimental effect in terms of durability. Although, sooner or later, mixtures will be classified with a very low probability for the penetration of chloride ions (37-251 $k\Omega\text{-cm}$), SER results exhibit that the detrimental effect will delay the time when these mixtures reach this level of impermeability; 30 and 50 days after reference mixture respectively. CNI also induced a delay of 15 days.
- Even though the differences in absolute values, SAP and CNI did not affect the qualitative impermeability, presenting an extremely high probability to resist the ingress of chlorides ($D_{nssm} < 2.5 \times 10^{-2} \text{m}^2/\text{s}$). The combination of SAP and CNI slightly affected the impermeability of the materials, presenting a very high probability to resist the ingress of chloride ($D_{nssm} = 2.5 \text{ to } 5 \times 10^{-12} \text{m}^2/\text{s}$).
- The qualitative evaluation criteria for SER and CNI results indicate that in terms of durability the incorporation of SAP and/or CNI to an HPC with silica fume and a water/binder ratio of 0.40, don't reduce the durability of concrete.
- The detrimental effect of SAP exhibited by the results of setting times, surface electrical resistivity and chloride migration coefficient are attributed to an increase of the water/binder ratio by an unquantified amount of internal curing water added during the hydration process between the time when specimens were casted and the final setting times.

5. ACKNOWLEDGEMENTS

The authors wish to express their gratitude and sincere appreciation to the different organizations that contributed in the development of this project; to the Consejo Nacional de Ciencia y Tecnología de Mexico (CONACYT) for the scholarship granted to Jennifer A. Canul-Polanco, to the Scientific and Technological Research Program of the Universidad Autónoma de Nuevo León (PACyT-UANL) and to the Program for the Promotion and Consolidation of Technological Research and Development Projects of the Facultad de Ingeniería Civil (FIC-UANL). Also, the authors wish to express their gratitude to José Alfredo Rodríguez Campos, from HOLCIM México S.A. de C.V.; and to Filiberto Marin, from EUCOMEX S.A. de C.V., for providing the Portland cement and the Chemical admixtures respectively.

6. REFERENCES

- American Association of State Highway and Transportation Officials. (2011). *AASHTO TP 95: Standard Method of Test for Surface Resistivity Indication of Concrete's Ability to Resist Chloride Ion Penetration*. Washington, DC.
- Ampadu, K. O. Torii, K., Kawamura, M. (1999), *Beneficial effect of fly ash on chloride diffusivity of hardened cement paste*, *Cement and Concrete Research*, 29 (4), 585–590. [https://doi.org/10.1016/S0008-8846\(99\)00047-2](https://doi.org/10.1016/S0008-8846(99)00047-2)
- Craeye, B., Geirnaert, M., DeSchuttera, G. (2011), *Super absorbing polymers as an internal curing agent for mitigation of early-age cracking of high-performance concrete bridge decks*. *Construction and Building Materials*. 25, 1-13. <https://doi.org/10.1016/j.conbuildmat.2010.06.063>.
- Cusson, D., Lounis, Z., Daigle, L. (2010), *Benefits of internal curing on service life and life-cycle cost of high-performance concrete bridge decks – A case study*. *Construction and Building Materials*, 32, 339-350 <https://doi.org/10.1016/j.cemconcomp.2010.02.007>.
- De la Varga, Castro, J., Bentz, D., Weiss, J. (2012), *Application of internal curing for mixtures containing high volumes of fly ash*. *Cement & Concrete Composites*, 34 1001–1008, <https://doi.org/10.1016/j.cemconcomp.2012.06.008>.
- Gaidis, J. M. (2004). *Chemistry of corrosion inhibitors*. *Cement and Concrete Composites*, Vol. 26, pp. 181–189. [https://doi.org/10.1016/S0958-9465\(03\)00037-4](https://doi.org/10.1016/S0958-9465(03)00037-4).
- Hansson, C. M., Mammoliti, L. Hope, B. B. (1998). *Corrosion Inhibitors in concrete Part I - Principles*. *Cement and Concrete Research*, Vol. 28, No. 12, pp. 1775–1781. [https://doi.org/10.1016/S0008-8846\(98\)00142-2](https://doi.org/10.1016/S0008-8846(98)00142-2).
- Jensen, O., Hansen, P. F. (2001), *Water-entrained cement-based materials*, PCT Patent Application WO01/02317A1.
- Jensen, O., Hansen, P. F. (2001), *Water-entrained cement-based materials I. Principles and theoretical background*, *Cement and Concrete Research*, Volume 31, Issue 4, pages 647-654. [https://doi.org/10.1016/S0008-8846\(01\)00463-X](https://doi.org/10.1016/S0008-8846(01)00463-X).
- Jensen, O. Hansen, P. F. (2002), *Water-entrained cement-based materials II. Experimental observations*, *Cement and Concrete Research*, Volume 32, Issue 6, June pages 973-978. [https://doi.org/10.1016/S0008-8846\(02\)00737-8](https://doi.org/10.1016/S0008-8846(02)00737-8).
- Lothenbach, B., Scrivener, K., Hooton, R. D. (2011), *Supplementary cementitious materials*, *Cement and Concrete Research* Num. 41 1244-1256. <https://doi.org/10.1016/j.cemconres.2010.12.001>.
- Mechtcherine, V., Reinhardt, H. (2012), *Application of Superabsorbent Polymers (SAP) in Concrete Construction* State of the Art Report Prepared by Technical Committee 225-SAP, <https://doi.org/10.1007/978-94-007-2733-5>.
- Nordest (1999), NT Build 492: *Concrete, mortar and cement-based repair materials: Chloride migration coefficient from non-steady-state migration experiments*.
- Nilsson, L., Ngo, M., & Gjrv, O. (1998). *High-performance repair materials for concrete structures in the port of Gothenburg*. En O. Gjrv, K. Sakai, & N. Banthia, *Concrete under severe conditions: environment and loading*, volumen 2, pp 1193-1198. Troms, Norway: E & FN Spon. <https://doi.org/10.1201/b16469>.
- Pendergrass, B., Darwin, D. (2014), *Low-cracking High-Performance Concrete (LC-HPC) bridge decks: Shrinkage-Reducing Admixtures, Internal Curing, and cracking performance*. *Structural Engineering and Engineering Materials SM Report no. 107*. The University of Kansas Center for Research, INC, Lawrence Kansas. <https://kuscholarworks.ku.edu/handle/1808/19821>.
- Powers, T. C., Brownyard, T. L. (1948) *Studies of the physical properties of hardened Portland Cement pastes*, *Journal of the American Concrete Institute*, USA.

- Quraishi, M. A., Nayak, D. K., Singh, B. N., Kumar, V., Pandey, K. K. (2016), *Experimental Studies on Effects of Sodium Citrate, Calcium Nitrite and Hexamine as Corrosion Inhibitor in Concrete*; Journal of Steel Structures & Construction, 5 pp; doi: [10.4172/2472-0437.1000117](https://doi.org/10.4172/2472-0437.1000117).
- Sellevoid, E. J. Radjy F. F. (1982), *Condensed silica fume in concrete*, Report BML 82.610. Division of Building Materials. The Norwegian Institute of Technology & The University of Trondheim, Norway.
- Shi, C. (2004), *Effect of mixing proportions of concrete on its electrical conductivity and the rapid permeability test (ASTM C1202 or ASSHTO T277) results*, Cement and Concrete Research, 34 (3), 537–545. <https://doi.org/10.1016/j.cemconres.2003.09.007>.
- Snoeck, D. Jensen O. M., De Belie N. (2015), *The influence of superabsorbent polymers on the autogenous shrinkage properties of cement pastes with supplementary cementitious materials*. Cement and concrete research 74, 59-67. <https://doi.org/10.1016/j.cemconres.2015.03.020>.
- Tange Hasholt, M., Mejlhede Jensen, O. (2015), *Chloride migration in concrete with superabsorbent polymers*, Cement and Concrete Composites, 55, 290-297. <https://doi.org/10.1016/j.cemconcomp.2014.09.023>.
- Zhutovsky S. and Kovler K. *Effect of internal curing on durability-related properties of high performance concrete*, Cement and concrete research (2012), vol. 42., 1, pages 20-26, <https://doi.org/10.1016/j.cemconres.2011.07.012>.

Image analysis on disintegrated concrete at the post-heating stage

A. H. Akca^{1*}, N. Özyurt²

*Contact author: aakca@yildiz.edu.tr

DOI: <http://dx.doi.org/10.21041/ra.v10i2.482>

Reception: 02/11/2019 | Acceptance: 05/02/2020 | Publication: 30/04/2020

ABSTRACT

The relation between crack growth and reduction in the compressive strength after high temperature exposure and after air re-curing was investigated in this study. Concrete specimens were heated to 1000 °C and they were subjected to air re-curing for 28 days. During re-curing period, their heated surfaces were monitored by using a digital single-lens reflex camera and the images were analyzed by using image analysis software. After cooling, the maximum reduction in the compressive strength of concrete was 49.5% and that of air re-cured concrete was 66.8%. Image analyses showed high correlations between crack growth and reduction in the compressive strength. This non-destructive method has the potential to represent the extent of damage in concrete after high temperature exposure.

Keywords: high temperature; fiber reinforced concrete; deterioration; crack development; black pixel analysis.

Cite as: Akcal, A. H., Özyurt, N. (2020), “*Image analysis on disintegrated concrete at the post-heating stage*”, Revista ALCONPAT, 10 (2), pp. 219 – 229, DOI: <http://dx.doi.org/10.21041/ra.v10i2.482>

¹ Department of Civil Engineering, Yıldız Technical University, İstanbul, Turkey.

² Department of Civil Engineering, Boğaziçi University, İstanbul, Turkey.

Legal Information

Revista ALCONPAT is a quarterly publication by the Asociación Latinoamericana de Control de Calidad, Patología y Recuperación de la Construcción, Internacional, A.C., Km. 6 antigua carretera a Progreso, Mérida, Yucatán, 97310, Tel.5219997385893, alconpat.int@gmail.com, Website: www.alconpat.org

Responsible editor: Pedro Castro Borges, Ph.D. Reservation of rights for exclusive use No.04-2013-011717330300-203, and ISSN 2007-6835, both granted by the Instituto Nacional de Derecho de Autor. Responsible for the last update of this issue, Informatics Unit ALCONPAT, Elizabeth Sabido Maldonado, Km. 6, antigua carretera a Progreso, Mérida, Yucatán, C.P. 97310.

The views of the authors do not necessarily reflect the position of the editor.

The total or partial reproduction of the contents and images of the publication is strictly prohibited without the previous authorization of ALCONPAT Internacional A.C.

Any dispute, including the replies of the authors, will be published in the first issue of 2021 provided that the information is received before the closing of the third issue of 2020.

Análisis de imagen sobre hormigón desintegrado en la etapa de post-calentamiento

RESUMEN

En este estudio se investigó la relación entre el crecimiento de grietas y la reducción de la resistencia a la compresión después de la exposición a altas temperaturas y después del curado con aire. Las muestras de hormigón se calentaron a 1000 °C y se sometieron a curado por aire durante 28 días. Durante el período de curado, sus superficies calentadas fueron monitoreadas usando una cámara réflex digital de lente única y las imágenes fueron analizadas usando un software de análisis de imágenes. Después del enfriamiento, la reducción máxima en la resistencia a la compresión del concreto fue del 49.5% y la del concreto curado al aire fue del 66.8%. Los análisis de imagen mostraron altas correlaciones entre el crecimiento de grietas y la reducción de la resistencia a la compresión. Este método no destructivo tiene el potencial de representar el alcance del daño en el concreto después de la exposición a altas temperaturas.

Palabras clave: alta temperatura; hormigón reforzado con fibra; deterioro; desarrollo de grietas; Análisis de píxeles negros.

Análise de imagem em concreto desintegrado na fase de pós-aquecimento

RESUMO

A relação entre o crescimento de fissuras e a redução da resistência à compressão após exposição a altas temperaturas seguida de resfriamento lento e ao ar foi investigada neste estudo. As amostras de concreto foram aquecidas a 1000 °C e, após submetidas ao resfriamento lento foram, na sequência sazoadas ao ar por 28 dias. Durante o período de resfriamento, sua superfície foi monitorada usando uma câmera reflex digital de lente única e as imagens foram analisadas usando o software de análise de imagens. Logo após o resfriamento, a redução máxima na resistência à compressão do concreto foi de 49,5% e a do concreto sazoadado ao ar, após 28 dias, foi de 66,8%. As análises de imagem mostraram altas correlações entre o crescimento da fissura e a redução da resistência à compressão. Este método não destrutivo tem o potencial de representar a extensão dos danos no concreto após a exposição a altas temperaturas.

Palavras-chave: temperatura alta; concreto reforçado com fibra; deterioração; desenvolvimento de fissuras; análise de pixel preto.

1. INTRODUCTION

Thermal gradients, evaporation of free water and chemical changes in concrete are the main reasons of deteriorations such as crazing, surface delamination, cracking and spalling (Poon et al. 2001; Akca and Özyurt, 2013) Moreover, deterioration in concrete may continue in the subsequent days of cooling due to continuing changes occurred in microstructure of concrete. For example, rehydration of CaO results in Ca(OH)₂ with a 44% volume expansion and this reaction may cause cracking of concrete especially at the heated surface level (Lin et al. 1996; Alonso and Fernandez, 2004; Mendes et al. 2011).

The changes on the heated surfaces of concrete can be used to evaluate the residual properties of concrete after heat exposure. For example, color changes on heated or fire exposed concrete surfaces give information about maximum temperature experienced and amount of deterioration of concrete (Yüzer et al. 2004; Ingham, 2009). Pink to red coloration occurs due to oxidation of iron compounds in sand particles after 300 °C and whitish color concrete surface means that temperature

of concrete exceeded 700 °C at which decarbonation of carbonates takes place. Thus, reduction in strength can be predicted roughly without applying destructive tests on concrete in some cases. Similarly, cracks on the heated surfaces can be evaluated to predict residual concrete strength after cooling. Therefore, concrete specimens were subjected to air re-curing process after heating up to 1000°C. In this project, one face heating condition was applied to the specimens since it can be considered more realistic and applicable. Then, heated surfaces of concrete specimens were monitored by using a DSLR camera after cooling and the images were evaluated to understand the relation between crack width and crack growth rate on the heated surfaces and the reduction in compressive strength after heating.

2. EXPERIMENTAL STUDY

2.1 Materials and specimens

CEM I type Portland cement (PC) was used in concrete groups and total amount of cement in 1 m³ of concrete was 450 kg and all concrete groups had a water to cement ratio of 0.45. Table 1 shows mix proportions of concrete groups. As chemical admixtures, oil alcohol and ammonium salt-based air entraining admixture (AEA) and modified polycarboxylate based superplasticizer were used in concrete mixes. AEA content was the same and 0.3 kg (0.7 % of total weight of cement.) in all concrete groups. Super plasticizer amount was varied in order to obtain slump levels in S4 limits given in EN 206-1. Steel fibers were used as high melting point fibers and PP fibers were used as low melting point fibers to reinforce concrete groups. In PP fiber reinforced groups PP fibers were used 0.2 % of volume of concrete and in steel fiber reinforced groups steel fibers were used 0.5 % of volume of concrete. PP fibers and steel fibers were added at contents of 0.1 % and 0.25 % per volume in hybrid fiber reinforced concrete groups, respectively. River sand and siliceous gravel were used in all concrete groups as aggregates. Depending on fiber types and also presence of air entraining agent, 8 different concrete groups were designed as can be seen in Table 1.

11 cubic specimens with dimensions of 15x15x15 cm were produced for each concrete group. One day after production, specimens were demolded and placed in curing water for 27 days. Then they were conditioned in laboratory environment for additional 2 months before tests (Poon et al. 2001; Chang et al. 2006). Three cubic specimens were used to determine initial properties of concrete before heating. Remaining 8 cubic specimens were heated to 1000 °C. Two of them were used to monitor temperatures in concrete cubes during heating, 3 of them were tested to determine properties after cooling and remaining 3 cubic specimens were subjected to air re-curing. Therefore, in tables and graphs 0, X, and Z represent tests before heating, after cooling and after air re-curing, respectively.

Table 1. Mix proportions.

Series	W/C	Cement	Water	Crushed Stone	Crushed Sand	Sand	SP ^a	AEA	PP Fibers	Steel Fibers
									(kg/m ³)	
C00	0.45	450	202.5	968	565	225	5.7	-	-	-
C0S	0.45	450	202.5	968	565	225	6.0	-	-	5
C0P	0.45	450	202.5	968	565	225	6.3	-	2	-
C0H	0.45	450	202.5	968	565	225	6.6	-	1	2.5
CA0	0.45	450	202.5	968	565	225	5.3	0.3	-	-
CAS	0.45	450	202.5	968	565	225	5.7	0.3	-	5
CAP	0.45	450	202.5	968	565	225	6.0	0.3	2	-
CAH	0.45	450	202.5	968	565	225	6.6	0.3	1	2.5

^a SP stands for superplasticizer

2.2 Heating procedure

An electrical furnace which has a 1250 °C maximum operation temperature was used in this study. Two stages of heating were determined and during the first stage, specimens were heated to 1000 °C and during the second stage specimens were kept at this temperature until the end of the total heating time (200 minutes). Figure 1 represents the heating procedure. Electrical furnace was operated at full power and temperature inside the furnace reached 1000 °C in approximately 120 minutes. Since furnace heating capacity was limited, heating rate was 20°C/min at the beginning but the rate decreased to 5 °C/min at the end of the first stage of heating. After the second stage completed, hot concrete specimens were not taken out until the furnace cooled down to 100 °C.

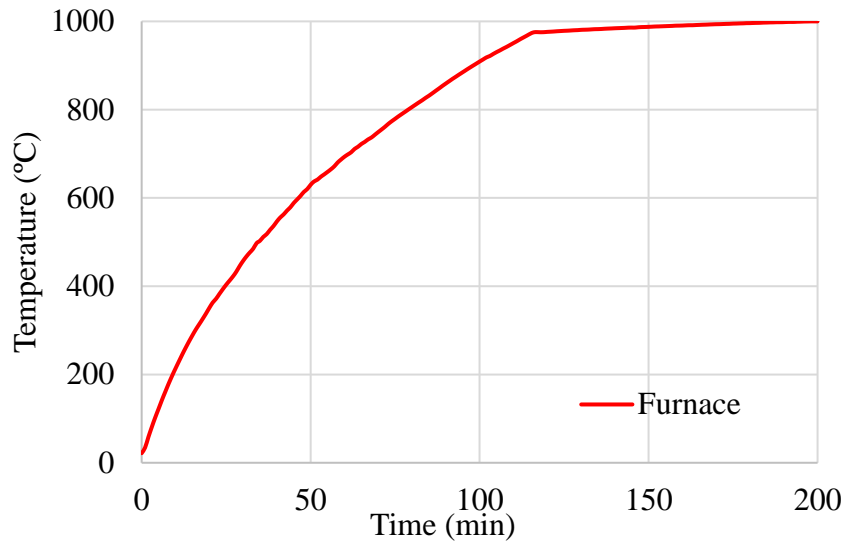


Figure 1. Heating procedure.

Four concrete cubes were placed together in the electrical furnace and in order to simulate one face heating conditions they were insulated with aerated concrete blocks as shown in Figure 2. For temperature monitoring K-Type thermocouples were placed inside a concrete specimen during heating.

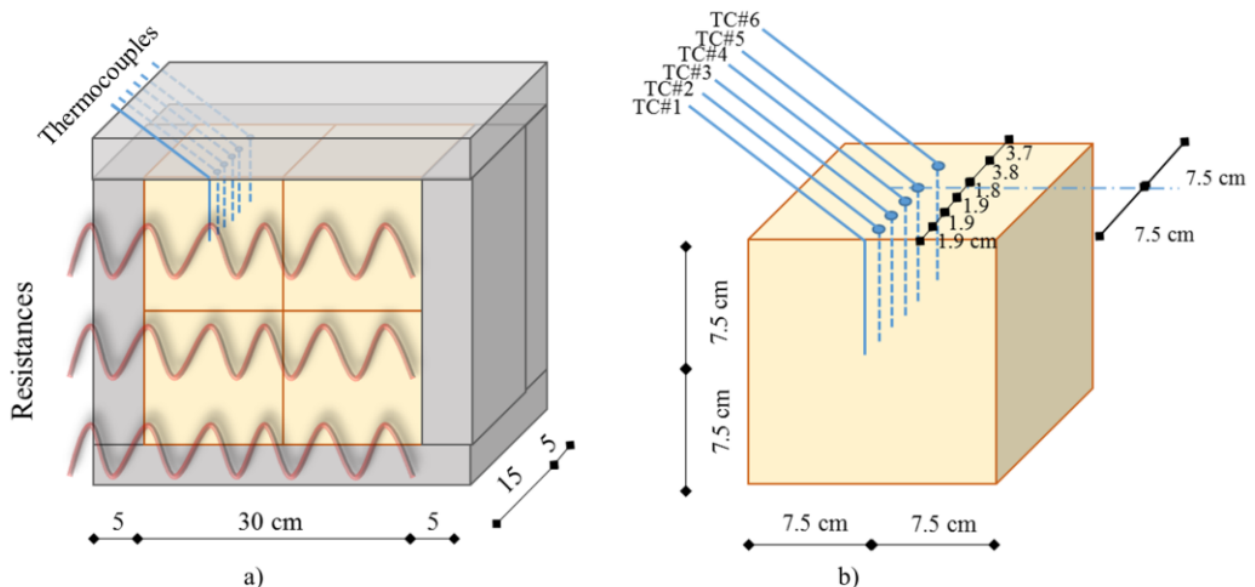


Figure 2. a) Heat insulation of concrete specimens in electrical furnace, b) positions of the K-type thermocouples used to monitor temperature change.

2.3. Re-curing process

After heating and cooling processes 3 specimens were subjected to air re-curing for 28 days. Specimens were kept in laboratory environment which has a relative humidity of $65\pm 10\%$ and temperature of $20\pm 2^\circ\text{C}$ during re-curing period.

2.4. Crack width measurements

Visual changes on heated or fire exposed concrete give information about maximum temperature experienced and amount of deterioration of concrete (Yüzer et al. 2004; Ingham, 2009). Therefore, photograph of the heated face of a survived specimen from each concrete group was taken by using a DSLR camera. These pictures were analyzed via software called Image J as can be seen in Figure 3. During an analysis the whole picture area was divided into 9 subareas and maximum crack widths of each subarea were measured and then mean crack widths were obtained.

2.5. Black pixel analyses

Development of cracks during air re-curing was monitored by taking photos of heated surfaces at every hour for a week. A high resolution DSLR camera and a 100 mm macro lens were used in order to obtain detailed images. As can be seen in Figure 4, these images were converted to 8-bit black and white images by using Image J and black pixel analyses (BPA) were conducted on them. Black pixels represent cracks, air voids, surface delamination and shadow (due to positions of spotlights) on the heated surfaces of specimens. Total areas of black pixels were calculated for all images separately. Then these calculated values were divided to black pixel area of first image in order to obtain normalized area values. Finally, normalized area-time graphs were drawn for all concrete groups except the groups experienced spalling during heating and trend lines were fitted on the graphs as shown in Figure 5. These curves were used to monitor deterioration of concrete for a week. The slopes of fitted trend lines were called BPA rates and they were compared to compressive strength reduction ratios of air re-cured concrete groups.

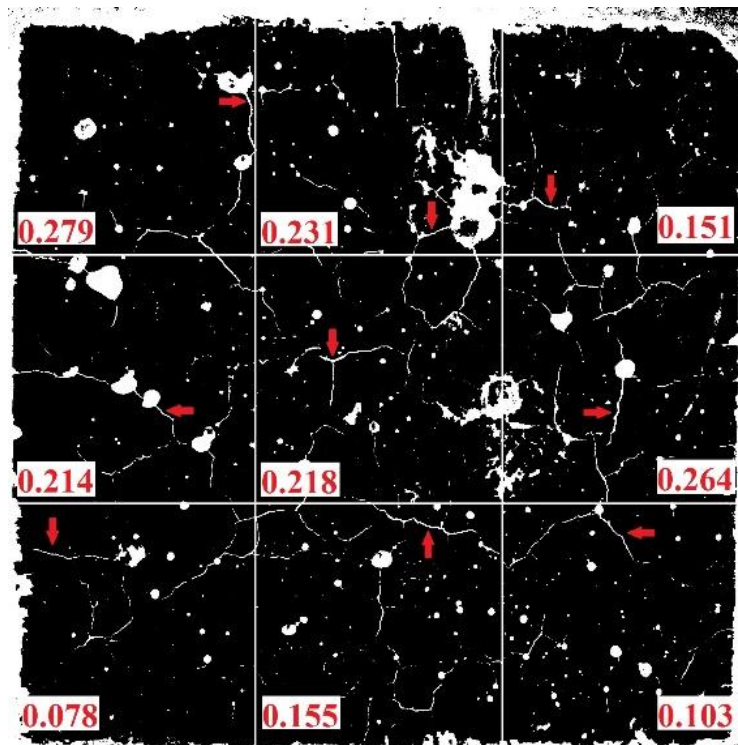


Figure 3. Crack width measurements on a C00X specimen (surface just after cooling).

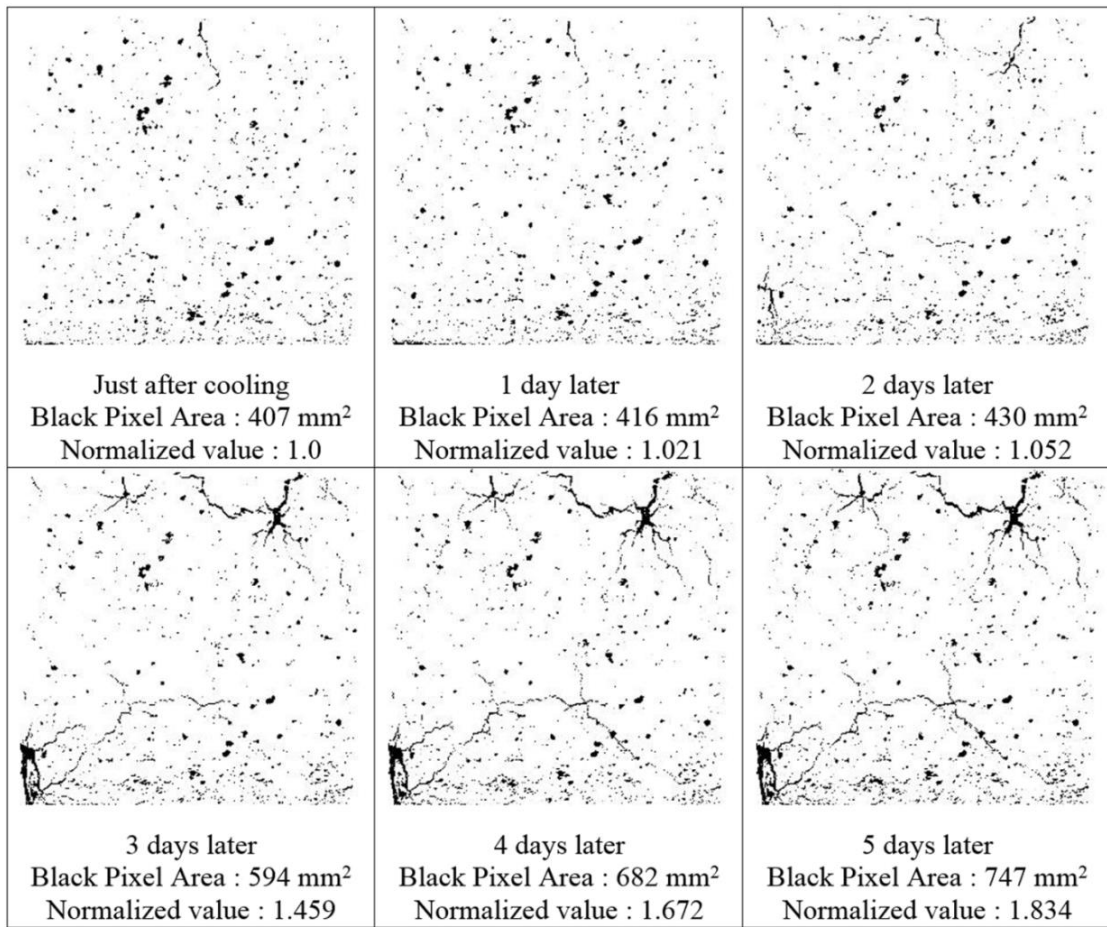


Figure 4. Crack growth monitoring on black and white images captured from COPZ specimen during air re-curing.

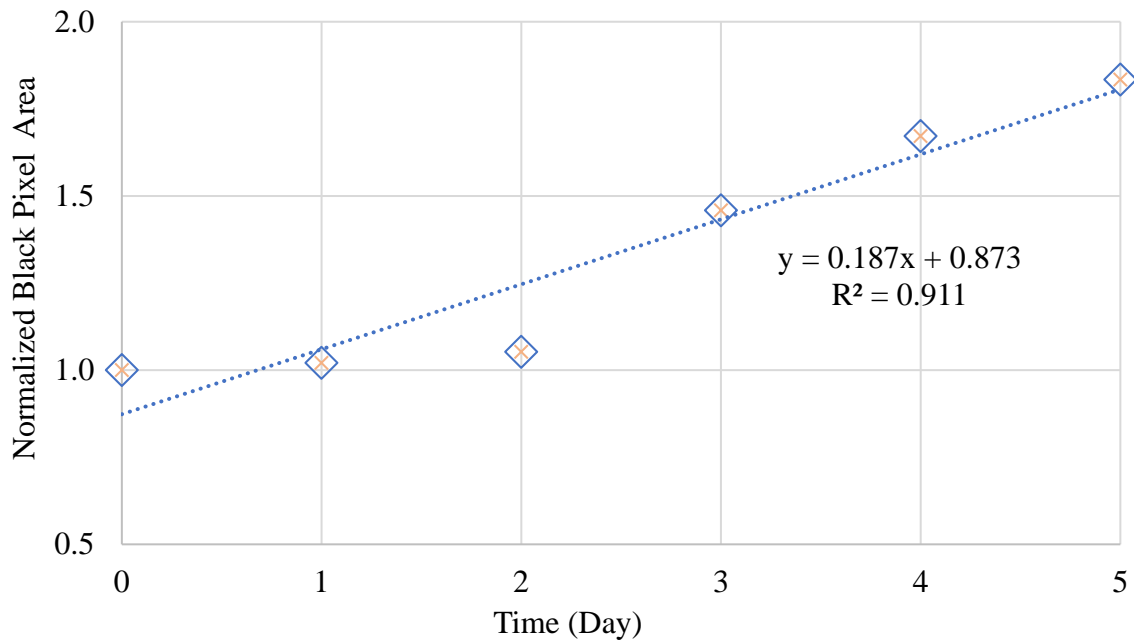


Figure 5. Black pixel analysis value of COPZ specimen.

3. RESULTS

3.1. Temperature monitoring

Temperatures of heated surface and inner parts of concrete cubes were monitored during heating and temperature monitoring continued further during cooling of the furnace (150 minutes more). In cooling period, although heating of furnace was stopped, temperatures in concrete continued to increase. Thermocouple data was very close when they were compared in terms of cementitious material types. Therefore, all concrete groups were gathered under two categories depending on use of AEA in them. Table 2 shows average maximum temperatures monitored in concrete categories with and without air entrainment during total temperature monitoring (200+150 minutes). Results showed that, temperatures experienced in air entrained concrete were less than that of concrete without air entrainment. When the whole heating and cooling period is considered it can be seen that concrete groups experienced at least 583 °C of temperature which may result in severe strength losses (Poon et al. 2001; Akca and Özyurt, 2013).

Table 2. Average maximum temperature values at predefined depths from the surface during total heating and cooling processes (at the end of 350 minutes).

Thermocouple No	TC#1	TC#2	TC#3	TC#4	TC#5	TC#6
Depth (mm)	0	19	38	57	75	113
Without AEA ¹ (°C)	1000	805	691	657	636	608
With AEA ² (°C)	1000	784	662	627	608	583
Difference (°C)	0	21	29	30	28	25

Without AEA¹ stands for all concrete groups without air entrainment.

With AEA² stands for all concrete groups with air entrainment.

3.2. Compression tests

Cubic concrete specimens were loaded before heating, after cooling and after air re-curing (for 28 days) and compressive strength values of concrete groups were determined at every stage. Compressive strength values of all concrete groups decreased after heating and further reduction in residual strength was observed after air re-curing period. Reduction ratios in compressive strength of all concrete groups after cooling and after air re-curing can be seen in Table 3.

Table 3. Reduction in compressive strength with respect to before heating strength.

Reduction in compressive strength	C00	C0S	C0P	C0H	CA0	CAS	CAP	CAH
After cooling (%)	31.9	25.8	36.7	33.9	35.2	36.5	49.5	45.5
After air re-curing (%)	64.1	44.9	66.8	49.2	56.3	49.6	58.7	56.5

3.3. Crack width measurement (after cooling specimens)

Photographs of the heated face of a survived specimen from each concrete group were taken by using a DSLR camera. These pictures were analyzed via software called Image J, then mean crack widths were obtained. Average crack widths of concrete groups after cooling were given in Table 4. According to the results it can be concluded that there were cracks on the heated faces of the specimens around 0.20 mm after heating. Also cracking tendency of PP fiber reinforced concrete can be considered higher and that of steel fiber reinforced concrete can be considered lower with respect to plain concrete groups after cooling. On the other hand, larger cracks were observed on the air entrained concrete groups than concrete groups without air entrainment.

Table 4. Average crack widths on the heated faces of concrete groups after cooling.

Crack width	C00X	C0SX	C0PX	C0HX	CA0X	CASX	CAPX	CAH X
Mean (mm)	0.188	0.175	0.196	0.181	0.195	0.182	0.206	0.204
Standard deviation (mm)	0.07	0.05	0.03	0.03	0.03	0.04	0.03	0.04

Calculated average crack widths were compared to reduction in compressive strength of specimens after cooling as can be seen in Figure 6. Results showed that increase in average crack width of specimens caused increase in reduction in compressive strength. This relation can be used to predict the extent of the deterioration in residual mechanical properties of concrete elements without applying destructive tests on them after an event of a fire.

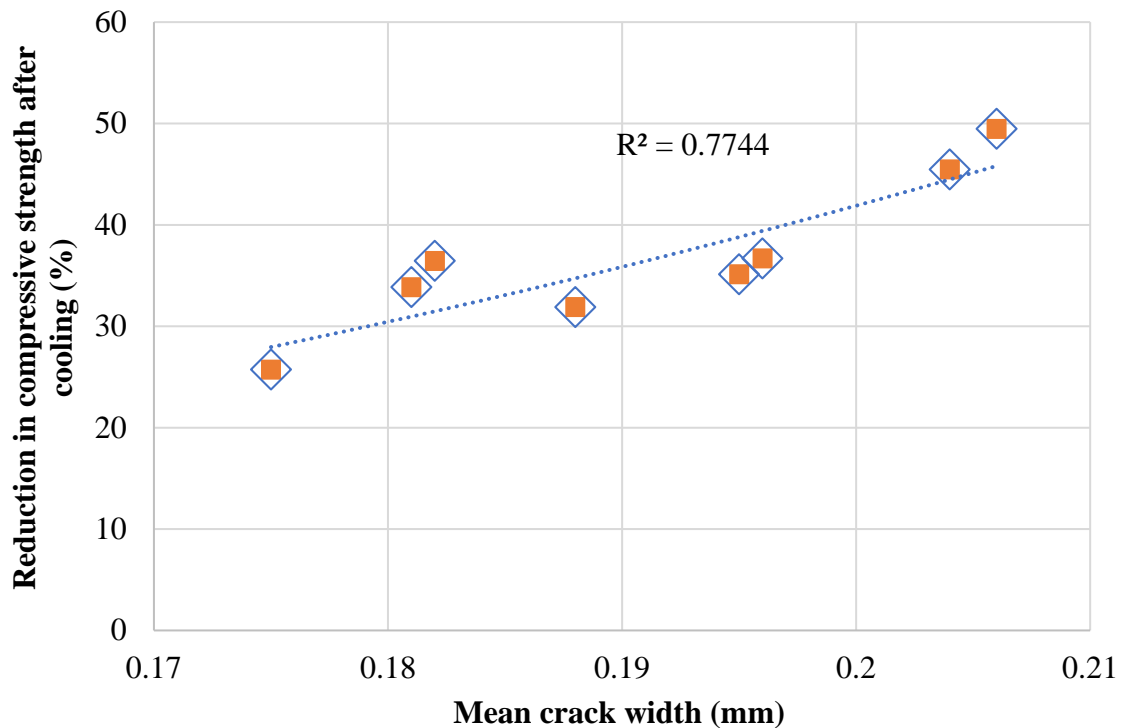


Figure 6. Relation between reduction in compressive strength and mean crack width after cooling.

3.4. Black Pixel Analysis (BPA) (for air re-curing period)

After cooling, sizes and numbers of cracks increased on the heated surfaces of concrete specimens probably due to expansive CaO rehydration. Therefore, surface pictures of specimens were captured during the first week of air re-curing and these pictures were evaluated in image analysis software in order to evaluate the relation between crack development rate and reduction in compressive strength during air re-curing period. Accordingly, BPA rates of air re-cured concrete specimens were calculated (as explained in Section 2.5) to monitor damage development and these values were compared to differences in compressive strength values after air re-curing period as shown in Table 5.

Table 5. Residual compressive strength and BPA values.

Group	X-Group ¹ (MPa)	Z-Individual ² (MPa)	(Z-X)/X (%)	BPA Rate (Day ⁻¹)
C00	Spalling was observed. BPA was not examined.			
C0S	Spalling was observed. BPA was not examined.			
C0P	36.9	20.1	- 45.5	0.187
C0H	36.7	24.6	- 32.8	0.056
CA0	35.5	22.2	- 37.5	0.087
CAS	34.9	25.6	- 26.9	0.087
CAP	25.3	21.2	- 16.1	0.007
CAH	27.2	24.3	- 10.5	0.019

X-Group¹ Represents average residual strength value of 3 specimens after cooling

Z-Individual² Represents individual residual strength value of monitored specimen after air re-curing

Individual compressive strength value of monitored specimen (air re-cured for 28 days following cooling period and tested at the end of this 28-day period) and average compressive strength value of 3 specimens tested after cooling (as an initial strength value before air re-curing period) were used to calculate the change in compressive strength during air re-curing period.

After comparison a scatter gram was obtained as shown in Figure 7 and it showed that there was a logarithmic relation between changes in compressive strength and BPA rates. Calculated R² value for all set of data was 0.77. This rate can be increased by using advanced photographing techniques, by analyzing in specific software, by increasing sample size etc. For example, air voids on the surface of the specimens influence the total amount of black pixels. If the effect of air voids is somehow eliminated more accurate BPA rates can be obtained.

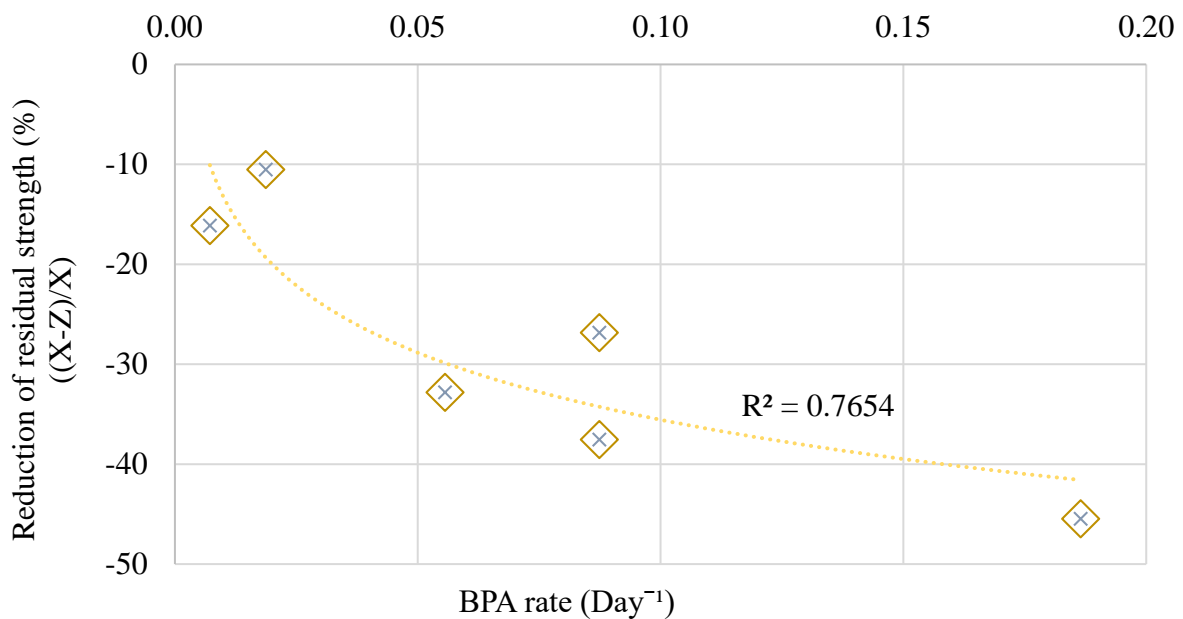


Figure 7. Black pixel analyses results.

4. CONCLUSIONS

In this study, disintegration of various kinds of concrete under air re-curing regime was investigated. BPAs were conducted on air re-cured specimens and the relation between crack development and reduction in compressive strength were evaluated. And the conclusions given below can be drawn regarding to the obtained results limited to the specimen geometry (cubic shape 15by15by15 cm)

1. Due to excessive temperature increase in concrete, compressive strength of concrete groups decreased approximately 35% after heating. Moreover, continuous cracking of concrete following to cooling caused further reduction in compressive strength.
2. Relation between cracks on heated surfaces and reduction in compressive strength was evaluated after cooling. The results showed that average crack width on the heated surface of concrete can give information about the decrease in compressive strength of concrete.
3. An image analysis technique was developed during this study which is called black pixel analysis (BPA) in order to understand the relation between the crack growth during air re-curing and compressive strength reduction after air re-curing. This method gave good results for high and it can be improved to better represent the extent of damage in concrete after high temperature exposure.

5. ACKNOWLEDGEMENTS

The authors gratefully acknowledge the financial support of Boğaziçi University Research Fund [Project Code 14A04D2]. The support of AKÇANSA Cement and BASF-YKS Construction Chemicals is also acknowledged. The authors also would like to thank Ümit Melep, Bilge Uluocak and Melike Babucci for their support during experimental measurements. The first author is grateful for the financial support given by The Scientific and Technical Research Council of Turkey (TÜBİTAK).

6. REFERENCES

- Akca, A. H., Özyurt, N. (2013). *High performance concrete under elevated temperatures*. Construction and Building Materials. 44:317-328. <https://doi.org/10.1016/j.conbuildmat.2013.03.005>
- Alonso, C., Fernandez, L. (2004). *Dehydration and rehydration processes of cement paste exposed to high temperature environments*. Journal of Materials Science. 39:3015-3024.
- Chang, Y. F. Chen, Y. H., Sheu, M. S., Yao, G. C. (2006). *Residual stress-strain relationship for concrete after exposure to high temperatures*. Cement and Concrete Research. 36 (10):1999-2005. <https://doi.org/10.1016/j.cemconres.2006.05.029>
- Ingham, J. P. (2009). *Application of petrographic examination techniques to the assessment of fire-damaged concrete and masonry structures*. Materials Characterization. 60 (7):700-709. <https://doi.org/10.1016/j.matchar.2008.11.003>
- Lin, W. M., Lin, T. D., Powers-Couche, L. J. (1996). *Microstructures of Fire-Damaged Concrete*. ACI Materials Journal. 93 (3):199-205.
- Mendes, A., Sanjayan, J. G., Collins, F. (2011). *Effects of slag and cooling method on the progressive deterioration of concrete after exposure to elevated temperatures as in a fire event*. Materials and Structures. 44:709-718. <https://doi.org/10.1617/s11527-010-9660-2>
- Poon, C. S., Azhar, S., Anson, M., Wong, Y. L. (2001). *Comparison of the strength and durability performance of normal- and high-strength pozzolanic concretes at elevated temperatures*. Cement and Concrete Research. 31 (9):1291-1300. [https://doi.org/10.1016/S0008-8846\(01\)00580-4](https://doi.org/10.1016/S0008-8846(01)00580-4)

Yüzer, N., Aköz, F., Dokuzer Öztürk, L. (2004). *Compressive strength–color change relation in mortars at high temperature*. Cement and Concrete Research. 34 (10):1803-1807. <https://doi.org/10.1016/j.cemconres.2004.01.015>

A numerical approach for evaluating residual capacity of fire damaged concrete members

V. K. R. Kodur^{1*} , A. Agrawal¹ 

*Contact author: kodur@egr.msu.edu

DOI: <http://dx.doi.org/10.21041/ra.v10i2.483>

Reception: 16/10/2019 | Acceptance: 05/02/2020 | Publication: 30/04/2020

ABSTRACT

This paper presents an approach to evaluate residual capacity of fire-damaged concrete structures. The approach involves capturing response in three stages; namely, structural response at ambient conditions (prior to fire exposure), thermo-mechanical response during fire exposure, and post-fire residual response after cooling down of the structural member. The proposed approach is implemented in a comprehensive numerical model developed in the finite element computer program ABAQUS for specifically evaluating residual capacity of an RC beam after exposure to different fire scenarios. Predictions from the numerical model are utilized to highlight importance of each stage of analysis in evaluating realistic residual capacity of fire damaged concrete members.

Keywords: reinforced concrete members, fire damage, cooling phase, post-fire residual capacity.

Cite as: Kodur, V. K. R., Agrawal, A. (2020), “A numerical approach for evaluating residual capacity of fire damaged concrete members”, Revista ALCONPAT, 10 (2), pp. 230 – 242, DOI: <http://dx.doi.org/10.21041/ra.v10i2.483>.

¹Department of Civil Engineering, Michigan State University, East Lansing, USA.

Legal Information

Revista ALCONPAT is a quarterly publication by the Asociación Latinoamericana de Control de Calidad, Patología y Recuperación de la Construcción, Internacional, A.C., Km. 6 antigua carretera a Progreso, Mérida, Yucatán, 97310, Tel.5219997385893, alconpat.int@gmail.com, Website: www.alconpat.org

Responsible editor: Pedro Castro Borges, Ph.D. Reservation of rights for exclusive use No.04-2013-011717330300-203, and ISSN 2007-6835, both granted by the Instituto Nacional de Derecho de Autor. Responsible for the last update of this issue, Informatics Unit ALCONPAT, Elizabeth Sabido Maldonado, Km. 6, antigua carretera a Progreso, Mérida, Yucatán, C.P. 97310.

The views of the authors do not necessarily reflect the position of the editor.

The total or partial reproduction of the contents and images of the publication is strictly prohibited without the previous authorization of ALCONPAT Internacional A.C.

Any dispute, including the replies of the authors, will be published in the first issue of 2021 provided that the information is received before the closing of the third issue of 2020.

Un enfoque numérico para evaluar la capacidad residual de los miembros de concreto dañados por el fuego

RESUMEN

Este artículo presenta un enfoque para evaluar la capacidad residual de las estructuras de hormigón dañadas por el fuego. El enfoque implica capturar la respuesta en tres etapas; a saber, la respuesta estructural en condiciones ambientales (antes de la exposición al fuego), la respuesta termomecánica durante la exposición al fuego y la respuesta residual posterior al incendio después del enfriamiento del miembro estructural. El enfoque propuesto se implementa en un modelo numérico integral desarrollado en el programa de computadora de elementos finitos ABAQUS para evaluar específicamente la capacidad residual de un haz RC después de la exposición a diferentes escenarios de incendio. Las predicciones del modelo numérico se utilizan para resaltar la importancia de cada etapa de análisis en la evaluación de la capacidad residual realista de los elementos de hormigón dañados por el fuego.

Palabras clave: elementos de hormigón armado, daños por incendio, fase de enfriamiento, capacidad residual posterior al incendio.

Uma abordagem numérica para avaliar a capacidade residual de elementos de concreto submetidos a incêndio

RESUMO

Este artigo apresenta uma abordagem para avaliar a capacidade residual de estruturas de concreto danificadas pelo fogo. A abordagem envolve capturar a resposta em três fases; ou seja, resposta estrutural em condições ambiente (antes da exposição ao fogo), resposta termomecânica durante a exposição ao fogo e resposta residual pós-incêndio após o resfriamento do membro estrutural. A abordagem proposta é implementada em um modelo numérico abrangente desenvolvido no programa computacional ABAQUS de elementos finitos para avaliar especificamente a capacidade residual de uma viga de CA após exposição a diferentes cenários de incêndio. Previsões do modelo numérico são utilizados para destacar a importância de cada fase de análise em avaliar a capacidade residual real de elementos de concreto danificado pelo fogo.

Palavras-chave: elementos de concreto armado, danos por incêndio, fase de resfriamento, capacidade residual pós-incêndio.

1. INTRODUCTION

Fire represents a severe environmental condition that civil infrastructure may experience during their design life. Hence, structural members in buildings have to satisfy required fire resistance requirements specified in building codes (CEN, 2004a; ASTM Internacional, 2018). However, statistical data clearly suggests that while fires do occur in structures, complete collapse of structural systems due to fire is a rare event (Beitel and Iwankiw, 2005). The probability of complete collapse in reinforced concrete or pre-stressed concrete (RC and PC) structures is even lower due to low thermal conductivity, high thermal capacity, and slower degradation of mechanical properties of concrete with temperature (Tovey and Crook, 1986; Kodur, 2014; Kodur, 2017). Therefore, it is reasonable to assume that concrete structures, after most fire incidents, can be opened to re-occupancy with adequate repair and retrofitting (Kodur and Agrawal, 2015; Kodur and Afrawal, 2016; Kodur and Phan, 2007).

Nonetheless, there is always uncertainty regarding level of remaining structural capacity in concrete members following a fire incident. It is imperative to assess if sufficient residual capacity exists in structural members prior to re-occupancy following a severe fire. Also, such an assessment forms the basis for developing relevant retrofitting (repair) strategies in fire-damaged concrete structures.

Residual capacity retained in fire damaged concrete structures is highly variable and depends on both temperature history as well as structural conditions present during fire exposure (Kodur and Agrawal, 2015; Kodur and Afrawal, 2016; Kodur and Phan, 2007). Number of factors, including fire severity, temperature dependent material properties of rebar and concrete, duration of fire (heating and cooling periods), temperature induced bond degradation, load level, and restraint conditions present during fire exposure influence residual capacity. Many of these factors are interdependent and can vary significantly in different scenarios. Thus, evaluation of residual capacity can be quite complex and depends on the assumptions used in analysis.

At present, there are limited approaches for residual capacity assessment of fire-damaged concrete structures (Bai and Wang, 2011; Kodur et al, 2013; Kodur et al, 2010). Majority of these approaches are based on sectional analysis which do not account for relevant load level, boundary conditions, and post-fire residual deformations in evaluating residual capacity. Also, most of the current residual capacity evaluation approaches do not account for strain hardening effect in reinforcement, which can lead to under-prediction of moment capacity by 15–25% than the actual value experienced in field applications (Kodur and Agrawal, 2016).

To overcome some of the above drawbacks, an approach is proposed for predicting residual capacity and residual deflections of fire exposed RC structures. The novelty of the current approach lies in the consideration of distinct material properties of reinforcing steel and concrete during heating phase of fire exposure, cooling phase of fire exposure, as well as residual phase (after cool down), and in incorporating post-fire residual (plastic) deformations of fire damaged RC members into post-fire response analysis. The proposed approach is implemented through in a comprehensive numerical model developed in a finite element based computer program ABAQUS (ABAQUS, 2012). Results from numerical studies are utilized to illustrate the significance of each stage of analysis in evaluating residual capacity of fire damaged RC members.

2. FIRE DAMAGE IN CONCRETE STRUCTURES

The extent of damage to concrete structures due to fire exposure is influenced by conditions existing just prior to the fire incident, as well as during complete fire exposure duration, including extended cooling phase when cross-sectional temperatures in the member reverts back to ambient conditions. The different phases encountered for a typical RC beam during and after a fire are illustrated in Fig. 1. Once the fire attains flashover, cross-sectional temperatures increase, and load carrying capacity decreases, together with rise in deflection due to temperature induced degradation in strength and stiffness of concrete and rebar. Furthermore, even as fire temperatures begin to decay during cooling phase, cross-sectional temperatures within the structural member remain significantly high for prolonged duration following burnout conditions or after fire is extinguished, owing to high thermal inertia of concrete. In fact, temperatures within the member may not cool down to ambient conditions until 24 to 72 hours after fire has been extinguished, depending on size (thermal mass) of the member and fire severity. After the member cools down to ambient conditions, an unrecoverable deflection exists in the structural member. These residual deformations represent the state of structural damage in the member resulting from fire exposure and the extent of damage depending on load level, boundary conditions, and temperature induced degradation in material properties.

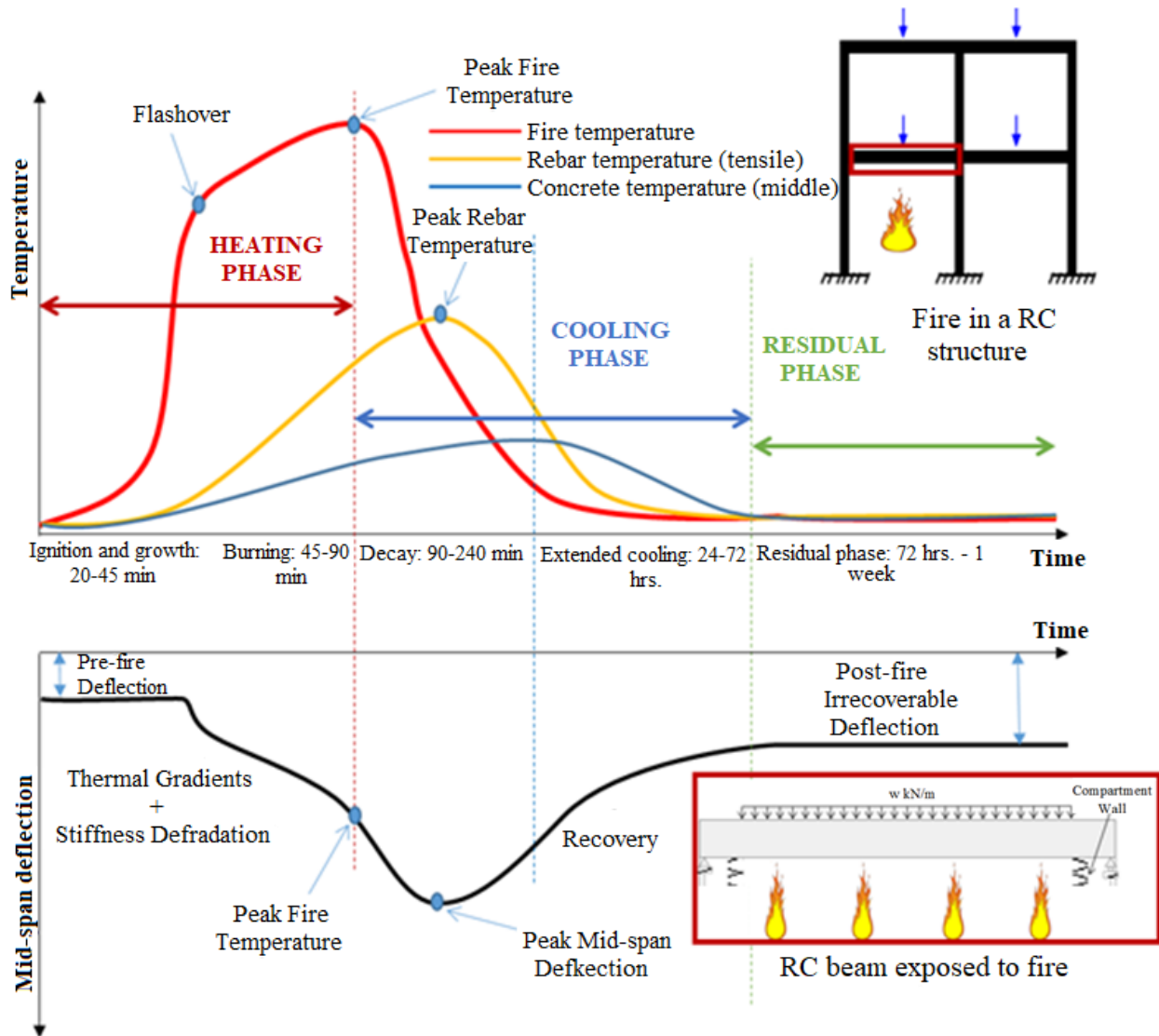


Figure 1. Response of a typical RC beam during and after fire exposure.

Thus, it is crucial to establish sectional temperatures experienced by the structural member, structural conditions present during the fire event, rate of cooling, and residual deformations to assess residual capacity of fire damaged concrete members.

3. APPROACH FOR EVALUATING RESIDUAL CAPACITY

The behavior of a RC member after fire exposure generally depends on parameters such as load level, temperatures experienced within the member during fire exposure, the rate of cooling and strength recovery after fire. A general approach comprising of three stages, which incorporate the interdependency of these parameters in evaluating residual capacity of RC members, is presented in this section.

3.1 General procedure

For evaluating residual capacity, strength analysis of an RC member has to be carried out in three stages, namely, ambient response analysis at room temperature (Stage 1), elevated temperature analysis comprising of both heating and cooling phase of fire exposure (Stage 2) and finally, post-fire residual analysis after cooling down of the concrete member (Stage 3). The three stages of the

analysis for evaluating residual capacity of fire damaged RC members are illustrated through a flow chart in Fig. 2. This type of approach can be applied through advanced analysis by utilizing commercial finite element software package such as ABAQUS (ABAQUS, 2012).

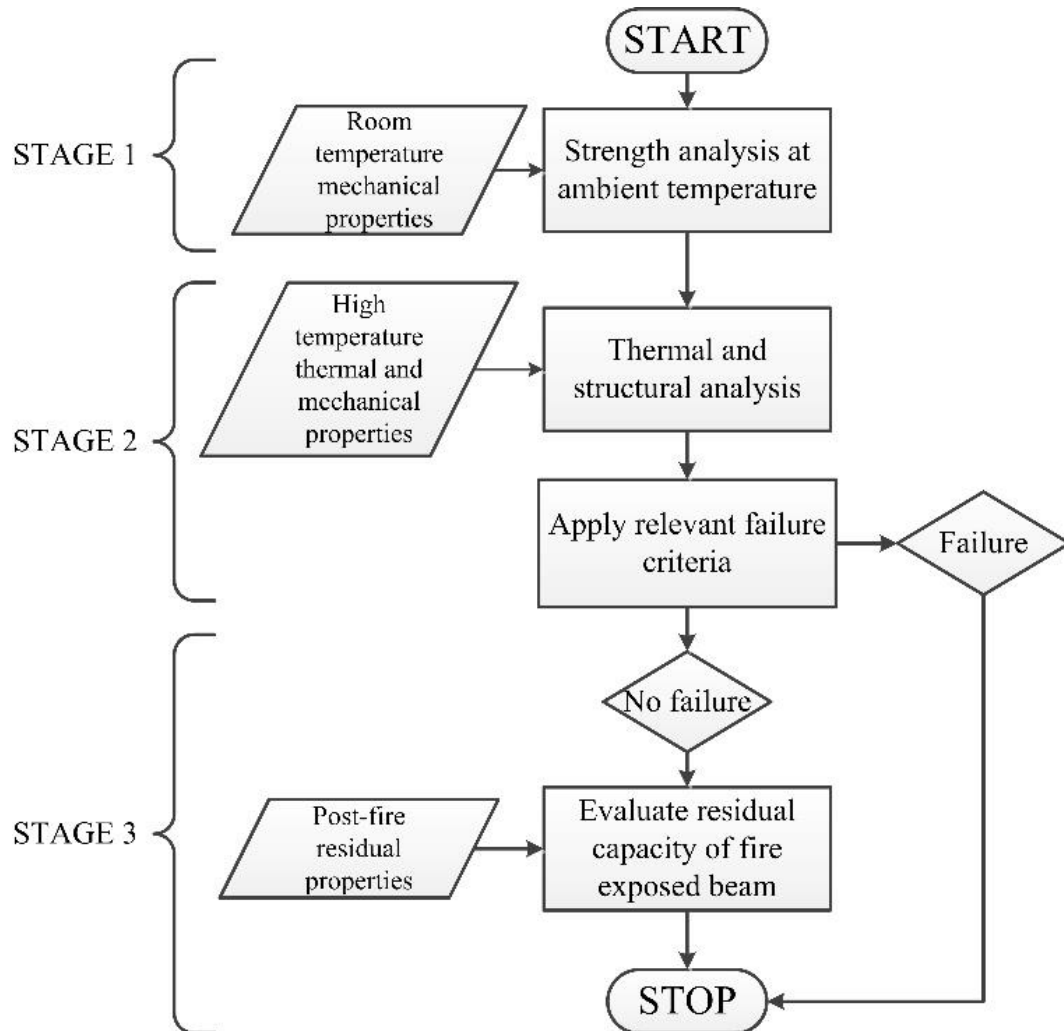


Figure 2. Flowchart describing three step approach for evaluating residual capacity of fire-damaged reinforced concrete structures.

In Stage 1, load (moment) carrying capacity of an RC member is evaluated through specified strength equations for room temperature capacity evaluation available in design standards. Alternatively, detailed finite element analysis can be carried out by gradually incrementing the load on the member till failure occurs. For this analysis, room temperature strength and stiffness properties of concrete and reinforcing steel are to be taken into consideration.

In Stage 2 of analysis, the response of RC member is evaluated under a given fire scenario, load level, and restraint conditions that are present during fire exposure. Both thermal and structural response of the member is traced to evaluate the fire performance of the RC member. In this stage, temperature dependent properties of concrete and reinforcing steel specific to heating and cooling phase of fire are to be input (Kodur and Agrawal, 2015; Kodur and Afrawal, 2016; Kodur and Phan, 2007). This stage of the analysis is carried out at various time increments till the failure of the member, or through total duration of fire exposure, whichever comes first. Response parameters from the thermal and structural analysis are to be utilized to check failure at the end of each time increment to evaluate the state of the RC member under different failure limit states.

Following the cooling down of the member, if there is no failure in Stage 2; Stage 3 of analysis is

to be carried out. In this stage of the analysis, the RC member is loaded incrementally, and the structural response of the member is traced. For this analysis, specific residual properties of material (concrete and steel reinforcement) are considered. The load increments continue until the member fails as per any of the specified limit states governing failure.

4. CASE STUDY

In order to illustrate the capability of the proposed approach for evaluating the residual strength of a fire exposed RC member, a finite element model was developed in ABAQUS (ABAQUS, 2012). This model was applied to evaluate response of fire damaged RC beams at three different stages of analysis as per the proposed approach. Full details of and validation of the proposed approach for residual capacity analysis of residual capacity evaluation of fire damaged concrete members can be found elsewhere (Kodur and Agrawal, 2016).

4.1 Beams analyzed

Two identical concrete beams, designated as beams B1 and B2, were analyzed for residual capacity after exposure to fire scenarios with distinct heating and cooling phases. Key response parameters including deflections and temperatures were calculated during different stages of analysis to monitor performance of each beam. The analysis parameters assumed for the two beams are summarized in Table 1.

Table 1. Summary of analysis parameters and results used for case study.

Beam designation	Support Condition	Fire exposure	ACI design capacity (kN-m)	Predicted fire resistance (min)	Predicted residual capacity (kN-m)
B1	Simply supported	SF*	191	No Failure	189
B2		LF**		No Failure	164

*Short fire scenario with 2h heating phase; **Severe fire scenario with 3h heating phase

4.2 Analysis details

The analysis was carried out using the finite element computer program ABAQUS (ABAQUS, 2012). The constitutive models for concrete and steel are defined within the framework of the software package and the modeling of fire exposed RC beams is undertaken using sequentially coupled thermo-mechanical analysis procedure. In this procedure, the mechanical analysis utilizes the results (temperatures) generated in the heat transfer analysis, but no reverse dependency exists. Furthermore, two sub-models are needed to carry out the three stages of analysis, namely, structural and thermal models. A structural model is needed to carry out strength analysis in Stages 1, 2, and 3, while Stage 2 of analysis requires heat transfer calculations to compute sectional temperatures in the RC beam.

In the case of structural model, eight-noded continuum elements with reduced integration (C3D8R) and two-node link elements (T3D2) are utilized for discretization of concrete and reinforcing steel respectively. In the case of thermal model in 3D space, concrete and reinforcement were discretized using DC3D8 elements (8 noded linear brick element) and DC1D2 elements (2 noded link element) available in ABAQUS (ABAQUS, 2012) library, having nodal temperature (NT11) as the only active degree of freedom.

4.3 Input parameters for analysis

Various input parameters such as model geometry, load distribution, boundary conditions, fire scenarios and material properties are required to carry out different stages of analysis. The details of the beams and the time-temperature curves of the fire scenarios assumed for analysis are presented schematically in Fig. 3a-c.

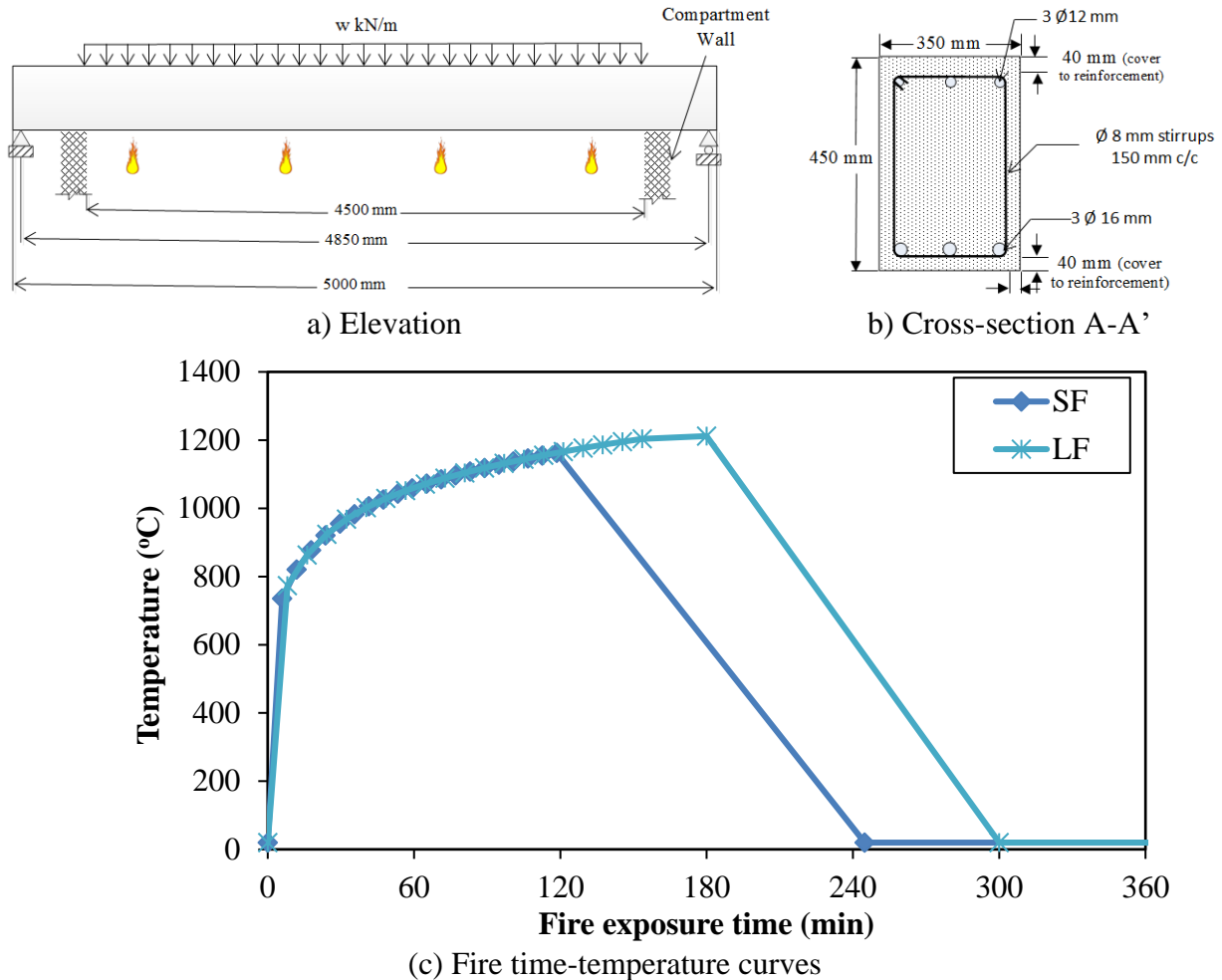


Figure 3. Dimensions, reinforcement details, loading and fire scenarios assumed for case study on RC beams

Both beams had identical cross-sectional dimensions and reinforcement details. The steel of the main reinforcing bars and stirrups was assumed to have yield strengths of 450 MPa and 280 MPa, respectively. Also, the average compressive (cylinder) strength of concrete was assumed to be 50 MPa. The beams were assumed to be simply supported for all stages of analysis. A uniformly distributed load was applied on each beam generating a bending moment of 50% of the beam capacity according to ACI 318 (American Concrete Institute, 2008), similar to load (stress) level typically present during pre-fire exposure conditions. The fire exposure scenarios adopted to simulate fire damage in the beams were calculated as per Eurocode 1 (CEN, 2004a) and comprised of a distinct heating and cooling phase. Varying the fuel load from 500 MJ/m² to 750 MJ/m² resulted in heating phase duration of 2h for the Short Fire (SF) scenario, and 3h for Severe Fire (LF) scenario respectively. Linear cooling (decay) in fire temperatures was adopted as per Eurocode 1 (CEN, 2004a) recommendations to simulate cooling phase in the structural member (see Fig. 3).

Besides these input parameters, various material properties are to be input during different stages of analysis as well. For Stage 1 analysis, at room temperature, typical uniaxial stress-strain relations for concrete and steel at room temperature are adopted. In Stage 2 of analysis, during heating phase, the temperature dependent thermal and mechanical properties of reinforcing steel and concrete are assumed to follow as that of Eurocode 2 and 3 provisions (CEN, 2004b; CEN, 2004d). In Stage 3 of analysis, after cooling of the fire exposed RC beam, the residual uniaxial compressive and tensile strength of concrete after cooling down to room temperature is assumed to be 10% less than the strength attained at the maximum temperature. This assumption is based on Eurocode 4 (CEN, 2004e) recommendations. The residual stress-strain relation for reinforcing steel is calculated using degradation observed by Neves et al. (1996).

4.4 Output results

Displacement and temperature fields are the primary output variables that are generated during different stages of analysis. Displacements due to applied loading in the first stage of analysis are used to ascertain condition of the beam during Stage 1 of analysis. In Stage 2 of analysis, the output from the thermal analysis, namely nodal temperatures, is applied as a thermal body load on the structural model to evaluate the mechanical response of RC beam under fire exposure. An identifier to ascertain if the material is under heating or cooling phase, so as to apply the appropriate material properties, is updated in the structural analysis using subroutine UFIELD available in ABAQUS (ABAQUS, 2012). Also, the maximum temperatures experienced at each node during thermal analysis are used to calculate residual mechanical properties to be used for the residual capacity evaluation in Stage 3 of analysis, when necessary. The load (moment)-deflection response from Stage 3 of the analysis is utilized to evaluate residual capacity of fire exposed reinforced concrete beams.

5. RESULTS AND DISCUSSION

In Stage 1 of analysis, the room temperature design capacity of beams B1 and B2 were calculated to be 191 kN-m as per ACI 318 (ACI, 2008) design equations. In addition, the realistic room temperature capacity of the RC beams prior to fire exposure, using finite element analysis when strain hardening and no material reduction factor is applied, was calculated to be 250 kN-m.

After evaluating room temperature capacity in Stage 1, each beam was subjected to distinct fire exposure scenario under constant load (stress) level in Stage 2 of analysis. During Stage 2 of analysis (fire exposure), thermal and structural response of the beams was evaluated not only till the end of fire exposure, but over an extending cooling period i.e. period covering between fire being extinguished to complete cooling down, which included time taken for the entire cross-section of the beam to revert back to room temperature.

The thermal response of the analyzed beams, B1 and B2, during fire exposure is shown in Fig. 4 by plotting rebar and concrete temperatures at different locations in the cross section, as a function of time. Unlike fire temperatures that rose rapidly in the first few minutes, the temperatures within the cross section of both beams started to rise at about 10 to 15 minutes into fire exposure, when fire temperatures were already in excess of 700°C. Temperatures within the beam cross-section rise monotonically during heating phase of beams B1 and B2, which last for 120 minutes and 180 minutes respectively.

Furthermore, cross-sectional temperatures in both beams continue to increase even as fire temperatures decay, owing to high thermal inertia of concrete. In fact, cross-sectional temperatures reach peak values during cooling (decay) phase of fire exposure in both beams. Peak rebar temperatures in B1 and B2 are calculated to be 592°C and 715°C at 170 min and 240 min respectively, well after heating phase of fire exposure has ended. Similarly, peak temperatures at

concrete mid-depth are calculated to be 240°C and 315°C respectively. Therefore, the relatively less severe fire exposure adopted for beam B1 leads to relatively lower cross-sectional temperatures as compared to those experienced in beam B2. Nonetheless, both beams do not fail during fire exposure or during extended cooling phase after fire exposure.

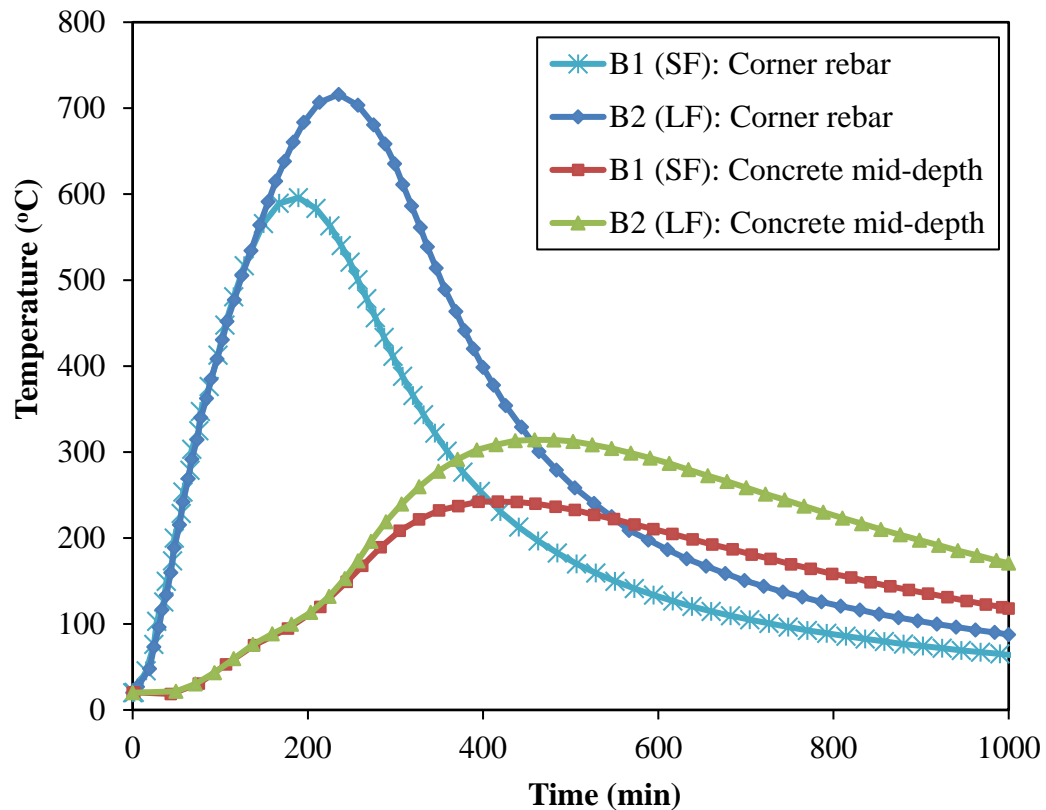


Figure 4. Predicted temperatures in beams B1 and B2

The structural response of beams B1 and B2 can be gauged through predicted mid-span deflections as a function of time as plotted in Fig. 5. During this early stage of fire exposure, deflection rise is mainly governed by level of applied loading and thermal gradients that develop within the beam cross-section. As fire exposure progresses further, cross-sectional temperature within the beam begin to rise and thermal gradients decrease along the depth. Mid-span deflection in beams continues to increase, but at a relatively gradual rate, owing to gradual reduction in mechanical properties, especially elastic modulus of reinforcing steel.

As the rebar temperatures continue to increase steadily, peak mid-span deflection was calculated to be approximately 80 mm and 120 mm in beams B1 and B2 respectively. It can be seen that as peak rebar temperature increased from approximately 600°C to 700°C, peak mid-span deflection increased significantly by almost 50%.

Both beams do not fail during fire exposure and mid-span deflections recover once the rebar and concrete temperatures revert back to ambient temperatures. This can be primarily attributed to the recovery in strength and modulus properties in reinforcing steel, once the beam enters the extended cooling phase. Also, recovery in mid-span deflection during the cooling phase of fire exposure is governed by cross-sectional temperatures, especially rebar temperatures.

A steady state mid-span deflection is attained in both beams B1 and B2 as rebar temperatures cool down below 150°C. In addition, noticeable residual deformation is left over in the fire exposed beams and it does not revert back to its pre-fire configuration after applied loading is removed.

This is primarily due to irreversible temperature induced damage in concrete, which does not recover any of its strength and stiffness properties upon cool down to ambient conditions, as well as residual plastic strains in steel reinforcement and concrete even after cooling down to room temperature. Such deformations adversely affect future serviceability of the fire damaged concrete structure, as these deformations are significantly larger than pre-fire (room temperature) deflection in the member. The residual deformation, with no load acting on the beam, was calculated to be 43 mm for beam B1 and 74 mm for beam B2 respectively (see Fig. 6), and this was assumed to be the initial state for the residual strength analysis in Stage 3.

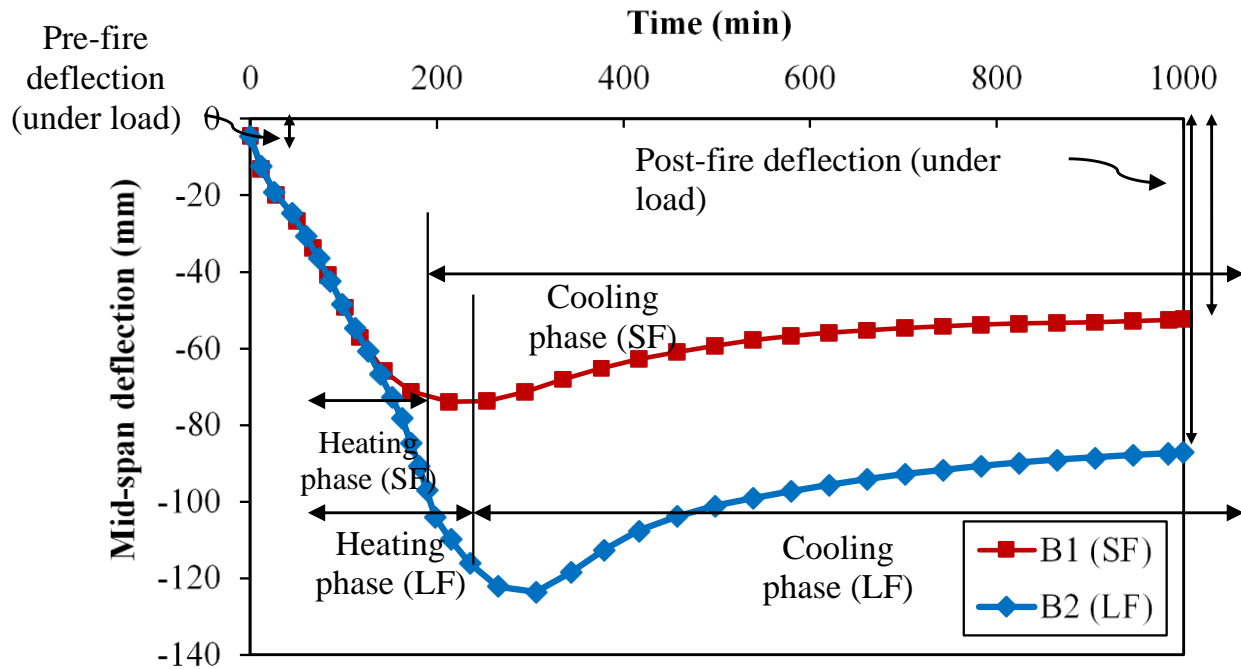


Figure 5. Predicted mid-span deflections during fire exposure in beams B1 and B2.

The residual moment-deflection response of beams B1 and B2 is evaluated in Stage 3 of analysis and shown in Fig. 6. Both fire damaged beams exhibit three key phases in deflection progression i.e., linear response (marked as A-B in Fig. 6), onset of yielding in steel reinforcement (marked as B in Fig. 6), and plastic deformation until failure (marked as B-C in Fig. 6). In the first phase (see A-B in Fig. 6), moment-deflection response of fire damaged beams follows a linear trend as seen in a cracked section, until the onset of yielding in steel reinforcement. This can be attributed to extensive tensile cracking and temperature induced material degradation that occur in the beams during fire exposure. The yielding moment for fire damaged beams B1 and B2 was calculated to be 135 kN-m and 150 kN-m respectively.

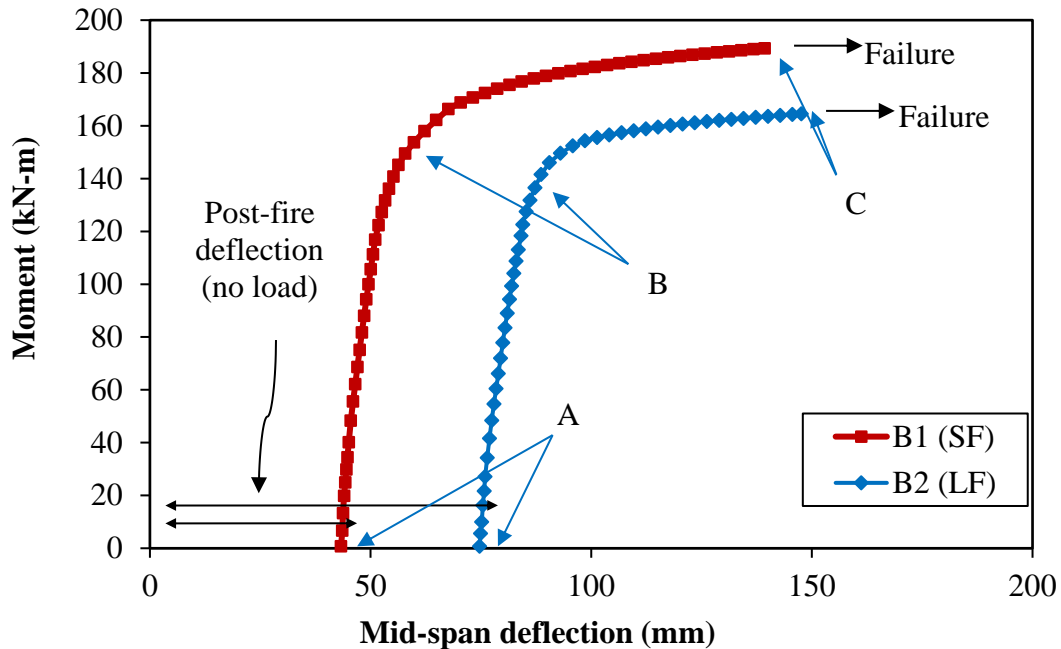


Figure 6. Predicted residual moment-deflection response for fire damaged beams.

Following yielding, the beams deform in a plastic fashion with further increase in moment carrying capacity due to strain hardening effect in steel reinforcement.

The peak moment-carrying capacity in fire damaged beams B1 and B2 was calculated to be 189 kN-m and 164 kN-m respectively. This calculated residual capacity was comparable to room temperature capacity computed as per ACI 318 (ACI, 2008) even after significant fire damage since strain hardening of steel is conservatively not accounted for in ACI 318 (ACI, 2008) design equations for estimating capacity of beam in Stage 1 (Kodur et al., 2010). However, the residual capacity of beams B1 and B2 represents a recovery of 76% and 65% respectively, with respect to realistic room temperature capacity of the beam calculated using finite element analysis. Thus, following a fire incident, fire damaged beams may satisfy design limit state from strength consideration but need to be retrofitted to provide comparable level of safety (capacity) which existed prior to the fire incident.

6. CONCLUSION

A general approach for evaluating residual capacity of fire exposed RC structural members is proposed. Based on the results of analysis the following conclusions can be drawn:

1. Three stages of analysis are required for evaluating the residual capacity of fire exposed reinforced concrete structural members, namely at pre-fire ambient conditions, during fire exposure, and following cooling of fire exposed RC member.
2. The finite element computer software ABAQUS, can successfully be applied for evaluating the response of fire exposed reinforced concrete structural members. Specific input parameters, including fire characteristics, structural parameters and material properties are to be input at each stage of analysis.
3. Irrecoverable residual plastic deformations occur in RC members due to temperature induced damage sustained during fire exposure. These residual deformations are significantly larger than pre-fire (room temperature) deformations and can adversely affect post-fire serviceability of the fire damaged concrete member.

Following a fire incident, fire damaged beams may satisfy design limit state from strength consideration but need to be retrofitted to provide comparable level of safety (capacity) which existed prior to the fire incident.

7. ACKNOWLEDGEMENTS

The authors wish to acknowledge the support of United States Agency for International Development (through Pakistan-US Science and Technology Cooperative Program grant PGA-2000003665) and Michigan State University for undertaking this research. Any opinions, findings, conclusions, or recommendations expressed in this paper are those of the author and do not necessarily reflect the views of the institution.

8. REFERENCES

- ABAQUS (2012), *ABAQUS Version 6.12 Documentation*. Dassault Systemes Simulia Corp., Providence, RI. URL: <http://130.149.89.49:2080/v6.12/index.html>
- American Concrete Institute (ACI) (2008). *ACI 318-08: Building code requirements for reinforced concrete*. Vol. 552. American Concrete Institute. 465 pp. Farmington Hills, MI.
- ASTM International (2018). *E119-18 Standard Test Methods for Fire Tests of Building Construction and Materials*. West Conshohocken, PA; ASTM International. doi: <https://doi.org/10.1520/E0119-18>
- Bai, L., Wang, Z. (2011). *Residual Bearing Capacity of Reinforced Concrete Member after Exposure to High Temperature*. *Advanced Materials Research*. 368–373:577–81. <https://doi:10.4028/www.scientific.net/AMR.368-373.577>.
- Beitel J., Iwankiw N. (2005). *Historical Survey of Multistory Building Collapses Due to Fire*. *Fire Protection Engineering*. 3rd Quart. issue 27: 42-49.
- European Committee for Standardization (CEN) (2004a). *EN 1991-1-2, Eurocode 1: Actions on structures. Part 1-2: General actions - Actions on structures exposed to fire*. Brussels, Belgium.
- European Committee for Standardization (CEN) (2004b). *EN 1992-1-1, Eurocode 2: Design of concrete structures. Part 1-1: General rules and rules for buildings*. Brussels, Belgium; 2004.
- European Committee for Standardization (CEN) (2004c). *EN 1992-1-2, Eurocode 2: Design of Concrete Structures. Part 1–2: General Rules – Structural Fire Design*, p. 97. Brussels, Belgium.
- European Committee for Standardization (CEN) (2004d). *EN 1993-1-2, Eurocode 3: Design of steel structures. Part 1-2: General rules-structural fire design*. Brussels, Belgium; 2004.
- European Committee for Standardization (CEN) (2004e). *EN 1994-1-2, Eurocode 4: Design of composite steel and concrete structures. Part 1-2: General rules-structural fire design*. Brussels, Belgium; 2004.
- Kodur, V. (2014). *Properties of concrete at elevated temperatures*. *International Scholarly Research Notices Civil Engineering*. 2014 (ID 468510): 1–15. <https://doi.org/10.1155/2014/468510>
- Kodur, V., Hibner, D., Agrawal, A. (2017). *Residual response of reinforced concrete columns exposed to design fires*. *Procedia Engineering*. 210: 574–81. <https://doi.org/10.1016/j.proeng.2017.11.116>.
- Kodur, V. K., Agrawal, A. (2015). *Critical Factors Governing the Residual Response of Reinforced Concrete Beams Exposed to Fire*. *Fire Technology*. 52(4): 967 pp. ISSN: 0015-2684 eISSN: 1572-8099. Springer US. <https://doi.org/10.1007/s10694-015-0527-5>.
- Kodur, V. K. R., Agrawal, A. (2016) *An approach for evaluating residual capacity of reinforced concrete beams exposed to fire*. *Engineering Structures*. 110:293–306. <https://doi.org/10.1016/j.engstruct.2015.11.047>.

- Kodur, V. K. R., Dwaikat, M. B., Fike, R.S. (2010). *An approach for evaluating the residual strength of fire-exposed RC beams*. Magazine of Concrete Research. 62 (7): 479–88. ISSN: 0024-9831, eISSN: 1751-763X. <https://doi.org/10.1680/macr.2010.62.7.479>.
- Kodur, V. K. R., Phan, L. (2007). *Critical factors governing the fire performance of high strength concrete systems*. Fire Safety Journal. 42 (6-7): 482-488. ISSN: 0379-7112. <https://doi.org/10.1016/j.firesaf.2006.10.006>.
- Kodur, V. K. R., Raut, N. K., Mao, X. Y. (2013). *Khaliq W. Simplified approach for evaluating residual strength of fire-exposed reinforced concrete columns*. Materials and Structures. 46:2059–2075. <https://doi:10.1617/s11527-013-0036-2>.
- Neves, I., Rodrigues, J. P. C., Loureiro A. D. P. (1996). *Mechanical properties of reinforcing and prestressing steels after heating*. Journal of Materials in Civil Engineering 8. (4):189–194. [https://doi.org/10.1061/\(ASCE\)0899-1561\(1996\)8:4\(189\)](https://doi.org/10.1061/(ASCE)0899-1561(1996)8:4(189))
- Tovey, A. K., Crook R. N. (1986). *Experience of Fires in Concrete Structures*. in SP-092: Evaluation and Repair of Fire Damage to Concrete. Special Publication. 92:1-14. American Concrete Institute.

Passivation process quality in reinforced concrete: effects of polarization periodicity and passivation consolidation parameters on data processing

J. A. Briceño-Mena¹ , M. G. Balancán-Zapata¹ , P. Castro-Borges^{1*} 

*Contact author: pcastro@cinvestav.mx

DOI: <http://dx.doi.org/10.21041/ra.v10i2.466>

Reception: 13/12/2019 | Acceptance: 24/04/2020 | Publication: 30/04/2020

ABSTRACT

The passivation process quality was studied considering polarization periodicity, passivation consolidation parameters, and data processing. Passivation process quality in steel reinforcement affects a structure's planned future service life. Some research has addressed this phenomenon, but its study is complicated by the limits of analog-era data, dispersion in corrosion rate data, and their interpretation. Two series of small reinforced concrete specimens were built using two water/cement ratios and two curing/storage combinations and exposed to the marine environment. Polarization periodicity did not affect passivation/depasivation during passivation but on the data processing. The curing and storage process influenced the tendency towards depasivation. Post-curing storage type affected the cumulative corrosion rate from 1 to 5 $\mu\text{A}\cdot\text{day}/\text{cm}^2$; this is equivalent to the margin of uncertainty in interpretation.

Keywords: cumulative corrosion rate, w/c ratio, reinforced concrete, tropical marine environment.

Cite as: Briceño-Mena, J. A., Balancán-Zapata, M. G., Castro-Borges, P. (2020), "Passivation process quality in reinforced concrete: effects of polarization periodicity and passivation consolidation parameters on data processing", Revista ALCONPAT, 10 (2), pp. 243 – 258, DOI: <http://dx.doi.org/10.21041/ra.v10i2.466>.

¹ Centro de Investigación y de Estudios Avanzados del IPN, Unidad Mérida, km. 6 Ant. Carr. a Progreso, 97310 Mérida, Yucatán, México

Legal Information

Revista ALCONPAT is a quarterly publication by the Asociación Latinoamericana de Control de Calidad, Patología y Recuperación de la Construcción, Internacional, A.C., Km. 6 antigua carretera a Progreso, Mérida, Yucatán, 97310, Tel.5219997385893, alconpat.int@gmail.com, Website: www.alconpat.org

Responsible editor: Pedro Castro Borges, Ph.D. Reservation of rights for exclusive use No.04-2013-011717330300-203, and ISSN 2007-6835, both granted by the Instituto Nacional de Derecho de Autor. Responsible for the last update of this issue, Informatics Unit ALCONPAT, Elizabeth Sabido Maldonado, Km. 6, antigua carretera a Progreso, Mérida, Yucatán, C.P. 97310.

The views of the authors do not necessarily reflect the position of the editor.

The total or partial reproduction of the contents and images of the publication is strictly prohibited without the previous authorization of ALCONPAT Internacional A.C.

Any dispute, including the replies of the authors, will be published in the first issue of 2021 provided that the information is received before the closing of the third issue of 2020.

Calidad del proceso de pasivación en concreto reforzado: efectos de la periodicidad de la polarización y los parámetros de la consolidación de la pasivación en el procesamiento de datos

RESUMEN

La calidad del proceso de pasivación se estudió considerando la periodicidad de polarización, los parámetros de consolidación de pasivación y el tratamiento de datos. Algunas investigaciones han abordado la calidad del proceso de pasivación, pero su estudio se complica por la limitación de los datos de la era analógica, la dispersión de éstos y la interpretación de la velocidad de corrosión. Se construyeron dos series de especímenes de concreto reforzado utilizando dos relaciones agua/cemento y dos combinaciones de curado/almacenamiento y se expusieron en un medio marino. La periodicidad de la polarización no tuvo efecto sobre la pasivación/despasivación durante la pasivación, sino sobre el tratamiento de los datos. El proceso de curado y almacenamiento influyó en la tendencia a la despasivación. El tipo de almacenamiento posterior al curado afectó la velocidad de corrosión acumulada de 1 a 5 $\mu\text{A}\cdot\text{día}/\text{cm}^2$; esto es equivalente al margen de incertidumbre en la interpretación.

Palabras clave: velocidad de corrosión acumulada; relación a/c; concreto reforzado; ambiente tropical marino.

Qualidade do processo de passivação em concreto armado: efeitos da periodicidade da polarização e parâmetros da consolidação da passivação no processamento de dados

RESUMO

A qualidade do processo de passivação foi estudada considerando a periodicidade da polarização, os parâmetros de consolidação da passivação e o tratamento dos dados. Algumas pesquisas abordaram a qualidade do processo de passivação, mas seu estudo é complicado pela limitação dos dados da idade analógica, pela dispersão destes e pela interpretação da taxa de corrosão. Duas séries de amostras de concreto armado foram construídas usando duas relações água / cimento e duas combinações de cura / armazenamento e expostas em um ambiente marinho. A periodicidade da polarização não teve efeito na passivação / despasivação durante a passivação, mas no tratamento dos dados. O processo de cura e armazenamento influenciou a tendência à despasivação. O tipo de armazenamento pós-cura afetou a taxa de corrosão cumulativa de 1 a 5 $\mu\text{A}\cdot\text{dia}/\text{cm}^2$; isso é equivalente à margem de incerteza na interpretação.

Palavras-chave: taxa de corrosão acumulada; relação a / c; concreto armado; ambiente marinho tropical.

1. INTRODUCTION

In natural conditions, a layer of oxides that protects reinforcing steel is consolidated over time (Poursaee & Hansson, 2007). This layer is formed due to the high alkalinity of the concrete and is known as the passivation layer (Andrade et al., 1995). This layer provides a barrier against aggressive agents, on whose stability of the passivation quality depends. Therefore, when the structures are exposed to an aggressive natural environment, the time for passivation to occur and consolidate is very important, since the electrochemical behavior of the reinforcing steel will

depend on it and, therefore, its corrosion process (Ahmad & Kumar, 2013), understanding as consolidation the electrochemical stability of the passive layer. There are studies on the passivation of the reinforcement, as well as the initiation and propagation stages of corrosion (Andrade et al., 1995; Huet et al., 2005; Jiang et al., 2017). However, the objectives of these studies did not necessarily take into account providing adequate times for steel to consolidate passivation (Poursaei & Hansson, 2007). Furthermore, the variability in the study methods of passivation (Alonso et al., 2000; Jiang et al., 2017; Page, 2009; Poursaei & Hansson, 2007) may cause a discrepancy in the interpretation of the same, causing it to have overestimation or underestimation values. Data on corrosion in reinforced concrete is commonly expressed as instantaneous corrosion rate, i_{corr} , as a function of time (Alonso et al., 2000; Andrade & Alonso, 1996; Castro-Borges et al., 2013; Castro-Borges et al., 2017; Lopez & Gonzalez, 1993; Pech-Canul & Castro, 2002; Pedrosa & Andrade, 2010; Rebolledo & Andrade, 2010). Many studies include analysis of i_{corr} behavior from the passivation zone to the moment when it begins to exhibit clear signs of depassivation. This helps in evaluating the corrosion resistance of different materials. Some works of both: before the 2000 year (Alonso et al., 2000; Andrade & Gonzalez, 1978; Lopez & Gonzalez, 1993) and after the 2000 year (Ghods et al., 2009; Pech-Canul & Castro, 2002; Poursaei & Hansson, 2007) sources, address the phenomena that occur before depassivation. However, the limitation of using analog data from earlier studies, and the intrinsic dispersion of i_{corr} data have delayed a deeper understanding of i_{corr} tendencies in the passivation zone. Previous studies (Andrade & Alonso, 1996; Castro-Borges et al., 2013, 2017; Melchers & Li, 2006; Pedrosa & Andrade, 2010; Rebolledo & Andrade, 2010) include passivation zone analyses and some of them found interpretations of the data trends by applying straightforward mathematical processing, which of course would need to be confirmed under different exposure conditions.

The current practice of designing reinforced concrete structures with nearly one-hundred-year service lives implies the application of durability criteria to prevent corrosion. This calls for a much deeper understanding of corrosion in the passivation zone. Attaining passivation zone stability and durability require optimum concrete quality (curing conditions, water/cement ratio), knowledge of the exposure environment (prevailing and non-prevailing winds, the regime of temperature and relative humidity) and damage prevention measures (concrete cover, surface sealing) among other factors. An inadequate combination of these at an early age can negatively affect the passivation quality and future service life. The study of the passivation quality in the steel embedded in concrete is vital since it can significantly affect later electrochemical behavior and consequently a structure's short-, medium- and long-term service life.

However, routine procedures for long-term field studies, with a variety of combined objectives and different materials, do not easily allow a detailed study of the passivation quality at an early age, and therefore the impact of this situation is not known in the service life of the element. An example of this is usually when the measurements are performed in the field at intervals of low periodicity. This situation could mask trends that could be useful for service life models. For these reasons, doubts arose after more than ten years of experimentation (from 2007) in field specimens in which a relatively early depassivation process was expected, which did not occur. Then, it was decided to do, ten years later, another set of specimens (from 2017), in which some parameters in their composition and exposure would be modified to be able to analyze in more detail the quality of the passivation.

On the other hand, studying passivation quality requires full knowledge of the general criteria used to define a reinforcement bar as passive, in transition or active. The most accepted criterion is that passivation ends when the corrosion rate exceeds the $0.1 - 0.2 \mu\text{A}/\text{cm}^2$ range (Andrade & Gonzalez, 1978; Berke et al., 1996), although some widely used criteria include a range of $0.1 - 0.5 \mu\text{A}/\text{cm}^2$ (Andrade & Alonso, 1996; NMX-C-501-ONNCCE, 2015; Troconis et al., 1998). For practical purposes, a conservative criterion of values $< 0.1 \mu\text{A}/\text{cm}^2$ indicates passivity in concrete

reinforcement. Considering the above, the present study objective was to analyze the passivation quality in concrete reinforcement in terms of polarization periodicity during measurement, passivation parameters and data processing.

For this paper, only the data corresponding to a concrete cover of 20 mm is analyzed, which is the most related to the typical situation of concrete in the region.

2. EXPERIMENTAL PROCEDURE

2.1 Specimen design

Using the ACI design method (ACI 211-91, 2002), twelve prismatic specimens (150x150x300 mm) were made using Portland Compound Cement (CPC30R) standardized by Mexican standard (NMX-C-414-ONNCCE, 2014), and limestone rock aggregate typical of southeast Mexico. Table 1 shows the basic characteristics of concrete: curing, storage condition, type of cement, and water/cement ratio, and Table 2 the dosage of concrete. Each specimen was reinforced with six, 42-grade, 3/8” diameter carbon steel bars (350 mm long), placed at depths of 15, 20 and 30 mm. Before placement in the specimens, the study area was marked on each bar, leaving a 150 mm long clear area in its center. The remaining bar was painted with epoxy paint and its end covered with isolating tape (Figure 1).

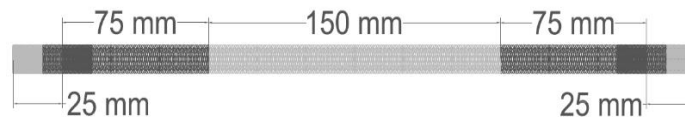


Figure 1. Marking of 150 mm unprotected area in the center of the bar (study zone).

The concrete was prepared using two water/cement (w/c) ratios: 0.45 (considered high-quality concrete in the study area), and 0.65 (considered low quality). Six specimens (old specimens - 2007) were cured in a moist room for 28 days and then kept in storage for 233 days. The second set of six (new specimens - 2017), was cured for seven days by direct application of tap water, common practice in the study area, and kept in storage for 27 days.

Table 1. Basic characteristics of concrete, curing and storage type

Specimen	Curing process	Storage condition (without control of relative humidity and temperature)	Type of cement	Water/cement ratio
2007	Moist room for 28 days	Kept in semi-controlled storage for 233 days after curing	Portland Compound Cement (CPC30R)	0.45 (3 specimens) 0.65 (3 specimens)
2017	Direct tap water, few times/day for 7 days	Kept in semi-controlled storage for 27 days after curing		0.45 (3 specimens) 0.65 (3 specimens)

Table 2. Mixture proportions for concrete

Specimen	w/c ratio	Content of material (kg/m ³)				f'c - 28 days (kg/cm ²)
		cement	sand	gravel	water	
2007	0.45	408	681	800	287	N/A
	0.65	277	739	868	280	N/A
2017	0.45	456	638	757	205	231
	0.65	315	740	757	205	159

Before exposure, the inferior and superior sides of the specimens were painted with epoxy paint to limit the influence of aggressive agents to the lateral faces (Figure 2).

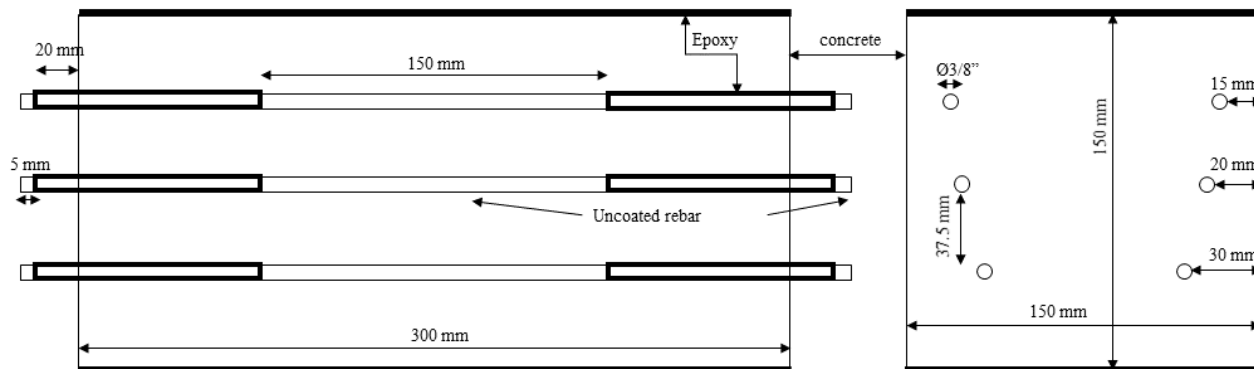


Figure 2. Specimen setup

2.2 Exposure environment

Specimens were exposed in a marine tropical environment on the north coast of the Yucatan Peninsula, Mexico. They were placed on the beach 50 m from the seashore and 0.95 m above the soil surface, positioning the area with most covering on the underside of the specimen. Their orientation was such that they were exposed to different regional climate conditions: prevailing winds out of the northeast (PW) and non-prevailing winds out of the southwest (NPW) (Figure 3). The first set of specimens (2007) was exposed 261 days after cast and the second set (2017) 34 days after cast.

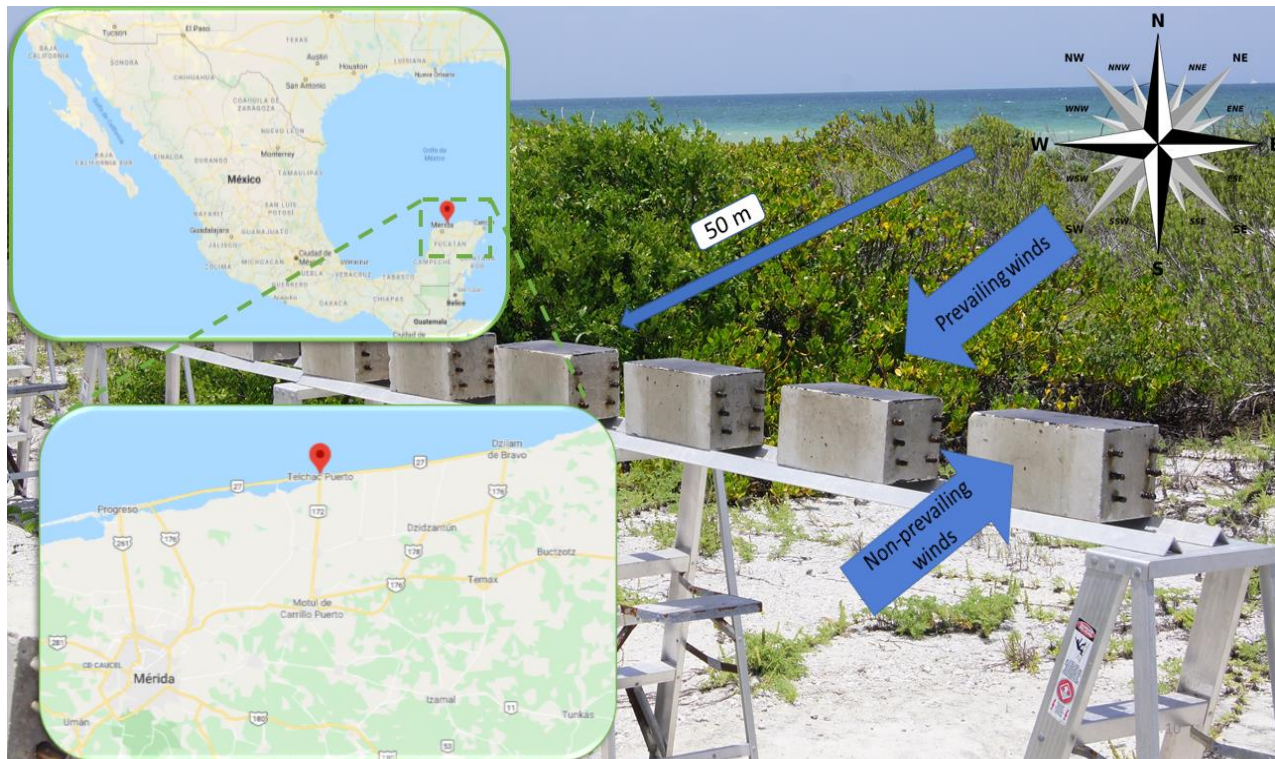


Figure 3. Setup of station for exposure of specimens.

2.3 Corrosion measurements

Steel reinforcement corrosion rate (i_{corr} , $\mu\text{A}/\text{cm}^2$), potential (E_{corr} , mV vs. Cu/CuSO₄), and concrete electrical resistance (R_s , k Ω) were measured with a commercial portable corrosimeter with a confinement system, which uses the linear polarization resistance technique (R_p) (Andrade & Alonso, 1996). The value for electrical resistivity (ρ , k Ω -cm) was calculated with equation (1), where D is the rebar diameter in cm.

$$\rho = 2 R_s D \quad (1)$$

For the 2007 specimens, electrochemical measurements were taken approximately every 90 days for 557 days, while for the second set, 2017, they were taken every 14 days for 279 days.

3. RESULTS AND DISCUSSION

3.1 Passivation quality at initial ages

For the present purposes, initial age is defined as the time during which the specimens exhibited electrochemical behavior in the passivation zone. Interpretation of passivation zone data was facilitated by using a conservative limit value of $0.1 \mu\text{A}/\text{cm}^2$ with a range of $0.1 - 0.5 \mu\text{A}/\text{cm}^2$ for depassivation. Figure 4 is a typical plot used for i_{corr} recording versus time in small specimens exposed to a natural marine environment in different seasons. Even though three concrete covers (15 mm, 20 mm and 30 mm) were studied, this work discusses only data for the 20 mm concrete cover. This one is very common in the region's marine zone although applicable regulations demand thicker cover (NMX-C-530-ONNCCCE, 2017). Other variables were the specimen's orientation (PW and NPW), included to identify any effect from wind, and concrete quality (w/c 0.45 and 0.65).

In the high-quality concrete (w/c 0.45) specimens, two data types were collected, one for exposure begun in 2007 (Table 1 and Figure 4a) and the other from 2017 (Table 1 and Figure 4b). The parameter of similar quality among specimens was mainly given by the type of cement and the w/c ratio. This was due to the lack of more information in 2007. However, one way to minimize the variability of the CPC was by comparing elements from the same family (2007 or 2017), where the difference between elements was more noticeable, from the same family, due to more important factors such as curing and storage. In fact, the data for exposure since 2007 (Figure 4a) were essentially stable during the first 557 days. The first 233 days corresponded to storage in a semi-controlled environment. From day 233 to day 557, they were exposed to a tropical marine environment, but the passivation condition continued almost unchanged.

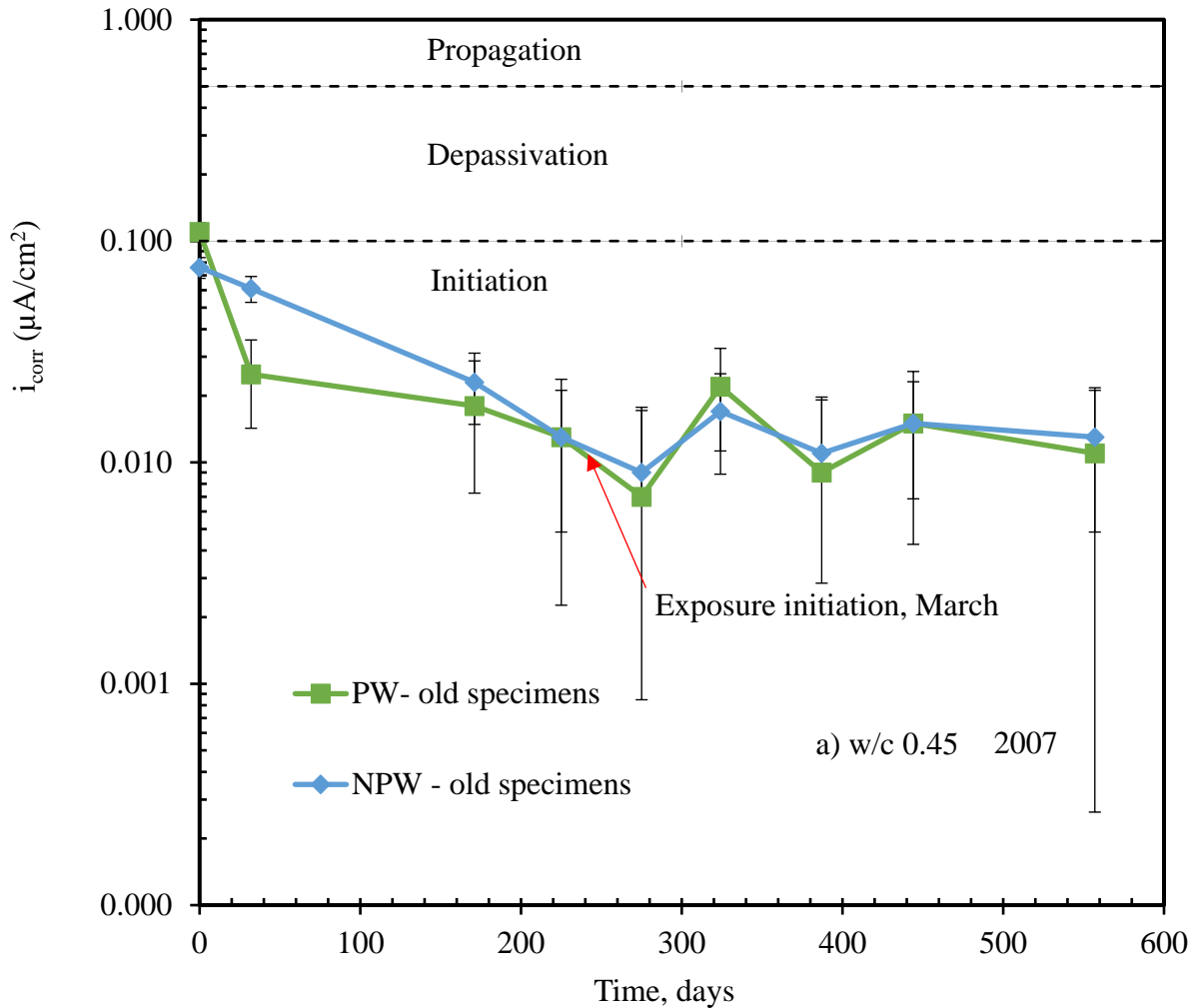
On the other hand, the data for exposure 2017 (Figure 4b), corresponding to 27 days in laboratory conditions and 211 days of natural exposure, started to show differences between PW and NPW. These figures are confirming a difference between both passivation qualities which is mainly due to the suitable curing and storage process of specimens for 233 days at the non-aggressive environment, without any aggressive agents, for specimens from 2007. Therefore, the quality of the passivation at initial ages allowed a subsequent better instantaneous electrochemical behavior for 2007 (Figure 4a) than for 2017 specimens (Figure 4b). The response of the low-quality concrete (w/c 0.65) was like that of the high-quality concrete (w/c 0.45) for both 2007 (Figure 4c) and 2017 (Figure 4d). However, instantaneous data for both w/c ratios seem to be a little bit dissimilar in 2017.

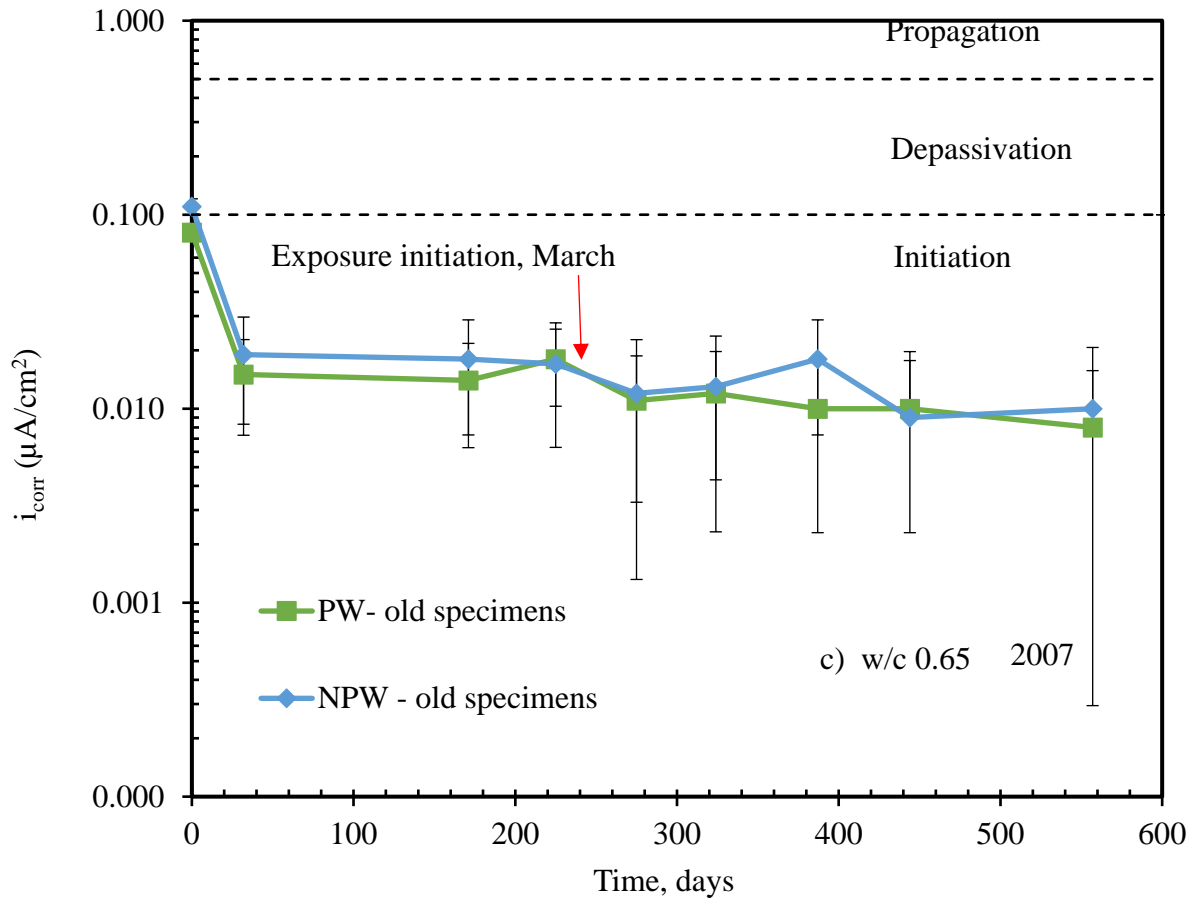
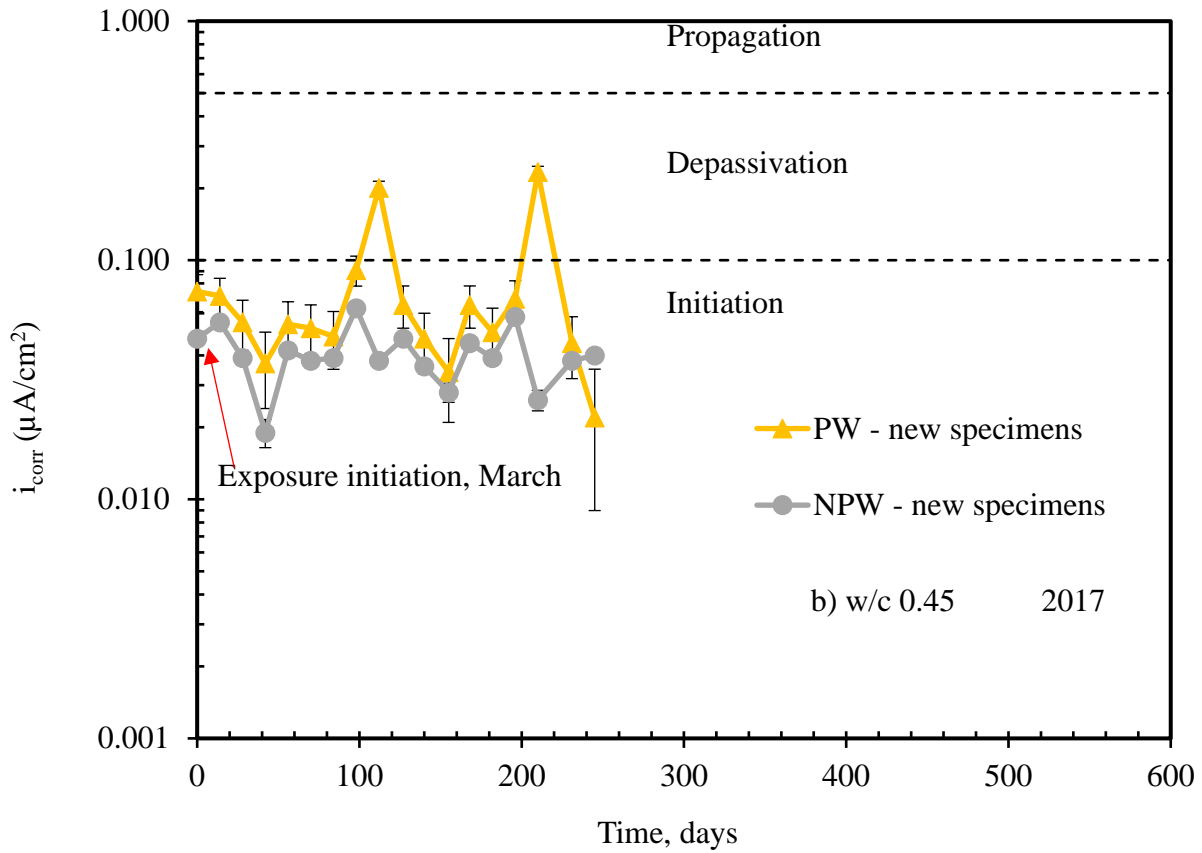
Although passivation zone behavior was stable, there were still doubts as to whether there were moments when, in response to changes in season (rainy and dry), the corrosion rate might have exceeded passivation zone values. As part of a larger project, specimens were built and exposed in 2017 for other purposes but clearly could serve to verify if this could influence the cumulative corrosion rate (i_{cum}), as reported recently (Castro-Borges et al., 2013, 2017; Melchers & Li, 2006; Pedrosa & Andrade, 2010; Rebolledo & Andrade, 2010). Unlike those built-in 2007, these new ones were exposed to the marine environment almost immediately after curing. In a comparison of the two processing over the same time scale (Figures 4a to 4d), the newer specimens exhibited behavior nearer the depassivation zone than the older specimens for all the studied variables. Curing, storage, and environmental variables affected, to a greater or lesser extent, the tendency towards depassivation. The parameters measured here helped to confirm passivation process quality at initial ages regardless of dependent variables (i.e. w/c and orientation). This will affect the planned specimen service life in terms of depassivation and propagation.

3.2 Effects of electrochemical measurement periodicity on the data processing

An obvious concern when taking frequent electrochemical measurements in passive steel reinforcement in concrete is possible damaging polarization which could affect the real i_{corr} value. In modern times the damaging polarization is controlled, for example, by measuring the i_{corr} through the linear polarization resistance with sweeping rates on the order of hundredths of millivolts and with cathodic polarization close to 20 mV at the most. Therefore, and within these ranges, a higher measurement periodicity in the polarizations to measure corrosion is not detrimental to the studied rebar, and especially in field tests. This general subject has been addressed extensively, but no previous studies (Andrade & Gonzalez, 1978; Andrade et al, 1986; Clément et al, 2012; Hansson et al, 2012) contain information about the possible effect of the periodicity of the measurements to interpret the meaning of the i_{cum} under natural conditions. The most obvious difference between laboratory and field studies is that under laboratory conditions measurement intervals can be minutes, whereas under natural conditions intervals are normally on the order of days. The possible effect of polarization periodicity at initial ages in cumulative corrosion could occur in a natural environment in response to peaks in temperature and humidity,

which would allow interpreting more accurately the changes in observed trends. Therefore, determining if electrochemical measurement periodicity influences the interpretation of passivation/depasivation in reinforced concrete with i_{cum} under a natural environment during the initiation stage (passivation zone) is therefore quite technically and economically important. The i_{corr} confirm that measurement periodicity in the older or newer specimens did not affect data credibility since both specimen series exhibited the same tendencies (Figure 4). However, when using i_{cum} , electrochemical measurement periodicity could create differences among trends that, if known, could be equivalent to tolerance levels used in destructive tests such as those used to compare electrochemical losses to gravimetric losses (Andrade & Martinez, 2005). To approximate these differences the data in Figure 4 were analyzed, resulting in the data in Figure 5.





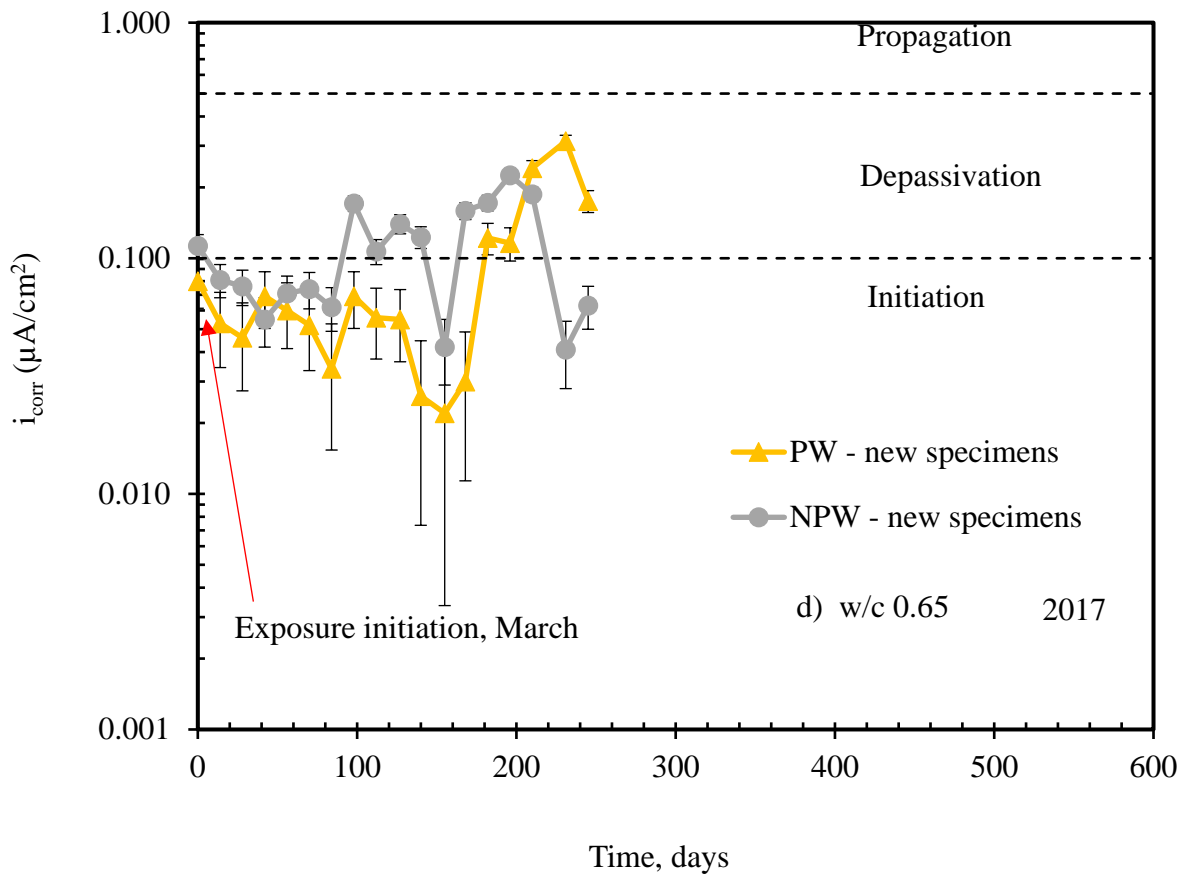


Figure 4. Instantaneous corrosion rate vs. time: a) w/c 0.45, march 2007; b) w/c 0.45, march 2017; c) w/c 0.65, march 2007; d) w/c 0.65, march 2017.

Figure 5 shows a relation between sixteen measurements from March 2017 and four measurements from March 2007 that correspond, in both cases, to an exposure period of 211 days just after the beginning of the exposure to the environment. This relation $16/4 = 4/1$ was taken as our reference to discuss the effect of the measurement periodicity on the interpretation of i_{cum} . The term i_{cum} can be defined as the sum of previous corrosion rates at each specific period (Castro-Borges et al., 2013) as given by equation (2):

$$i_{cum} = \frac{(t_f - t_i) * (i_{corrf} + i_{corri})}{2} + i_{cum_i} \quad (2)$$

Where:

t_f = Final day of the considered period

t_i = Initial day of the considerer period

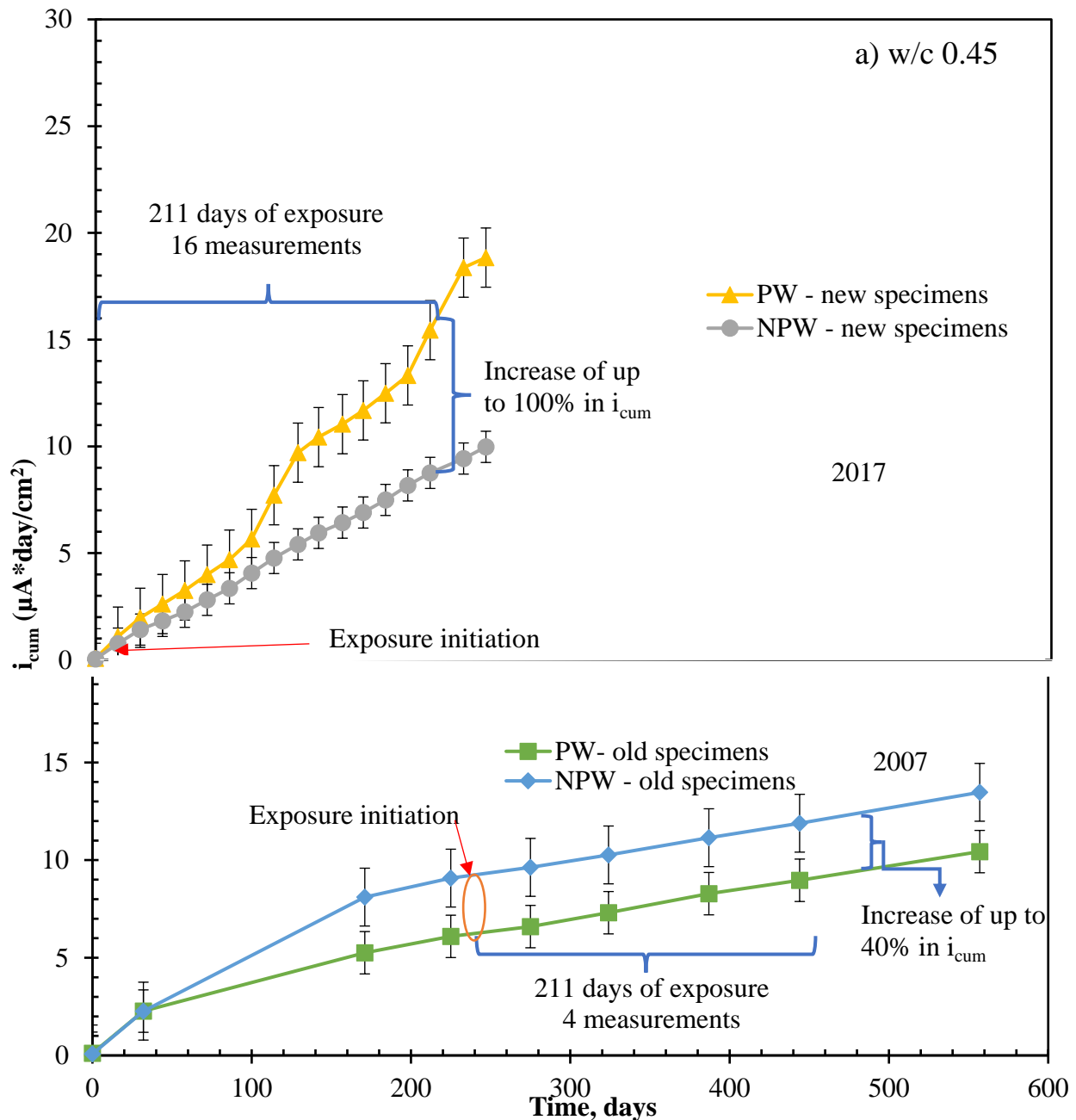
i_{corrf} = Final i_{corr} of the considered period

i_{corri} = Initial i_{corr} of the considered period

i_{cum_i} = Previously accumulated corrosion rate

When the Figure 5 data were analyzed using a 4/1 electrochemical measurement periodicity ratio, the difference between PW and NPW was up to 100% on the i_{cum} value on specimens that did not have time to consolidate their passivation correctly (2017). Moreover, the tendencies between PW and NPW were inverted when considering the quality of concrete (w/c 0.45 or 0.65). This coincides and could be compared with tolerance due to errors that are attributed to data collection when electrochemical losses are compared to gravimetric losses (Andrade & Martinez, 2005). However,

this did not happen with those (2007) that were stored for 233 days and then exposed for 211 days, and that influenced the i_{cum} between PW and NPW of up to 40%. In this case, it could mean the possibility of having a sharper tolerance if electrochemical losses were compared to gravimetric ones. The values of 100% and 40% probably mean a characteristic difference between specimens with not consolidated or consolidated passivation just before the beginning of the depassivation stage for the 4/1 ratio of measurement periodicity. The experimental and data collection limitations could slightly influence the results, so they do not necessarily apply under different conditions than those reported in this work. In equivalent form, if measurement ratios $> 4/1$ were found and give even higher numerical differences in cumulative corrosion would place data credibility in question at initial ages (passivation zone). This is supported by the fact that the values of i_{corr} (Figure 4) begin to show limit values close to $0.1 \mu A/cm^2$, the 100% of tolerance when comparing electrochemical vs gravimetric losses, and the inverted position of the PW and NPW tendencies in Figure 5.



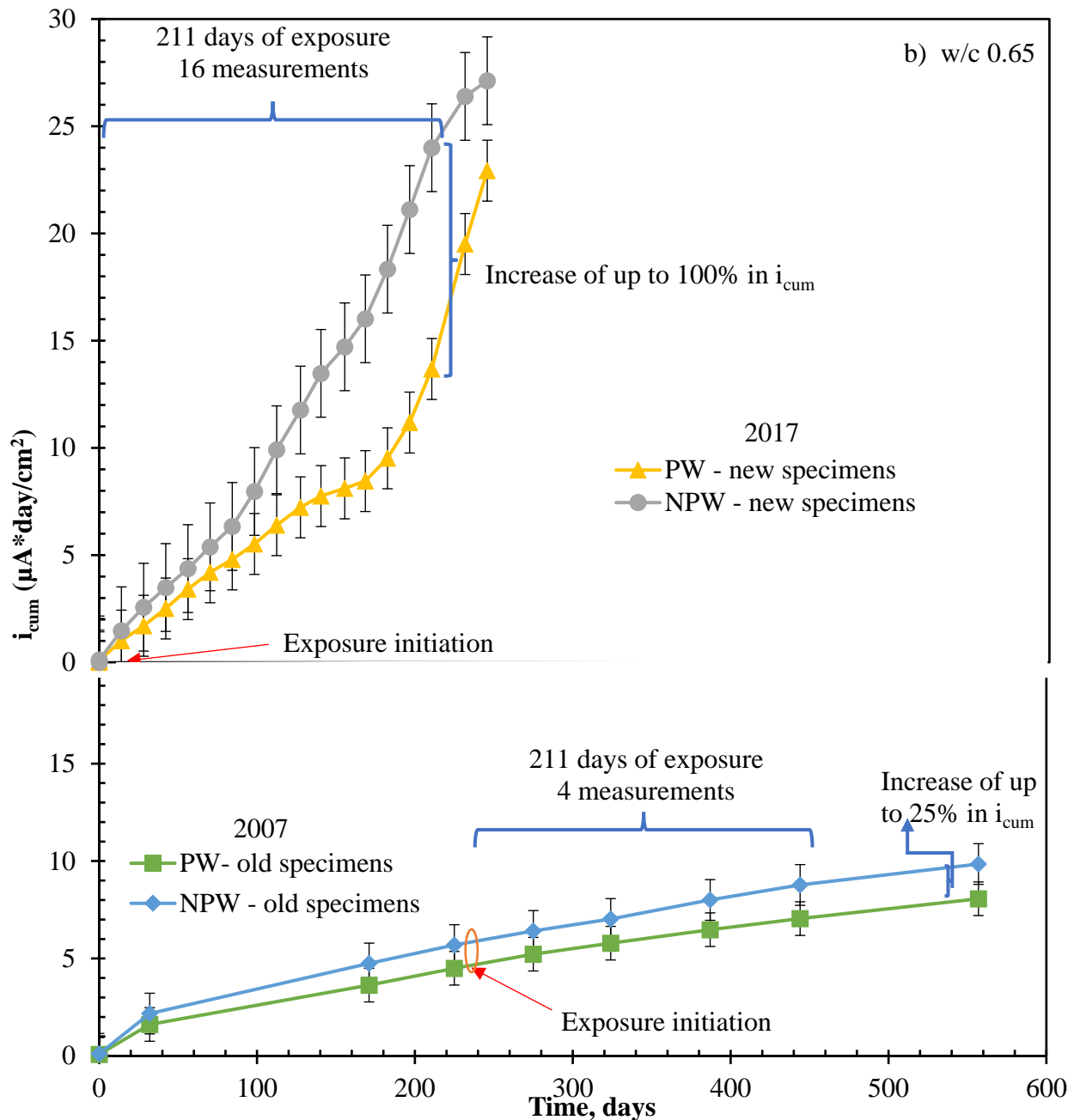


Figure 5. Cumulative corrosion rate vs. time: a) w/c 0.45; b) w/c 0.65.

3.3 Margin of uncertainty in cumulative corrosion

In Figure 6, the i_{cum} of the specimens made in 2007 corresponds to the moment just before exposure to the tropical marine environment. These specimens were under semi-controlled conditions (storage in a laboratory, sheltered from the rain and the sun and without control of relative humidity and temperature) for the entire period. No significant variations were noted at a measurement periodicity of approximately three months (Figure 4). Considering that they were electrochemically stable in the passivation zone, cumulative corrosion immediately before exposure to the natural environment differed between surfaces (PW and NPW), from $1 \mu\text{A}\cdot\text{day}/\text{cm}^2$ for w/c 0.65 to $5 \mu\text{A}\cdot\text{day}/\text{cm}^2$ for w/c 0.45. Ahmad (2003) mentions that the lower the cement content, the lower the plastic consistency in the mix, which causes that the passivation of the steel does not occur uniformly, resulting in the depassivation; therefore, the results found could represent the margin of

uncertainty when interpreting i_{cum} at initial ages (passivation zone) and these differences ($1 \mu A \cdot day/cm^2$ for w/c 0.65 to $5 \mu A \cdot day/cm^2$ for w/c 0.45) can be deemed as characteristics of the materials used.

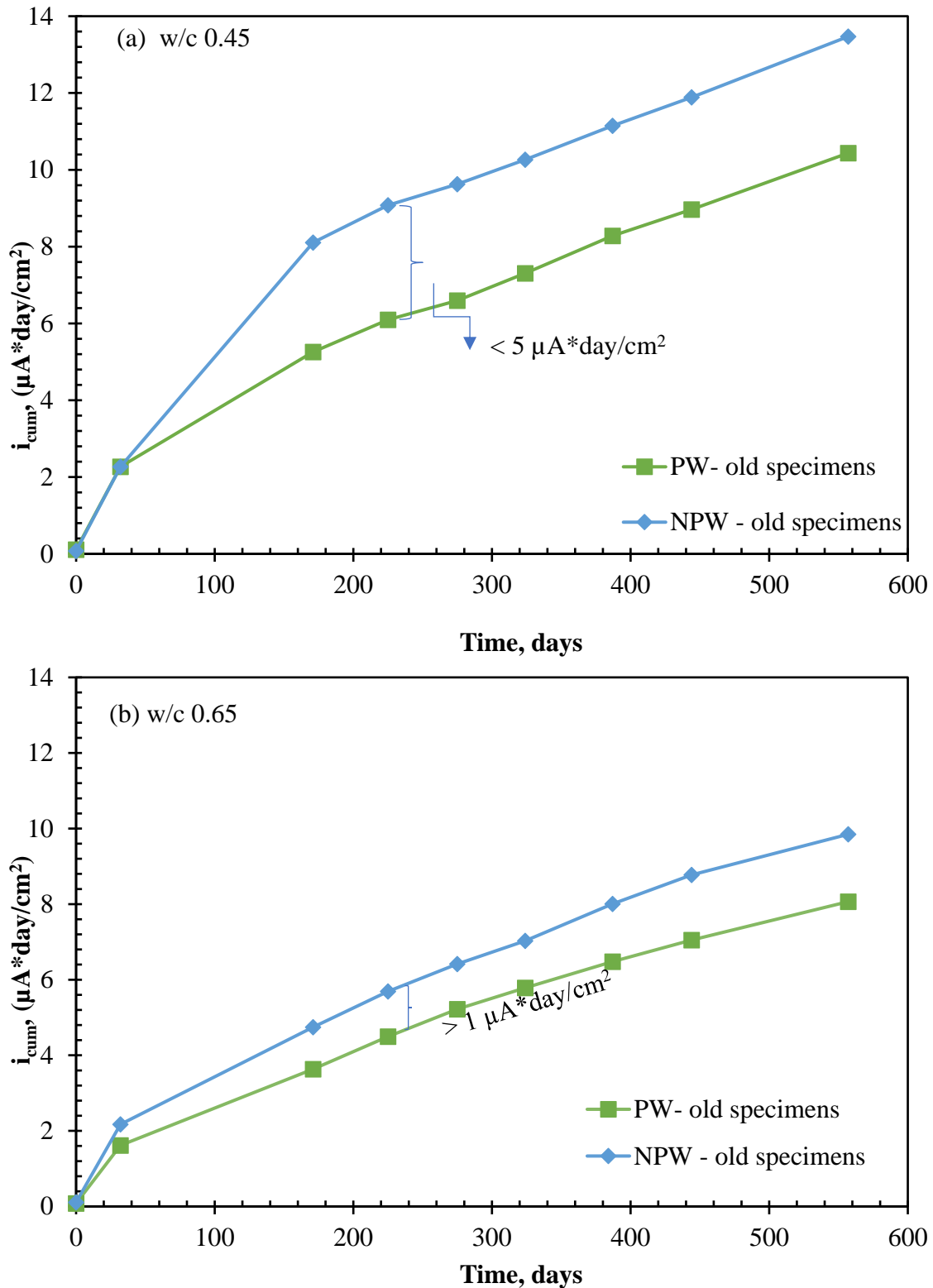


Figure 6. Uncertainty in cumulative corrosion rate vs. time: a) w/c 0.45; b) w/c 0.65.

4. CONCLUSIONS

The reported results apply to these specific study conditions. Therefore, they can be extrapolated taking the appropriate precautions to other situations. In the present data, the parameters used in consolidating passivation quality at initial ages (i.e. curing, storage, and environmental variables) affect the tendency to depassivation regardless of the dependent variables (w/c ratio and orientation). This can affect the planned service life.

As and expected, the polarization produced by electrochemical measurement periodicity (days) in a tropical marine environment did not influence reinforced concrete passivation/depassivation during the initiation stage (passivation zone).

When electrochemical measurement periodicity was calculated at a 4/1 ratio, it was found that it could numerically influence the cumulative corrosion value by up to 100%. This is equivalent to the tolerance used in destructive tests comparing electrochemical losses to gravimetric losses.

Even though it is considered a largely qualitative method, i_{cum} allows the detection of changes in the electrochemical behavior of reinforced concrete in the initiation stage (passivation). From a quantitative perspective, storage type after curing and before exposure to the environment, even in the initiation stage (before depassivation), had an influence that differed from $1 \mu A \cdot day/cm^2$ for 0.65 w/c to $5 \mu A \cdot day/cm^2$ for 0.45 w/c in i_{cum} . This is equivalent to the margin of uncertainty when interpreting cumulative corrosion in the studied concrete qualities.

5. ACKNOWLEDGMENTS

The authors wish to acknowledge CINVESTAV-IPN Unidad Mérida and CONACyT for partial support. One of the authors, Jorge Briceño-Mena wish to acknowledge his scholarship from CONACyT for his Ph.D. studies.

6. REFERENCES

- American Concrete Institute Committee (ACI) (2002). *ACI 211-91. Standard Practice for Selecting Proportions for Normal, Heavyweight, and Mass Concrete*. American Concrete Institute Committee 211, (Reapproved), 1–38.
- Alonso, C., Andrade, C., Castellote, M., Castro, P. (2000). *Chloride threshold values to depassivate reinforcing bars embedded in a standardized OPC mortar*. Cement and Concrete Research, 30(7), 1047–1055. [https://doi.org/10.1016/S0008-8846\(00\)00265-9](https://doi.org/10.1016/S0008-8846(00)00265-9)
- Andrade, C., Alonso, C. (1996). *Corrosion rate monitoring in the laboratory and on-site*. Construction and Building Materials, 10(5), 315–328. [https://doi.org/10.1016/0950-0618\(95\)00044-5](https://doi.org/10.1016/0950-0618(95)00044-5)
- Andrade, C., Gonzalez, J. A. (1978). *Quantitative measurements of corrosion rate of reinforcing steels embedded in concrete using polarization resistance measurements*. Materials and Corrosion, 29(8), 515–519. <https://doi.org/10.1002/maco.19780290804>
- Andrade, C., Martinez, I. (2005). *Calibration by gravimetric losses of electrochemical corrosion rate measurement using modulated confinement of the current*. Materials and Structures, 38(283), 833–841. <https://doi.org/10.1617/14297>
- Andrade, C., Merino, P., Nóvoa, X. R. R., Pérez, M. C. C., & Soler, L. (1995). *Passivation of Reinforcing Steel in Concrete*. Materials Science Forum, 192–194, 891–898. <https://doi.org/10.4028/www.scientific.net/MSF.192-194.891>

- Andrade, C., Castelo, V., Alonso, C., González, J. A. (1986). *The determination of the corrosion rate of steel embedded in concrete by the polarization resistance and AC impedance methods*. Corrosion Science, 26, 961–970. [https://doi.org/10.1016/0010-938X\(86\)90086-7](https://doi.org/10.1016/0010-938X(86)90086-7)
- Ahmad, A., Kumar, A. (2013), *Chloride ion migration/diffusion through concrete and test methods*. International Journal on Advanced Scientific and Technical Research, 6(3), 151–180.
- Ahmad, S. (2003), *Reinforcement corrosion in concrete structures, its monitoring and service life prediction - A review*. Cement and Concrete Composites, 25(4-5 SPEC), 459–471. [https://doi.org/10.1016/S0958-9465\(02\)00086-0](https://doi.org/10.1016/S0958-9465(02)00086-0)
- Berke, N. S., Escalante, E., Nmai, C. K., & Whiting, D. (1996). *Techniques to Assess the Corrosion Activity of Steel Reinforced Concrete Structures - ASTM STP 1276*. American Society for Testing and Materials.
- Castro-Borges, P., Balancán-Zapata, M., López-González, A. (2013). *Analysis of tools to evaluate chloride threshold for corrosion onset of reinforced concrete in tropical marine environment of Yucatán, México*. Journal of Chemistry, 2013, 1–9. <https://doi.org/10.1155/2013/208619>
- Castro-Borges, P., Balancán-Zapata, M., Zozaya-Ortiz, A. (2017). *Electrochemical meaning of cumulative corrosion rate for reinforced concrete in a tropical natural marine environment*. Advances in Materials Science and Engineering, Article ID 6973605. <https://doi.org/10.1155/2017/6973605>
- Clément, A., Laurens, S., Arliguie, G., & Deby, F. (2012). *Numerical study of the linear polarisation resistance technique applied to reinforced concrete for corrosion assessment*. European Journal of Environmental and Civil Engineering, (3–4), 1–17. <https://doi.org/10.1080/19648189.2012.668012>
- Ghods, P., Isgor, O. B., McRae, G., Miller, T. (2009). *The effect of concrete pore solution composition on the quality of passive oxide films on black steel reinforcement*. Cement and Concrete Composites, 31(1), 2–11. <https://doi.org/10.1016/j.cemconcomp.2008.10.003>
- Hansson, C. M., Poursae, A., Jaffer, S. J. (2012). *Corrosion of Reinforcing Bars in Concrete*. The Masterbuilder, 15(3). <https://doi.org/10.1179/000705980798275535>
- Huet, B., L'Hostis, V., Miserque, F., Idrissi, H. (2005). *Electrochemical behavior of mild steel in concrete: Influence of pH and carbonate content of concrete pore solution*. Electrochimica Acta, 51(1), 172–180. <https://doi.org/10.1016/j.electacta.2005.04.014>
- Jiang, J. Y., Wang, D., Chu, H. Y., Ma, H., Liu, Y., Gao, Y., Shi, J., Sun, W. (2017). *The passive film growth mechanism of new corrosion-resistant steel rebar in simulated concrete pore solution: Nanometer structure and electrochemical study*. Materials, 10(4). <https://doi.org/10.3390/ma10040412>
- Lopez, W., & Gonzalez, J. A. (1993). *Influence of the degree of pore saturation on the resistivity of concrete and the corrosion rate of steel reinforcement*. Cement and Concrete Research, 23(2), 368–376. [https://doi.org/10.1016/0008-8846\(93\)90102-F](https://doi.org/10.1016/0008-8846(93)90102-F)
- Melchers, R. E., Li, C. Q. (2006). *Phenomenological modeling of reinforcement corrosion in marine environments*. ACI Materials Journal, 103(1), 25–32. Retrieved from <http://0-proquest.umi.com.library.newcastle.edu.au:80/pqdweb?did=1090660671&Fmt=7&clientId=29744&RQT=309&VName=PQD>
- ONNCCE (2014). *NMX-C-414-ONNCCE. Industria de la Construcción - Cementos Hidráulicos - Especificaciones y métodos de prueba*. Organismo Nacional de Normalización y Certificación de la Construcción y Edificación, S. C.
- ONNCCE (2015). *NMX-C-501-ONNCCE. Industria de la construcción-Durabilidad de estructuras de concreto reforzado-Medición de velocidad de corrosión en campo-Especificaciones y método de ensayo*. Organismo Nacional de Normalización y Certificación de la Construcción y Edificación, S. C.
- ONNCCE (2017). *NMX-C-530-ONNCCE. Industria de la construcción – Durabilidad – Norma*

- general de durabilidad de estructuras de concreto reforzado – Criterios y Especificaciones.* Organismo Nacional de Normalización y Certificación de la Construcción y Edificación, S. C.
- Page, C. L. (2009). *Initiation of chloride-induced corrosion of steel in concrete: Role of the interfacial zone.* *Materials and Corrosion*, 60(8), 586–592. <https://doi.org/10.1002/maco.200905278>
- Pech-Canul, M. A., Castro, P. (2002). Corrosion measurements of steel reinforcement in concrete exposed to a tropical marine atmosphere. *Cement and Concrete Research*, 32(3), 491–498. [https://doi.org/10.1016/S0008-8846\(01\)00713-X](https://doi.org/10.1016/S0008-8846(01)00713-X)
- Pedrosa, F., Andrade, C. (2010). *Study of corrosion rate variability in indoor and outdoor specimens.* In Carmen Andrade & J. Gulikers (Eds.), *Advances in Modeling Concrete Service Life: Proceedings of 4th International RILEM* (pp. 33–42). Madrid: Springer. <https://doi.org/10.1007/978-94-007-2703-8>
- Poursae, A., Hansson, C. M. (2007). *Reinforcing steel passivation in mortar and pore solution.* *Cement and Concrete Research*, 37(7), 1127–1133. <https://doi.org/10.1016/j.cemconres.2007.04.005>
- Rebolledo, N., Andrade, C. (2010). *From corrosion rate to accumulated corrosion depth or loss in cross section of reinforcements.* In Carmen Andrade & J. Gulikers (Eds.), *Advances in Modeling Concrete Service Life: Proceedings of 4th International RILEM* (Vol. 3, pp. 43–51). Madrid: Springer. <https://doi.org/10.1007/978-94-007-2703-8>
- Troconis, O., Romero, A., Andrade, C., Helene, P., Díaz, I. (1998). *Manual de inspección, evaluación y diagnóstico de corrosión en estructuras de hormigón armado* (2nd ed.). Red Durar.

Recommendations for rehabilitation and corrosion protection of a 100-year-old steel bridge (Durgadee) across heavily polluted river near Mumbai, India

S. S. Bhonge¹, P. Dalwi²,
J. K. Kulkarni³, S. K. Manjrekar⁴

*Contact author: bhongess@gmail.com

DOI: <http://dx.doi.org/10.21041/ra.v10i2.476>

Reception: 09/12/2019 | Acceptance: 15/04/2020 | Publication: 30/04/2020

ABSTRACT

This paper describes the rehabilitation proposal, methodology of evaluation of distress and likely remedial measures for 100 years old steel bridge on Ulhas river, near Mumbai. The bridge is constructed in year 1914 during British era apparently now heritage bridge as it was constructed with unique structural arrangement of jack arch decking and warren truss girder with verticals. After structural audit in 2000, it revealed the deterioration of steel parts and concrete initiated long back because of humid atmosphere and pollution in the area. Durgadee bridge showed various signs of bridge distress like major cracks in masonry abutments, heavy corrosion of Mild Steel (MS) structural members, non -functioning of expansion joints and bearings, failure of jack arch roof plates, de-bonding of concrete and exposed reinforcement etc. Paper discusses recommendations for rehabilitation and corrosion protection.

Keywords: corrosion protection; rehabilitation; distress; steel structure; LCNR.

Cite as: Bhonge, S. S., Dalwi, Pradeep, Kulkarni, J. K., Manjrekar, S. K. (2020), "Recommendations for rehabilitation and corrosion protection of a 100-year-old steel bridge (Durgadee) across heavily polluted river near Mumbai, India", Revista ALCONPAT, 10 (2), pp. 259 – 273, DOI: <http://dx.doi.org/10.21041/ra.v10i2.476>

¹ The Superintending Engineer, Designs Circle (BR), P.W.D., Govt of Maharashtra, India.

² Executive Engineer, PW Division Thane, India.

³ Retired Executive Engineer, MIDC, Govt of Maharashtra, Mumbai, India.

⁴ Director, Sunanada Speciality coatings, Mumbai, Hon. Member ACI India, India.

Legal Information

Revista ALCONPAT is a quarterly publication by the Asociación Latinoamericana de Control de Calidad, Patología y Recuperación de la Construcción, Internacional, A.C., Km. 6 antigua carretera a Progreso, Mérida, Yucatán, 97310, Tel.5219997385893, alconpat.int@gmail.com, Website: www.alconpat.org

Responsible editor: Pedro Castro Borges, Ph.D. Reservation of rights for exclusive use No.04-2013-011717330300-203, and ISSN 2007-6835, both granted by the Instituto Nacional de Derecho de Autor. Responsible for the last update of this issue, Informatics Unit ALCONPAT, Elizabeth Sabido Maldonado, Km. 6, antigua carretera a Progreso, Mérida, Yucatán, C.P. 97310.

The views of the authors do not necessarily reflect the position of the editor.

The total or partial reproduction of the contents and images of the publication is strictly prohibited without the previous authorization of ALCONPAT Internacional A.C.

Any dispute, including the replies of the authors, will be published in the first issue of 2021 provided that the information is received before the closing of the third issue of 2020.

Recomendaciones para la rehabilitación y protección contra la corrosión de un puente de acero de 100 años de antigüedad (Durgadee) sobre un río muy contaminado cerca de Mumbai, India

RESUMEN

Este documento describe la propuesta de rehabilitación, la metodología de evaluación de la angustia y las posibles medidas correctivas para el puente de acero de 100 años de antigüedad en el río Ulhas, cerca de Mumbai. El puente se construyó en el año 1914 durante la era británica, aparentemente ahora puente de patrimonio, ya que se construyó con una disposición estructural única de cubierta de arco de gato y vigas de celosía con verticales. Después de una auditoría estructural en 2000, reveló el deterioro de las piezas de acero y el hormigón iniciado hace mucho tiempo debido a la atmósfera húmeda y la contaminación en el área. El puente Durgadee mostró varios signos de angustia en el puente, como grietas importantes en los pilares de mampostería, corrosión intensa de los miembros estructurales de acero dulce (MS), no funcionaban las juntas de expansión y los cojinetes, falla de las placas de techo de arco de gato, desacoplamiento de concreto y refuerzo expuesto. El documento discute recomendaciones para rehabilitación y protección contra la corrosión.

Palabras Clave: protección contra la corrosión; rehabilitación; angustia; estructura de acero; LCNR.

Recomendações para reabilitação e proteção contra a corrosão de uma ponte metálica de 100 anos de idade (Durgadee) sobre um rio fortemente poluído perto de Mumbai, Índia

RESUMO

Este artigo descreve a proposta de reabilitação, metodologia de avaliação de perda de capacidade resistente e prováveis medidas corretivas para uma ponte metálica de 100 anos de idade no rio Ulhas, perto de Mumbai. A ponte foi construída no ano de 1914, durante a era britânica, agora como ponte histórica, uma vez que foi construída com arranjo estrutural exclusivo de decks em arco e viga vertical treliçada. Após uma inspeção estrutural em 2000, foi revelada a deterioração dos elementos de aço e concreto iniciadas há muito tempo por causa da atmosfera úmida e da poluição na área. A ponte Durgadee mostrou vários sinais de deterioração da sua estrutura, como grandes fissuras nos pilares de alvenaria, corrosão avançada dos elementos metálicos estruturais, não funcionamento das juntas de dilatação e aparelhos de apoio, falha das chapas metálicas do deck em arco, deslocamento do concreto e armadura exposta. O documento discute recomendações para reabilitação e proteção contra corrosão.

Palavras chave: proteção contra corrosão; reabilitação; perda de capacidade resistente; estrutura de aço; LCNR.

ABBREVIATIONS AND ACRONYMS:

Heritage Bridge Structure: Structure recognized by State Govt for its historical and aesthetical significance.

PWD: Public Works Department of State Govt in charge of infrastructure construction and maintenance.

MPCB: Maharashtra State pollution Control Board who monitors pollution.

LCNR: Long Chain Nylon Reticulant protective coating.

IRC: Indian Road Congress, an organization in India controlling road and bridge design standards.

1. INTRODUCTION

This paper describes the need for rehabilitation proposal, methodology of evaluation of distress and likely remedial measures for 100 years old steel bridge (also known as Durgadee bridge) on Ulhas River at km 1/ 800 on Bhiwandi road, Kalyan, near Mumbai.

The bridge is constructed in year 1914 during British era apparently now heritage bridge as it was constructed by British engineers with unique structural arrangement of jack arch decking and warren truss girder with verticals. The bridge is a steel structure with two columns filled with concrete with Steel superstructure consisting of jack arch type deck support sheet.

Steel structures in severe atmosphere must face a variety of environmental forces. Although several deteriorating processes, chemical attack still represent severe challenges and problems to many important steel structures. Rapid development in technology in recent years has made easier to control such deteriorating processes.

Structural steel offers several advantages:

High strength: the yield stress of steel in tension and compression is almost the same which helps us in the use of steel as long span bridges and tall structures.

Durability: this property of steel allows successive deformation without significant loss of strength and stiffness including resistance to weathering action.

Prefabrication: steel parts are manufactured at factory under strict supervision and quality control due to which there is a very less variation in material properties. The material can be transported at site and assembled which helps in speedy construction ensuring better quality.

Demountability: steel structure can be disassembled and reused if required. It can be recycled easily reducing the wastage. Even the repairs and retrofitting of steel structure and their strengthening is much simpler and easier than the concrete structure.

Limitations: steel structure are susceptible to corrosion when exposed to air and water.

Although structural Steel are not combustible, they lose their strength rapidly during fire. Aesthetically, steel structure does not give pleasing appearance. The cost of steel structure is more than that of concrete

The choice of section in steel structure is governed by:

- Cross section area, to resist tension or compression.
- Section modulus to resist bending and shearing stress.
- The radius of gyration to provide rigidity towards buckling in compression

2. GENERAL- INDIAN SCENARIO

India is home to various geographical features such as rivers, mountains, valleys, tablelands, long seashores, deserts, and flat terrains. India is the seventh largest country in the world and covers a total area of 3,287,263 sq km. The shoreline of the country extends for 7,517 km.

India has one of the largest road networks in the world with about 59 lakh km of road length including National Highways (NHs), Expressways, State Highways, District roads, Other District Road and Village roads. In India, road infrastructure is used to transport over 60% of total goods and 85% of total passenger traffic. India has inventoried more than 4 lakh bridges/structures constructed through various Government bodies.

The bridges in coastal areas were constructed in the face of several adverse factors, such as difficulty of fixing water way, navigational requirements, approach alignments, foundation problems, saline conditions, difficulty of construction of superstructure and approach banks, Navigational requirements. These in turn, sometimes required bridges having long spans involving sophisticated construction procedures. Foundations were usually deep in the creek bridges and standing water posed major problem in construction.

Due to extraordinary increase in traffic densities, particularly in and around main cities of the state, the Government has undertaken a program of constructing flyovers, underpasses and bye-pass roads. But before a decision of new construction, priority to rehab and retro fitting of existing bridge is given. As the Durgadee bridge has outperformed and proved its durability because of its robust structural arrangement. Bridge after rehabilitation, can act as bypass for LMV (light and medium vehicles) and city users in the city of Kalyan.

3. PRESENT SCENARIO OF DURGADEE BRIDGE

Kalyan is near Mumbai and is historical place and was famous Trade Centre due to Kalyan creek coast. There exists one fort known as Durgadee fort along the side of the bridge which is around 400 years old. Similarly, Bhiwandi is a Taluka place and equally important historical Trade Centre. In early parts of 19th century the British Government decided to connect Kalyan and Bhiwandi by steel bridge across Ullas river near Durgadee fort. The construction of bridge started somewhere in 1908 and was commissioned in 1914. (Bridge site location: 19°14'43" N 73° 6'59" E)

- **Abutments:** These are rubble masonry abutments on both sides, however abutment on Bhiwandi side seems to be in very dangerous condition and need the replacement.
- **Bridge consist of 10 spans of 36m each having total length of 360m with through truss arrangement Superstructure and Decking arrangement:** There is a continuous flooring system of Jack arch over the stringer beam for all 10 numbers of spans. Signs of upheaval of BT layer shows that there is immediate need of replacement. The expansion joints of the bridge are completely damaged and blocked.
- **Wearing course:** There is an immediate need of dismantling bituminous wearing course removing cleaning the debris on bridge bearing and over the jack arch decking sheet. The condition of deck steel plates in Jack arch due to corrosion would be visible only after removal of wearing course and the layers below it. The distress mapping of superstructure is needed by exposing the one or two spans after dismantling wearing course.
- **Bearings:** The type of bearing is steel rocker and roller type and not visible due to lots of debris deposited on the bearing location. Arrangement of Rocker / roller type bearings is nonfunctional because of lack of maintenance.
- **Substructure:** It consist of twin hollow steel column filled with concrete and tied with cross bracings.
- **Bridge foundation:** Consist of pile foundation with steel liners. MS liner in splash zone, i.e. portion between high and low water levels, shows extreme corrosion.
- **Present corrosion protection arrangements:** No protection is given to exposed surfaces from Corrosion /carbonation and other atmospheric pollution.

In addition, above, general causes of distress in structure, following have played major role in damaging the structure and reduction in service life.

After structural audit in 2000, it revealed the deterioration of steel parts and concrete initiated long back because of humid atmosphere in the Kalyan area, carbonation of concrete, chloride ingress, leaching, sulphate attack, which all lead to the corrosion and ultimately reduction in life of structure. Bridge is closed for traffic since 2001. Figure 1 shows Google map of bridge.

Any bridge structure in service life will be subjected to chemical and physical changes. A durable structure is one in which these changes occur at a slower rate which does not detrimentally affect its performance within its intended lifespan. As per Indian codes and other contemporary codes, the steel structures are designed for a maintenance-free operating life of 60 to 100 years. However, the various structures in and around Mumbai area show severe deterioration (or failure in many cases) within a very short span due to aggressive environment and humidity in atmosphere. In

present case generally aggressive environment added by polluted water of Ulhas river is playing major role for deterioration.

Based on the studies, the water from river cannot be considered safe even for irrigation purpose. The chloride content in the wastewater effluent was with an average value of 1,377 mg/L. The results indicate that the chloride content is very much above the acceptable limit of 200 mg/L set by WHO. The results indicated high level of pollution due to toxic heavy metals like chromium (Cr), cadmium (Cd), nickel 6 (Ni), zinc (Zn), copper (Cu), lead (Pb) and iron (Fe). The concentration of all these heavy metals were found to be much above the acute toxicity level.

Because of heavy pollution in Ulhas river, water and the humidity due to nearness to seashore, the bridge condition is very dilapidated. There is heavy corrosion of steel parts used in the structure. The structure must have been designed for normal river water in 1914. It is however seen that the color of river water is blackish which may be due to mixing of wastewater of surrounding urban areas and industrial waste. River water contains both organic and inorganic chemicals in addition to various gases like H₂S, CO₂, CH₄, and NH₃ etc., that are formed due to the decomposition of sewage. This leads to faster deterioration of steel structure and concrete.



Figure 1. Google map of bridge.

4. DISTRESSES NOTICED IN DURGADEE BRIDGE

Durgadee bridge showed various signs of distress as under:

- Minor to major cracks in Masonry abutments on both sides. Abutment on Bhiwandi side is in dangerous condition on the verge of giving way.
- Non -functioning of expansion joints and bearings.
- Heavy Corrosion of MS structural members. However, loss of section up-to 3mm due to corrosion was noticed at less than 10 % of the area.
- Leakages through Jack Arch deck and near bearings.
- Failure and deterioration of Jack Arch roof plates for decking of bridge as well as concrete filling above it is including wearing course.
- De-bonding of concrete and exposed reinforcement in concrete below wearing course.

State Transport Department (called as PWD) has already stopped the vehicular traffic on the bridge since 2001.

5. DRAFT POLICY/ PROPOSED STAGES OF REHABILITATION AND REPAIR

The whole program of restoration of this bridge can be divided into the following parts.

1. Study of old records related to bridge

- Verify the original design work done by PWD, Material specifications used during the construction period.
- Study of Restoration, repair done by PWD from time to time in past.
- Detailed mapping, dimensions and preparation of detailed drawings for Old Bridge structure with help of Drone and physical survey. It will include use of drone survey for preparation of Auto cad drawings and dimensioned drawing which will be needed for structural modelling and analysis.

2. Inspection

Steel bridge will be inspected with the purpose of identifying any defects that may be present in the structure and to establish causes for these defects. Defects that are likely to affect the strength, safety or serviceability of a bridge are planned to attend as part of the remedial and maintenance work cycle.

- Photographs (both recent and historic); The most recent inspection reports; Recent maintenance history.
- Strength and rating calculations. Condition survey of bridge will lead to estimation of residual life of the structure.
- A visual inspection will systematically cover the whole surface of the steel structure at close quarters paying particular attention to areas.
- The following matters are critical to the success of a steel bridge inspection:
- Detailed notes must be taken of the condition of the protective coating on all parts of the structure using a standard method of assessment
- Signs of rust staining should be looked for around the heads of fasteners. This may indicate that they are loose.
- Fasteners which do not conform with proper standards of installation should be noted.
- The highest loaded bolt or rivet in a joint should be carefully examined in areas which are expected to be susceptible to fatigue.
- The presence of a suspected crack should be confirmed by non-destructive testing, Dye penetrant and magnetic particle techniques are likely to be used in the first instance. Radiographic and ultrasonic methods may also be used for specific cases.
- Deformations and distortions will often show up as cracking or flaking paint. Measurements of any significant deviations from the true line should be recorded.
- The location and description of all defects must be methodically recorded to allow proper evaluation of their effects and subsequent monitoring or repair.

3. Study of corrosion parameters related to various bridge components that is corrosion mapping.

4. Various types of NDT (Non-Destructive Testing) to assess the damage

5. Testing of river water.

6. Planning for working platform for working of labor and machinery

Suspended or hanging platform will be needed for working below the soffit. Detailed drawings will be prepared for above cases considering site situation and methodology of repair. Ideally floating pontoon with small boat along with winch machine will be very useful for speedy execution of work. Figure 2 is a photo of bridge showing bearing and expansion joint location.

7. Underwater assessment of the part of the substructure and foundation

Special types of cameras and certified divers will be needed as water due to turbid due to pollution. It will involve underwater videography and taking photographs and Submission survey details in soft copies and status report of underwater survey. Total number of piers to be survey will be 9 piers of bridge.

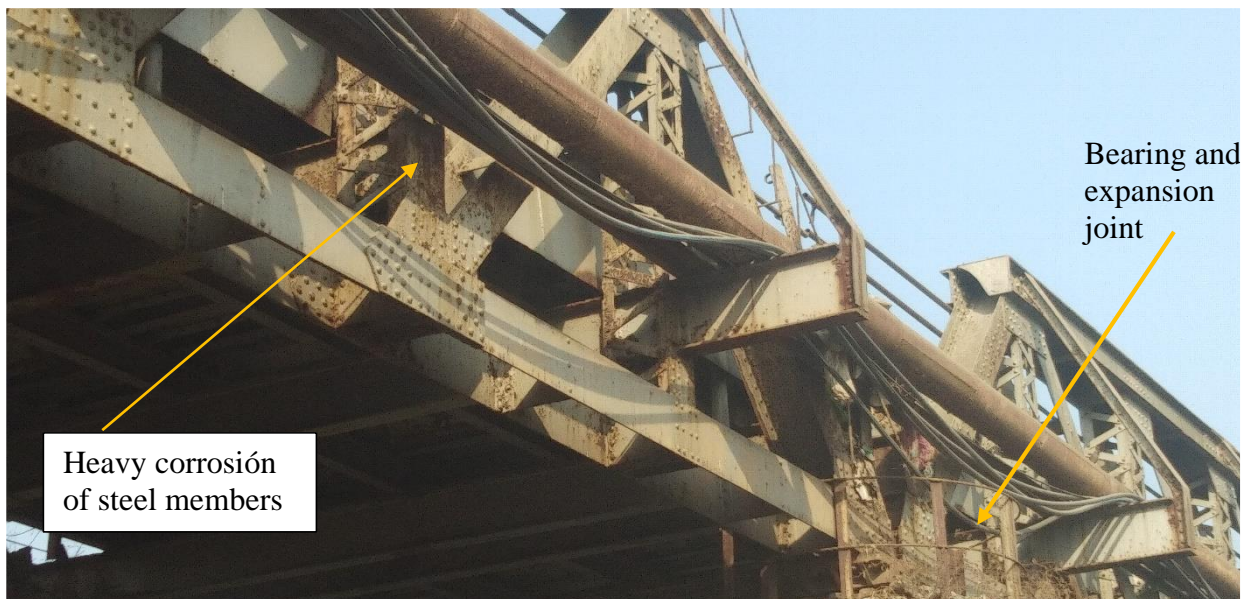


Figure 2. Photo of bridge showing bearing and expansion joint location

8. Evaluation of defects

All observed defects will influence the strength or serviceability of the bridge. Defects which reduce the capacity or durability of the bridge do require remedial action. The purpose of evaluation is to determine the relative significance of each defect so that the load-carrying capacity of the bridge can be reassessed and so that any remedial work required can be given proper priority. Evaluation will also assist in determining future strategies for maintenance or replacement.

The evaluation of the effect of some defects requiring a thorough understanding of the behaviour of the structure concerned. The interaction of primary and secondary load-carrying members, the effect of imperfectly pinned joints and the possible presence of alternative load paths need to be appreciated. A basic understanding of metal fatigue and crack mechanics is necessary to evaluate problems of this nature.

9. Analysis of factors to decide methodology of rehabilitation/ strengthening

Structural repair and maintenance of steelwork includes the replacement and maintenance of protective coatings, repair of corroded members, replacement of damaged members and defective fastenings, and remedial work associated with fatigue cracking. These problems have been identified during the inspection and evaluation process.

Fatigue behavior is very much influenced by the presence of stress concentrations such as holes, welds, abrupt changes of shape, cracks or other defects.

10. Residual life Assessment and bridge rating

- a) Residual life Assessment and bridge rating as per design analysis before and after rehab.
- b) Assessments to enhance the residual life by further by about 15 to 20 years.
- c) Assessing the existing load rating which may vary from 30 R to 60 R to decide the suitability of bridge for vehicle traffic.

11. Action plan for Corrosion Protection

The detailed evaluation of corroded material is to be carried out by laboratory testing in ICT (Institute of Chemical Technology), Matunga Mumbai, India and Metallurgical testing of steel at Metallurgical Department, IIT (Indian Institute of Technology) Powai Mumbai, India.

Plan on the various technology and material available for repair and its methodology with reference to economic consideration. Corrosion protection system to protect the bridge for further 25 years including sacrificial anode system to prevent the further corrosion and its damaging action.

12. Selection of appropriate repair, restoration and rehabilitation measures to various structures.

6. METHODOLOGY PROPOSED: SALIENT FEATURES AND PARAMETERS TO BE CONSIDERED

6.1 Steel girder repair

Figure 3 is a photo of the bridge showing the warren truss type structure. The work of repairing built-up steel girders by restoring or replacing damaged or deteriorated elements include, but is not limited to, providing temporary supports for jacking; modifying girders to accept jacking loads; temporarily supporting or reducing loads carried by girders; disconnecting or removing elements from girders by removing bolts or rivets; drilling and reaming holes; grinding to provide required finish or tolerances on steel surfaces; making minor repairs to decks within the work area; erecting repaired or replaced elements and incidental items by welding or high tensile strength bolting; and preparing surfaces damaged or left bare by the work and applying a prime coat of paint.



Figure 3. Photo of bridge showing warren truss type structure.

6.2 Protective coating failure

It is rare for a protective coating to outlast the life of the structure. Breakdown of paint or loss of any coating is inevitable and should be anticipated. This usually results from condensation and may be increased by absorption of moisture by wind-borne salts on areas not subject to rain washing. Accumulation of debris, bird droppings, flaking paint etc. will all retain moisture and promote corrosion.

In addition to eventual failure of a coating system by weathering, premature failure may result from:

- Loss of coating adhesion due to faulty specification or application;
- Incompatibility of successive coats;
- Subsurface rusting due to inadequate surface preparation and/or priming paint;
- Localized failure due to mechanical damage;
- Inadequate film-build on sharp edges, welds and paint shadow areas.

6.3 Loss of section

Where the protective coating has not been maintained or an area of damaged coating not been repaired, corrosion resulting in a loss of section usually follows. The corrosion rate largely depends on the proximity of the bridge to the coast.

Corrosion can also be accelerated by the following situations:

- Presence of cracks and crevices.
- Different metals in contact.
- Ponding of moisture.
- Concentration of salts through evaporation; rust and debris.
- Loss of section may also result from wear in pins or from mechanical abrasion where members rub together.

6.4 Loose or defective fastenings

Whether operating in shear or in a friction grip joint, fastenings must be properly installed to function correctly. Sometimes, because of excessive vibration, over-straining, corrosion or improper installation, fastenings can become loose and should be replaced.

Specific problems typically associated with various types of fastenings are:

- Mild steel bolts tend to corrode rapidly if the protective coating is not intact. This type of bolt may also loosen with vibration unless suitable washers or lock nuts are provided;
- High-strength bolts will also corrode unless the protective coating is maintained. Galvanized bolts are usually better than painted 'black' steel. Improperly torqued bolts will loosen and bolts which have been installed through heavily tapered flanges without suitably tapered washers may flex and become overstressed.

6.5 Cracks

Cracking of any bridge component is potentially serious and needs to be thoroughly investigated. Cracks in steel bridge members can be caused by metal fatigue, embrittlement, impact damage or manufacturing defects such as rolling flaws, and can extend with time. Structural cracks are most likely to have started at obvious stress concentrations such as a bolt or rivet hole, extremities of welds, abrupt changes of section, or at nicks and notches.

Fatigue cracks might not become obvious until a member has been subject to many stress reversals or fluctuations.

6.6 Impact damage

Accidental damage to bridge members through vehicle impact is a serious matter and one which needs to be investigated promptly. Obvious damage will usually be in the form of bent and distorted members and overstrained fastenings.

6.7 Deformation and distortion

A structural member's resistance to compressive forces is considerably reduced if components are buckled or distorted out of plane. Tensile members can act unpredictably. Deformation and distortion can occur as a result of:

- Accidental damage.
- Axial over-strain.
- Excessive shear in thin webs.
- Seized bearings.
- Inadequate provisions for expansion.
- Substructure settlement may also lead to distortion in members.

Deformations cause members designed for tension being forced to take compressive loads.

6.8 Manufacturing defects

Despite the rigorous specifications and the tight manufacturing tolerances to which structural components are rolled and formed, manufacturing and fabrication defects can and do find their way into completed structures.

Rolling flaws may show up as delamination, cracks, blisters, pits or inclusions as well as out-of-tolerance straightness or lack of squareness.

6.9 Faults in detailing

Regrettably, defects can be built into a bridge structure through poor design, detailing and specification. In this category are found such details as:

- The abrupt curtailment of steel section flanges in tension members.
- Excessive eccentricities (both in plane and out of plane) in joint intersections.
- Inadequate provision for rotation.
- Poor drainage provisions.
- Curtailment of welds in inappropriate locations.

Manufacturing defects as well as design flaws can sometimes be noticed through a drone tour as illustrated in figure 4.

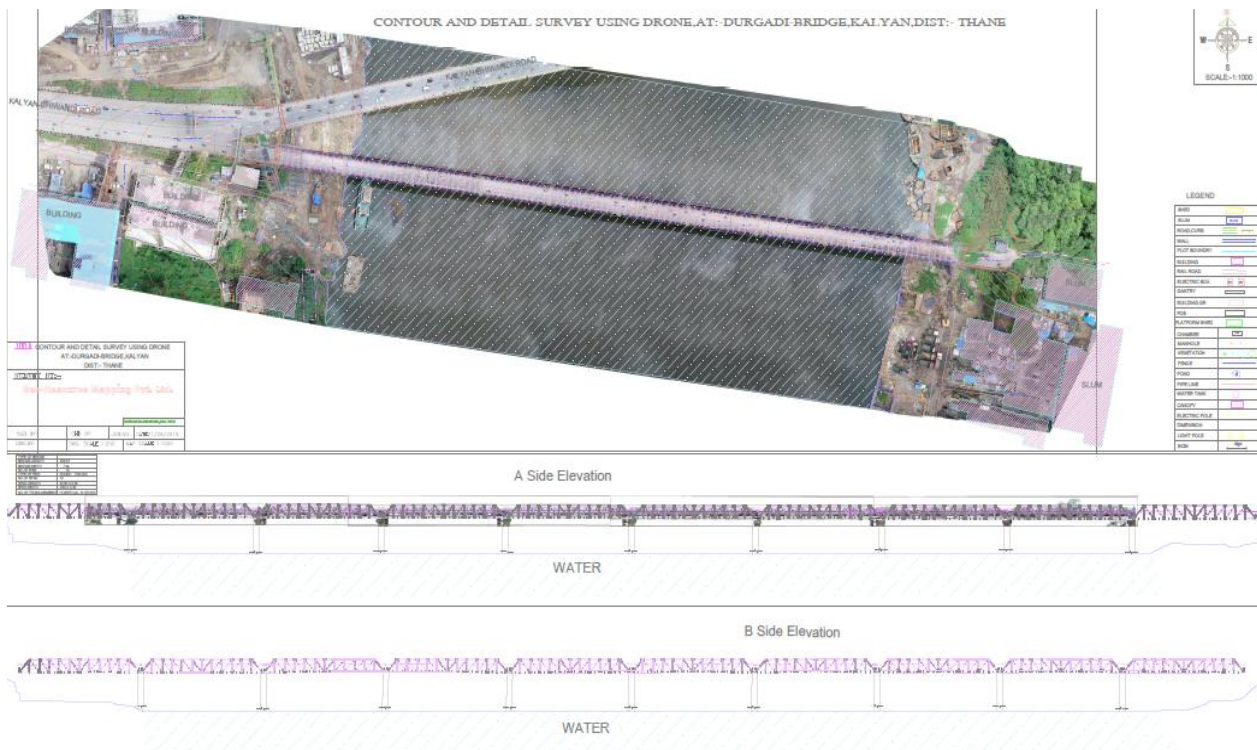


Figure 4. Drone survey map of bridge

7. PROPOSED METHODOLOGY AND PROCEDURE FOR CORROSION PROTECTION

7.1. The Composite Treatment of LCNR (Long Chain Nylon Reticulant) UV (Ultraviolet) Resistant Coating along with Electrochemical Protection by sacrificial anodes

It will be necessary to evolve 'State of the Art' corrosion removal, highly adhesive, UV resistant coating system and include electro-chemical protection to further prolong the life of protective system. This paper attempts to choose such composite system based on test parameters and past track records of innovative systems.

The points to be considered for rendering new protective systems:

- The surface should be totally bereft of any residual paint as well as even the traces of corrosion product as life of corrosion protection systems are dependent solely on surface preparation.
- The corrosion free surface should remain so (after corrosion removal treatment) until the next logical treatment of appropriate polymer primer is received by the surface.
- Primer should be followed by especially cross linked and highly impenetrable matrix of polymers.
- These coatings should have full immunity from the decomposition due to attack of ultraviolet radiation in the sunlight.
- Corrosion is an electro-chemical process and in highly susceptible conditions like Durgadee bridge, it is possible for it to get promptly initiated whenever smallest amount of exposure to bare metal either due to defects inadvertently left during the execution due to extremely high intricate arrangement of steel members or during the initial service life due to unintentional injuries to protective systems happens and then the entire corrosion could be vigorous. Thus, it is preferable to give electro-chemical protection like use of sacrificial anodes at regular intervals typically at the junctions.

7.2. Procedure of rectifications

- Since the removal of entire residual remains of the paint as well as adamant corrosion products to the extent of absolute 100% is a challenging situation by steel wire brushing etc., the only option is to sand blast the whole steel structure.

As a result of sand blasting, the corrosion products and residual paint are removed fully, however it also leads to creating a very vulnerable steel surface which is susceptible for ‘flash corrosion’ due to moisture and oxygen in the ambient conditions. This layer of flash rust can be visible within even 2 to 3 hours of sand blasting in the form of reddish iron oxide layer. This layer then onward creates compromise to some extent in the loss of adhesion of subsequent polymer/epoxy/polyurethane coatings.

- In order to avoid this weakness in the protection system, as soon as sand blasting is over, one layer of Rusticide is applied.

Rusticide can be applied by cotton waste, soft brush etc. Rusticide not only removes the residual rust but also reacts with corrosion products to convert them to a stable passivating nano film on the surface of the steel and return the steel back to its original grayish white color the steel from flash rusting. As a result of application of Rusticide, the steel surface turns into whitish-black colour.

- Now this surface is totally free of corrosion product and ready to receive the priming coat of 100% pure LCNR - epoxy primer - Sunepoxy 358. Epoxy coat is always a primer coat for two reasons:
 - a. It has extraordinary adhesion to steel or any other dry surface.
 - b. The outstanding adhesion of epoxy ensures the successful performance of subsequent protective coats.

Epoxy coatings are not to be given as finishing layers as it easily gets disintegrated by ultraviolet rays or any form of external energy.

Sunepoxy 358 is a specially made epoxy primer which has longer chain nylon reticulant molecule which enhances its performance as compared to ordinarily available general epoxy coatings.

- Corrosion Protection with Acyclic Polyisocyanate Reticulant (APR) based Sungard APR Epoxy coatings are not UV stable and hence it needs additional protection of UV stability.

After 24 hours of application of Sunepoxy 358, provide and apply 2 coats of Sungard APR using soft paint brush / spray gun, etc. Polyurethane coatings are resistant to attack of ultraviolet rays. However, in case of Sungard APR the normal polyurethane molecule has been added with the characteristics of acyclic polyisocyanate reticulantness, making the matrix more complex due to additional cross linking and hence added denseness of the cured polymer. This adds to the robustness and protection to a higher degree.

There will be need of Rollers with long handles (metal sticks), spike shoes on horizontal surfaces.

- As mentioned earlier corrosion is an Electro chemical process and LCNR coating system will give protection to the surface covered by the same. However, Durgadee bridge structure is having several intricate steel members welded together. Also, at several places the steel flats or channels are arranged on each other which means that the coating cannot be physically done in such an area either by spray or brush. Hence, the surfaces so unattended are vulnerable to corrosion. The corrosion thus initiated will be very rigorous as seen in some of the photographs. At such situations, it is very useful to operate sacrificial anode. This sacrificial anode is connected to the vulnerable areas by welding and wherever corrosion attack takes place sacrificial anode being more vulnerable will corrode preferentially leaving the steel surface unaffected.

The placement of sacrificial anodes shall be more focused at gusset plate weld joints and at major junctions etc. Where the possibility of proper protective coating will be difficult.

- Deck slab will be re-concreted by using welded studs for anchoring purpose. Required slope of 2.5% for camber and to facilitate drainage will be provided. Stripe seal type expansion joint and new steel rocker roller bearing will be provided.

8. PREVENTIVE MAINTENANCE

8.1 The preventive maintenance of a steel bridge starts after completion of rehabilitation as proposed above.

Provision of access to facilitate future inspections and maintenance should also be considered. Other practices which will assist in minimizing maintenance of an in-service bridge include:

- Proper selection of protective coating type, proper surface preparation and application over the entire coated surface and its periodicity of application.
- Regular washing and cleaning of protective coating surfaces.
- Regular clearing and cleaning of drainage ports. Improving drainage in areas which are not adequately drained.
- Ensuring bearings are operating correctly.
- Maintaining the presence of adequate expansion joints.
- In addition, potential problem areas should be identified, and appropriate action taken before structural defects become manifest. Such matters include:
 - i. Details involving abruptly curtailed cover plates on flanges should be improved if they are likely to become fatigue risks;
 - ii. Poor welds should be ground out and replaced;
 - iii. Selected rivets can be replaced with high- strength friction-grip, fasteners to improve the fatigue characteristics of a rivet group (e.g. the leading rivets in a joint or cover plate);
 - iv. Eccentricities in joints and connections may be improved to reduced unwanted bending stresses;
 - v. The point of support of bearings may be redefined to improve eccentric movement effects.

8.2 Bridge instrumentation systems for dynamic monitoring of bridge.

Baseline model development of a bridge is essential for structural health monitoring which can play an important role in securing system integrity, minimizing maintenance cost, and maintaining longevity of bridges. Structural health monitoring and baseline model are required periodically, especially after damaging earth quacks, degradation of a structure due to aging or environmental actions or if there is a damage-causing event such as impact due to accident or natural disaster.

Global structural health monitoring technology consists of two aspects: (1) Instrumentation of bridges with sensors such as accelerometers and strain gauges and more importantly, (2) Methodologies for obtaining meaningful information concerning the structural health conditions, if any, from the measured data.

Advances in sensing, digitizing, recording, and data communications have led to current monitoring systems capable of sensing, recording, and remotely analyzing/displaying dynamic input and response information for bridges and other structures.

The current generation of sensors for earthquake accelerometers has large dynamic ranges, allowing simultaneous measurement of earthquake shaking, low-frequency wind-induced vibration, and ambient vibration.

Proposed baseline model development of this bridge, which will be instrumented for global structural health monitoring. Monitoring systems including accelerometers, strain gauges, pressure sensors, and displacement sensors to be installed.

A structural health monitoring system may detect unusual structural behavior at an early stage, thereby reducing the risk of sudden and catastrophic failure. Appropriate monitoring requires the development of an accurate computer model that effectively characterizes the entire structure, including the continuity and boundary conditions.

9. CONCLUSION

The steel bridge though has outlived its service life; however, it is still in serviceable condition with Engineered Strengthening and Corrosion protection. It also enjoys status of Heritage structure. Appropriate strengthening of steel and concrete deterioration is brought out. Its service life enhancement can be done with Life 365 Model of ACI since the damage and rectification is focused around with enhanced properties coatings and the attack of chloride and other aggressive pollutants. Major emphasis in corrosion control will be creating long term barriers for protection against heavy pollutants to come in contact of steel. Protective treatment is also suggested considering coastal conditions of Mumbai and around. The protection program is drawn on the basis of successful past track record of similar structure in similar conditions. The restoration will serve purposes like retaining heritage structure at the same time it will be useful for at least LMV for few more years reducing traffic load on the existing bridge.

10. ACKNOWLEDGEMENTS

The authors acknowledge the support of Designs Circle, PWD, Govt of Maharashtra, Mumbai and PW Division (Thane), Thane in writing of this paper.

11. BIBLIOGRAPHY AND STANDARDS

- Malhotra, M. M. (2007), *Design od steel structure*. Edition: 7, Reprint Publisher: Jain Brothers.
- Indian Road Congress (IRC) (1990), *IRC: SP:35-1990: Guidelines for Inspection and Maintenance of Bridges*. (Reprint-2000), Indian Road Congress Special Publication. New Delhi.
- Indian Road Congress (IRC) (1996), *IRC: SP:18-1996: Manual for Highway Bridge Maintenance Inspection*. Indian Road Congress Special Publication. New Delhi.
- Indian Road Congress (IRC) (1999), *IRC: SP:52-1999: Bridge Inspector's Reference Manual*. Indian Road Congress Special Publication. New Delhi.
- Indian Road Congress (IRC) (2007), *IRC: SP:74-2007: Guidelines for Repair and Rehabilitation of Steel Bridges*. Indian Road Congress Special Publication. New Delhi.
- Indian Road Congress (IRC) (2008), *IRC: SP:75-2008: Guidelines for Retrofitting of steel Bridges by Pre-stressing*. Indian Road Congress Special Publication. New Delhi.
- Indian Road Congress (IRC) (2002), *IRC: SP:60-2002: An Approach Document for Assessment of Remaining Life of Concrete Bridges*. Indian Road Congress Special Publication. New Delhi.
- Indian Road Congress (IRC) (2004), *IRC SP 61-2004: An Approach Document on Whole Life Costing for Bridges in India*. Indian Road Congress Special Publication. New Delhi.
- Indian Road Congress (IRC) (1993), *IRC: SP:40-1993: Guidelines on Techniques for strengthening and Rehabilitation of Bridges*. Indian Road Congress Special Publication. New Delhi.
- Indian Road Congress (IRC) (2010), *IRC: SP:37-2010: Guidelines Evaluation of Load Carrying Capacity of Bridges*. Indian Road Congress Special Publication. New Delhi.
- MPCP (2019), *Maharashtra State Pollution Control Board (MPCP)*, URL: <http://www.mpcb.gov.in/node>

- Maharashtra Pollution Control Board (2015), *Comprehensive Study on Polluted River Stretch of Ulhas River – Downstream of Mohane, Kalyan*, MPCB Kalyan.
- Karve, S. R. Shah, V. I. (1998), *Structural Design Databook Steel Structures*, Structures Publications.
- NZ Transport Agency (2001), *Bridge Inspection and Maintenance Manual*. URL: <https://www.nzta.govt.nz/resources/bridge-inspection-maintenance-manual/>